CAR-iNKT cells as a novel immunotherapy for B cells malignancies

A thesis submitted for the degree of Doctor of Philosophy

April 2018

Antonia Rotolo

Imperial College London

Declaration of Originality

I can declare that the work in this thesis is my own and that any work performed by anyone other than myself, has been appropriately credited, referenced and acknowledged.

Antonia Rotolo

Copyright Declaration

The copyright of this thesis rests with the author and is made available under a Creative Commons Attribution Non-Commercial No Derivatives licence. Researchers are free to copy, distribute or transmit the thesis on the condition that they attribute it, that they do not use it for commercial purposes and that they do not alter, transform or build upon it. For any reuse or redistribution, researchers must make clear to others the licence term of this work.

Acknowledgements

I would like to express my deep gratitude to Professor Anastasios Karadimitris, my research supervisor, for his inspiring guidance and influential mentorship, that led me through a greater awareness of my enthusiasm for science, while maturing the idea of my professional self.

My sincere thanks go to Dr John Maher, for his advice and assistance throughout my doctoral studies, and Professor Irene Roberts, for her invaluable time and precious suggestions.

My grateful thanks are extended to Professor Jane Apperley and all clinical and research staff of the Department of Haematology at Hammersmith Hospital, for giving me the fantastic opportunity to work in such a highly stimulating environment.

To my friends, Valentina, Andi and Chiara, I owe a very big thank you. They have been my greatest comfort during stressful and hard times. Always there, to encourage, help and support me with their extraordinary patience, genuine advice and optimistic attitude. Thank you, Valentina, for always believing in my research potential and following my progress, day-by-day, enhancing my commitment to pursue an academic career. Thank you, Andi, for all your intellectual inputs and guidance through uncertain moments, that strengthen even more my motivation and excitement for science. Thank you, Chiara, for reminding me that nothing worthwhile comes easily and no one can discourage us or tell us that we can't do it.

A bear, virtual hug to Katerina and Kyriaki, amazing colleagues and loveable friends, who were there with me during my very first important achievements, making them possible with their contagious enthusiasm.

Jacob and Martha, Monika and Bryant and all people of the ‘fourth floor’ will remain in my memory and heart, as nice friends and fantastic colleagues, with their unique power of making long days sweeter and happier…

My thesis is dedicated to my parents and sister. They have never been far. They have been always next to me, believing in me, ready to share good and bad times. They have been patiently reminding me to have perseverance and above all confidence in myself, never fearing difficult moments, because the best comes from them. Nothing would have been possible without them. GRAZIE, con tutto il cuore...

It has been an exciting journey. Looking forward to the next adventure…

'Think of the future that awaits you. Think of what you can do.'

Rita Levi Montalcini

Abstract

Anti-CD19 chimeric antigen receptor T cell (CAR19-T) immunotherapy has shown curative potential in B cell malignancies. However, clinical remissions in relapsed/refractory $CD19^+$ lymphomas and lymphoproliferative disorders are often short-lived, with therapeutic benefit for less than half of patients, highlighting the need for more effective CAR-based strategies.

iNKT cells are rare but powerful immunoregulatory and cytotoxic T lymphocytes, playing a pivotal anti-tumour role. They are restricted by CD1d, a non-polymorphic, glycolipid-presenting HLA I-like molecule, expressed on malignant $CD19^+$ B cells in mantle cell lymphoma (MCL) and marginal zone lymphoma (MZL) cells, while in up to 50% of patients with chronic lymphocytic leukaemia (CLL) CD1d expression is very low or negative.

I tested the hypotheses that a) bi-specific CAR19-iNKT cells, targeting simultaneously CD19 and CD1d, via the CD19-specific CAR and their natural invariant TCR respectively, would be more effective than CAR19-T cells against $CD19^+CD1d^+$ B cell malignancies and b) transcriptional enhancement of CD1d expression would increase the CAR19-iNKT cytotoxic effect, including against CLL cells.

I established and optimized a novel, highly efficient protocol for manufacturing clinical scale CAR19-iNKT cells. *In vitro* validation demonstrated that CAR19-iNKT cells are CD19-specific, retain their natural CD1d-restricted reactivity and exert additive dual-specific cytotoxicity against $CD1d^+CD19^+$ targets. Compared to same-donor CAR19-T, CAR19-iNKT cells display a significantly higher expandability and proliferative potential, they are equally or more effective in killing $CD19^+CD1d^+$ lymphoid cell lines and consistently more effective against primary MCL, MZL and CLL cells.

Notably, I found that in $CD1d^{low/-}$ primary CLL cells, surface CD1d expression can be restored by clinically relevant concentrations of all-trans retinoic acid (ATRA) and, in line with my

hypothesis, CAR19-iNKT but not CAR19T cells displayed higher cytotoxic activity against ATRA-treated CLL cells.

Finally, in an NSG xenograft model of lymphoma, CAR19-iNKT cell immunotherapy led to a significantly improved overall survival, with earlier, more profound and sustained complete responses, which resulted in a significantly improved tumour-free survival as well as eradication of CNS lymphoma.

I conclude that CAR19-iNKT are more effective than CAR19-T cells against $CD1d^{+}CD19^{+}$ B cell malignancies *in vitro* and *in vivo*. This, together with the previously demonstrated ability of third donor-derived iNKT cells to protect from acute Graft-versus-Host Disease (aGVHD), raise the prospect of developing a more effective '*off-the-shelf*' CAR19-iNKT immunotherapy for lymphomas. Furthermore, the finding that ATRA-mediated restoration of CD1d expression enhances the anti-lymphoma effect of CAR19-iNKT immunotherapy against CD1d low/negative tumour cells *in vitro* suggests that CAR-iNKT cells, in combination with transcriptional/epigenetic modulation of CD1d, may represent a highly efficient platform for CAR-based immunotherapy also for other CD1d-negative disorders.

Table of Contents

1 Introduction 21

1.1 Background 21

1.1.1 Non-Hodgkin lymphoma: an unmet clinical need 21

1.1.2 CAR immunotherapy 22

1.1.3 iNKT cells 31

1.2 Hypothesis 35

1.3 Aims 36

2 Materials & Methods 37

2.1 CD19-specific CARs 37

2.2 CD1d and CD19 antigens 42

2.3 Firefly luciferase 44

2.4 Primary Cells 45

2.4.1 iNKT cell isolation 45

2.4.2 Primary cell medium and culture 46

2.5 Cell lines 47

2.6 Pharmacological agents 48

2.7 Retroviral and lentiviral production and cell transduction 48

2.7.1 Virus production 48

2.7.2 Cell transduction 51

2.8 Antibodies and intracellular staining 52

2.9 Cytokine release assay 53

2.10 Proliferation assay 54

2.11 *In vitro* real-time monitoring of CAR cell cytotoxic activity 54

2.12 Cytotoxicity assay 55

2.13 Gene expression analysis by Real-Time PCR 56

2.14 Chromatin immunoprecipitation assays 57

2.14.1 Chromatin preparation 57

2.14.2 Immunoprecipitation and DNA extraction 57

2.14.3 Real time polymerase chain reaction 58

2.14.4 ChIP primers for QRT-PCR 58

2.15 Systemic xenograft tumour model 59

2.16 Bioluminescence imaging (BLI) 59
2.17 Magnetic resonance imaging (MRI), diffusion-weighted imaging (DWI) and MR spectroscopy (MRS) 60
2.18 Immunohistochemistry 61
2.19 Statistics 62
2.19.1 Sample size 62
2.19.2 Replicates 62
2.19.3 In vivo randomisation 62
2.19.4 Statistical analysis 62
3 Development and optimization of protocol for manufacturing of clinical scale CAR-iNKT cells 65
3.1 Introduction 65
3.2 Generation of CAR19-T cells 66
3.2.1 Expression of CAR19 in primary human T lymphocytes – standard procedure 66
3.2.2 Expansion of CAR19-T cells from transduced T cells according to standard procedure 68
3.2.3 Selection of CAR19-T cells 69
3.3 Generation of CAR19-iNKT cells 71
3.3.1 Protocol 1 71
3.3.2 Protocol 2 73
3.3.3 Protocol 3 75
3.3.4 Protocol 4 76
3.3.5 Protocol 5 80
3.4 'Scale-up steps' for clinical scale manufacturing of CAR19-iNKT cells 86
3.5 Phenotypic and functional characterisation of CAR19-iNKT cells 88
3.5.1 Preservation of $CD4^-$ iNKT cell subset 88
3.5.2 CAR-iNKT cells display a Th1-like, poly-functional cytokine profile 90
3.5.3 Low PD-1 expression by CAR19-iNKT cells 94
3.6 Discussion 100
4 *In vitro* validation: dual specificity and cytotoxic activity of CAR19-iNKT cells 105
4.1 Introduction 105
4.2 Optimisation of a flow cytometry based cytotoxicity assay 106

4.3 Characterization of CAR19-iNKT cell reactivity 107
4.3.1 Cooperative killing of CD1d^{+}CD19^{+} targets by dual specific CAR19-iNKT cells 107
4.3.2 Specific killing of B cell lymphoma cell lines by CAR19-iNKT cells 109
4.3.3 Enhanced reactivity of CAR19-iNKT cells against B cell lymphoma cell lines 111
4.3.4 Sustained proliferative response coupled to enhanced killing by CAR19-iNKT cells 117
4.3.5 Enhanced reactivity of CAR19-iNKT cells against primary B cell lymphoma cells 125
4.4 Discussion 131
5 Transcriptional and epigenetic basis for enhancing CAR-iNKT cell reactivity 139
5.1 Introduction 139
5.2 CAR19-iNKT cells effectively kill B-CLL cells *in vitro* 142
5.3 Molecular basis of CD1d expression in B-CLL cells 146
5.4 Discussion 149
6 *In vivo* validation: enhanced anti-tumour activity of CAR19-iNKT cells 153
6.1 Introduction 153
6.2 Establishment of luciferase-expressing C1R-CD1d cells 154
6.3 Luc^{+}C1R-CD1d cells are capable of xenografting NSG mice 156
6.4 Single infusions of CAR19-iNKT cells are feasible and well tolerated in NSG xenografts. 159
6.5 Enhanced anti-lymphoma activity of CAR19-iNKT cell *in vivo* 165
6.6 CAR19-iNKT cell eradicate brain tumour 170
6.7 CAR19-iNKT cell second complete responses of lymphoma relapse 178
6.8 Discussion 181
7 Conclusions & Perspectives 187
8 References 193

List of Figures

Figure 1-1 CAR structure and immunotherapy 23

Figure 1-2 CAR-T cell manufacturing 24

Figure 1-3 Drawbacks and current areas of optimisation of CAR-T immunotherapy 27

Figure 1-4 Advantages of CAR19-iNKT cells over CAR19-T cells 36

Figure 2-1 Generation of CAR19 constructs with reduced scaffold by Gibson cloning approach 38

Figure 2-2 Insert sequences for the generation of CAR19 constructs with reduced-size scaffold 39

Figure 2-3 DNA sequencing of CAR19 constructs with reduced scaffold 40

Figure 2-4 2nd and 3rd generation CD19-specific CARs with reduced-size scaffold. 41

Figure 2-5 Generation of SFG.CD1d and SFG.CD1d.2A.dCD19 constructs by Gibson approach 42

Figure 2-6 Insert sequences for SFG.CD1d and SFG.CD1d.2A.dCD19 constructs 43

Figure 2-7 Cloning confirmation of SFG.CD1d and SFG.CD1d.2A.dCD19 constructs 44

Figure 2-8 Flow cytometry based method for viral vector titration 51

Figure 2-9 Flow cytometry-based cytotoxicity assay - Gating strategy 56

Figure 3-1 Assessment of CAR19-T cells by flow cytometry 67

Figure 3-2 CAR19-T cell percentage and fold change over 3 weeks 68

Figure 3-3 Impact of different expansion methods on CAR19-T cells 68

Figure 3-4 CAR19-T cell selection. 69

Figure 3-5 CAR19-T cell expansion post selection 70

Figure 3-6 CAR19-iNKT cell engineering – protocols 1-3 76

Figure 3-7 Low-purity iNKT cell expansion with aCD3/CD28 beads 78

Figure 3-8 Expansion of upfront selected iNKT cells with aCD3/CD28 beads 79

Figure 3-9 Viability of CAR19-transduced iNKT cells engineered according to protocol 4 80

Figure 3-10 CAR19-iNKT cell engineering – protocol 4 82

Figure 3-11 CAR19-iNKT cell engineering – protocol 5 83

Figure 3-12 CAR19-iNKT engineering protocols 84

Figure 3-13 2nd and 3rd generation CAR19-iNKT and CAR19-T cells – protocol 5 85

Figure 3-14 Lymphoma patient-derived CAR19-iNKT cells 86

Figure 3-15 CAR19-iNKT expandability and clinical scale expansion 87

Figure 3-16 Timeline of optimised procedure for manufacturing of large scale CAR19-iNKT cells 88

Figure 3-17 CD4^{-} CAR19-iNKT cells – protocol 5 compared to baseline 89

Figure 3-18 CD4^{-} CAR19-iNKT cells – protocol 5 compared to protocol 2 89

Figure 3-19 CAR19-iNKT intracellular cytokine profile 91

Figure 3-20 CAR19 -iNKT vs -T intracellular cytokine profile – resting cells 92

Figure 3-21 Polyfunctional CAR19 -iNKT vs -T cells 93

Figure 3-22 CAR19 -iNKT vs -T cytokine release assay 94
Figure 3-23 End-of-manufacturing PD-1^{+} CAR19-cells 95
Figure 3-24 PD-1^{+} CAR19-cells after 2 restimulations 96
Figure 3-25 PD-1^{+} CAR19-cells after 3 restimulations 97
Figure 3-26 PD-1^{+} CAR19-cells in resting phase after 3 restimulations 98
Figure 3-27 PD-1^{+} CAR19-iNKT vs -T cells after weekly restimulations 99
Figure 3-28 CAR19 -iNKT vs -T cell expandability after weekly restimulations 99
Figure 4-1 Validation of flow-cytometry-based cytotoxicity assay 107
Figure 4-2 CD1d^{+} and/or CD19^{+} K562 cells 108
Figure 4-3 CAR19-iNKT cell cytotoxic activity against CD1d$^{+/-}$ and/or CD19 $^{+/-}$ K562 targets 109
Figure 4-4 CAR19-iNKT cell cytotoxic activity against CD19^{low} and CD19^{high} targets 110
Figure 4-5 CAR19-iNKT cell cytotoxic activity against CD1d^{low} and CD1d^{high} targets 110
Figure 4-6 Cytotoxicity of 2nd generation CAR19-iNKT vs -T cells at E/T of 1 111
Figure 4-7 Cytotoxicity of 3rd generation CAR19-iNKT vs -T cells at E/T 2.5 112
Figure 4-8 Cytotoxicity of 2nd and 3rd generation CAR19-iNKT vs -T cells at E/T of 10, 5, 2.5, 1.25 113
Figure 4-9 Effector-target conjugates analysis 114
Figure 4-10 Conjugate formation and associated activation-induced effector-cell death 115
Figure 4-11 CD4^{+} and CD4^{-} conjugates 116
Figure 4-12 CD4^{+} vs CD4^{-} CAR19-iNKT cells cytotoxicity against B cell targets 117
Figure 4-13 Real-time monitoring and analysis of proliferation of CAR19-iNKT vs CAR19-T cells 118
Figure 4-14 CAR19-iNKT vs -T cells cell clustering and confluency analysis by IncucyteZOOM 120
Figure 4-15 Visualization of third CAR19-T cell proliferation by IncucyteZOOM 121
Figure 4-16 Control wells for cell clustering and confluency analysis by IncucyteZOOM 122
Figure 4-17 Real-time monitoring of proliferation and cytotoxicity of CAR19-iNKT vs CAR19-T cells 124
Figure 4-18 CD1d surface expression on primary B cell lymphoma cells 125
Figure 4-19 CAR19-iNKTvs CAR19-T vs iNKT cell cytotoxicity against primary B cell lymphoma cells 126
Figure 4-20 Gating strategy of FCCA with lymphoma cell targets 127
Figure 4-21 Primary B cell lymphoma cell death analysis by FCCA 128
Figure 4-22 CD1d expression on primary monocytes 129
Figure 4-23 Monocyte specific cell death in lymphoma patients derived PBMCs 130
Figure 4-24 Flow cytometry analysis of MZL-derived PBMCs 135
Figure 5-1 Transcriptional regulation of *CD1D* gene 140
Figure 5-2 In silico analysis of the CD1D promoter in B-LCLs and murine GC B cells. 141
Figure 5-3 CD1d surface expression on CLL malignant and normal B cells 142
Figure 5-4 CAR19-iNKT cell cytotoxicity against CLL cells 143
Figure 5-5 Effect of ATRA treatment on CD1d expression and viability in B-CLL cells 144

Figure 5-6 CAR19-iNKT vs CAR19-T cytotoxicity against ATRA-treated B-CLL cells..... 145
Figure 5-7 CD1d expression in CLL cells pre and post treatment with ATRA..... 147
Figure 5-8 ChIP-qPCR assay in baseline B-CLL cells 148
Figure 6-1 Generation and *in vitro* validation of luciferase expressing C1R-CD1d cell line 155
Figure 6-2 *In vivo* pilot experiment 1 156
Figure 6-3 *In vivo* C1R-CD1d bioluminescence titration 157
Figure 6-4 *In vivo* tumour burden monitoring 158
Figure 6-5 Weight chart and terminal BLI scans 158
Figure 6-6 *In vivo* pilot 2 experiment 160
Figure 6-7 Systemic infiltration by C1R-CD1d cells 160
Figure 6-8 IHC analysis of xenograft tissues 161
Figure 6-9 Tumour burden monitoring in pilot 2 experiment 162
Figure 6-10 Feasibility study for preclinical *in vivo* investigation of CAR19-iNKT cell immunotherapy for B lymphoma 163
Figure 6-11 CD19 and CD1d expression on xenograft-derived C1R-CD1d cells 163
Figure 6-12 Histological analysis of GvHD target organs in CAR19-iNKT-treated xenografts 164
Figure 6-13 Layout for characterisation of *in vivo* anti-lymphoma activity of CAR19-iNKT cells 165
Figure 6-14 Skin GvHD 166
Figure 6-15 Anti-tumour activity of CAR19-iNKT cells in a systemic B-lymphoma xenograft model 167
Figure 6-16 Overall and tumour-free survival according to experiment..... 168
Figure 6-17 Early response to treatment..... 169
Figure 6-18 Mouse MRI brain sections and macroscopic anatomy 170
Figure 6-19 Representative MRI images of brain tumour 170
Figure 6-20 Representative MRI monitoring of brain tumour..... 171
Figure 6-21 Representative MR Spectroscopy of sellar mass 173
Figure 6-22 Representative DWI analysis of low-burden brain disease..... 175
Figure 6-23 Correlation of BLI images with immunohistochemistry..... 176
Figure 6-24 Head tumour burden as assessed by BLI..... 177
Figure 6-25 Tumour burden profiles 178
Figure 6-26 Second remissions in CAR19-iNKT mice 179
Figure 6-27 Absence of CAR19-iNKT related neurotoxicity 180
Figure 7-1 CAR19-iNKT cell overview 192

List of Tables

Table 2-1 Primers to amplify inserts for the generation of reduced-size scaffold CAR19 constructs..... 39

Table 2-2 Primers for the generation of SFG.CD1d and SFG.CD1d.2A.dCD19 retroviral constructs..... 43

Table 2-3 Plasmid mixture for virus production 49

Table 2-4 Calcium phosphate methods for virus production 49

Table 2-5 List of reagents used for virus production..... 50

Table 3-1 CAR19-T cell transduction efficiency according to standard procedure 67

Table 3-2 CAR19-T cell selection 69

Table-3-3 Upfront expansion of iNKT cells from mononuclear cells in the presence of αGalCer 72

Table 3-4 Expansion of upfront selected iNKT cells 74

Table 3-5 CAR19-iNKT cell expansion with aCD3/CD28 beads 77

Table 3-6 CAR19-iNKT engineering protocols 84

Table 3-7 Overview of optimisation steps towards CAR19-iNKT cell manufacturing protocol..... 102

Table 6-1 MRI study – all animals 174

Table 6-2 Head tumour burden..... 177

List of Abbreviations

ab	Antibody
aCD3/CD28	Anti-CD3/CD28 Coated Beads
ACT	Adoptive Cell Therapy
aGVHD	Acute Graft-Versus-Host Disease
AICD	Activation-Induced Cell Death
ALL	Acute Lymphoblastic Leukaemia
Allo-HSCT	Allogeneic Haematopoietic SCT
APC	Antigen Presenting Cell
ATRA	All-Trans Retinoic Acid
BBB	Blood-Brain Barrier
BLI	Bioluminescent Imaging
bp	Base Pair
BSA	Bovine Serum Albumin
CAIX	Carbonic Anhydrase 9
CAR	Chimeric Antigen Receptor
CAR19	CD19-Specific CAR
CB	Cord Blood
CBMNC	CB Mononuclear Cells
CBS	Centre For Biological Service
CEA	Carcinoembryonic Antigen
ChIP	Chromatin Immunoprecipitation
Cho	Choline
CLL	Chronic Lymphocytic Leukaemia
CNR	Contrast-To-Noise Ratio
CNS	Central Nervous System
Cr	Creatine
CR	Complete Remission
CRA	Chromium-51 Release Assay
CRS	Cytokine Release Syndrome
-CSF	-Colony Stimulating Factor
CSF	Cerebro-Spinal Fluid
DC	Dendritic Cell
DLBCL	Diffuse Large B Cell Lymphoma
DN	Double Negative
ESC	Embrionic Stem Cells
Exp	Experiment
EZH2	Enhancer Of Zeste Homolog 2
FACS	Flow Cytometry Activated Cell Sorting
FCCA	Flow Cytometry-Based Cytotoxicity Assay
EGFR	Epidermal Growth Factor Receptor
FDA	Food And Drug Administration
FL	Follicular Lymphoma
FOV	Field Of View
GC	Germinal Centre
GM-CSF	Granulocyte-Monocyte-CSF
GVL	Graft-Versus-Leukaemia
H3K4me3	Histone 3 Lysine 4 Trimethylation
H3K27me3	Histone 3 Lysine 27 Trimethylation
HSV-TK	Herpes Simplex Virus Tyrosine Kinase
iAPC	Irradiated Antigen Presenting Cell
i-autoPBMC	Irradiated Autologous PBMC
iCAR	Inhibiting CAR
iCasp9	Inducible Caspase 9
ID	Donor Identifier
IFN-γ	Interferon-Gamma
IL	Interleukin
IL-6R	Interleukin-6 Receptor
iNKT	Invariant Natural Killer T Cell
ip	Intraperitoneal
Itx	Immunotherapy
Iv	Intravenous
LAK	Lymphokine Activated Killer
LAph	Lymphapheresis
LPD	Lymphoproliferative Disorder
LTE	Long Echo Time
moAb	Monoclonal Antibody
MACS	Magnetic Activated Cell Sorting
MCL	Mantle Cell Lymphoma
MHC	Major Histocompatibility Complex
MIF	Mean Image Fluorescence
MNC	Mononuclear Cells
MOI	Multiplicity Of Infection

MZL	Marginal Zone Lymphoma
NHL	Non-Hodgkin Lymphoma
NK	Natural Killer
NOD	Non-Obese Diabetes
OS	Overall Survival
PB	Peripheral Blood
PBMC	Peripheral Blood Mononuclear Cells
PBS	Phosphate Buffered Saline
PcG	Polycomb Group
PCM	Primary Cell Medium
PCR	Polymerase Chain Reaction
PD-1	Programmed Death-1
PD-L1	PD-1 Ligand 1
RARE	Retinoic Acid Receptor Element
RARα	Retinoic Acid Receptor Alpha
ROI	Region Of Interest
RQ-PCR	Real-Time Quantitative PCR
rr	Relapsed/Refractory
SCT	Stem Cell Transplant
SEM	Standard Error Mean
sr	Steradian
SLL	Small Lymphocytic Leukaemia
STE	Short Echo Time
TALEN	Transcription Activator-Like Effector Nucleases
TFS	Tumour-Free Survival
Th	T Helper Lymphocyte
TLI	Total Lymphoid Irradiation
TNC	Total Nucleated Cells
TNF-α	Tumour Necrosis Factor Alpha
TRAC	T Cell Receptor Alpha Constant
TrxG	Trithorax Group
TSS	Transcription Starting Site
ULA	Ultra-Low Attachment
vs	versus
vWF	Von-Willebrand Factor
Xeno-GvHD	Xenogeneic Gvhd
ZFN	Zinc Finger Nuclease
αGalCer	Alpha-Galactosylceramide
γc	Gamma Chain

1 Introduction

1.1 Background

1.1.1 Non-Hodgkin lymphoma: an unmet clinical need

Non-Hodgkin lymphomas (NHL) are a heterogeneous group of diseases comprising diverse B- and T-cell-derived malignancies. Collectively NHL account for approximately 4% of all cancers in the UK[1]. In 2015, an estimated 414,772 patients worldwide were diagnosed with NHL[2] and 215,074 patients died as a result of the disease[3]. The incidence and mortality trend are increasing, with 2020 projections of 465,000[4] and 240,000[5] respectively.

Eighty five per cent of NHL originate from the B-cell lineage and therefore express B-lymphocyte differentiation antigens, including CD20 and CD19[6]. Their clinical course may be either indolent or aggressive. Aggressive subtypes include mantle-cell lymphoma (MCL), which accounts for up to 10% of all lymphomas, presents in advanced stage and lacks durable responses to standard chemo-immunotherapy[7], with median survival of 5 years in young and 3 years in older patients[8]. Indolent subtypes include marginal zone lymphoma (MZL), small-cell lymphocytic lymphoma/chronic lymphocytic leukaemia (SLL/CLL)[9]. MZL comprises approximately 10% of all NHL[10]. Advanced disease is generally incurable, with most patients experiencing serial relapses[10]. In up to 30% of cases the clinical course becomes aggressive with less than 4 years median survival[11]. CLL is the most prevalent leukaemia of adults in the West, with a median age at diagnosis of 70 years[12]. Where indicated, first line chemo-immunotherapy can induce remissions in the majority of patients with this largely incurable disease, but the prognosis remains poor in the case of relapsed/refractory disease[13].

There is an unmet clinical need for new therapies for lymphomas such as MCL, MZL and for chronic lymphoproliferative disorders in adults and in particular CLL. Allogeneic haematopoietic stem cell transplantation (allo-HSCT) could be curative, but it is associated with

considerable morbidity and transplant-related mortality and only few patients are eligible. Novel targeted therapies, such as the B cell receptor kinase inhibitors idelalisib[14] and ibrutinib[10,15,16], have yielded encouraging responses, including higher complete remission (CR) rates, which are not durable, underpinning their lack of curative potential. In contrast, adoptive immunotherapy with CD19-redirected T lymphocytes by means of chimeric antigen receptor (CAR) transgenes have proved the ability to induce deep, long-lasting remissions and possibly cures in patients where all previous lines of treatment had failed, thus dramatically changing the therapeutic perspective of B cell malignancies.

1.1.2 CAR immunotherapy

1.1.2.1 CAR structure

CAR immunotherapy represents one of the most significant breakthroughs for the treatment of B cell neoplasms[17]. It entails transfer of a CAR transgene into T lymphocytes to enable otherwise non-tumour specific T cells to specifically recognize and fight cancer cells[18,19].

CARs are synthetic molecules consisting of an antibody-derived antigen-binding moiety, recognizing a tumour-associated surface protein, coupled with a TCR complex signalling domain (**Figure 1-1**). They have a tetramodular structure characterized by: 1) an extracellular binding region, mostly derived from monoclonal antibodies (moAbs) and less frequently from ligand analogues, peptides, receptors and nanobodies; 2) an extracellular spacer/hinge sequence which is borrowed from the Ig, CD4, CD8 or CD28 molecules and is a key factor in determining the distance between effectors and targets at the immunological synapse as well as the outcome of CAR-T cell interactions with cancer and bystander cells; 3) a transmembrane sequence, which may impact on the final CAR-T cell reactivity, and 4) an activating CD3ζ or FcRγ-derived endodomain. This is the simplest, 1st generation structure of a CAR prototype. Further 2nd and 3rd generation CARs incorporate in the endodomain one or two co-stimulatory components respectively that were developed to promote prolonged and sustained activation of the CAR-T cells while compensating for the lack of co-stimulatory signals on malignant cells. Different co-stimulatory domains have been tested and associated with distinct T cell functional profiles, thus providing the opportunity for modulating and shaping the ensuing

immune response. For instance, CD28 induces higher levels of IL-2 and TNF-α, ICOS promotes greater cytotoxicity while 4-1BB enhances survival of CAR-T cells[20].

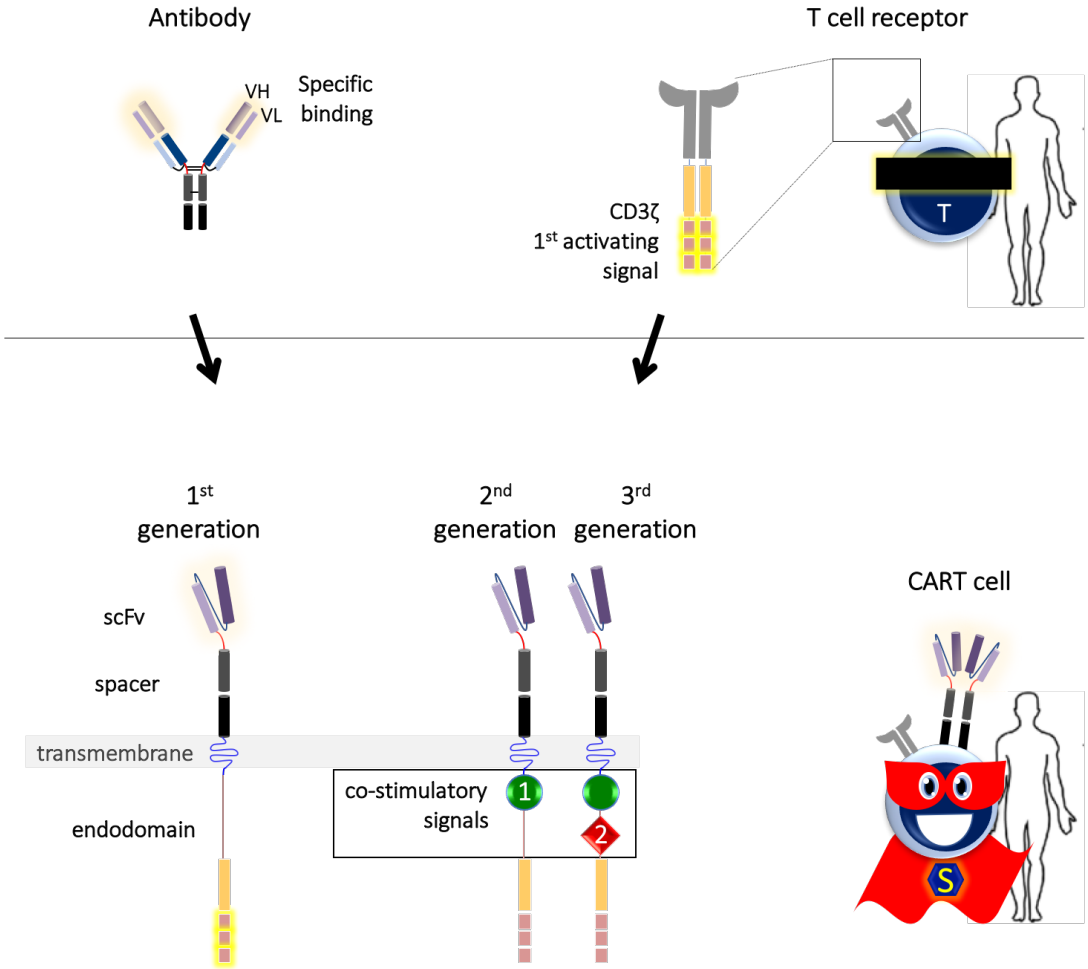


Figure 1-1 CAR structure and immunotherapy
A 1st generation CAR is a synthetic protein derived from the fusion of the antigen-recognizing domains of a moAb (in the form of a single-chain variable fragment) and the intracellular signalling domain of the T cell receptor CD3ζ chain, used to genetically modify autologous T lymphocytes otherwise unresponsive to cancer cells (top). 2nd and 3rd generation CARs also include co-stimulatory domains (typically 4-1BB or CD28) which enhance the final level of activation of the CAR-engineered effectors (*bottom*).

1.1.2.2 CAR-T cell manufacturing

Figure 1-2 summarizes the main steps for CAR-T cell manufacturing. Briefly, (1) patients undergo leukapheresis, aiming to obtain >10^7 $CD3^+$ T cells suitable for CAR-engineering, followed by (2) T cell activation, generally by means of anti-CD3/CD28 coated (aCD3/CD28) beads. Next, (3) activated T cells are incubated with viral supernatants carrying the CAR-

transgene vector and expanded up to clinical scale numbers (typically over 10-15 days). At the end of the expansion, (4) the beads are removed, the cell culture is concentrated and the CAR-cell product is either immediately reinfused or cryopreserved until usage. Variations to the above procedure may include differences in: 1) starting material (peripheral blood versus (vs) leukapheresis); 2) methods of delivering the CAR transgene (e.g. usually by viral transduction systems but also via a sleeping beauty transposon system or by mRNA transfection); 3) T cell activation prior to CAR engineering (e.g. use of artificial antigen presenting cells (APC) or anti-CD3 moAb plus IL-2 instead of aCD3/CD28 beads); 4) cell culture conditions (e.g. G-Rex static systems in case of initial low seeding densities vs bioreactors with rocking platform). Development of fully automated procedures for CAR-T cell manufacturing could potentially be critical to sustain the increase in demand for CAR immunotherapy.

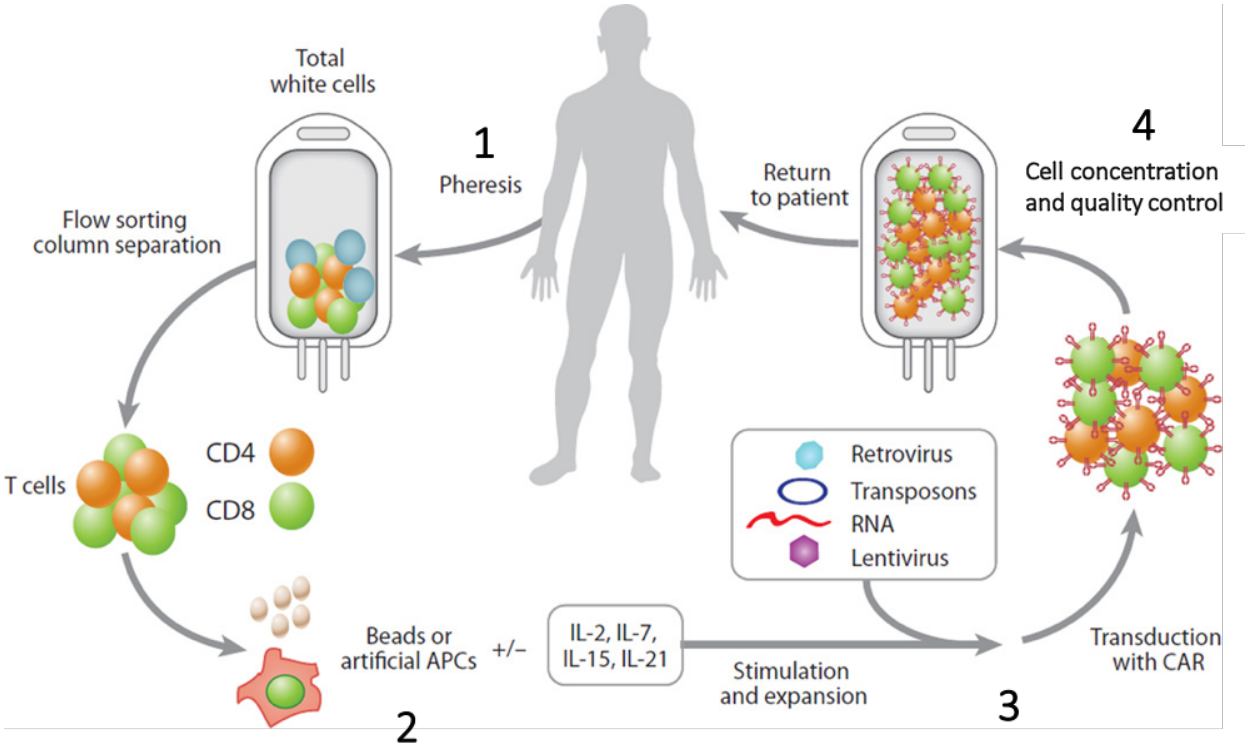


Figure 1-2 CAR-T cell manufacturing

Peripheral blood mononuclear cells collected by lymphapheresis (1) are activated (2) and expanded *ex vivo* prior to transduction with a retroviral or lentiviral vector (3) to express the CAR molecule before infusion into the patient (4) (adapted from Barrett DM et al. Ann Rev Med 2014;65:333, PMID: 24274181[21]).

1.1.2.3 CAR-T cell immunotherapy

The first clinical experiences with CAR-T immunotherapy were reported in the late '90s. First generation CAR-T cells were initially investigated in patients with solid tumours, targeting colorectal carcinoma (TAG72 and carcinoembryonic antigen, CEA), breast cancer (CEA), ovarian cancer (folate receptor-α), renal cell carcinoma (carboxy anhydrase IX, CAIX) and neuroblastoma (L1 cell adhesion molecule and GD2 ganglioside). Minimal to no clinical benefit was reported, that was attributed to poor *in vivo* activation and rapid immune-mediated clearance of CAR-T cells[22]. Furthermore, grade 3 and 4 adverse events were observed, including unexpected on-target off-tumour toxicity due to unanticipated expression of the CAR-target in different organs, e.g. CAIX-driven attack of bile duct epithelial cells and subsequent cholangitis in a renal cell carcinoma patient treated with CAIX-specific CAR-T cells[23]. Nevertheless, these first-in-man experiences turned to be of great relevance since they proved that CAR-T cells are capable of trafficking to the tumour sites and reacting against malignant cells. Subsequently, CD20 and CD19 -specific CAR-T cells were used in a cohort of haematological patients with relapsed/refractory B cell lymphoma[24]. All patients received lymphodepleting chemotherapy and some of them concomitant IL-2[25]. Compared to solid tumours trials, there were no CAR-T-related adverse events and no anti-CAR immune responses. Although clinical responses remained disappointing, these proof-of-principle studies represent a milestone in the history of CAR immunotherapy and provided the basis for further clinical development and optimization of CAR technology. Importantly, they suggested a link between *in vivo* CAR-T cell persistence and sustained clinical responses. Hence, to improve CAR-T cell survival, 2nd generation CARs were developed.

2nd generation CD19-specific CAR-T (CAR19-T) cells have led to impressive, unprecedented results in the treatment of B-cell acute lymphoblastic leukaemia (B-ALL), with up to 90% complete remissions (CR) reported in refractory B-ALL patients and durable molecular responses[26-33]. Sustained CR after CAR19-T cell therapy have been described also in a subset of heavily pre-treated patients with chemo-refractory CLL, diffuse large-B cell lymphoma (DLBCL) and follicular lymphoma (FL), further corroborating the emerging clinical evidence of a curative potential of CAR technology[34-39]. Yet, response rates in CLL and NHLs are generally lower compared to B-ALL patients[40], with approximately 50% or less response rates in

lymphoma/chronic lymphoproliferative disorders vs 90% in B-ALL. Moreover, very preliminary experience in MCL and MZL patients (reviewed in Brudno, J.N. & Kochenderfer, J.N. *Nat Rev Clin Onc*, 2017[41]) suggests that autologous stem cell transplant[42] and/or CR at the time of immunotherapy[43] may be required to achieve clinically relevant responses. The reasons for the differences remain to be determined, but may include differences in CAR-T cell access to tumour antigen and/or immune suppression in the tumour microenvironment in each disease.

1.1.2.4 Unsolved issues related to CART immunotherapy

CAR-immunotherapy has to address at least three main challenges: i) better clinical outcomes; ii) safer profile; iii) broader applicability[44].

1.1.2.4.1 Efficacy of CAR immunotherapy

Several strategies are under investigation to enhance the therapeutic efficacy of CAR T cells against lymphoma. These include:

1) ***multi-targeting***, i.e. targeting more than one B-cell antigens (e.g., CD20 and CD22) by means of either multi-specific CARs (e.g. tandem CARs), microcircuits or mixtures of CAR T cells endowed with different specificities. This strategy is required to prevent disease relapse observed in up to 30% of CAR19-T cell treated patients and caused by loss of relevant CD19-epitopes leading to tumour escape;

2) ***targeting the tumour microenvironment***, either directly, by using CAR effectors capable of reacting against both malignant and neighbouring immunosuppressive cells[45], or indirectly, by increasing the actual effector-to-target ratio at the tumour site while 'awakening' endogenous anergic immune cells. Such multi-tasking CAR-T cells, namely '*armored CAR cells*' or '*TRUCKs'*, may co-express chemokines, homing receptors and costimulatory ligands, they release homeostatic cytokines and can even be engineered to secrete scFv derived from therapeutic checkpoint-blocking moAb [46];

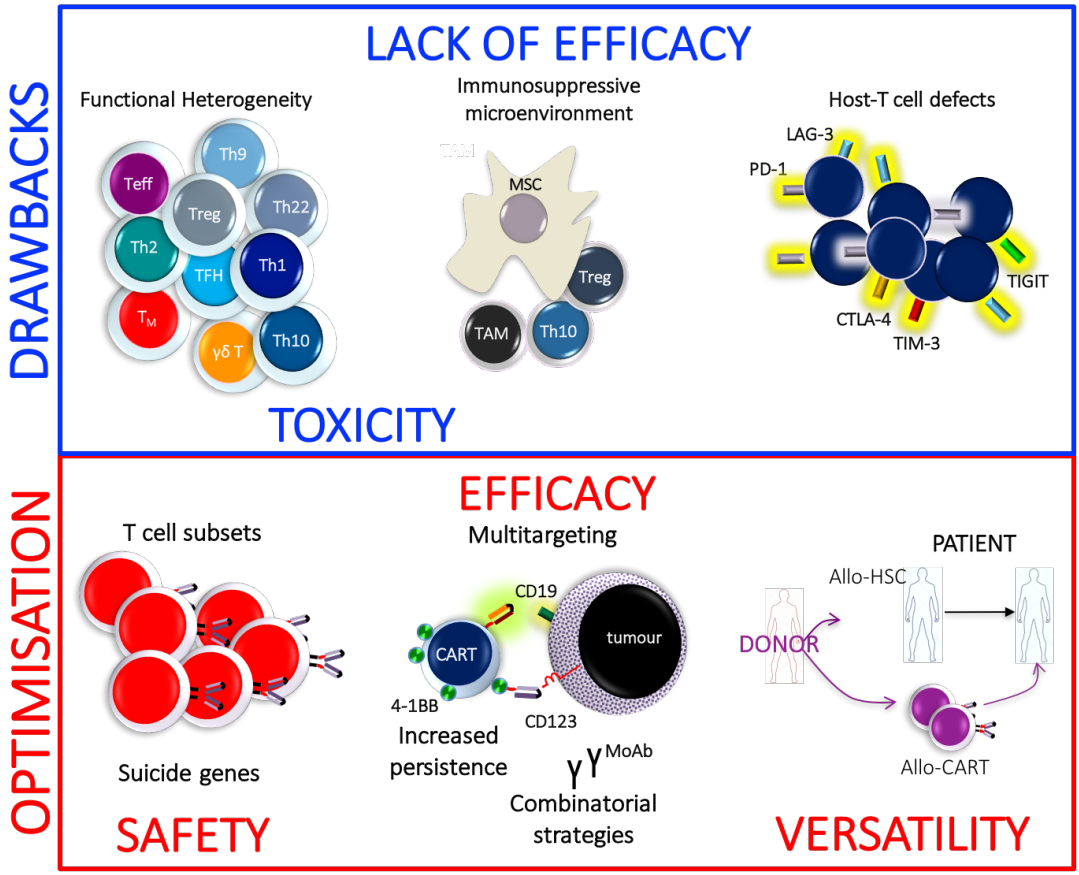


Figure 1-3 Drawbacks and current areas of optimisation of CAR-T immunotherapy
CAR-T cells fail and have unacceptable toxicity in a number of cases, which impact on the high social and financial costs of CAR-immunotherpay and limit faster and broader applicability. Improving efficacy, safety and versatility represent the three main challenges for further clinical development of CAR-T cells.

3) ***increasing CAR potency***, by using different co-stimulatory domains or transmembrane and hinge regions to ensure a more robust, sustained activation and longer persistence;

4) ***improving CAR expression***, by inserting anti-CD19 CARs into specific genetic loci, e.g. CRISPR–Cas9-mediated insertion of CAR19 in the T-cell receptor alpha constant region (TRAC) gene, to promote higher and more stable expression of the CAR construct over time[47];

5) ***CAR-engineering of selected T-cell subpopulations*** *(e.g. $CD4^+$, $CD8^+$ T cells, etc.)* with more homogenous (and predictable) functional profile and/or enhanced anti-tumour activity[40,44,48-51].

6) ***combinatorial approaches***, by combining CAR-T-immunotherapy with small molecules and moAb-based therapies such as Bruton tyrosine kinase inhibitors and inhibitors of immune checkpoint pathways (e.g., programmed death 1 [PD-1] protein or its ligand [PD-L1]). However, such approaches would be expected to be associated with higher risk of severe toxicity which may limit their clinical development [52].

1.1.2.4.2 CAR immunotherapy safety

CAR-T cells are '*living drugs'* that can persist even more than 10 years *in* vivo[53]. As a result, their therapeutic effects as well as related toxicities may manifest far beyond those of conventional pharmaceuticals. Adverse events may be immediate or delayed, mild to severe, and/or persist for the duration of the CAR-T cell lifespan.

To date, the most prevalent side effect is the onset of an overwhelming and potentially life-threatening immune activation, termed cytokine release syndrome (CRS)[54]. The hallmark of CRS is dramatic elevation of cytokines, particularly interferon-gamma (IFN-γ), granulocyte-monocyte colony stimulating factor (GM-CSF), interleukin (IL)-10, IL-6, which is proportional to the degree of activation and expansion of CAR-T cells. While tumour burden is a key determinant of CRS severity, clinical outcomes are not dictated by the evolution of CRS, although the evidence of any sign of immune reactivity, including mild fever, is generally associated with positive clinical responses. Appropriate management may require aggressive interventions to swiftly dampen the inflammatory forward-loop without blunting the anti-tumour specific reactivity of CAR-T cells. Administration of the anti-IL-6 receptor (IL-6R) moAb tocilizumab has demonstrated near-immediate reversal of CRS[31,55] and has been approved by the Food and Drug Administration (FDA) as front-line treatment for CRS following CAR-T-cell infusion[54,56,57], thus emphasising the key role of IL-6 in the pathogenesis of CAR-T related CRS.

Neurotoxicity is another prominent, although non-CAR-T specific[58-60], toxicity occurring in up to 64% of patients. The clinical course is heterogeneous, often severe, with reports of seizures, cerebral oedema and deaths[61-70]. The exact mechanism of CAR-T cell associated neurotoxicity is still poorly understood. CAR-T cells may directly attack central nervous system (CNS) tissues that have the yet-to-be-detected expression of targeted antigen, as it has been reported for other systems[71]. However, there is no evidence of CD19 expression on CNS tissues. By contrast,

CNS endothelial cell activation, associated with high levels of serum IL-6, IFN-γ, and tumour necrosis factor-alpha (TNF-α) followed by release of angiopoietin-2 (Ang-2) and von Willebrand Factor (vWF) from endothelial Weibel-Palade bodies, endothelial dysfunction and increased blood-brain barrier (BBB) permeability, may play a key role upon infusion of CAR19-specific T cells[72]. Crucially, increased permeability of the BBB allows sequestration of Il-6, IFN-γ and TNF-α into CSF, thus initiating a feed-forward loop of continued endothelial cell and pericyte activation. In the most severe cases, this feed-forward loop can cause breakdown of the parenchymal basement membrane and vascular disruption, with cerebral oedema, haemorrhage, infarction, necrosis and neuronal death as observed in autopsy studies of 2 patients who had fatal neurotoxicity. Once again, IL-6 seems to be key in promoting and sustaining this feed-forward loop[64].

In the setting of CD19-specific CAR-T cells, off-tumour on-target effects are of lesser clinically consequences[73]. B cell aplasia due to targeting of normal B cells is relatively easily manageable with intermittent infusion of pooled immunoglobulin as prophylaxis from infectious complications[74,75]. Lately, clinical trials have reported recovery of normal B cell in patients with durable clinical response[39], suggesting that such toxicity may be transient.

Given the risk of life-threatening side effects, incorporation of safety switches in CAR-T cells have become compulsory for further clinical development. Safety switches are suicide or elimination genes that allow to suppress CAR-T cells in a spatio/temporal controlled manner. Suicide genes may be human herpes simplex virus thymidine kinase type 1 (HSV-TK) and genes encoding for proteins with caspase-like activity (iCasp9), in frame with a drug dimerizer domain, capable of triggering CAR-T cell apoptosis upon binding with ganciclovir or specific dimerizer (Rimiducid) respectively[76,77]. Elimination genes, e.g. CD20 and epidermal grow factor receptor (EGFR)-derived extracellular epitopes, are surface antigens that can mediate *in vivo* depletion by clinical grade moAbs. Alternatively, CAR transient expression by means of RNA-electroporation has also been explored [78]. On the flip side, in both cases CAR cell loss results in loss of immunosurveillance and risk of disease relapse. In order to overcome such limitation, affinity-optimized CAR variants that can discriminate between aberrant and healthy cells based on different levels of expression of the target antigen have been under investigation[79]. Indeed, low-affinity CARs have been proved to mediate strong cytotoxicity against transformed cells

expressing high levels of the relevant antigen with minimal or no reactivity against antigen-low normal cells. More recently, preclinical work has demonstrated the feasibility of exerting a remote control of CAR-T cells *in vivo* by using micro-circuits and transcriptional loops[20] to modulate surface expression, as well as split co-stimulatory configurations and AND/OR gate platforms, combining conventional activating constructs with inhibitory CARs (iCAR), carrying CTLA-4- or PD-1-derived inhibitory domains to allow full activation only against targets expressing a defined array of tumour-associated antigens[80].

1.1.2.4.3 CAR immunotherapy versatility

Lately there has been a great interest in developing universal CAR-T cells that could be used for any patient without the need of HLA-matching between T cell donor and recipient. Autologous T cells are generally obtained from heavily pre-treated patients. Hence, it is conceivable that such T cells carry inherent defects that contribute to the heterogeneous clinical outcomes reported. Furthermore, failure to harvest the target number of $CD3^+$ cells and/or rapidly progressing disease represent the main limitations to CAR-T cell manufacturing in a significant proportion of patients. Allogeneic, donor-derived CAR-T cells have been generated and infused to their respective allogeneic stem cell transplant recipients. Such donor-derived CAR-T cells exert anti-ALL activity and have been considered as a valid alternative to improve CAR-T immunotherapy outcomes. However, acute graft-versus-host disease (aGVHD) has been observed in a number of cases. In addition, the manufacturing of donor-derived CAR T cells is not always feasible and can be more time consuming and expensive than that of autologous CAR T cell products. Therefore, establishment of an '*off-the-shelf*', third-party cell bank is an attractive solution with the possibility of reducing time-to-treatment and costs. CAR-transduced viral (EBV or CMV)-specific cells and deletion of the endogenous T-cell receptor via zinc finger nucleases (ZFN), TAL effector nuclease (TALEN) or CRISPR/Cas9 gene-editing are the main two approaches currently under clinical development. Preliminary clinical evidence suggests that TCR-edited CAR19-T cells retain their anti-leukaemia activity without causing significant aGVHD [81-85].

1.1.3 iNKT cells

Invariant natural killer T (iNKT) cells are a rare T cell subset (~0.01-0.1% of CD3+ T cells[86-88]), with memory-like phenotype[89,90] and innate-like reactivity[89,91,92]. Compared to conventional T cells, iNKT cells have a number two unique features: a) they display a highly restricted TCR repertoire, in humans consisting of an invariant TCRVα24Jα18 chain (detected by the anti-idiotypic moAb 6B11) coupled with a diverse TCRVβ11 chain[89,91,93,94], b) they are activated by endogenous or exogenous glycolipid antigens presented in the context of the non-polymorphic major histocompatibility complex (MHC) class I-like CD1d molecule.

CD1d-iTCR interactions are key to iNKT cell development and activation biology (see also below *1.1.3.2 CD1d* paragraph). Upon direct CD1d-iTCR interaction (signal 1), that can be further modulated by surface co-stimulatory molecules (signal 2), iNKT cells may achieve full activation, followed by swift release of large amounts of cytotoxic granules such as perforin and granzymes and T helper (Th)1/2/17 cytokines. Constant stimulation of the iTCR by CD1d-self-glycolipids promotes enhanced chromatin acetylation at the *IFNG* regulatory locus[95], which results in constitutive transcription and prompt production in a iTCR-independent manner of IFN-γ in response to cytokines such as IL-12, IL-18, and type I IFN.

Human iNKT cells are mainly $CD4^{-}CD8\beta^{-}$ double negative (DN) and $CD4^{+}$ $CD8^{-}$. CD4 expression is preferentially associated with the potential to generate Th2 cytokines, such as IL-4, GM-CSF, and IL-13, whereas Th1 cytokines can be equally produced by both $CD4^{+}$ and $CD4^{-}$ subsets[86,96]. As a result, $CD4^{+}$ cell reactivity is characterised by a balanced profile (Th0), while IFN-γ and other Th1 cytokines are predominant upon stimulation of $CD4^{-}$ iNKT cells. $CD4^{-}$ iNKT cells may also be $CD8\alpha^{+}$, less frequently $CD8\alpha\beta^{+}$[86,97], and CD8 expression predicts an even more pronounced Th1 profile, i.e. greater levels of IFN-γ and cytotoxic potential[98].

1.1.3.1 Anti-tumour potential of iNKT cells

Owing to the above features, iNKT cells exhibit potent effector and immunoregulatory functions and play a key role in various immune responses, including against tumours.

Importantly, the iNKT cells are often qualitatively and quantitatively defective cancer patients[92,99-105]. Compared to healthy individuals, patients with advanced solid tumours and haematological malignancies, such as myelodysplastic syndrome and multiple myeloma[92,99-105],

have lower frequency of circulating iNKT cells, generally accompanied by functional, although reversible defects, including decreased proliferation, impaired IFN-γ production and detrimental Th2-biased cytokine profile. By contrast, the presence of circulating iNKT cells capable of making IFN-γ has positive prognostic value for survival[92,103-107]. Similar defects have been shown in mouse models, where iNKT cell *in vivo* stimulation and/or adoptive transfer could induce strong direct and indirect anti-tumour responses[108-113] characterized by robust activation of NK, B and $CD8^+$ T cells[89,91,93,94,109,113].

The synthetic glycolipid α-galactosylceramide (αGalCer), originally derived from marine sponges in a screen for anti-tumour agents[112], is a potent iNKT cell agonist that has been proved to elicit effective anti-tumour activity in murine models of colon carcinoma, lymphomas, sarcoma, melanoma, prostate, and lung carcinoma[89,91,93,94,109-113]. On this basis, phase 1 trials evaluated the effect of administration of αGalCer in cancer patients. Although no dose-limiting toxicity was observed[114], there was minimal therapeutic activity. Importantly, immunological responses, i.e., increases in serum GM-CSF and TNF-α levels, were only observed in patients with at least normal iNKT cell counts[114], thus emphasising that both qualitative and quantitative iNKT cell defects are clinically relevant and adoptive transfer of fully functional iNKT cells might be the key for successful iNKT cell-based cancer immunotherapy. Further, administration of autologous, αGalCer-pulsed APC, e.g. adherent peripheral blood mononuclear cells (PBMC) treated with GM-CSF and IL-2 or monocyte-derived dendritic cells (DCs), led to enhanced anti-tumour responses[106,110,115-118], with evidence of activation of iNKT, T and NK cells and improved NK cell cytotoxicity[106,115-121]. Notably, intravenous (iv) administration of autologous, purified αGalCer-pulsed matured monocyte-derived DCs in 5 patients with cancer[119] induced more than 100-fold expansion of circulating iNKT cell numbers for up to 6 months post-vaccination. This was also associated with an increase in memory $CD8^+$T cells. Toxicity was mild (grade ≤1), with no reports of autoimmunity[119]. More recently, the adoptive transfer of *ex vivo* expanded and activated iNKT cells has shown the highest therapeutic potential in preclinical models of melanoma and lung cancer[122-124] as well as melanoma patients with metastatic disease[125].

Specifically, autologous iNKT cells were sorted from leukapheresis products by using a paramagnetic microbead-conjugated 6B11 moAb[87,126], followed by *in vitro* expansion over

several weeks in the presence of IL-2 prior to adoptive transfer. All patients received three doses of 3 to 250 million cells/infusion with a 2-week interval, reporting more than 4 and 5 years tumour-free progression in 1 and 2 cases respectively and no more than grade 2 toxicity. This proof-of-principle trial demonstrated that few iNKT cells may be sufficient to induce durable clinically relevant responses, suggesting that indeed iNKT cell therapy for advanced cancers is feasible and safe. Moreover, transfer of up to 10^9 total iNKT cells was well tolerated, while producing evidence of subsequent activation of other immune cells. Yet, optimization is needed to fully exploit the anti-tumour potential of iNKT cells. Several strategies are currently under preclinical and clinical investigation, including the usage of iNKT cells as a more effective platform for CAR-based immunotherapy[48,49] (see also NCT02656147).

1.1.3.2 CD1d

CD1d, the restriction element of iNKT cells, is a non-polymorphic HLA type I-like molecule presenting phospho- and glycosphingo- lipid antigens. CD1d is required for iNKT cell development and activation. CD1d is expressed on thymocytes and APC, including DCs and mature B cells, as well as granulocytes, monocytes, plasma cells and some epithelial tissues[127,128]. Similar to their normal counterparts, malignant B cells can also express CD1d. Specifically, MCL and MZL consistently express CD1d[129-131], whereas CLL generally express low-to-no CD1d molecules, although they have been detected in cases of advanced, progressing disease[132,133].

Expression of CD1d is regulated by multiple transcription factors (TFs). Transcription of the human *CD1D* gene is regulated by a proximal and a distal promoter[134], with the former between -106 and +24 base pair (bp) and the latter within the -665 and -202 bp regions relative to the ATG codon, containing an activating SP1 (proximal)[134,135] and a repressing LEF-1(distal)[136] binding sites respectively. In addition, the 5' untranslated region contains a retinoic acid response element (RARE), approximately 1.5 kb upstream the ATG[137]. All-trans retinoic acid (ATRA) and retinoic acid receptor alpha (RARα) agonists have been demonstrated to increase CD1d expression in myeloid and B cells *in vitro*[138-140].

1.1.3.3 iNKT cell alloreactivity

Owing to its non-polymorphic nature, CD1d has also a central role in iNKT cell alloreactivity. Specifically, minor or major conventional HLA disparities between donor and recipient are responsible for the initiation of alloreactive immune processes in the context of allogeneic organ and haematopoietic stem cell transplantation. The clinical correlate of this disparity in allo-HSCT is the multi-organ syndrome called aGVHD, a relatively frequent cause of transplant-related morbidity and mortality characterized by immunological attack of normal recipient tissues by donor alloreactive T cells activated by host APC[141-143]. In contrast to conventional T cells, iNKT cells do not cause aGVHD. Extensive preclinical work showed that both recipient and donor iNKT cells can suppress incipient alloreactions and protect from aGVHD[144]. In the setting of experimental reduced intensity immunoablation including total lymphoid irradiation (TLI), recipient conventional T cells are depleted while iNKT cells, which constitutively express high levels of the prosurvival protein Bcl2, are relatively radio-resistant and thus highly enriched following TLI [145]. Such surviving iNKT cells are polarized to a Th2 phenotype and actively suppress donor alloreactive T cells while promoting the activity of Tregs[146]. Likewise, donor iNKT cells can also protect from aGVHD[147,148], while exerting a potent GVL effect[149]. Clinical observational studies demonstrated a direct correlation between higher donor iNKT cell count in the graft ($CD4^-$ iNKT cells), prompt recovery of iNKT cells after allotransplant and a significantly reduced risk of aGVHD[150-152]; in addition, in paediatric haploidentical allo-HSCT, earlier and higher iNKT cell recovery is associated with a significantly reduced risk of leukaemia relapse[153]. It is likely that donor human iNKT cells protect against aGVHD by killing recipient, CD1d-expressing APC, as suggested by *in vitro* data showing that iNKT cells swiftly react and lyse allogeneic APC in a process that requires a CD1d–iTCR interaction and activating killer immunoglobulin receptors[154].

1.2 Hypothesis

Since malignant B cells may co-express CD19 and CD1d and the CD1d-iTCR axis is required for the anti-tumour activity of iNKT cells, I hypothesised that CAR19-engineering of iNKT cells would enhance their anti-lymphoma activity via simultaneous and dual targeting of CD19 and CD1d on tumour cells. Therefore, I hypothesised that CAR19-iNKT cells would be more effective than unmodified iNKT and CAR19-T cells against $CD19^{+}CD1d^{+}$ B cell malignancies.

I also predicted that CAR-iNKT cells would have additional advantages compared to their CAR-T and unmodified iNKT counterparts as follows:

- It is likely that iNKT cells could utilize both their endogenous iTCR and engineered CAR to simultaneously target the tumour with two different targeting moieties.
- CAR therapy-related potential toxicities could be more easily addressed in the case of an iNKT platform without the need of extra, laborious effector cell manipulation, e.g. co-engineering of suicide and/or elimination genes. Indeed, a GMP-grade anti-iNKT moAb is already clinically available and has been proven effective at eliminating pathogenic iNKT cells in patients with sickle cell disease.
- While aGvHD is a common concern for T cell based adoptive therapies, with their endogenous TCRs being responsible for initiating aGvHD and causing off-target toxicities, iNKT cells have been proven to protect from GvHD, with evidence of aGvHD suppression in pre-clinical models and reduced aGvHD frequency in allotransplanted patients[146,147,155-157]. Therefore, CAR-iNKT cells would be suitable for '*off-the-shelf*', third party manufacturing and usage, thus conferring wider applicability of the CAR technology. This would come along with predicted decrease of manufacturing related-costs, which represent one the of main limitations to broader applicability and long-term sustainability of CAR-T based therapies.

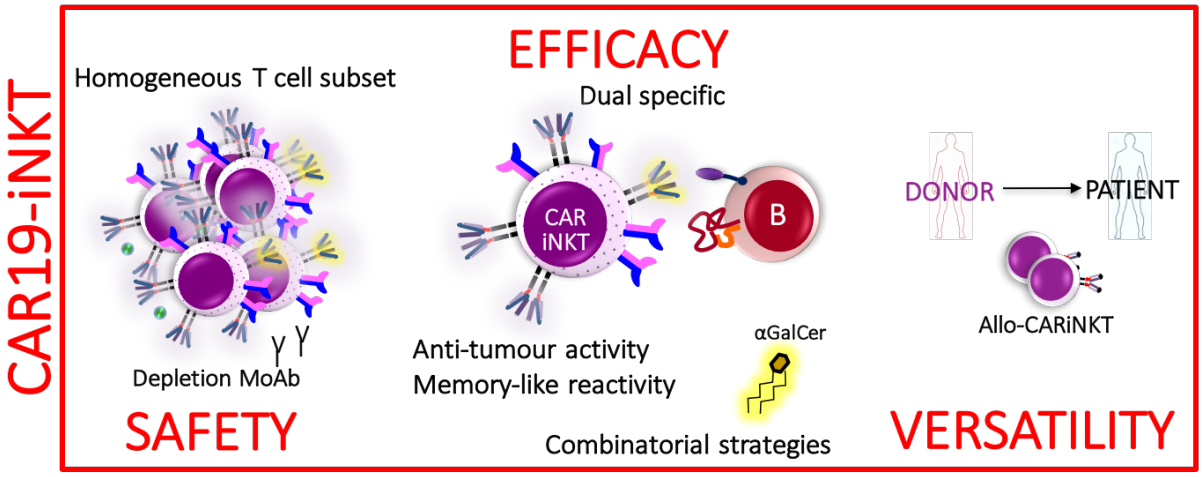


Figure 1-4 Advantages of CAR19-iNKT cells over CAR19-T cells
By combining the potent direct (iTCR) and indirect (perforin, granzymes, IFN-γ) antitumour activity, fast innate-like responses and unique alloreactivity (protection against aGvHD) together with the activating properties of CARs, CAR19-iNKT cells may overcome the limitations of both unmodified iNKT and CAR19-engineered conventional T cells in terms of efficacy, safety and versatility.

1.3 Aims

The aim of this project was to address whether CD19-specific CAR-iNKT (CAR19-iNKT) cells would be more effective than conventional CAR19-T and unmodified iNKT cells against $CD19^{+}CD1d^{+}$ mature B lineage malignancies.

The specific objectives were to:

1) optimise a protocol for clinical scale manufacturing of CAR-engineered iNKT cells,

2) functionally validate CAR19-iNKT cells *in vitro* and *vivo* and

3) compare side-by-side CAR19-iNKT, CAR19-T and unmodified iNKT cells for immunotherapy of B cell malignancies *in vitro* and *in vivo.*

2 Materials & Methods

2.1 CD19-specific CARs

To generate CD19-specific CAR-iNKT and -T cells, a 2nd generation 19-IgGFc-CD28ζ and 3rd generation 19-IgGFc-CD28OX40ζ CAR constructs with FMC63-derived scFv[158] were kindly donated by Dr Martin Pule, University College London. To protect CAR-expressing cells from *in vivo* opsonisation[158], the original IgGFc-derived spacers were modified by removing the CH2 and CH3 extracellular domains and the resulting new constructs were re-cloned into pSew lentiviral vector *via* overlapping PCR using Gibson assay (New England Biolabs, **Figure 2-1, Figure 2-2** and **Figure 2-3**). The primer pairs used are listed in **Table 2-1**.

The final modular structure is provided in **Figure 2-4**. The RQR8 marker/suicide[159] gene was maintained upstream of the CARs with an intervening FMD-2A peptide sequence to allow detection of CAR-transduced cells as previously described[159].

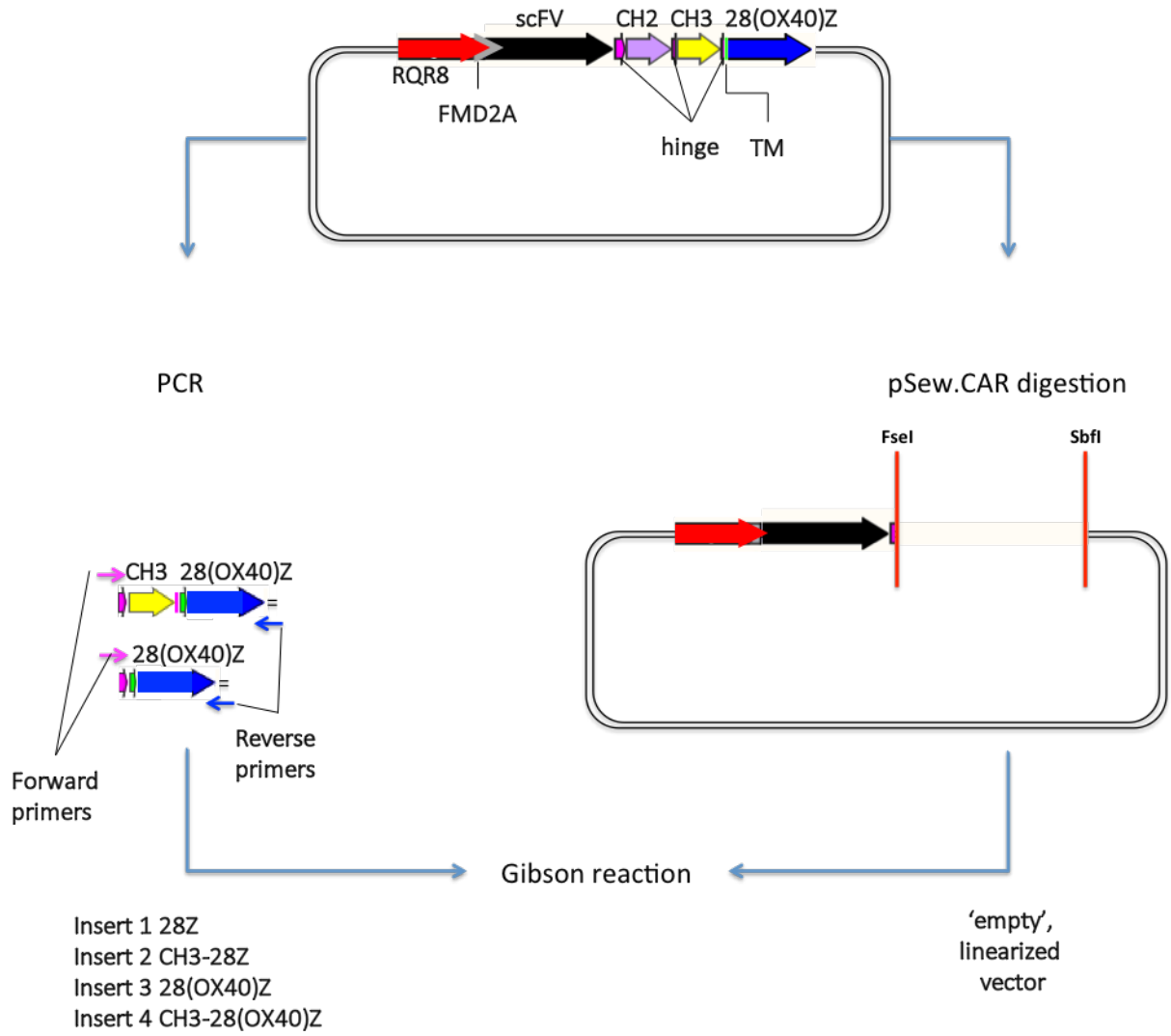


Figure 2-1 Generation of CAR19 constructs with reduced scaffold by Gibson cloning approach
Representative scheme for cloning strategy. 2nd generation 19-IgGFc-CD28ζ and 3rd generation 19-IgGFc-CD28OX40ζ plasmids were used as templates (*top*). 4 inserts were prepared by polymerase chain reaction (PCR) using Phusion Green High-Fidelity DNA Polymerase (2 U/µL, Thermo ScientificTM) (*left*) according to the manufacturer's instructions. Primers were designed to generate overlapping DNA fragments and the final PCR products were electrophoresed on a 1% agarose gel for identification and gel extraction. pSew plasmid vectors were then linearised by double digestion with FseI and SbfI (Thermo Scientific) according to the manufacturer's instructions (*right*) and electrophoresed on 0.8% agarose gel for identification and gel extraction of vectors lacking of CH2CH3-spacer, transmembrane tract and intracellular moiety sequences (pSew 'empty' vectors). DNA fragments were visualised under Safe Imager™ blue-light transilluminator and the relevant bands were excised and purified using GeneJET Gel Extraction Kit (Thermo Scientific). DNA concentrations were determined by Nanodrop instrument. Finally, insert fragments were mixed with pSew empty vectors together with Gibson Assembly Master Mix as per Gibson Assembly protocol and incubated at 50°C for 50 minutes.

Insert 1 – IgGhinge-CD28ζ (2nd generation, short scaffold)

CCCACCGTGCCCAGCACCTCCCGTGGCCGGCCCGTCAGTCTTCTGGGTCCTGGTGGTGGTGGGAGGCGTGCTGGCCTGTTACTCTCTCCTGGTGACCGTGGCCTTCATCATCTTCTGGGTGCGCTCCAAGAGGAGCAGG
CTCCTGCACAGTGACTACATGAACATGACTCCCCGCCGCCCCGGGCCCACCCGCAAGCATTACCAGCCCTATGCCCCACCACGCGACTTCGCAGCCTATCGCTCCCGGGTGAAGTTCTCTCGCTCTGCCGATGCCCCAGC
CTATCAGCAGGGCCAGAATCAGCTGTACAATGAACTGAACCTGGGCAGGCGGGAGGAGTACGACGTGCTGGATAAGCGGAGAGGCAGAGACCCCGAGATGGGCGGCAAACCACGGCGCAAAAATCCCCAGGAGGG
ACTCTATAACGAGCTGCAGAAGGACAAAATGGCCGAGGCCTATTCCGAGATCGGCATGAAGGGAGAGAGAAGACGCGGAAAGGGCCACGACGGCCTGTATCAGGGATTGTCCACCGCTACAAAAGATACATATGATG
CCCTGCACATGCAGGCCCTGCCACCCAGATGACCTGCAGGCATGCAAGCTTGATATCAAGCTTATCG

Insert 2 – IgG.CH3hinge-CD28ζ (2rd generation, half scaffold)

CCCACCGTGCCCAGCACCTCCCGTGGCCGGCCCGTCAGTCCAGGTGTACACCCTGCCCCCATCCCGGGATGAGCTGACCAAGAACCAGGTCAGCCTGACCTGCCTGGTCAAAGGCTTCTATCCCAGCGACATCGCCGTG
GAGTGGGAGAGCAATGGGCAACCGGAGAACAACTACAAGACCACGCCTCCCGTGCTGGACTCCGACGGCTCCTTCTTCCTCTACAGCAAGCTCACCGTGGACAAGAGCAGGTGGCAGCAGGGGAACGTCTTCTCATGC
TCCGTGATGCATGAGGCCCTGCACAATCACTATACCCAGAAATCTCTGAGTCTGAGCCCAGGCAAGAAGGACCCCAAGTTCTGGGTCCTGGTGGTGGTGGGAGGCGTGCTGGCCTGTTACTCTCTCCTGGTGACCGTGG
CCTTCATCATCTTCTGGGTGCGCTCCAAGAGGAGCAGGCTCCTGCACAGTGACTACATGAACATGACTCCCCGCCGCCCCGGGCCCACCCGCAAGCATTACCAGCCCTATGCCCCACCACGCGACTTCGCAGCCTATCGC
TCCCGGGTGAAGTTCTCTCGCTCTGCCGATGCCCCAGCCTATCAGCAGGGCCAGAATCAGCTGTACAATGAACTGAACCTGGGCAGGCGGGAGGAGTACGACGTGCTGGATAAGCGGAGAGGCAGAGACCCCGAGAT
GGGCGGCAAACCACGGCGCAAAAATCCCCAGGAGGGACTCTATAACGAGCTGCAGAAGGACAAAATGGCCGAGGCCTATTCCGAGATCGGCATGAAGGGAGAGAGAAGACGCGGAAAGGGCCACGACGGCCTGTAT
CAGGGATTGTCCACCGCTACAAAAGATACATATGATGCCCTGCACATGCAGGCCCTGCCACCCAGATGACCTGCAGGCATGCAAGCTTGATATCAAGCTTATCG

Insert 3 – IgGhinge-CD28OX40ζ (3nd generation, short scaffold)

CCCAGCACCTCCCGTGGCCGGCCCGTCAGTCTTTTGGGTGCTGGTGGTGGTTGGTGGAGTCCTGGCTTGCTATAGCTTGCTAGTAACAGTGGCCTTTATTATTTTCTGGGTGAGGAGTAAGAGGAGCAGGCTCCTGCAC
AGTGACTACATGAACATGACTCCCCGCCGCCCCGGGCCCACCCGCAAGCATTACCAGCCCTATGCCCCACCACGCGACTTCGCAGCCTATCGCTCCAGGGACCAGAGGCTGCCCCCCGATGCCCACAAGCCCCCTGGGG
GAGGCAGTTTCCGGACCCCCATCCAAGAGGAGCAGGCCGACGCCCACTCCACCCTGGCCAAGATCAGAGTGAAGTTCAGCAGGAGCGCAGACGCCCCCGCGTACCAGCAGGGCCAGAACCAGCTCTATAACGAGCTC
AATCTAGGACGAAGAGAGGAGTACGATGTTTTGGACAAGAGACGTGGCCGGGACCCTGAGATGGGGGGAAAGCCGAGAAGGAAGAACCCTCAGGAAGGCCTGTACAATGAACTGCAGAAAGATAAGATGGCGGAG
GCCTACAGTGAGATTGGGATGAAAGGCGAGCGCCGGAGGGGCAAGGGGCACGATGGCCTTTACCAGGGTCTCAGTACAGCCACCAAGGACACCTACGACGCCCTTCACATGCAGGCCCTGCCTCCTCGCTAACCTGCA
GGCATGCAAGCTTGATATCAAGCTTATCG

Insert 4 – IgG.CH3hinge-CD28OX40ζ (3rd generation, half scaffold)

CCCAGCACCTCCCGTGGCCGGCCCGTCAGTCCAGGTGTACACCCTGCCCCCATCCCGGGATGAGCTGACCAAGAACCAGGTCAGCCTGACCTGCCTGGTCAAAGGCTTCTATCCCAGCGACATCGCCGTGGAGTGGGA
GAGCAATGGGCAACCGGAGAACAACTACAAGACCACGCCTCCCGTGCTGGACTCCGACGGCTCCTTCTTCCTCTACAGCAAGCTCACCGTGGACAAGAGCAGGTGGCAGCAGGGGAACGTCTTCTCATGCTCCGTGAT
GCATGAGGCTCTGCACAACCACTACACGCAGAAGAGCCTCTCCCTGTCTCCGGGTAAAAAAGATCCCAAATTTTGGGTGCTGGTGGTGGTTGGTGGAGTCCTGGCTTGCTATAGCTTGCTAGTAACAGTGGCCTTTATTA
TTTTCTGGGTGAGGAGTAAGAGGAGCAGGCTCCTGCACAGTGACTACATGAACATGACTCCCCGCCGCCCCGGGCCCACCCGCAAGCATTACCAGCCCTATGCCCCACCACGCGACTTCGCAGCCTATCGCTCCAGGGA
CCAGAGGCTGCCCCCCGATGCCCACAAGCCCCCTGGGGGAGGCAGTTTCCGGACCCCCATCCAAGAGGAGCAGGCCGACGCCCACTCCACCCTGGCCAAGATCAGAGTGAAGTTCAGCAGGAGCGCAGACGCCCCCG
CGTACCAGCAGGGCCAGAACCAGCTCTATAACGAGCTCAATCTAGGACGAAGAGAGGAGTACGATGTTTTGGACAAGAGACGTGGCCGGGACCCTGAGATGGGGGGAAAGCCGAGAAGGAAGAACCCTCAGGAAGG
CCTGTACAATGAACTGCAGAAAGATAAGATGGCGGAGGCCTACAGTGAGATTGGGATGAAAGGCGAGCGCCGGAGGGGCAAGGGGCACGATGGCCTTTACCAGGGTCTCAGTACAGCCACCAAGGACACCTACGAC
GCCCTTCACATGCAGGCCCTGCCTCCTCGCTAACCTGCAGGCATGCAAGCTTGATATCAAGCTTATCG

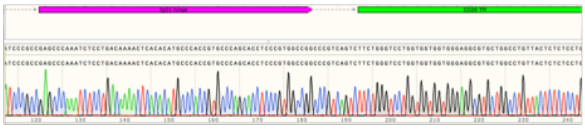
Figure 2-2 Insert sequences for the generation of CAR19 constructs with reduced-size scaffold

The CH2 segment was removed by PCR to generate inserts including hinge (pink), CH3 segment (yellow), CD28 trans-membrane tract (green), CD3Z domain (blue) and a small sequence overlapping with pSew vector (grey).

Table 2-1 Primers to amplify inserts for the generation of reduced-size scaffold CAR19 constructs

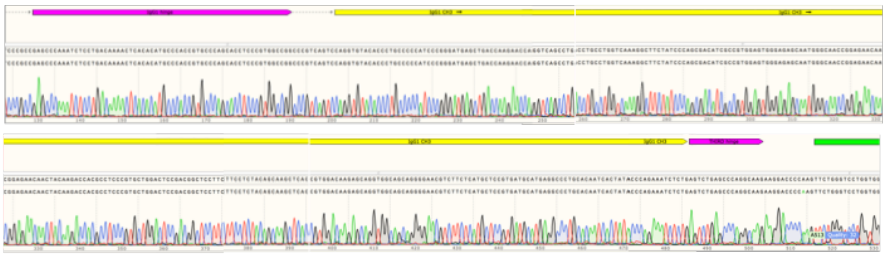
Primer	bp	Sequence	Primer - insert		Insert size	Insert - vector	
			Tm	Annealed		Overlap	Tm
Insert 1 F	50bp	CCCAGCACCTCCCGTGGCCGGCCCGTCAG TCTTCTGGGTCCTGGTGGTGG	590C	19bp	609bp	31bp	690C
Insert 2 F	48bp	CCCAGCACCTCCCGTGGCCGGCCCGTCAG TCCAGGTGTACACCCTGCCC	580C	18bp	924bp	31bp	690C
Insert 1&2 R	48bp	CGATAAGCTTGATATCAAGCTTGCATGCCT GCAGGTCATCTGGGTG	600C	19bp	-	33bp	650C
Insert 3 F	50bp	CCCAGCACCTCCCGTGGCCGGCCCGTCAG TCTTTTGGGTGCTGGTGGTG	590C	19bp	717bp	31bp	760C
Insert 4 F	48bp	CCCAGCACCTCCCGTGGCCGGCCCGTCAG TCCAGGTGTACACCCTGCCC	580C	18bp	1032bp	31bp	690C
Insert 3&4 R	48bp	CGATAAGCTTGATATCAAGCTTGCATGCCT GCAGGTTAGCGAGGAGGC	590C	19bp	-	33bp	650C

Construct #1 - 19-IgGhinge-CD28ζ



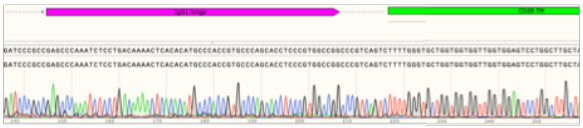
Clone 2G: *4076*-GATCCCGCCGAGCCCAAATCTCCTGACAAAACTCACACATGCCCACCGTGCCCAGCACCTCCCGTGGCCGGCCCGTCAGTCTTC
TGGGTCCTGGTGGTGGTGGGAGGCGTGCTGGCCTGTTACTCTCTCCTGGTG-*4210*

Construct #2 – 19-IgG.CH3hinge-CD28ζ



Clone 5D2: 4076-GATCCCGCCGAGCCCAAATCTCCTGACAAAACTCACACATGCCCACCGTGCCCAGCACCTCCCGTGGCCGGCCCGTCAGTCCAGG
TGTACACCCTGCCCCCATCCCGGGATGAGCTGACCAAGAACCAGGTCAGCCTGACCTGCCTGGTCAAAGGCTTCTATCCCAGCGACATCGCCGTGGAGTGG
GAGAGCAATGGGCAACCGGAGAACAACTACAAGACCACGCCTCCCGTGCTGGACTCCGACGGCTCCTTCTTCCTCTACAGCAAGCTCACCGTGGACAAGAG
CAGGTGGCAGCAGGGGAACGTCTTCTCATGCTCCGTGATGCATGAGGCCCTGCACAATCACTATACCCAGAAATCTCTGAGTCTGAGCCCAGGCAAGAAGG
ACCCCAAGTTCTGGGTCCTGGTGGTGGTGGGAGGCGTGCTGGCCTGTTACTCTCTCCTGGTG-4525

Construct #3 19-IgGhinge-CD28OX40ζ



Clone E: 4076-GATCCCGCCGAGCCCAAATCTCCTGACAAAACTCACACATGCCCACCGTGCCCAGCACCTCCCGTGGCCGGCCCGTCAGTCTTTTGG
GTGCTGGTGGTGGTTGGTGGAGTCCTGGCTTGCTATAGCTTGCTAGTA- 4210

Construct #4 – 19-IgG.CH3hinge-CD28OX40ζ



Clone 4: 4076-GATCCCGCCGAGCCCAAATCTCCTGACAAAACTCACACATGCCCACCGTGCCCAGCACCTCCCGTGGCCGGCCCGTCAGTCCAGGTG
TACACCCTGCCCCCATCCCGGGATGAGCTGACCAAGAACCAGGTCAGCCTGACCTGCCTGGTCAAAGGCTTCTATCCCAGCGACATCGCCGTGGAGTGGGA
GAGCAATGGGCAACCGGAGAACAACTACAAGACCACGCCTCCCGTGCTGGACTCCGACGGCTCCTTCTTCCTCTACAGCAAGCTCACCGTGGACAAGAGCA
GGTGGCAGCAGGGGAACGTCTTCTCATGCTCCGTGATGCATGAGGCTCTGCACAACCACTACACGCAGAAGAGCCTCTCCCTGTCTCCGGGTAAAAAAGAT
CCCAAATTTTGGGTGCTGGTGGTGGTTGGTGGAGTCCTGGCTTGCTATAGCTTGCTAGTA-4525

Figure 2-3 DNA sequencing of CAR19 constructs with reduced scaffold

DNA sequencing confirmed the absence of insertions/deletions and/or mutations in the modified constructs.

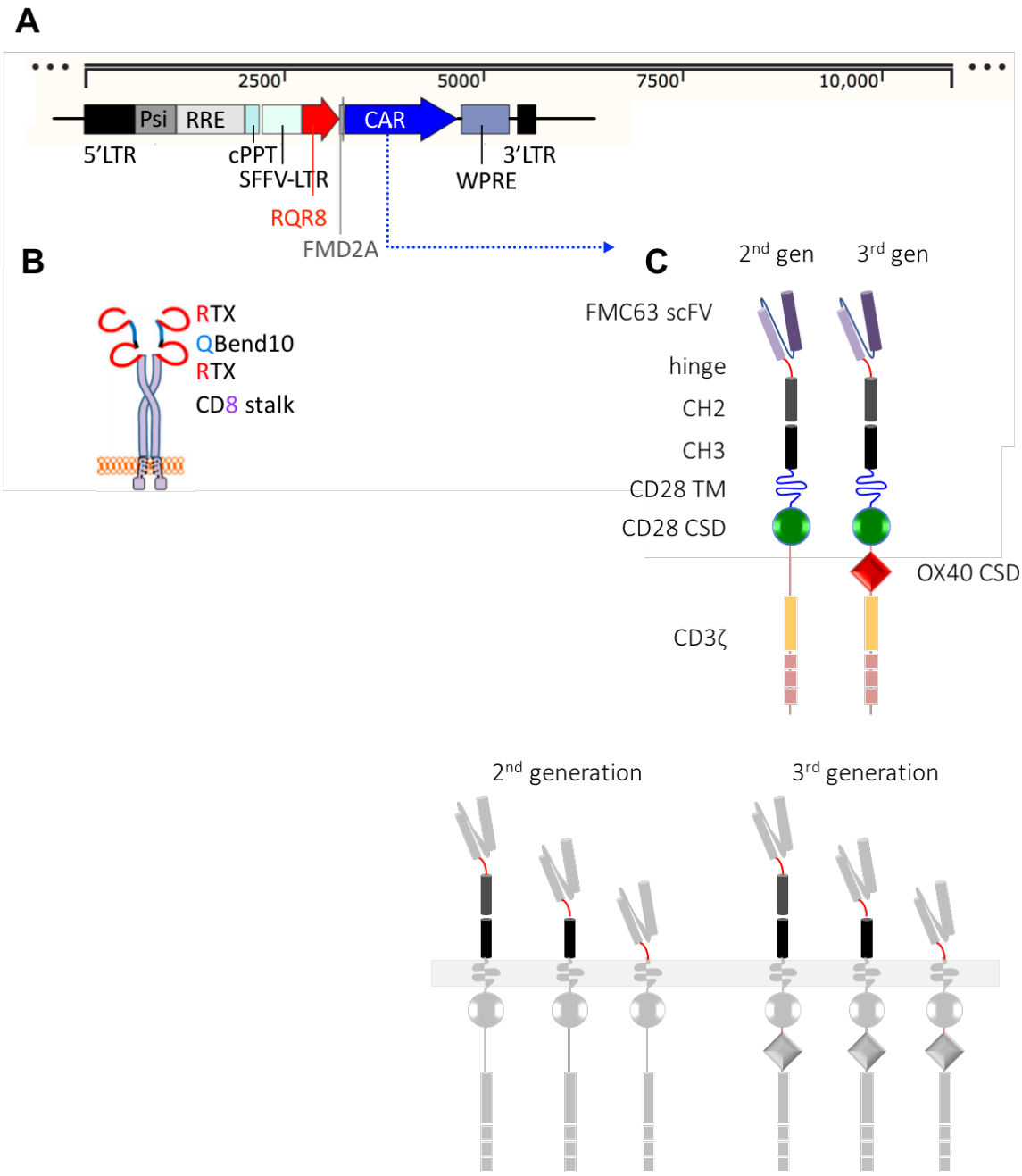


Figure 2-4 2nd and 3rd generation CD19-specific CARs with reduced-size scaffold.

A. Lentiviral constructs. Recombinant transgenes were cloned in the pSew lentiviral vector.

B. RQR8 protein. RQR8 is a marker/suicide gene construct enabling both clinical grade sorting and effective *in vivo* killing of administered T-cells in the face of toxicity using off-the-shelf clinical grade reagents/pharmaceuticals, namely CD34 cliniMACS and Rituximab. It comprises two rituximab (R) binding epitopes flanking a single CD34-QBEnd10 (Q) epitope on the CD8 (8) stalk[159]. RQR8 and CAR equimolar co-expression was achieved by using an intervening FMD-2A autocleaving peptide. C. CAR19 modular structures. Original (*top*) and modified (*bottom*) CAR19 proteins.

2.2 CD1d and CD19 antigens

To generate CD19 and CD1d single- or double-expressing -cells, two cDNA sequences encoding for the human CD19 and CD1d, obtained from Dr Martin Pule and Prof Vincenzo Cerundolo, University of Oxford, respectively, were cloned singly or together with an interposed FMD2A fragment into a retroviral SFG vector (

Figure 2-5**, Figure 2-6,**

Figure 2-7 and **Table 2-2**). For the purposes of real-time *in vitro* monitoring of CAR cell cytotoxic activity, mCherry-labeled $CD1d^{+}$ B cell targets were generated by using a lentiviral pHR-SIN plasmid encoding for a hCD1d-mCherry fusion protein (Prof Vincenzo Cerundolo).

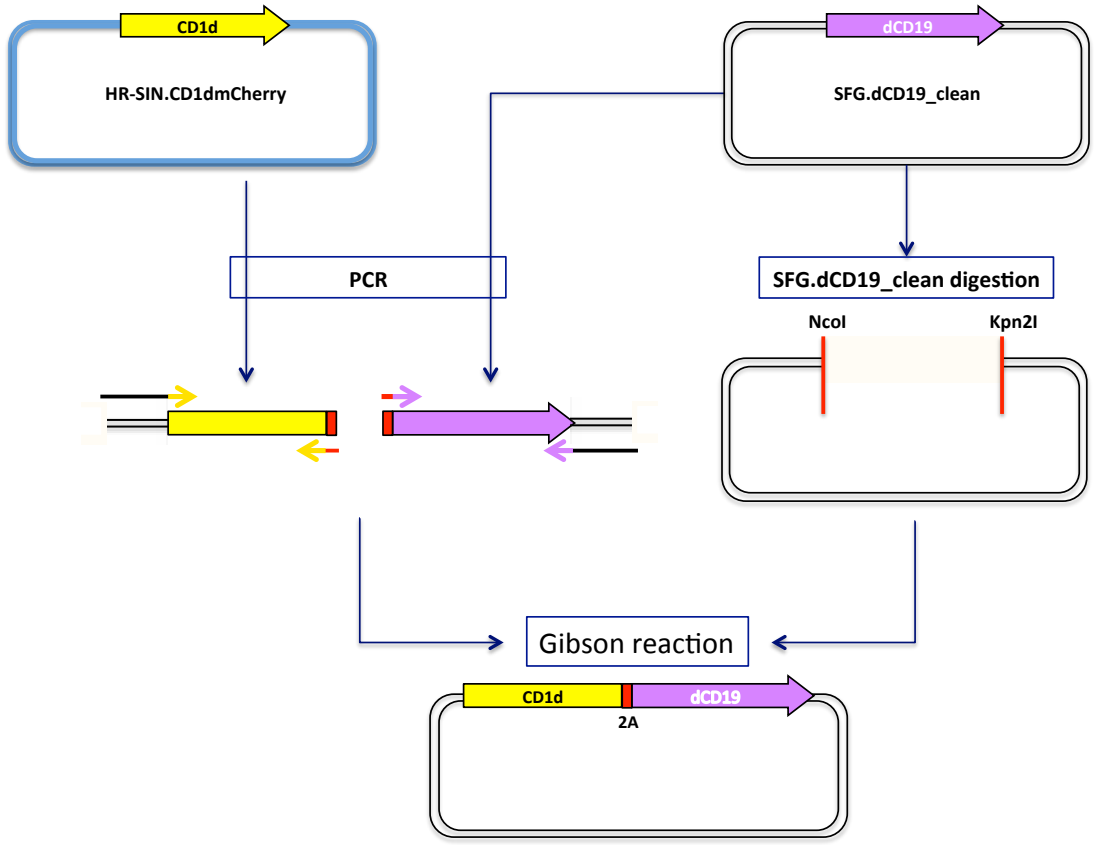


Figure 2-5 Generation of SFG.CD1d and SFG.CD1d.2A.dCD19 constructs by Gibson approach
The HR-SIN.CD1dmCherry and SFG.dCD19_clean plasmids (*top*) were used as templates to generate CD1d and CD19 sequences respectively. The hCD1d plasmid encodes for full-length hCD1d fused with mCherry fluorescent protein in a pHR-SIN lentiviral vector. The hCD19 plasmid encodes for the endodomain-truncated CD19 (dCD19, internal NcoI site removed) in an SFG retroviral vector. The CD1d and dCD19 sequences (*middle left*) were amplified by using Phusion Green High-Fidelity DNA Polymerase (2 U/µL, Thermo ScientificTM) according to the manufacturer's instructions. The primers

were designed to generate overlapping DNA fragments. The PCR products were electrophoresed on a 1% agarose gel. Next, SFG.dCD19_clean plasmid was linearised by double digestion with NcoI and Kpn2I (Thermo Scientific, middle right) according to the manufacturer's instructions and electrophoresed on 0.8% agarose gel for identification and gel extraction of pSFG vector lacking of dCD19 sequence (pSFG 'empty' vector). DNA fragments were visualised under Safe Imager™ blue-light transilluminator and the corresponding pSFG band was excised and purified using GeneJET Gel Extraction Kit (Thermo Scientific). DNA concentrations were determined by Nanodrop instrument. Finally, insert fragments were mixed with pSFG empty vector together with Gibson Assembly Master Mix (*bottom*) as per Gibson Assembly protocol and incubated at 50°C for 50 minutes. Gibson reaction products were transformed in DH5α competent E. Coli cells.

Insert 1 – CD1d

GGCTGCCGACCCCGGGGGTGGACCATCCTCTAGACTGCCATGGGGTGCCTGCTGTTTCTGCTGCTCTGGGCGCTCCTCCAGGCTTGGGGAAGCGCTGAAGTCCCGCAAAGGCTTTTCCCCCTCCGCT
GCCTCCAGATCTCGTCCTTCGCCAATAGCAGCTGGACGCGCACCGACGGCTTGGCGTGGCTGGGGGAGCTGCAGACGCACAGCTGGAGCAACGACTCGGACACCGTCCGCTCTCTGAAGCCTTGGTCCCAGGGCACGT
TCAGCGACCAGCAGTGGGAGACGCTGCAGCATATATTTCGGGTTTATCGAAGCAGCTTCACCAGGGACGTGAAGGAATTCGCCAAAATGCTACGCTTATCCTATCCCTTGGAGCTCCAGGTGTCCGCTGGCTGTGAGGT
GCACCCTGGGAACGCCTCAAATAACTTCTTCCATGTAGCATTTCAAGGAAAAGATATCCTGAGTTTCCAAGGAACTTCTTGGGAGCCAACCCAAGAGGCCCCACTTTGGGTAAACTTGGCCATTCAAGTGCTCAACCAGG
ACAAGTGGACGAGGGAAACAGTGCAGTGGCTCCTTAATGGCACCTGCCCCCAATTTGTCAGTGGCCTCCTTGAGTCAGGGAAGTCGGAACTGAAGAAGCAAGTGAAGCCCAAGGCCTGGCTGTCCCGTGGCCCCAGTC
CTGGCCCTGGCCGTCTGCTGCTGGTGTGCCATGTCTCAGGATTCTACCCAAAGCCTGTATGGGTGAAGTGGATGCGGGGTGAGCAGGAGCAGCAGGGCACTCAGCCAGGGGACATCCTGCCCAATGCTGACGAGACA
TGGTATCTCCGAGCAACCCTGGATGTGGTGGCTGGGGAGGCAGCTGGCCTGTCCTGTCGGGTGAAGCACAGCAGTCTAGAGGGCCAGGACATCGTCCTCTACTGGGGTGGGAGCTACACCTCCATGGGCTTGATTGCC
TTGGCAGTCCTGGCGTGCTTGCTGTTCCTCCTCATTGTGGGCTTTACCTCCCGGTTTAAGAGGCAAACTTCCTATCAGGGCGTCCTGTAGCCGGATTAGTCCAATTTGTTAAAGACAGGATATCAGT

Insert 2 – CD1d.2A.dCD19

GGCTGCCGACCCCGGGGGTGGACCATCCTCTAGACTGCCATGGGGTGCCTGCTGTTTCTGCTGCTCTGGGCGCTCCTCCAGGCTTGGGGAAGCGCTGAAGTCCCGCAAAG
GCTTTTCCCCCTCCGCTGCCTCCAGATCTCGTCCTTCGCCAATAGCAGCTGGACGCGCACCGACGGCTTGGCGTGGCTGGGGGAGCTGCAGACGCACAGCTGGAGCAACGACT
CGGACACCGTCCGCTCTCTGAAGCCTTGGTCCCAGGGCACGTTCAGCGACCAGCAGTGGGAGACGCTGCAGCATATATTTCGGGTTTATCGAAGCAGCTTCACCAGGGACGTG
AAGGAATTCGCCAAAATGCTACGCTTATCCTATCCCTTGGAGCTCCAGGTGTCCGCTGGCTGTGAGGTGCACCCTGGGAACGCCTCAAATAACTTCTTCCATGTAGCATTTCAA
GGAAAAGATATCCTGAGTTTCCAAGGAACTTCTTGGGAGCCAACCCAAGAGGCCCCACTTTGGGTAAACTTGGCCATTCAAGTGCTCAACCAGGACAAGTGGACGAGGGAAA
CAGTGCAGTGGCTCCTTAATGGCACCTGCCCCCAATTTGTCAGTGGCCTCCTTGAGTCAGGGAAGTCGGAACTGAAGAAGCAAGTGAAGCCCAAGGCCTGGCTGTCCCGTGGC
CCCAGTCCTGGCCCTGGCCGTCTGCTGCTGGTGTGCCATGTCTCAGGATTCTACCCAAAGCCTGTATGGGTGAAGTGGATGCGGGGTGAGCAGGAGCAGCAGGGCACTCAGCC
AGGGGACATCCTGCCCAATGCTGACGAGACATGGTATCTCCGAGCAACCCTGGATGTGGTGGCTGGGGAGGCAGCTGGCCTGTCCTGTCGGGTGAAGCACAGCAGTCTAGAG
GGCCAGGACATCGTCCTCTACTGGGGTGGGAGCTACACCTCCATGGGCTTGATTGCCTTGGCAGTCCTGGCGTGCTTGCTGTTCCTCCTCATTGTGGGCTTTACCTCCCG
GTTTAAGAGGCAAACTTCCTATCAGGGCGTCCTGAGAGCCGAGGGCAGAGGCAGCCTGCTGACCTGCGGCGACGTGGAGGAGAACCCAGGCCCCATGGAGACCGACAC
CCTGCTGCTGTGGGTGCTGCTGCTGTGGGTGCCCGGCAGCACCGGCGAGGAACCTCTAGTGGTGAAGGTGGAAGAGGGAGATAACGCTGTGCTGCAGTGCCTCAAGGGGACC
TCAGATGGCCCCACTCAGCAGCTGACCTGGTCTCGGGAGTCCCCGCTTAAACCCTTCTTAAAACTCAGCCTGGGGCTGCCAGGCCTGGGAATCCACATGAGGCCCCTGGCCAT
CTGGCTTTTCATCTTCAACGTCTCTCAACAGATGGGGGGCTTCTACCTGTGCCAGCCGGGGCCCCCCTCTGAGAAGGCCTGGCAGCCTGGCTGGACAGTCAATGTGGAGGGCA
GCGGGGAGCTGTTCCGGTGGAATGTTTCGGACCTAGGTGGCCTGGGCTGTGGCCTGAAGAACAGGTCCTCAGAGGGCCCCAGCTCCCCTTCCGGGAAGCTCATGAGCCCCAAG
CTGTATGTGTGGGCCAAAGACCGCCCTGAGATCTGGGAGGGAGAGCCTCCGTGTCTCCCACCGAGGGACAGCCTGAACCAGAGCCTCAGCCAGGACCTCACAATGGCCCCTG
GCTCCACACTCTGGCTGTCCTGTGGGGTACCCCCTGACTCTGTGTCCAGGGGCCCCCTCTCCTGGACCCATGTGCACCCCAAGGGGCCTAAGTCATTGCTGAGCCTAGAGCTGA
AGGACGATCGCCCGGCCAGAGATATGTGGGTAATGGAGACGGGTCTGTTGTTGCCCCGGGCCACAGCTCAAGACGCTGGAAAGTATTATTGTCACCGTGGCAACCTGACCATG
TCATTCCACCTGGAGATCACTGCTCGGCCAGTACTATGGCACTGGCTGCTGAGGACTGGTGGCTGGAAGGTCTCAGCTGTGACTTTGGCTTATCTGATCTTCTGCCTGTGTTCCC
TTGTGGGCATTCTTCATCTTCAAAGAGCCCTGGTCCTGAGGAGGAAAAGAAAGCGAATGACTGACCCCACCAGGAGATGAACGCGTCATCATCGATCCGGATTAGTCCAAT
TTGTTAAAGACAGGATATCAGTGGTCCAGGCT

Figure 2-6 Insert sequences for SFG.CD1d and SFG.CD1d.2A.dCD19 constructs

Sequences recognized by primers are underlined with double line. CD1d sequence, including leader signal (pink), extracellular (black), trans-membrane (green) and internalizing (blue) domains, was followed by CD19 sequence (purple), with the intervening 2A element (highlighted in red). The stop codon and vector sequence are in bold purple and grey respectively.

Table 2-2 Primers for the generation of SFG.CD1d and SFG.CD1d.2A.dCD19 retroviral constructs

Primer	bp	Sequence	Primer - insert		Insert size	Insert - vector	
			Tm	Annealed		Primer	Length
CD1d F	58bp	ggctgccgaccccgggggtggaccatcctctag actgccATGGGGTGCCTGCTGTTTC	590C	19bp	1083bp	38bp	770C
CD1d.STOP R	60bp	actgatatcctgtctttaacaaattggactaatcc ggCTACAGGACGCCCTGATAGGAAG	600C	23bp		37bp	710C
CD1d.2A R	60bp	cgtcgccgcaggtcagcaggctgcctctgccctc ggctctCAGGACGCCCTGATAGGAAG	580C	20bp	1084bp	24bp	710C
2A.CD19 F	60bp	gcagcctgctgacctgcggcgacgtggaggaga acccaggccccATGGAGACCGACACCC	540C	16bp	1105bp	24bp	710C

CD19 R	22bp	AGCCTGGACCACTGATATCCTG	600C	19bp		47bp	690C

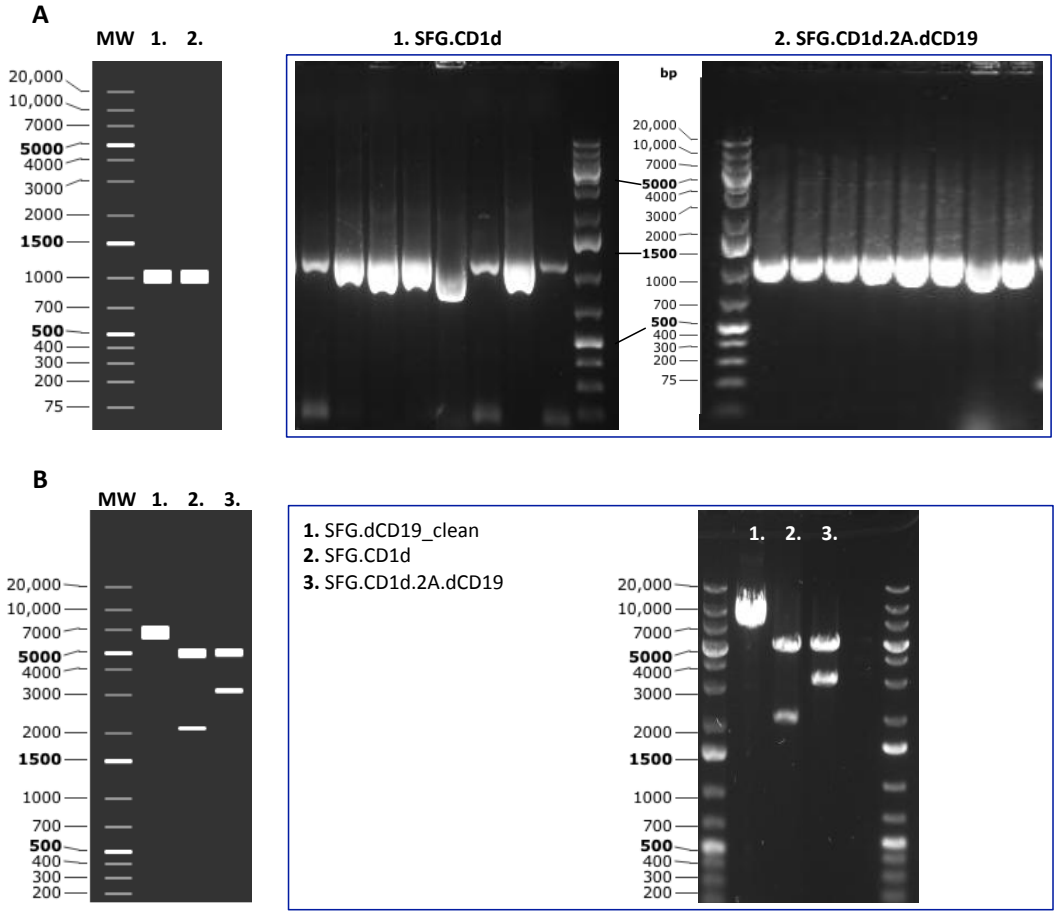


Figure 2-7 Cloning confirmation of SFG.CD1d and SFG.CD1d.2A.dCD19 constructs

A. Colony PCR was performed by using the primer pairs CD1d F/CD1d.STOP R and CD1d F/CD1d.2A R to amplify CD1d sequence in SFG-CD1d (*left*) and SFG-CD1d.2A.dCD19 (*right*) constructs respectively. Several colonies resulted positive for an insert of size between 1000 and 1500bp, consistent with the expected length of CD1d sequence. B. miniprep DNA digestion using EcoRI. After 30min digestion at 37oC, DNA fragments were electrophored on a 0.8% agarose gel. By comparing the actual DNA bands (*right*) with the expected ones (SnapGene simulation, left), successful cloning could be confirmed in samples 1C (SFG.CD1d) and 11B (SFG.CD1d.2A.dCD19).

2.3 Firefly luciferase

To detect tumour cells and monitor tumour growth *in vivo*, a luciferase construct was obtained from Dr John Maher, consisting of firefly luciferase co-expressed with tandem dimer Tomato red fluorescent protein (tdRFP) in a single SFG vector[160].

2.4 Primary Cells

Healthy volunteer PB and lymphapheresis samples as well as PB samples from MCL, MZL and CLL patients were obtained after written informed consent and research ethics committee approval (Research Ethics Committee reference: 11/H0308/9). Fresh PBMCs were isolated from diluted heparinized blood by density gradient centrifugation (400 x g for 30 min at room temperature (RT) with the brake off) using Histopaque-1077 or Lymphoprep gradient medium (Sigma-Aldrich) warmed to room temperature. Cryopreserved cells from lymphapheresis products were thawed in a 37˚C waterbath and washed in warm medium containing heparin and DNAse I up to a maximum of 600,000 IU to prevent cell clumping. Mononuclear cells were then used as a source of either $CD3^+$ lymphoid cells for CAR engineering or $CD19^+$ tumour cell targets for functional assays.

In order to generate CAR iNKT cells, $TCRV\alpha24J\alpha18^+$ lymphocytes were immunomagnetically purified from PBMCs and apheresis mononuclear cells using anti-human iNKT cell microbeads (Miltenyi Biotech), according to the manufacturer's instructions, with minor modifications in the labelling step in order to minimise 6B11 non-specific binding.

2.4.1 iNKT cell isolation

2.4.1.1 1. Anti-iNKT MicroBead labelling

Up to 10^8 PBMC were resuspended in ice-cold binding buffer (phosphate-buffered saline (PBS)/0.5% bovine serum albumin [BSA]) to a final volume of 500µl and hold for 5 up to 15 min on ice. Next 50µL of sterile anti-iNKT MicroBeads per 10^8 total cells, followed by either incubation on ice for 40 min combined with gentle shaking by finger tapping every 5 min or incubation for 30 minutes at 4˚C under continuous shaking. At the end of incubation, cells were washed twice, first with up to 50ml ice-cold binding buffer followed by centrifugation at 300 x g for 10 min, 4˚C, then with 10-20 ml ice-cold binding buffer and subsequent centrifugation as above. Cell pellet was then resupended in ice-cold binding buffer at 500µl/10^8 cells.

2.4.1.2 2. Selection

Two magnetic columns (Miltenyi, MS for up to 1 x 10^8 PBMCs, LS for larger samples) were placed in the magnetic field of suitable magnetic-activated cell sorting (MACS) separators and hydrated with ice-cold MACS buffer (PBS, 0.5% BSA and 2 mM EDTA). Cell suspension was applied onto the first column. An aliquot of the unbound PBMCs (≥10^7) was set aside from the flow-through containing unlabelled cells (negative fraction 1, NF1) for further irradiation (3500 cGy), to be used as feeder and stimulating cells (see below). Next, the column was washed three times by adding the appropriate amount of MACS buffer, i.e. MS: 3×500 µL, LS: 3×3 mL, removed from the separator and placed on a 15ml collection tube. Appropriate amount of binding buffer (MS: 1 mL; LS: 5 mL) was then pipetted into the column and labelled cells were immediately flushed out by firmly pushing the plunger into the column. The eluted cell suspension was reapplied onto the hydrated column and the procedure repeated in order to increase the purity of the 6B11+ cell fraction to ≥80% of CD3+ cells. The second eluted fraction was finally diluted in at least ten volumes of primary cell medium (PCM, see below), residual MACS buffer removed by centrifugation at 300 × g for 10 min at RT and iNKT cell pellet resuspended in TCM at 10^5/ml. Cell purity was confirmed by flow cytometry (see below) before proceeding to CAR-engineering protocol.

2.4.2 Primary cell medium and culture

Primary cell medium (PCM) consisted of RPMI1640, 10% FBS, 2% glutamine, 1% Penicillin-Streptomycin, 1% sodium pyruvate; 1% essential and non-essential aminoacids, 10mM Hepes buffer (Sigma-Aldrich) and 5.5x10^{-5}M beta-mercaptoethanol (Gibco®, Life Technologies). For CD3+ cells, human IL2 and/or IL-15 and/or IL-7 (premium grade, Miltenyi Biotec) were added at 100IU/ml unless otherwise stated.

Cells were cultured in U-bottom 96-well plate at a concentration of 1 x 10^4 cells/well in 200µl/well or flat-bottom 96-well plate at a concentration of 1 x 10^5 cells/well in 200µl/well or 24-well plate at a concentration of 1 x 10^6 cells/well in 1ml/well. Half medium replacement was carried out every 2-3 days or when required based on medium colour change.

2.5 Cell lines

Human Embryonic Kidney 293 (293T) cells were purchased from ATCC and used for lentivirus production. The K562 cells were obtained from ATCC, while the ARH-77, KMS12, H929 and U266 cell lines were purchased from DSMZ. C1R and C1R-CD1d cell lines were provided by Prof Cerundolo. The Farage cell line was kindly donated by Prof Ronald Gartenhaus at University of Maryland School of Medicine, Baltimore. The B lymphoblastoid AK cell line was produced by Joana Costa at the Karadimitris lab. All cell lines were tested for mycoplasma contamination using the MycoAlert Mycoplasma Detection Kit (Lonza). The K562, C1R and ARH-77 cell lines were transduced to express the human CD19 and/or CD1d. For the purposes of *in vitro* functional assays, ARH-77 cells were also modified with the pHR-SIN plasmid described above to co-express the mCherry red fluorescent protein together with CD1d. The C1R-CD1d cell line was modified with the luciferase-tdRFP plasmid for *in vitro* and *in vivo* monitoring by fluorescence and bioluminescence imaging (BLI) respectively.

The adherent 293T cells were grown in 75cm2 culture flasks in Dulbecco's Modified Eagle Medium (DMEM) (Sigma-Aldrich), supplemented with 10% Fetal Bovine Serum (FBS) (Sigma-Aldrich), 2mM L-Glutamine and 10ml/L Penicillin-Streptomycin (Stem Cell Technologies). Cells were maintained at 75% confluency and split as required using x1 trypsin-EDTA solution (Sigma-Aldrich) according to the manufacturer's instructions.

The suspension cell lines were grown in RPMI 1640 medium (Sigma-Aldrich) supplemented with 10-20% Fetal Bovine Serum (FBS) (Sigma-Aldrich), 2mM L-Glutamine and 10ml/L Penicillin-Streptomycin (Stem Cell Technologies), at 37°C, 5% CO2. Where required, sodium pyruvate 1:100, essential and non-essential aminoacids, 1:100 (Gibco®, Life Technologies) were added to the medium. Cells were maintained at a concentration of $4x10^5$ - $5x10^5$ cells/ml in order to be in exponential growth phase. The trypan blue (Sigma-Aldrich) exclusion method was used to determine cell concentrations on a Neubaeur haemocytometer. For each counting, three squares ($1mm^2$) were used to count cells and then the average was calculated for the final concentration. Blue stained dead cells were excluded from counting.

2.6 Pharmacological agents

α-galactosylceramide (KRN7000, Cambridge Bioscience) and all-trans retinoic acid (ATRA, Sigma-Aldrich) were purchased in lyophilized form. Stock solutions were prepared in 100% dimethyl sulfoxide (DMSO) at 1mg/ml (0.001M) and 3mg/ml (0.01M) respectively. The DMSO solution of α-galactosylceramide (αGalCer) was completely dissolved by heating at 80˚ for 1 hour, aliquoted and stored at -20˚C until use. Prior to use, a working solution was prepared by heating for another 60 seconds at 80˚C, followed by dilution in PBS at 100μg/ml (1000x). ATRA was used to assess the transcriptional regulation of CD1d in primary CLL cells. The ATRA solution in DMSO was freshly prepared before each experiment protected from light and diluted in PBS to 1mM (1000X) for immediate use. After preliminary dose-finding experiment, a final dose of 10^{-6}M was chosen, equivalent to pharmacological dose used in clinical settings[161].

2.7 Retroviral and lentiviral production and cell transduction

2.7.1 Virus production

VSV-G pseudotyped retroviruses and lentiviruses were generated by transfection of 80% confluent HEK293T cells, passage ≤6, with the transfer, packaging and envelope plasmids (**Table 2-3**) using the $CaCl_2$ method (**Table 2-4** and **Table 2-5**)[162]. pCMV-Gag-Pol and pVSV-G were used for retrovirus, or pRsv-REV, pMDlg-pRRE and pMD2G were used for lentivirus respectively.

Table 2-3 Plasmid mixture for virus production

Retroviral plasmids		Plasmid name	DNA µg/reaction*
Gene transfer	retroviral backbone	SFG.dCD19_cleanI2.eBFP2 SFG.CD1d SFG.CD1d.2A.dCD19 LuckyTom	10-12 µg
Packaging	two-plasmid system	pCMV-Gag-Pol	12 µg
Envelope	retroviral backbone	pVSV-G	3 µg
Lentiviral plasmids			
Gene transfer	lentiviral backbone	pSew.RQR8-2A.aCD19-CAR.full pSew.RQR8-2A.aCD19-CAR.half pSew.RQR8-2A.aCD19-CAR.short pHR-SIN-hCD1d.mCherry	10-12 µg
Packaging	two-plasmid system	psPAX2	7.5 µg
	three-plasmid system	pMDLg/pRRE (gag/ pol)	5 µg
		pRSV-REV	2.5 µg
Envelope	lentiviral backbone	pMD2.G (VSVG)	3

* 1 reaction = plasmid mix to transfect HEK293T in a 10cm tissue culture dish (2.5-3 x 106 at the time of seeding 24hrs before transfection)

Table 2-4 Calcium phosphate methods for virus production

Virus mix reagents*	Volume (µl)	Procedure
low TE buffer	Up to 500µl	
plasmid mixture	See Table 2-3	two-/three-plasmid packaging system that separates gag, pol, rev, and VSV-G genes onto separate vectors
2.5M CaCl2	50µl	(optional) 5 min incubation
2x HBS	500µl	dropwise while vortexing at full speed
total	1000µl	immediately add dropwise to the 293T cells.

* per 1 reaction

Table 2-5 List of reagents used for virus production

Reagents	Stock solution	Final concentration	per 500 ml
Low-TE buffer	0.5 M TRIS HCl pH8.0	10 mM	10 ml
	0.5 M EDTA pH8.0	0.1 mM	100 µl
	H2O (autoclaved)	-	489.9 ml
HBS	NaCl	8 g	
	KCl	0.37 g	
	Na2HPO4 anydrus	106.5 mg	
	Dextrose	1 g	
	Hepes	5 g	
	H20 (autoclaved)	-	up to 500ml (adjust pH to 7.05 with NaOH)

Full medium change (10%FBS/DMEM) was performed 8hrs later and cells were further incubated for up to 48 hours. Virus supernatant was then harvested at 48 and 72 h post transfection, centrifuged and filtered through a 0.45 µm cellulose acetate filter, concentrated by ultracentrifugation at 23,000 × g 4 °C for 120 min and re-suspended with 1 × RPMI 1640 medium. Virus titres (**Figure 2-8**) were determined by transducing 293T cells using a 2-fold serial dilution of the viral stock and calculated as transducing units (TU) per mL according to the following formula:

$$\text{TU/ml} = \frac{(F \times N \times D \times 1{,}000)}{V}$$

F = % infected cells

N = cell number at the time of transduction

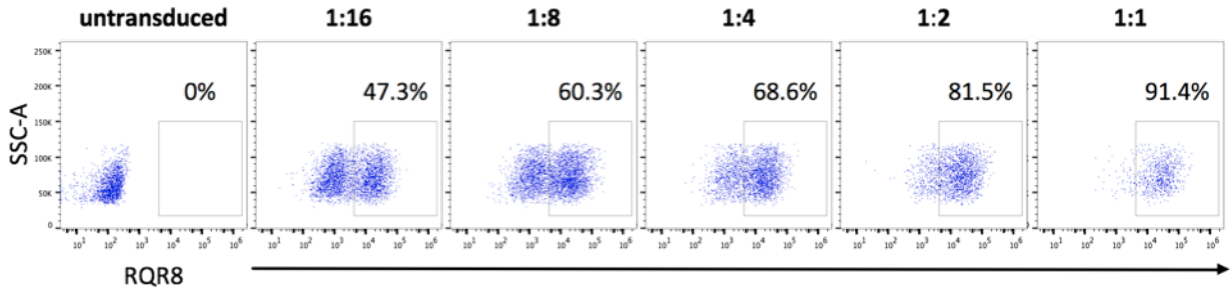
D = fold dilution of viral stock

V = volume (ml) of diluted viral stock

Ultraconcentration generally resulted in titres of 10^{10} TU/ml.

Concentrated virus was either used immediately aliquoted (50-200µl), snap frozen with LN and stored at -80˚C for up to 3 years.

A



B

D	V	N	F	TU/ml
medium	0.05	50,000	0	0
32	0.05	50,000	47.3	1.51 x10^{10}
16	0.05	50,000	60.3	9.65 x10^{9}
8	0.05	50,000	68.6	5.49 x10^{9}
4	0.05	50,000	81.5	3.26 x10^{9}
2	0.05	50,000	91.4	1.83 x10^{9}

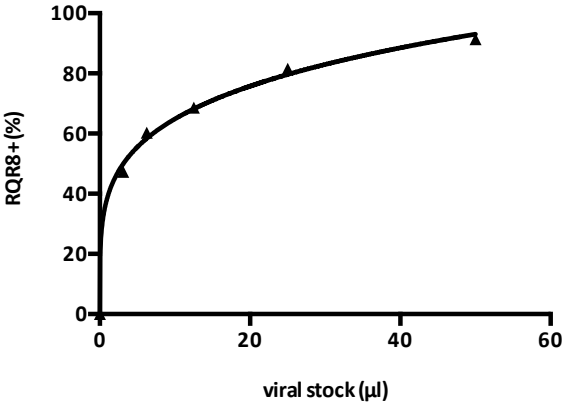


Figure 2-8 Flow cytometry based method for viral vector titration

A. Representative FACS plots for gating strategy, showing a correlation between viral load (viral stock fold dilution) and transduction efficiency (RQR8+ cell percentage, %). Data were used to determine virus titre expressed as transducing units (TU) per ml. B. Percentage of RQR8+ cells as function of the amount (µl) of lentiviral vector added. In this case, the average titre was about 1 x1010 TU/ml.

2.7.2 Cell transduction

Cell lines were transduced with retrovirus in the presence of 8µg/ml polybrene (Sigma-Aldrich). Two days later, transduction efficiency was determined by flow cytometry as percentage of

$CD19^+$ and/or $CD1d^+$ cells or $tdRFP^+$ cells. Where required, positive cells were sorted by immuno-magnetic selection or fluorescence-activated cell sorting (FACS) and further expanded in RPMI 1640 supplemented with 10% Fetal Bovine Serum (FBS, Gibco) and 1% Penicillin-Streptomycin (Pen/Strep, Stem Cell Technologies) (standard culture medium). To generate CAR-engineered iNKT cells (optimised procedure, see Protocol 5 in chapter 3), 6B11-sorted cells were seeded at 1:1 ratio with irradiated (3500 cGy) autologous mononuclear cells (iAPC). An equal number of same-donor mononuclear cells was used as a source of conventional T cells. Next, T and iNKT lymphocytes were activated for up to 48 hours with Dynabeads Human T-Activator CD3/CD28 (ThermoFisher) at 1:1 beads-to-cell ratio in RPMI 1640 medium supplemented with 10% FBS and 1% Pen/Strep with 30 U ml^{-1} IL-15 (Miltenyi Biotech) at a density of 1-5 x 10^4 cells per ml. Activated T and iNKT cells were then transduced at 2-5 MOI in the presence of 4μg/ml polybrene. Within 4 days post transduction, cells were assessed for viability and expansion by Trypan blue as well as purity by flow cytometry. Transduction efficiency was determined by flow cytometry as percentage of $RQR8^+$ cells as previously described[159]. Where required, positive cells were sorted by immunomagnetic selection with anti-CD34-microbeads (Miltenyi), re-plated at the same density and re-stimulated with 1:1 irradiated C1R-CD1d cells, 30 IU/ml IL-15 and 100ng/ml αGalCer. After 7 days cells were reassessed for viability by Trypan blue and purity by flow cytometry using a F(ab')2-Goat anti-Mouse antibody (Invitrogen) and switched to low-IL-15 medium (≤20IU/ml) towards resting phase prior to functional studies. Alternatively, the cells were maintained with 100IU/ml IL-2 and/or IL-15 and harvested during exponential growth phase prior to cryopreservation.

2.8 Antibodies and intracellular staining

CAR^+ cells were identified by using the mouse anti-human APC-CD34 (QBend10, R&D Systems) or FITC-CD34 (QBend10, Abcam) monoclonal antibody (MoAb) against the RQR8 marker or the goat anti-mouse FITC-F(ab')2 fragment (Invitrogen) against the CAR hinge. For T cell phenotyping, the following antibodies were used: mouse anti-human PerCP-Cy5.5-CD3 (OKT3, eBioscience), Pe-Cy7-CD8 (RPA-T8, eBioscience) and eFluor450-CD4 (OKT4, eBioscience). iNKT

cells were defined as TCRVα24^{+}, TCRVβ11^{+}, TCRVα24Jα18^{+} T cells using mouse anti-human PE-TCRVα24 (C15, Beckman Coulter), APC-TCRVβ11 (C21, Beckman Coulter), or FITC-TCRVα24Jα18^{+} (6B11, BD) pairwise combinations. Either a minimum of 0.5 x10^{6} CD3^{+} cells or 200 iNKT cells were recorded to facilitate accurate calculation of the total, CD4^{+} and CD4^{-} iNKT cell frequencies. The B cell panel included the mouse anti-human BV421-CD19 (HIB19, BD Biosciences), APC-CD1d (42.1, BD Pharmingen™ and 51.1, Biolegend), PerCP-eFluor710-CD5 (UCHT2, eBioscience), APC-eFluor780-CD3 (OKT3, eBioscience). 4',6-Diamidino-2-Phenylindole, Dihydrochloride (DAPI) staining was used to exclude dead cells. For intracellular cytokine profiling, T cells were fixed and permeabilized using BD Cytofix/Cytoperm Plus kit as per the recommendation of the manufacturer, followed by staining with mouse anti-human eFluor450-CD3 (UCHT1, eBioscience), PerCP-eFluor710-CD4 (SK3, eBioscience), BUV395-CD8a (RPA-T8, eBioscience), FITC-Perforin (δ-G9, eBioscience and B-D48, 2BScientific), PE-GranzymeB (GB11, eBioscience), APC-IFNγ (4S.B3, eBioscience), PE-IL-2 (MQ1-17H12, eBioscience), PeCy7-IL-4 (8D4-8, eBioscience) and APC-eFluor780-IL17A (eBio64DEC17, eBioscience). Cytokine profile was assessed in resting cells and upon stimulation for 4 hours with Dynabeads (1:1) or PMA/ionomycin (eBioscience) or C1R CD1d cells (1:1) in the presence of Monensin and Brefeldin (eBioscience).

2.9 Cytokine release assay

Resting CAR iNKT and T cells were extensively washed, counted, plated in 96 U-bottom well plates (5x10^{4} cell/well) and stimulated with aCD3/CD28 coated beads at 1:1 ratio. Unstimulated CAR cells and medium only wells were included as controls to measure spontaneous release and background signal. Supernatants were collected after 3 and 8 hours and stored at –80^{o}C until analysis. Released cytokines (GM-CSF, IL-13, IFN-γ, TNF-α, TNF- β, IL-2, IL-4, IL-5, IL-6, IL-7, IL-9, IL-10, IL-15, IL-17A, IL-21, IL-22, IL-23, IL-27, IL-1α, IL-1β, IL-1RA, IL-31, IL-12p70, INF-α) were evaluated by using the ProcartaPlex™ Multiplex Immunoassay (eBioscience) according to manufacturer's instructions. Analyte detection and quantification was performed by Luminex instrument (Bio-rad Bioplex200). The concentration of the samples

was calculated based on the standard curve generated by plotting the expected concentration of the standards against the MFI generated by each standard. Sample values were then normalised to the control values (unstimulated CAR cells and medium only).

2.10 Proliferation assay

Up to 10^4 irradiated C1R-CD1d cells were plated in poly-L-ornithine-coated, flat-bottom 96-well microplates. Where required, αGalCer or vehicle were added for 4 hours before the addition of up to 10^4 CAR-modified cells in RPMI 1640 medium supplemented with 10% FBS, 1% Pen/Strep and 20 IU ml^{-1} IL-15. The cell plate was maintained at 37˚C and 5% CO_2 into the IncuCyte ZOOM® instrument (Sartorius) for up to one week without any further manipulation. CAR cell proliferation was determined by the IncuCyte™ software, with a 24-hr scanning scheduled for every 1 hour with 10x or 4x objectives and using the confluence algorithm according to the manufacturer's instructions (EssenBio protocol 8000-0331-A00).

2.11 *In vitro* real-time monitoring of CAR cell cytotoxic activity

CD1d-mCherry-transduced ARH-77 cells were seeded in a 96-well round-bottom ultra-low attachment (ULA) microplate (Corning) with standard culture medium at a density of 500 cells/well and let settle for 1 hour. Effector cells were then resuspended in standard medium with 20 IU ml^{-1} IL-15 and added at the indicated ratio in triplicates. Wells with targets alone and effectors were included as controls. The microplate was maintained at 37˚C and 5%CO_2 into the IncuCyte ZOOM® instrument for up to one week without any further manipulation and scanned using a phase and a red channel every 1 hour with 10x objective during the first 48 hours and 4x objective from day 3 until the end of the experiment. Targets cells were monitored as red fluorescent objects and quantified with IncuCyte™ software by using red mean image fluorescence (MIF) and red fluorescence area (μm^2/image) according to the manufacturer's instructions (EssenBio protocol 8000-0330-B00). CAR cell proliferation was determined as described in 'Proliferation assay'.

2.12 Cytotoxicity assay

OrangeCell Tracker (CTA type1) or CellTrace™ Violet (CTA type2)-labeled targets (1µM, Invitrogen) were incubated at the indicated ratios with effector cells for 3 hours. Where required, targets were labeled with an antibody mix containing PeCy7-conjugated mouse anti-human CD3 (OKT3, Biolegend), CD56 (5.1H11, Biolegend), CD11b (ICRF44, Biolegend), CD14 (HCD14, Biolegend) and CD16 (B73.1, Biolegend) MoAbs to allow discrimination between $CD19^+$ and $CD19^-$ mononuclear cells. Similarly, in order to characterise Effector-Target Conjugates, CAR-effectors could be labelled with the following fluorophore conjugated mouse anti-human MoAb: APC-CD34 (QBend-10, R&D Systems), PerCP-Cy5.5-CD3 (OKT3, eBioscience), eFluor450-CD4 (OKT4, eBioscience) and PeCy7-CD8 (RPA-T8, eBioscience). As controls, targets and effectors alone were simultaneously incubated to determine spontaneous cell death. Where indicated, targets were also pre-incubated with αGalCer or vehicle at 37˚C for 4 hours before addition of the effector cells. Cells were then harvested and DAPI (CTA type1) or 7-AAD (CTA type2) was added prior to flow cytometric analysis on BD Fortessa Flow Cytometer, using BD FACSDiva software version 6.0. Specific cytotoxic activity was determined as ((% sample ($DAPI^+$, $Orange^+$) − % spontaneous ($DAPI^+$, $Orange^+$)) / (100 - %spontaneous ($DAPI^+$, $Orange^+$))) x 100 or ((% sample (7-AAD^+, $Violet^+$) − % spontaneous (7-AAD^+, $Violet^+$)) / (100 - %spontaneous (7-AAD+, $Violet^+$))) x 100. The gating strategy is shown in (**Figure 2-9**). All assays were run in duplicates or triplicates. Data analysis was performed using FlowJo 10.2.

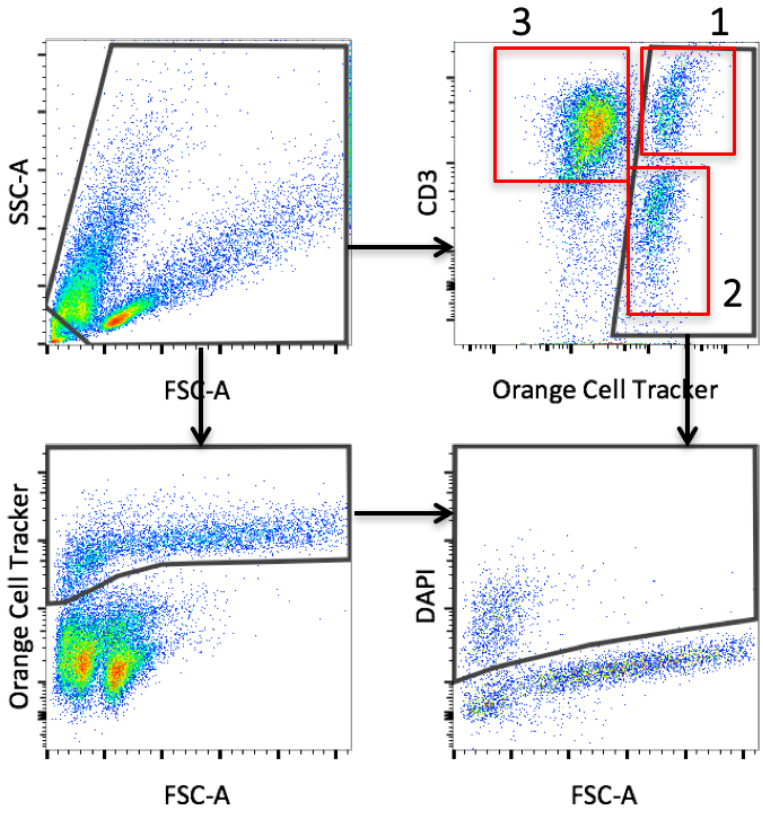


Figure 2-9 Flow cytometry-based cytotoxicity assay - Gating strategy

After excluding cell debris (*top left*), targets were identified as vital dye-labeled events (*bottom left*). For further dissection, conjugates were identified as $CD3^{+}$, vital dye-labeled events (*top right*). Dead targets resulted stained by DAPI (or 7-AAD). In CTA type2, OrangeCell Tracker and DAPI were replaced by VioletCell Trace and 7-AAD. 1: conjugates (targets+effectors); 2: targets only; 3. effectors only. For more complex analysis, see chapter 4.

2.13 Gene expression analysis by Real-Time PCR

Total RNA from primary CLL cells was extracted by using the NucleoSpin RNA kit (Macherey Nagel), followed by cDNA synthesis with RevertAid first strand cDNA synthesis kit (Thermo Fisher Scientific), as per the manufacturer's instructions. For gene expression quantification, RQ-PCR of template cDNA was performed in triplicate on StepOnePlus™ Real-Time PCR System using Taqman Gene Expression Master Mix and Assays (Applied Biosystems). CD1d transcript levels were determined relative to the reference genes *ACTB* and *GAPDH*, using the ΔΔCT method. Taqman probes were *CD1D* Hs00939888_m1, *ACTB* Hs99999903_m1 and *GAPDH* Hs03929097_g1.

2.14 Chromatin immunoprecipitation assays

Primary CLL cells were assessed for histone 3 lysine 4 and histone 3 lysine 27 tri-methylation (H3K4me3 and H3K27me3 respectively) by chromatin immunoprecipitation (ChIP) combined with real-time quantitative polymerase chain reaction (ChIP-RQ-PCR) as previously described[163]. Cross-link was performed within 4 hours from sample collection on PBMC isolated by gradient centrifugation, upon confirmation of B-CLL purity by flow-cytometry.

2.14.1 Chromatin preparation

30 $x10^6$ cells were used per immunoprecipitation. Cells were collected by centrifugation at 1200rpm. Chromatin was prepared using the Shearing ChIP kit (Diagenode). A formaldehyde-based buffer was initially used to cross link proteins to DNA. Sequential washing in cell lysis buffers allowed isolation of chromatin. Chromatin was sonicated at 4°C for 20 minutes in a 0.5/0.5 on/off cycle using high intensity in a Bioruptor UCD-200 (Diagenode). Post-sonication fragments of average 500bp length were confirmed on a 1.5% agarose gel. Sheared chromatin was either used immediately in downstream experiments or was flash frozen in liquid nitrogen and stored at -80°C for later use.

2.14.2 Immunoprecipitation and DNA extraction

Chromatin was diluted at least 10 times in chromatin immunoprecipitation (ChIP) dilution buffer (0.01% SDS, 1.1% Triton X-100, 1.2mM EDTA, 16.7mM Tris-HCL pH 8, 167mM NaCl) containing protease inhibitors. The diluted chromatin was pre-cleared by incubation with magnetic beads (Dynabeads Protein G from Thermo Fisher Scientific) for 1hr at 4°C on a rotating wheel. Pre-cleared chromatin was incubated with 3µg of antibodies overnight at 4°C on a rotating wheel. Protein G magnetic beads were added and incubated for 2-4hrs at 4°C on a rotating wheel. The immunoprecipitates were washed for 5 min at 4°C in a rotating wheel with low salt buffer (0.1% SDS, 1% Triton X-100, 2mM EDTA, 20mM Tris-HCl pH 8, 150mM NaCl), high salt buffer (0.1% SDS, 1% Triton X-100, 2mM EDTA, 20mM Tris-HCl pH 8, 500mM NaCl), LiCl buffer (0.25M LiCl, 1% IGEPAL, 1% sodium deoxicolate, 1mM EDTA, 10mM Tris-HCl pH 8) and 2 times with TE. Immunocomplexes were eluted by adding 150µl elution buffer

(50mM Tris-HCl pH 8, 50mM NaCl, 1mM EDTA and freshly added 1% SDS and 20mg/ml of RNaseA) at 65°C for 4h and a second time for 30 min. Both elutions were pooled and treated with proteinase K. DNA was purified by phenol extraction and DNA precipitation. QRT-PCR was also used to quantify genomic DNA following ChIP.

2.14.3 Real time polymerase chain reaction

QRT-PCR was performed using SYBR Green/ROX qPCR mastermix. Appropriate primers for relevant genomic loci (see below for details of design), template DNA and qPCR mastermix were combined, as per the manufacturer's instructions. Reactions were run in a 96 well plate in the Applied Biosystems 7500 Real Time PCR System using the following programme:

1. 95°C for 10min
2. 40 cycles of: 95°C for 15s, 60°C for 30s, 72°C for 30s

Enrichment of immunoprecipitated DNA was calculated, either relative to input DNA or DNA immunoprecipitated by control IgG antibody, using the ΔΔCT method.

2.14.4 ChIP primers for QRT-PCR

3 primer sets were designed using OligoPerfect™ Designer (**https://tools.lifetechnologies.com)** to analyse 2 regions upstream the ATG start codon at -3047 (distal, DP) and -1240 (proximal, PP) and 1 region within exon 2 at +382 (I2P). The aim was to generate 50-200bp long amplicons. The final sequences consisted of 20-23mer with annealing temperatures between 55-65°C. As per design, there were no potential self-annealing sites, 3' complementarity or potential for hairpin formation.

The corresponding sequences were:

DP 5'-TGGACGTCCGAGAGGTAAGAG and 3'-CACAGTAACCTGGAGATCCACTA,

PP 5'-AATGATGCTGGGGTGTGAGG and 3'-GCACGGCCTGCAAGATTATG,

I2P 5'-CTCCAGATCTCGTCCTTCGC 3'-CTGGGACCAAGGCTTCAGAG.

2.15 Systemic xenograft tumour model

Six-week old NOD/SCID/IL-2Rγ-null (NSG) sex-matched mice were handled in accordance with the 1986 Animal Scientific Procedures Act and under a United Kingdom Government Home Office–approved project licence. The animals were housed at the Hammersmith Central Biomedical Services (CBS) facility, Imperial College London. On the basis of two pilot experiments (see details in chapter 6), the final layout of the *in vivo* experiments was as follows. On day 0 all animals received 5×10^6 luciferase-expressing C1R-CD1d cells by tail vein (iv) injection, followed by BLI monitoring twice a week. Upon confirmation of engraftment defined on the basis of increased photon signal in two consecutive scans performed 72 hours apart, on day 11 the mice were randomized to no treatment or immunotherapy with either T, iNKT, 2nd generation CAR19-T or 2nd generation CAR19-iNKT cells generated from the same donor. Thereafter, BLI was performed twice a week until day 21 and weekly until the end of experiment on day 90. Primary endpoints were overall survival (OS) and tumour-free survival (TFS). Secondary endpoint was brain-TSF. All mice were sacrificed according to the protocol when either experimental or humane endpoints were reached.

2.16 Bioluminescence imaging (BLI)

Bioluminescence images were collected on an IVIS Lumina XR III Imaging System using Living Image software (PerkinElmer). Before imaging, mice were anesthetized and maintained under inhalational anaesthesia via a nose cone with 2% isoflurane (Zoetis UK)/medical oxygen. All mice received a single intraperitoneal (IP) injection of 150mg/Kg D-luciferin (Goldbio) in PBS 10 minutes before scanning. Up to three mice were imaged simultaneously in a 12.5cm field of view (FOV) with minimum target count of 30,000 and exposure times ranging from 0.5 to 2 minutes at medium binning, with additional images acquired at low binning levels to maximize sensitivity and spatial resolution where required. Both ventral and dorsal scans were acquired for each mouse. The dorsal and ventral signals were quantitated separately through region of interest (ROI) analysis using Living Image software and expressed in radiance (unit of

photons/sec/cm^2/sr) as a total signal summation normalized to the ROI area. Where required, normalized background signal from similarly sized ROIs was subtracted.

2.17 Magnetic resonance imaging (MRI), diffusion-weighted imaging (DWI) and MR spectroscopy (MRS)

Brain tumours were assessed and monitored with MRI and MRS in 12 animals. All MRI scans were performed on a pre-clinical 9.4 T scanner (94/20 USR Bruker BioSpec; Bruker Biospin, Ettlingen, Germany) housed at the Biological Imaging Centre, Imperial College London. Mice were anesthetized as described above and positioned prone in a dedicated mouse bed provided with a circulating warm water heat mat to control body temperature. Respiration and body temperature were continuously monitored (1030-MR, SA Instruments, Stony Brook, NY, USA) and the amount of isoflurane and heat delivered were adjusted through the MRI scans to maintain the respiratory rate within the range of 35-45 breaths per minute and the body temperature at 36.5˚C. Brain images were acquired with Paravision 6.01 (Bruker, BioSpin) using an 86mm inner diameter volume transmit quadrature coil combined with an actively decoupled mouse brain array receiver. The imaging datasets consisted of T_1 weighted FLASH, T_2 weighted RARE and echoplanar, diffusion-weighted sequences in sagittal, axial and coronal orientation obtained within 10 minutes and 25 minutes respectively after iv injection of Gadovist (Gadobutrol, Bayer). The contrast agent was diluted in 0.9% saline and used at a concentration of 0.3 mmol/kg in all but 1 mouse. For T1 FLASH images the following settings were applied: T_1 sagittal: TR/TE = 250/2.6 ms; FOV = (18 x 14) mm^2, in plane spatial resolution (58 x 56) µm^2, slice thickness 500 µm, 10 µm slice gap, 20 slices, scan time 6 min 30 s; T_1 axial: TR/TE=320/2.6 ms; FOV = (16 x 14) mm^2, in plane spatial resolution (62 x 61) µm^2, slice thickness 500 µm, 10 µm slice gap, 30 slices, scan time 6 min 30 s, T_1 coronal: TR/TE = 200/3 ms, FOV = (14 x x16) µm^2, in plane resolution (34 x 62) µm^2, 500 µm slice thickness, slice gap 50 µm, 10 slices. Scan time 3 min 50s. T_2 RARE images were generated with: T_2 sagittal: TR/TE = 3000/40 ms, FOV = (18 x 14) mm^2, in plane spatial resolution (70 x 55) µm^2, slice thickness 500 µm, 10 µm slice gap, 20 slices, scan time 5 min. T_2 axial: TR/TE = 2500/45 ms, FOV = (14 x 14)

μm^2, in plane resolution (55 x 55) μm^2, 700 µm slice thickness, slice gap 50 µm, 12 slices. Scan time 4 min. T_2 coronal: TR/TE = 3600/40 ms, FOV = (18 x 14) mm^2, in plane spatial resolution (70 x 55) μm^2, slice thickness 500 µm, 10 µm slice gap, 30 slices, scan time 6 min. Measurement of Diffusion ADC (measurement of diffusion trace, equivalent to mean diffusivity) was performed with EPI readout (4 shots) using the following settings: TR/TE = 6000/18.8 ms, in spatial resolution (135 × 135 × 500) μm^3, B value = 950 s/mm^2, 11 slices, scan time = 8 min (respiratory triggered). All images were analyzed using OsiriX software. For MRS, the voxel was positioned within the pituitary gland avoiding inclusion of surrounding tissue. Field-map based shimming (up to 4^{th} order) was performed prior to the MRS acquisition to optimize the main field homogeneity in the voxel of interest. Single voxel spectra (SVS) were acquired at both long and short echo times (LTE and STE respectively), with: LTE PRESS: TR/TE = 2500/100 ms, voxel size (2 x 1.2 x 1.35) mm3, total scan time 13 min 20 s; STE STEAM: 2500/3 ms, voxel size (2 x 1.2 x 1.35) mm3, total scan time 13 min 20s. Relative quantification of Creatine/NAA, Choline/NAA ratios was computed from the LTE spectra. The spectra were pre-processed (phased, apodized) and quantified afterwards using AMARES (jMRUI software).

2.18 Immunohistochemistry

Sample preparation for immunohistochemistry analysis was performed as previously described [164]. Rabbit anti–human CD19 (polyclonal, Abcam, ab99965) and CD3 (SP7, Abcam, ab16669) were used as primary antibodies to identify tumour and CAR-cells respectively in paraffin sections from mouse tissues. Stained sections were viewed and images acquired using an EVOS XL Imaging System (ThermoFisher Scientific).

2.19 Statistics

2.19.1 Sample size

In vitro assays were planned to achieve at least 3 biological replicates per set of experiments. For in vivo experiments, sample size was determined to show a 30% survival improvement in CAR19-iNKT vs CAR19-T -treated animals at 5% significance and 80% power.

2.19.2 Replicates

The in vitro data were reproduced in technical duplicates or triplicates using samples from different donors and lymphoma patients as a source of CAR-engineered and target cells respectively. For in vivo studies, to show enhanced anti-lymphoma activity of CAR19-iNKT compared to CAR19-T cells, after completing two pilot experiments, two repeats were performed, obtaining similar results.

2.19.3 In vivo randomisation

At the beginning of the in vivo experiment a numeric ID was randomly assigned to each mouse. At the time engraftment, all animals were assessed in a consecutive order according to their ID, from the smaller to the larger. Same sex mice with comparable weight were assigned to one of the 5 treatment arms only based on the bioluminescent signal, aiming to ensure an equal distribution of tumour burden across the groups.

2.19.4 Statistical analysis

Statistical analysis was performed on GraphPad Prism 7 software. For comparisons between two groups, the Wilcoxon (paired) or Mann–Whitney *U* (unpaired) test were used, with correction for multiple t tests according to the two-stage step-up method of Benjamini, Krieger and Yekutieli. For comparison between more than two groups, either one of the following tests were performed depending on the number of variables: non-parametric Friedman (paired) or Kruskal-Wallis (unpaired) test with post-hoc Dunn's test (one variable, non-parametric for one-way ANOVA) or two-way ANOVA adjusted by Tukey (more than one variables). Survival was calculated using the Kaplan-Meier method, with log rank analysis for comparing survival

between groups. All experimental data are presented as mean ± standard error mean (S.E.M.) All P-values given are two-tailed values. A P-value below 0.05 was considered significant.

3 Development and optimization of protocol for manufacturing of clinical scale CAR-iNKT cells

3.1 Introduction

iNKT cells are rare, CD1d restricted T lymphocytes comprising ~0.01-0.1% of circulating CD3+ cells in humans[86-88]. Owing to their innate-like reactivity, robust, direct and indirect anti-tumour activity and ability to modulate alloreactivity, they represent a very attractive platform for adoptive immunotherapy. However, their very low frequency, which is even lower in cancer patients than in healthy individuals[100,165,166], has been a major obstacle for the clinical development of iNKT cell-based adoptive therapy so far.

Isolation and selective expansion of TCRVα24Jα18+ (moAb 6B11+) cells are important requirements for iNKT cell manipulation *in vitro*. Two main approaches have been described. One approach entails iNKT cell expansion from bulk PBMCs in the presence of the iNKT cell-specific agonist αGalCer and IL-2[167]. A more effective procedure, described by Exley et al., relies on upfront moAb 6B11-based iNKT cell selection followed by their specific activation and expansion with glycolipid compounds presented by $CD1d^{+}$ APCs[168]. Such method allows to establish iNKT cell lines in 2-3 weeks. Non-specific mitogens, e.g. activating anti-CD3 moAb, have been also used with success, but their application remains limited to highly purified iNKT cell preparations and/or clones established by previous rounds of αGalCer-CD1d-driven expansion[88,169].

The curative potential of CAR technology has been supported over the last 20 years by unprecedented responses in patients with refractory/relapsed B cell malignancies. However, inconsistent clinical outcomes, safety issues and unsustainable costs may limit widespread clinical applications. Indeed, given the expression of CD1d on malignant B cells, CAR

engineering of iNKT cells may represent a more suitable platform for CAR immunotherapy than bulk conventional T lymphocytes. Hence, the first aim of my study was to generate CAR19-iNKT cells to investigate their therapeutic potential against B lymphoproliferative disorders.

When I started to work on this project, there was no literature suggesting how best to CAR-engineer iNKT cells. By contrast, conventional T cells have been successfully manipulated and several protocols have been published over the past 20 years. Therefore, I first planned a preliminary set of experiments aiming to explore whether the procedures validated for conventional T cells engineering could be applied to iNKT cells.

3.2 Generation of CAR19-T cells

3.2.1 Expression of CAR19 in primary human T lymphocytes – standard procedure

Standard methods for CAR19-T cell manufacturing include steps of (1) PBMC enrichment, usually by gradient centrifugation; (2) $CD3^+$ cell activation by means of CD3-specific stimulating agents, mostly CD3/CD28 agonists; (3) viral transduction of activated T lymphocytes using retro- or lenti- viral vectors encoding for the cell surface receptor with MOI up to 20; (4) short-term expansion of the transduced T cell population to achieve clinically relevant numbers for adoptive therapy, generally 1-3 weeks depending on the protocol[170].

Based on this reference approach, I produced lentiviral supernatant carrying a 2^{nd} generation CAR19 and transduced primary T cells upon activation with aCD3/CD28 beads for 48 hours at an MOI of 10. The detailed procedure is described in *'Material and Methods'*. Twelve independent experiments were performed using either fresh PBMC or frozen lymphapheresis samples obtained from eight different healthy donors. The transduction efficiency was assessed by flow cytometry within 3 days after gene transfer on the basis of the RQR8 marker/suicide gene co-expressed with the CAR19 protein, as the percentage of RQR8 positive cells relative to untransduced total T cells. Transduction was successful in all cases (**Table 3-1**). The mean transduction efficiency was 55.63% ± 4.875 (range 20.6% - 78.2%, **Figure 3-1**).

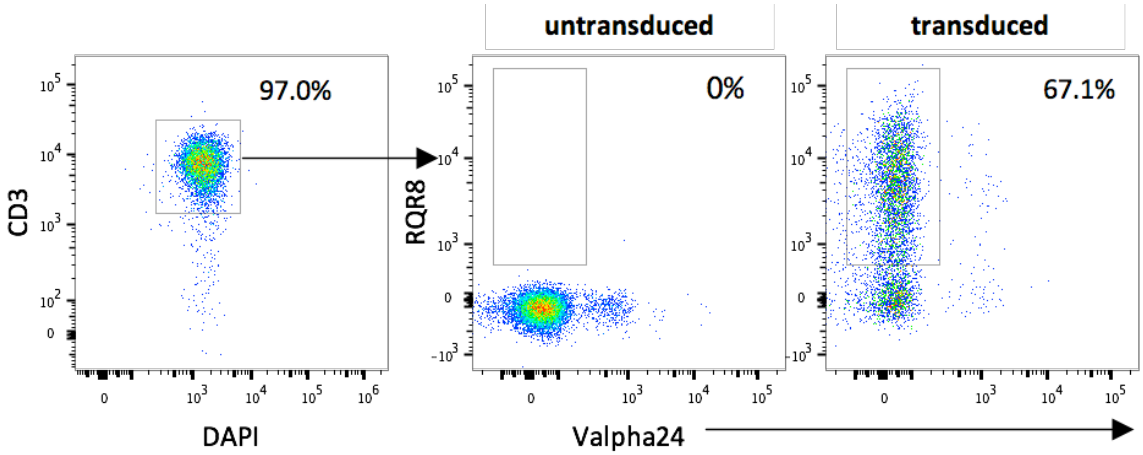


Figure 3-1 Assessment of CAR19-T cells by flow cytometry

Representative dot plots illustrating the gating strategy for assessment of CAR19 transduction efficiency of conventional T cells. Gating on live $CD3^+$ cells (*left*), CAR-cells were identified as $RQR8^+$ cells (*right*) relatively to untransduced control cells (*middle*).

Table 3-1 CAR19-T cell transduction efficiency according to standard procedure

Exp	ID	Source	Baseline		CAR19-T
			TNC	T %	%
Fresh samples					
1	#1 PB	PB	3.10E+07	40.0	56.3
2	#2 PB	PB	1.20E+07	52.1	57.5
3	#2 PB	PB	2.25E+07	55.5	44.2
4	#3 PB	PB	5.50E+07	53.1	41.4
5	#4 PB	PB	2.53E+07	41.5	68.5
6	#1 LAph	LAph	2.50E+09	57.5	67.5
Frozen samples					
7	#2 LAph	LAph	1.12E+08	43.2	41.2
8	#2 LAph	LAph	1.20E+09	40.6	20.6
9	#2 LAph	LAph	7.70E+08	44.4	49.4
10	#3 LAph	LAph	7.00E+08	51.0	73.9
11	#4 LAph	LAph	8.00E+08	60.9	78.2
12	#5 LAph	LAph	6.00E+08	34.6	68.9
		Mean			55.63
		S.E.M.			4.875
		Min			20.60
		Max			78.20

Exp: experiment number; ID: donor identifier; TNC: total nucleated cell count; PB: peripheral blood; LAph: lymphapheresis

3.2.2 Expansion of CAR19-T cells from transduced T cells according to standard procedure

Next, I sought to evaluate the expandability of 2nd generation CAR19-T cells cultured under different conditions. When maintained in standard T cell medium (TCM), i.e. PCM supplemented with IL-2 100IU/mL, transduced T cells showed a stable or modestly increased proportion of CAR19+ T cells over a period of 3 weeks (n=3). However, the absolute CAR19-T cell number increased by nearly 100-fold (mean ± S.E.M.: 97.18 ± 29.64; **Figure 3-2**).

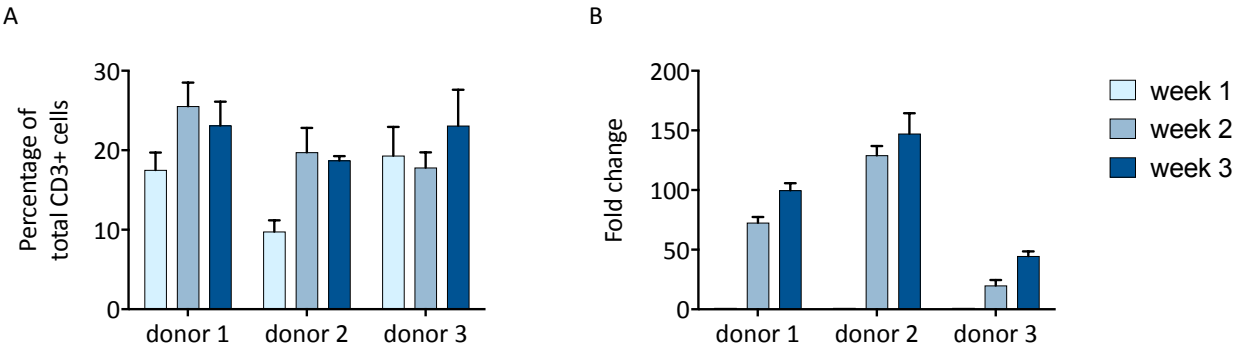


Figure 3-2 CAR19-T cell percentage and fold change over 3 weeks

Bar graphs summarising the percentage of CAR19-T cells as assessed by flow cytometry (A) and the fold change of live transduced cells as assessed by Trypan blue (B). There was no significant difference in the amounts of CAR19-T cells between week 2 and 3 (n=3; error bars show S.E.M. of technical triplicates).

Likewise, stimulation with CD19+ APCs, i.e. irradiated AK (CD19high) and C1R (CD19low) B lymphoblastoid cells at different responder-stimulator ratios, induced a similar increase of total cell number, with minimal preferential expansion of 2nd gen CAR19+ cells compared to control cells maintained in IL-2 (**Figure 3-3**).

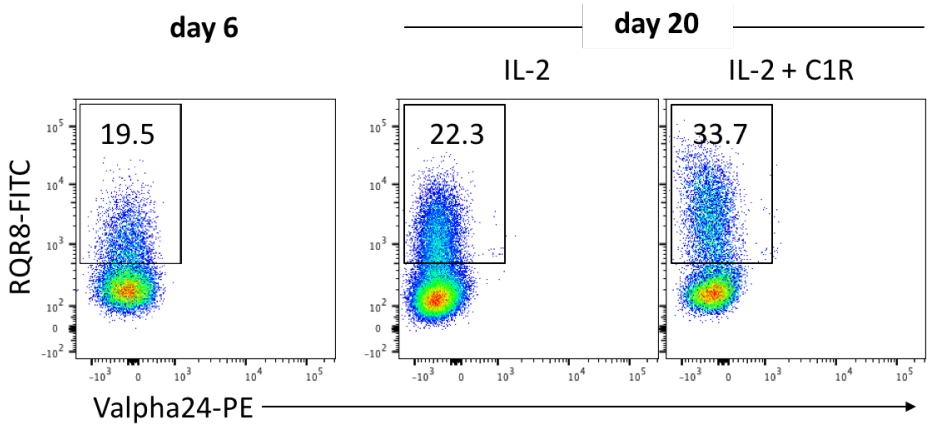


Figure 3-3 Impact of different expansion methods on CAR19-T cells

Representative FACS plots of 2nd generation CAR19-T cells (*left*) expanded in the presence of IL-2 (*middle*) or IL-2 and irradiated C1R cells (*right*) at responder (CAR19-T)-stimulator (C1R) ratio of 1:1. C1R cells were added 6 days after aCD3/CD28 bead stimulation, with only mild improvement of CAR19+ cell percentage at the end of the protocol compared to control cells maintained in IL-2 only TCM.

3.2.3 Selection of CAR19-T cells

In order to functionally characterize CAR19-expressing cells, I transduced T cells with 2nd and 3rd generation CAR19 virus and immunomagnetically purified RQR8^{+} cells by the end of the first week. Briefly, CAR19-T cells were labelled with an anti-CD34-QBend/10 antibody conjugated to paramagnetic beads either directly (anti-CD34 microbeads kit, Miltenyi; method 1) or indirectly (anti-CD34-QBend/10-APC combined with anti-APC microbeads kit, Miltenyi; method 2). Starting from 1.5 x10^{7} transduced T cells, of which 54.2% were RQR8^{+} (n=4 samples), I obtained approximately 7.45 x10^{6} CAR19-T cells, that were >90% pure after a single round of positive immunomagnetic selection (**Table 3-2**). The selection efficiency was comparable with both methods, leading to 90.8% ± 7.7 and 91.8% ± 7,6 pure CAR19-T cells respectively (**Figure 3-4**).

Table 3-2 CAR19-T cell selection

Exp	ID	CAR	Pre-selection	Post-selection	
				Method 1	Method 2
1	#5 PB	2nd gen	57.6	99.6	98.9
2	#5 PB	3rd gen	69.2	96.8	99.0
3	#6 PB	2nd gen	66.3	99.4	99.5
4	#6 PB	3rd gen	23.6	68.1	68.7
	mean		54.2	90.8	91.8
	S.E.M.		±10.5	±7.7	±7.6

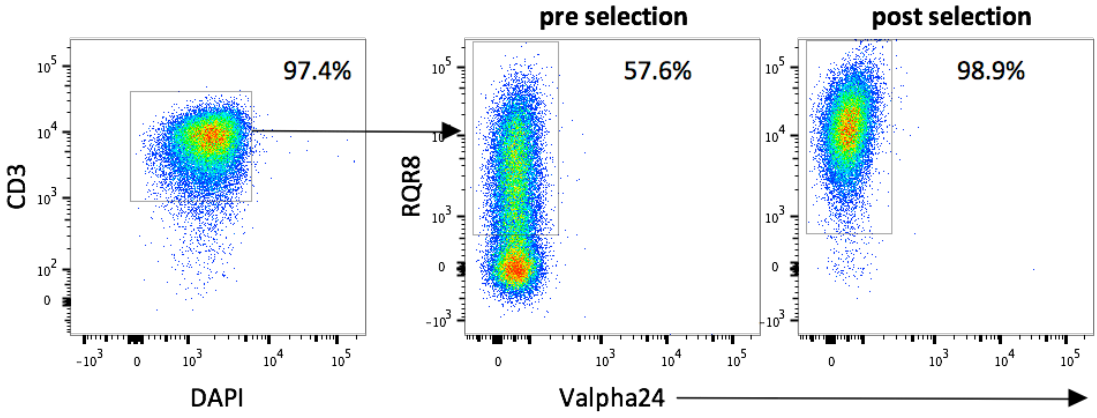


Figure 3-4 CAR19-T cell selection.
Representative FACS plots showing CAR19-T cells pre and post RQR8-based selection. In this example, pure CAR19-T cells were obtained by sequentially labelling transduced cells with anti-CD34-QBend/10-APC moAb and anti-APC microbeads.

Finally, I expanded purified CAR19-T cells in TCM with or without irradiated CD19^{+} C1R cells for one week. In the presence of APC at a responder-stimulator ratio of 1:1, 2nd generation CAR19-T cells displayed a 23-fold increase, that was approximately 10 times greater than control cells maintained in IL-2 supplemented medium (P=0.0033, **Figure 3-5**). By contrast, expansion of C1R stimulated 3rd generation CAR19-T was irrelevant, at least in part due to activation induced cell death (AICD).

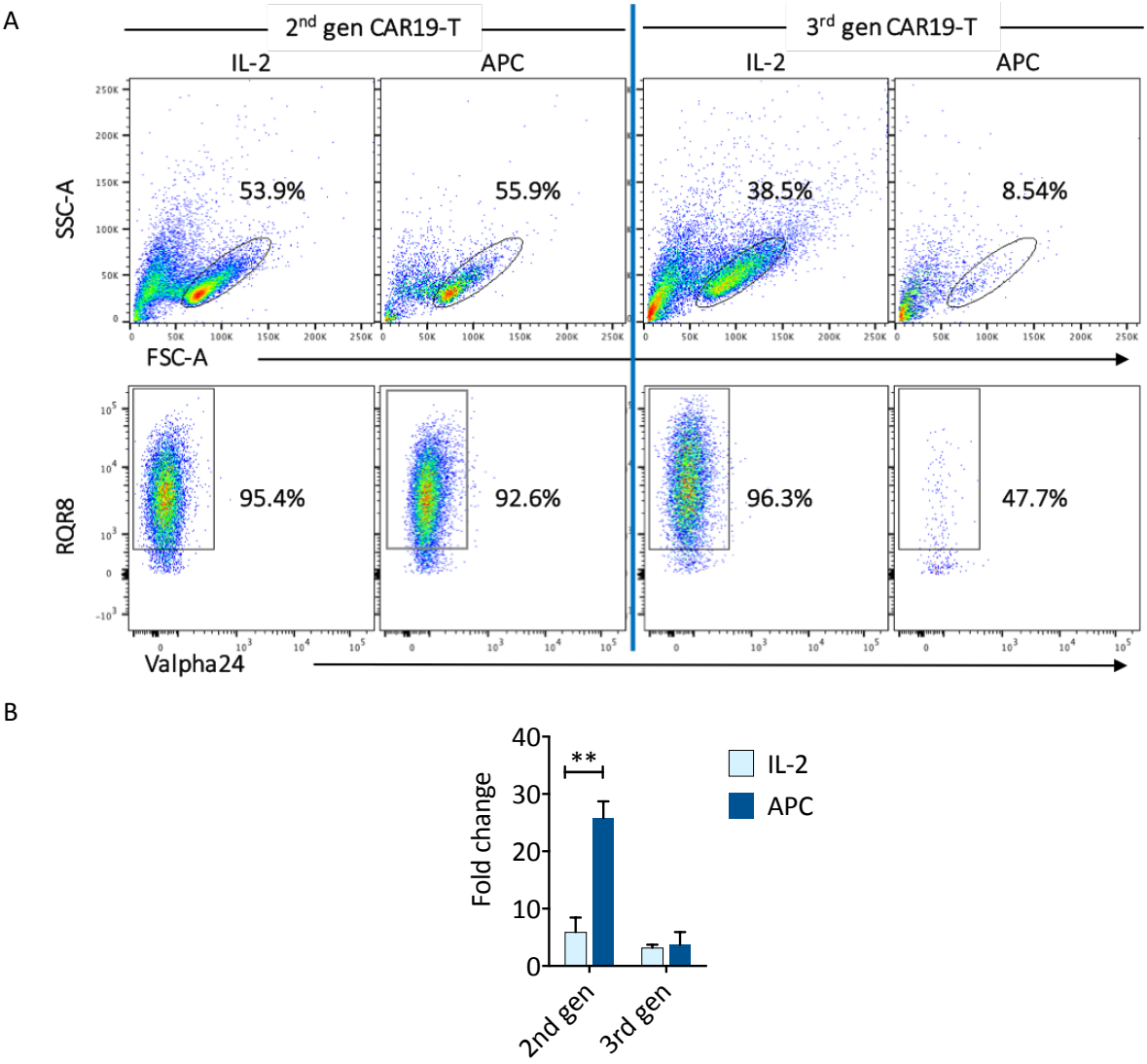


Figure 3-5 CAR19-T cell expansion post selection

Purified (>90%) CAR-T cells were stimulated with irradiated C1R and counted 7 days after stimulation. Control cells were cultured in IL-2 100 IU/ml (n=2). At assessment on day +7, all populations were proliferating but the C1R-stimulated 3rd generation CAR19-T one, where the very few live cells (live gate in the top right representative FSC-A/SSC-A plot) were mainly untransduced T cells (A). As a result, C1R-stimulated 2nd and 3rd CAR19-T cells achieved a 25.8±2.9 and 3.7±2.2 -fold increase respectively, compared to 5.9±2.5 and 3.2±0.6 of control 2nd and 3rd generation CAR19 -T cells (B). Data are shown relative to post-selection pre-stimulation CAR-cell number. Error bars represent S.E.M. of technical triplicates.

3.3 Generation of CAR19-iNKT cells

Having set up a method to transduce primary human T lymphocytes that was representative of the most commonly used and clinically validated methods for CAR-T cell adoptive therapy[171], I aimed to generate CAR19-iNKT cells by using a similar procedure, although with some modifications as required by the very low frequency of circulating iNKT cells compared to conventional T cells.

3.3.1 Protocol 1

As mentioned above, selective expansion of 6B11+ cells is key for iNKT cell manipulation *in vitro.* Towards this goal, I first tested an upfront expansion-based approach (*protocol 1)*, i.e. incubation of bulk PBMCs in the presence of the iNKT cell-specific agonist αGalCer followed by transduction. Specifically, peripheral blood or cord blood MNC were resuspended in TCM supplemented with αGalCer at 100 ng/ml and plated in a 24-well plate at 1-2 x10^6 cells/ml; IL-2 was added on day 3 at 100 IU/ml and every 3-4 days thereafter until assessment on day 10. Transduction was performed during week 3 of expansion, i.e., during exponential growth phase.

The rationale behind *protocol 1* was to achieve higher iNKT cell numbers at the time of gene-transfer, ideally comparable to those of conventional T cells under standard CAR-engineering protocols, while minimizing the requirement for additional manufacturing steps. However, this protocol consistently failed to provide a pure population of iNKT cells from PBMCs (n=7, mean ±S.E.M. iNKT cells 26.65% ±11.39, **Table-3-3**) and resulted in low transduction efficiency of iNKT cells (n=4, mean ±S.E.M. 3.17% ±1.68, range 0.92%-8.17%, **Figure 3-6**). I then attempted the incorporation of a moAb 6B11-based selection step prior to transduction (*protocol 1b*) and found that the subsequent transduction efficiency of iNKT cells was improved (n=4, mean ±S.E.M. 45.76% ±12.17, range 12.64%-68.5%, **Figure 3-6**), suggesting that purity of iNKT cells at the time of lentiviral infection might be a key determinant for successful gene transfer.

Table-3-3 Upfront expansion of iNKT cells from mononuclear cells in the presence of αGalCer

Exp	ID	Blood product					Protocol for expansion					Post expansion	
		source		TNC	T	iNKT	αGalCer	IL2			days	TNC	iNKT
							ng/mL	IU/mL					
				x 10^6	%	%	d1	d1	d3	d6		x 10^6	%
1	#1 PB	frozen	PBMCs	10.00	42.3	0.023	100	500	500	500	20	34	9.85
2	#1 PB	fresh	PBMCs	10.00	49.9	0.050	100	500	500	500	14	22	18.95
3	#7 PB	fresh	PBMCs	31.00	68.5	0.020	100	100	100	100	17	31	4.58
4	#7 PB	fresh	PBMCs	12.00	69.5	0.051	100	-	10	100	13	25	28.00
5	#8 PB	fresh	PBMCs	25.00	69.8	0.110	100	100	100	100	17	44	4.00
6	#2 PB	fresh	PBMCs	22.50	55.5	0.120	100	10	10	10	21	30	30.60
7	#3 PB	fresh	PBMCs	11.00	50.9	2.060	100	-	1	10	8	24	90.60
8	#1 CB	fresh	CBMNCs	65.00	45.9	0.067	100	10	10	10	20	35	31.90
9	#2 CB	fresh	CBMNCs	89.00	20.0	0.108	100	10	10	10	18	38	72.20
10	#1 CB	fresh	CBMNCs	65.00	45.9	0.067	100	10 + IL7 100	10 + IL7 100	10 + IL7 100	20	18	21.70
11	#2 CB	fresh	CBMNCs	89.00	20.0	0.108	100	10 + IL7 100	10 + IL7 100	10 + IL7 100	18	22	68.40
												Mean	**34.62**
												S.E.M.	8.85
												Min	4.00
												Max	90.60

Live cell counts (TNC) as assessed by Trypan blue and percentages of T and iNKT cells as assessed by flow cytometry.

TNC: total nucleated cell count; PB: peripheral blood; CB: cord blood; PBMCs: peripheral blood mononuclear cells; CBMNCs: cord blood mononuclear cells

3.3.2 Protocol 2

Therefore, I set up a second series of experiments characterized by upfront selection followed by selective expansion of iNKT cells prior to transduction (*protocol 2*). Specifically, selected iNKT cells were plated in a U-bottom 96-well plate at a density of $1x10^4$ cells/200µl TCM/well, in the presence of 1:1 irradiated (3500 rad) autologous mononuclear cells (iAPC) and αGalCer 100ng/ml. 100IU/ml IL-2 was added on the following day. Cells were reassessed for expansion and purity on day 10-12 and transduced with CAR19-lentivirus in a 24-well plate, at a density of 3×10^5 cell/ml as per conventional T cell standard protocol, during exponential growth phase, between day 14 and 24. The rationale behind *protocol 2* was to improve the transduction efficiency while ensuring an adequate number of iNKT cells at the time of transduction, based on the very successful procedure for *in vitro* expansion of iNKT cells published by Exley et al. in 2010[88]. Indeed, in all cases I obtained $\geq 1 \times 10^6$ iNKT cells within 2 weeks (**Table 3-4**) and the subsequent CAR19 engineering process was more efficient (n=11, mean ±S.E.M. 32.66% ±5.43, range 13.8%-69.5%, **Figure 3-6**). Yet, the overall procedure was not optimal: (1) the average CAR transduction efficiency was < 50%; (2) the time of in vitro manipulation was relatively long, comprising 14 days prior to transduction and another additional 2-to-3 weeks to further purify and expand CAR-iNKT cells.

Table 3-4 Expansion of upfront selected iNKT cells

Exp	ID	Blood product					Post selection		Expansion		Post expansion	
		Source		TNC	T	iNKT	iNKT	Live cells	Stimulated iNKT	days	TNC	iNKT
				x 10^8	%	%	%	x 10^3	x 10^3		x 10^6	%
1	#2 LAph	frozen	lymphapheresis	7.700	44.4	0.020	88.2	350.0	10.0	14	9.8	>95
2	#2 LAph	frozen	lymphapheresis	1.100	45.0	0.020	96.8	10.0	10.0	14	8.2	>95
3	#3 LAph	frozen	lymphapheresis	7.000	51.0	0.200	97.6	650.0	10.0	14	10.1	>95
4	#2 CB	frozen	CBMNCs	0.030	22.0	0.130	96.1	6.0	6.0	14	6.7	>95
5	#1 BC	fresh	buffy coat	6.500	66.3	0.068	91.8	250.0	10.0	14	10.5	>95
6	#2 PB	fresh	PBMCs	0.160	65.9	0.220	96.5	22.0	22.0	14	24.0	>95
7	#6 PB	fresh	PBMCs	0.440	52.0	0.040	97.3	9.0	9.0	14	9.4	>95
8	#7 PB	fresh	PBMCs	0.520	70.0	0.022	73.9	7.0	7.0	14	4.2	>95
9	#8 PB	fresh	PBMCs	0.500	62.0	0.200	90.0	60.0	60.0	14	7.5	>95
10	#9 PB	fresh	PBMCs	0.350	60.4	0.370	72.4	30.0	30.0	14	18.0	>95
11	#3 CB	fresh	CBMNCs	1.100	20.0	0.520	95.0	110.0	10.0	14	38.0	>95
										Mean	**13.3**	
										S.E.M.	2.9	
										Min	4.2	
										Max	38.0	

Live cell counts as assessed by Trypan blue and percentages of T and iNKT cells as assessed by flow cytometry

TNC: total nucleated cells; LAph: Lymphapheresis; PB: peripheral blood; CB: cord blood; PBMCs: peripheral blood mononuclear cells; CBMNCs: cord blood mononuclear cells

3.3.3 Protocol 3

In an effort to shorten the length of the manufacturing process, I sought to explore whether iNKT cells could be effectively engineered immediately after 6B11-selection and set up a micro-scale procedure where iNKT cells were plated in a 96-well U-bottom plate at a density of 1 x 10^4 cells/well in the presence of 1:1 iAPC and αGalCer 100ng/ml. IL-2 100 IU/ml was added 12 hours later, followed by CAR19-lentiviral transduction within 24-48 hours (*protocol 3*). CAR-transduced cells could be assessed only at the end of the second week of culture, according to the cell growth kinetics of αGalCer-expanded iNKT cells. In 4 out of 4 experiments less than 20% cells were $RQR8^+$ (mean ±S.E.M. 13.12% ±2.089, range 8.45%-18.3%, **Figure 3-6**).

There is a plethora of comparative studies addressing how best to stimulate and expand conventional T cells for the purposes of adoptive cancer immunotherapy. Specifically, it has been demonstrated that aCD3/CD28 beads are associated with greater and faster T cell growth compared to APC-based strategies, including the so-called 'rapid expansion protocol'. Hence, aCD3/CD28 beads have been incorporated in most GMP-grade procedures for CAR-T cell manufacturing[172]. Furthermore, lentivirus DNA integration is more efficient in highly and homogeneously activated T cell populations[173]. Therefore, I addressed whether aCD3/CD28 beads would allow to improve CAR19-iNKT transduction efficiency, while reducing the time of *ex vivo* manipulation.

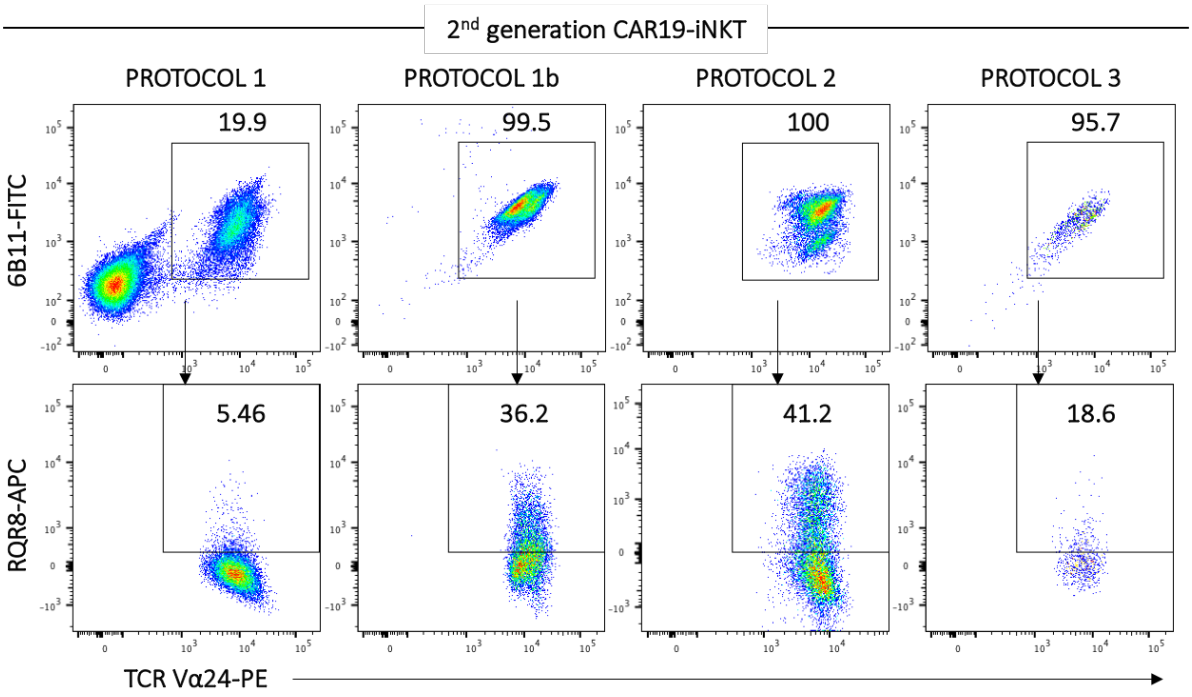


Figure 3-6 CAR19-iNKT cell engineering – protocols 1-3
Representative flow cytometry plots of CAR19-iNKT cell transduction efficiency according to protocol.

3.3.4 Protocol 4

As previously mentioned, non-specific mitogens such as anti-CD3 moAb have been proved to successfully activate iNKT cells, although their application remains limited to highly purified cell preparations. However, there is no literature addressing the effect aCD3/CD28 beads on iNKT cells.

In a preliminary set of experiments, I tested the feasibility of aCD3/CD28 beads stimulation as a method to activate and expand iNKT cells selected from frozen lymphapheresis (n=3) and fresh PB (n=2) products. In 4 out of 5 cases, a ≥29-fod increase was observed by day 9 (**Table 3-5**).

Table 3-5 CAR19-iNKT cell expansion with aCD3/CD28 beads

Exp	ID	Source		Blood product			Post selection		Expansion		
				TNC	T	iNKT	iNKT	Live cells	PRE	1 week POST	
				x 10^6	%	%	%	x 103	x 103	x 103	fold
1	#2 LAph	frozen	lymphapheresis	150	42.7	0.018	87.9	10.0	10.0	300.0	30.0
2	#3 LAph	frozen	lymphapheresis	140	58.9	0.185	96.5	120.0	10.0	350.0	35.0
3	#4 LAph	frozen	lymphapheresis	500	49.1	0.130	95.2	250.0	10.0	290.0	29.0
4	#10 PB	fresh	PBMCs	42	61.0	0.027	84.2	4.8	4.8	170.0	35.4
5	#11 PB	fresh	PBMCs	65	81.0	0.008	65.4	6.5	6.5	20.0	3.1

Live cell counts as assessed by Trypan blue and percentages of T and iNKT cells as assessed by flow cytometry.

TNC: total nucleated cells; LAph: Lymphapheresis; PB: peripheral blood; PBMCs: peripheral blood mononuclear cells.

The only exception was represented by a sample with relatively lower 6B11^{+} cell purity after immunomagnetic selection (**Figure 3-7**).

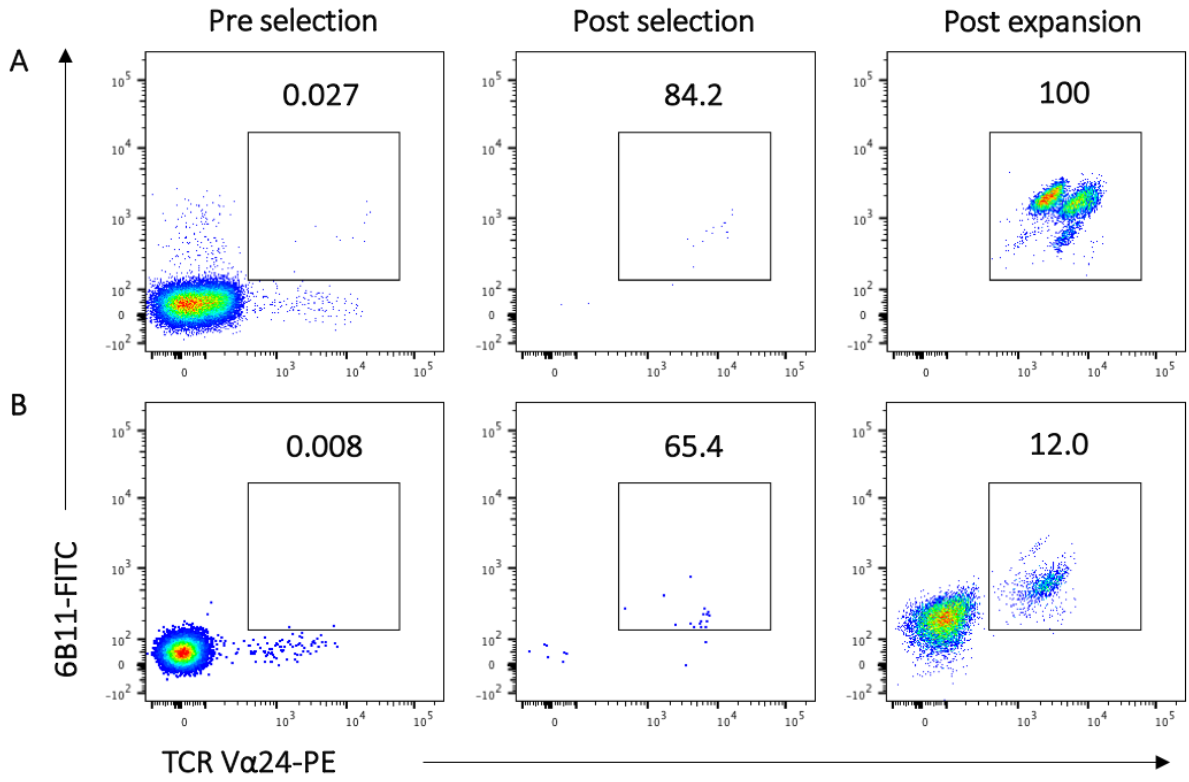


Figure 3-7 Low-purity iNKT cell expansion with aCD3/CD28 beads

6B11^{+} sorted cells from healthy volunteers #10 PB (A) and #11 PB (B) were 84.2% and 65.4% respectively (*middle panels*). Both samples were stimulated with aCD3/CD28 beads. At reassessment, preferential expansion of conventional T cells was observed in the sample with initial lower 6B11^{+} cell purity.

Next, I compared the expansion of upfront selected, unmodified iNKT cells under 3 different conditions: a) 1: 1 aCD3/CD28 beads, b) 1 : 1 αGalCer-pulsed iAPC and c) 1 : 1 aCD3/CD28 beads and iAPC, without αGalCer. As shown in **Figure 3-8**, iNKT cells could be expanded >450-fold in 16 days by all 3 methods, with a yield of ≥50 x10^{6} cells from an initial 1 x10^{5} iNKT cell count (n=2). However, the expansion was more substantial in the aCD3/CD28 stimulated wells.

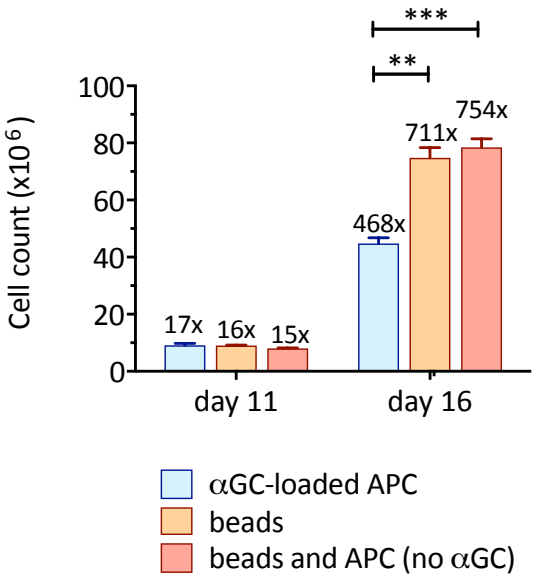


Figure 3-8 Expansion of upfront selected iNKT cells with aCD3/CD28 beads

Comparison of different strategies for expansion of iNKT cells. Bars represent the final cell counts, whereas the corresponding fold increase is shown on top of each bars. iNKT cells were expanded >450 fold in less than 3 weeks by all methods. Bead-based strategies were associated with a higher increase. αGC: αGalCer, Beads: aCD3/CD28 beads.

Encouraged by the consistent purity of the iNKT cell products generated according to my optimized 6B11-based magnetic sorting (MACS) procedure (see '*Material and Methods*'), I decided to use 1:1 aCD3/CD28 beads instead of αGalCer-pulsed iAPC as a method for iNKT cell activation before transduction (*Protocol 4*). Indeed, transduction efficiency greatly improved (n=8, mean ±S.E.M. 62.2% ±7.745, range 34.6%-91.5%), although at the expense of cell viability. Specifically, viable cells were very few one week after viral infection (**Figure 3-9**), which often precluded the possibility of completing downstream functional studies and represented the main limitation in the prospect of clinical applications.

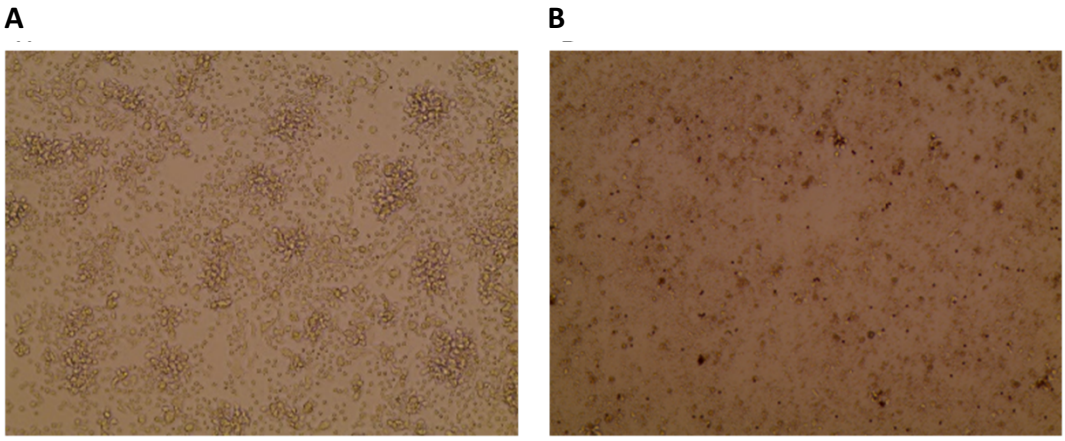


Figure 3-9 Viability of CAR19-transduced iNKT cells engineered according to protocol 4
Representative images acquired on day +3 of protocol 4, showing viability of untransduced control (A) and transduced (B) iNKT cells exposed to CAR19 lentivirus (day 0) after upfront selection (day -2) and 48h-activation with aCD3/CD28 beads. While untransduced iNKT cells were forming large cell clusters, indicating active proliferation, most transduced cells were dead. That was also confirmed by Trypan blue staining (not shown).

3.3.5 Protocol 5

As previously mentioned, there is a dearth of information about the impact of aCD3/CD28 stimulation on iNKT cells, although strong stimulation with anti-CD3 moAb *in vivo* has been associated with activation-induced anergy[43] and cell death[12] of iNKT cells. By contrast, *in vitro* co-stimulation of conventional T cells by anti-CD28 moAb has been demonstrated to induce telomerase expression and activity, with detrimental effects particularly on $CD8^+$ conventional T cells, which acquire an effector memory phenotype, become dysfunctional and may eventually die within 14 days[42]. Furthermore, while promoting expansion of Ag-nonspecific T cells, aCD3/CD28-mediated stimulation has been associated with depletion of particular Vβ subsets, including $V\beta11^{+}$[44].

IL-15 has been shown to inhibit AICD of T cells[174]. Interestingly, it has been also proved to play a central role in iNKT cell biology, by promoting cell survival through induction of BCL2 family proteins[175], while inducing expression of effector molecules such as granzymes and IFN-γ. IL-7 is another common cytokine receptor gamma-chain-dependent (γc) cytokine with well-recognized role in conventional T cell survival and homeostasis[176]. More recently, a STAT5-

driven transcriptional program downstream of IL-7 signalling has been also shown to promote survival and maintain iNKT cell homeostasis through similar mechanisms[177].

Finally, iNKT cells interact with CD1d-expressing APCs, including monocytes and $CD19^+$ B cells within PBMCs, with a propensity to autoreactivity in response to endogenous lipid ligands that may contribute to their activated/memory phenotype[90,178]. On this basis, co-culture of iNKT cells with iAPC as nurturing cells has been widely used to provide pro-survival signals capable of supporting selective expansion and sustained proliferation of such CD1d-resticted lymphocytes[88,179]. In addition, the usage of $CD19^+$ artificial APC has been incorporated in a number of GMP-procedure for rapid expansion and clinical scale production of CAR19-T cells[180], suggesting that the co-existence of autologous $CD19^+$ B cells at the time of CAR19-enginerring of iNKT cells could also favour preferential expansion of the newly generated CAR19-expressing cells, with a positive impact on the final transduction efficiency.

Therefore, I set up a final series of experiments aimed to compare side-by-side the effect of the incorporation of different cytokines and/or iAPC (without αGalCer) within protocol 4, in combination with aCD3/CD28 beads in the pre-transduction activation step. As shown in **Figure 3-10**, supplementation of TCM with either 100 IU/mL IL-7 or 100 IU/mL IL-15 instead of IL-2 during the first week of the CAR engineering protocol was sufficient to prolong iNKT cell viability in vitro, without producing significant effects on transduction efficiency (n=3, 81.13% vs 84.04% vs 81.9% for IL-2, IL-7 and IL-15 respectively). Further incorporation of 1 : 1 iAPC allowed to consistently produce the highest numbers of long-term viable and actively proliferating CAR19-iNKT cells, the best results being associated with the combination of iAPC plus IL-15 supplemented medium (protocol 5; n=6, transduction efficiency mean ±S.E.M. 76.87% ±5.475, **Figure 3-11**). Notably, the MOI was reduced down to 2-5, i.e. 2 to 10µl of lentiviral supernatant per experiment were sufficient, without affecting the transduction efficiency.

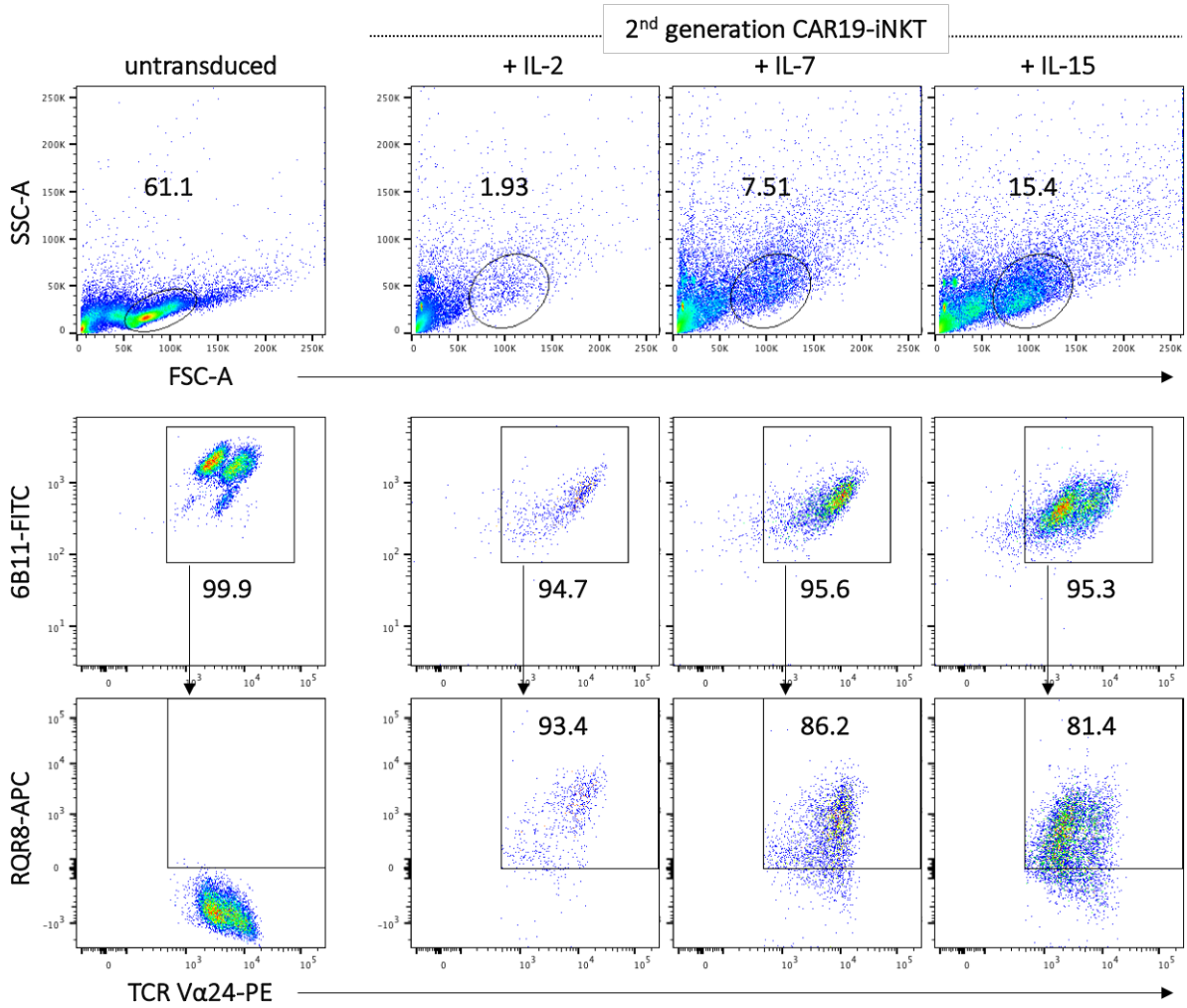


Figure 3-10 CAR19-iNKT cell engineering – protocol 4

Flow cytometry assessment on day +3 post transduction. Representative plots of upfront selected, pure 6B11^{+} cells transduced upon pre-activation with aCD3/CD28 beads. The addition of either IL-7 or IL-15 at 100 IU/mL during the pre-activation phase and the first week post infection was sufficient to prolong iNKT cell viability in vitro, as demonstrated by the cell percentage increase in the live gate (FSC-A/SSC-A, *top*). In all cases, iNKT cell purity was preserved (*middle*). Transduction efficiency (TCR Vα24^{+}, RQR8^{+} events) was >80% (*bottom*).

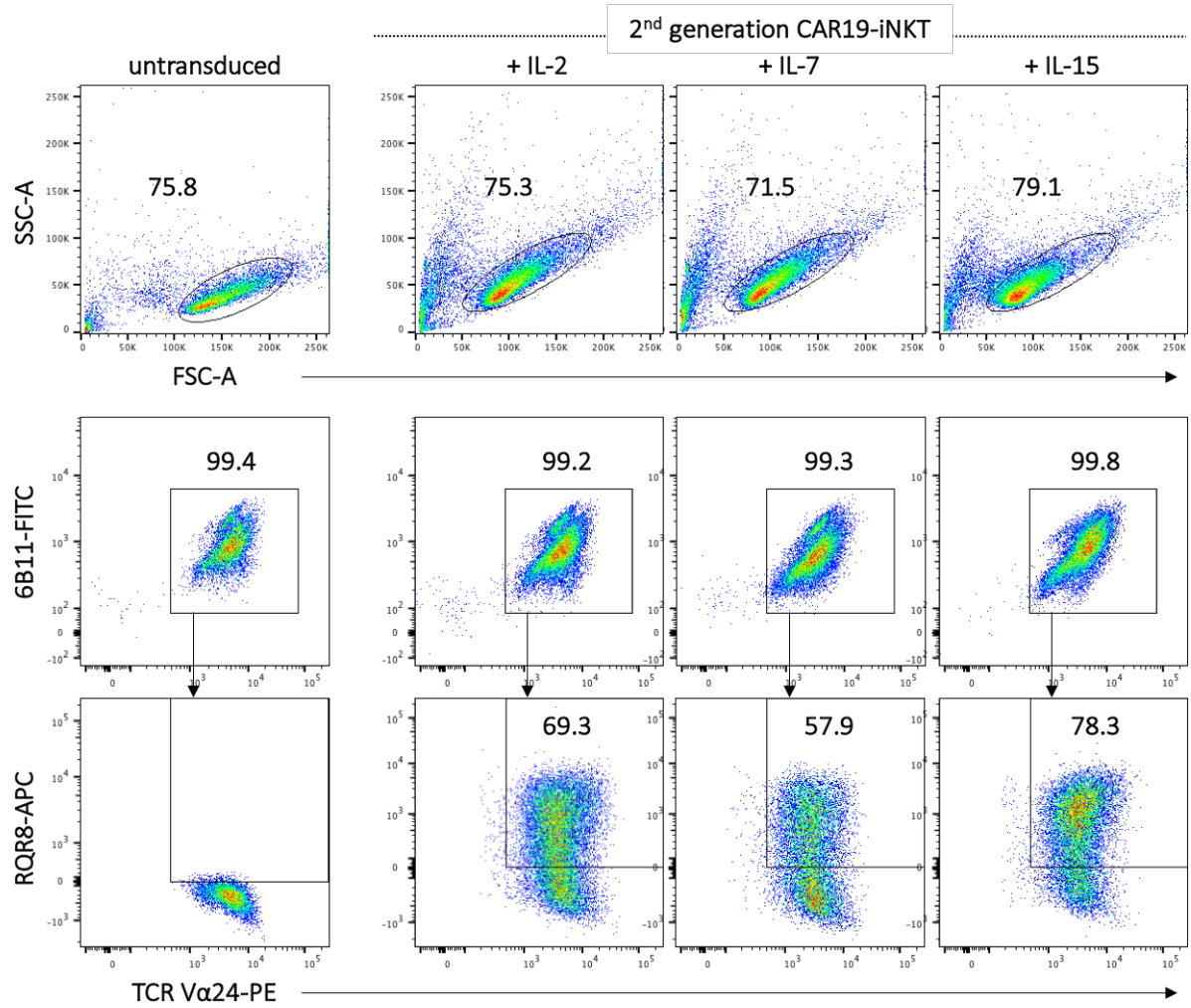


Figure 3-11 CAR19-iNKT cell engineering – protocol 5

Flow cytometry assessment on day +3 post transduction. Representative plots of upfront selected, pure 6B11^{+} cells transduced upon pre-activation with aCD3/CD28 beads in the presence of autologous irradiated PBMCs (i-autoPBMC), serving as feeders as well as APCs. The incorporation of i-autoPBMC allowed to preserve viability of transduced cells at comparable levels as untransduced cells (*top*). iNKT cell purity was maintained as well (*middle*). The combination with IL-15 supplemented medium resulted in the best transduction efficiency (*bottom*).

A summary of all optimisation steps is provided in **Figure 3-12** and **Table 3-6.**

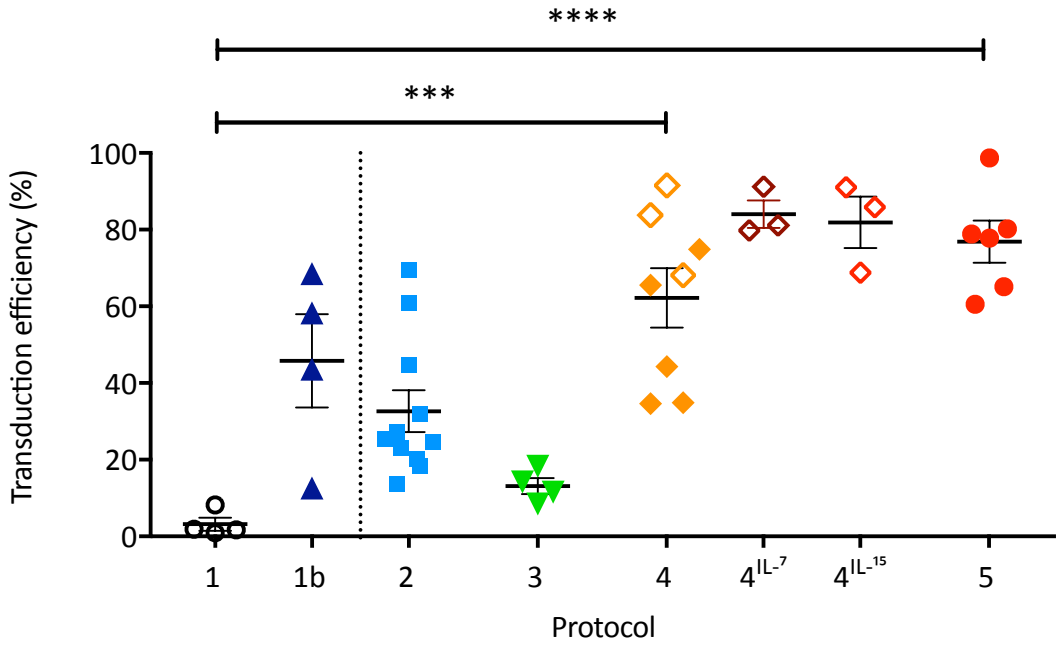


Figure 3-12 CAR19-iNKT engineering protocols

Cumulative data showing CAR transduction efficiency of iNKT cells according to each protocol. Only protocol 4 and 5 allowed to consistently generate highly transduced CAR19-iNKT, although viability was irreversibly compromised by protocol 4. Clear symbols represent side-by-side comparisons of protocol 4 variants.

Table 3-6 CAR19-iNKT engineering protocols

Protocol	1		2	3	4				5
Variant	1	1b	2	3	4	4 - IL-2	4 - IL-7	4 - IL-15	5
n	4	4	11	4	8	3	3	3	6
Min	0.92	12.64	13.80	8.45	34.60	68.10	79.80	68.80	60.50
Median	1.80	50.95	25.30	12.86	66.80	83.80	81.13	85.90	78.35
Max	8.17	68.50	69.50	18.30	91.50	91.50	91.20	91.00	98.70
Mean	3.17	45.76	32.66	13.12	62.20	81.13	84.04	81.90	76.87
S.E.M.	1.68	12.17	5.43	2.09	7.75	6.89	3.60	6.71	5.48

On the basis of these observations, I propose an optimal protocol for transducing primary human iNKT cells entailing (a) upfront 6B11-based selection in order to obtain a pure iNKT cell starting population, and (b) 24-48-hour aCD3/CD28 bead-activation in the presence of irradiated autologous PBMC and IL-15-supplemented medium, (c) followed by transduction with CAR19 lentivirus at a MOI of 2-5.

Importantly, such 'micro-scale' protocol allows to efficiently CAR-engineer iNKT as well as bulk T lymphocytes (**Figure 3-13**) and can be equally used with fresh and frozen blood products from either healthy donors or patients (**Figure 3-14**).

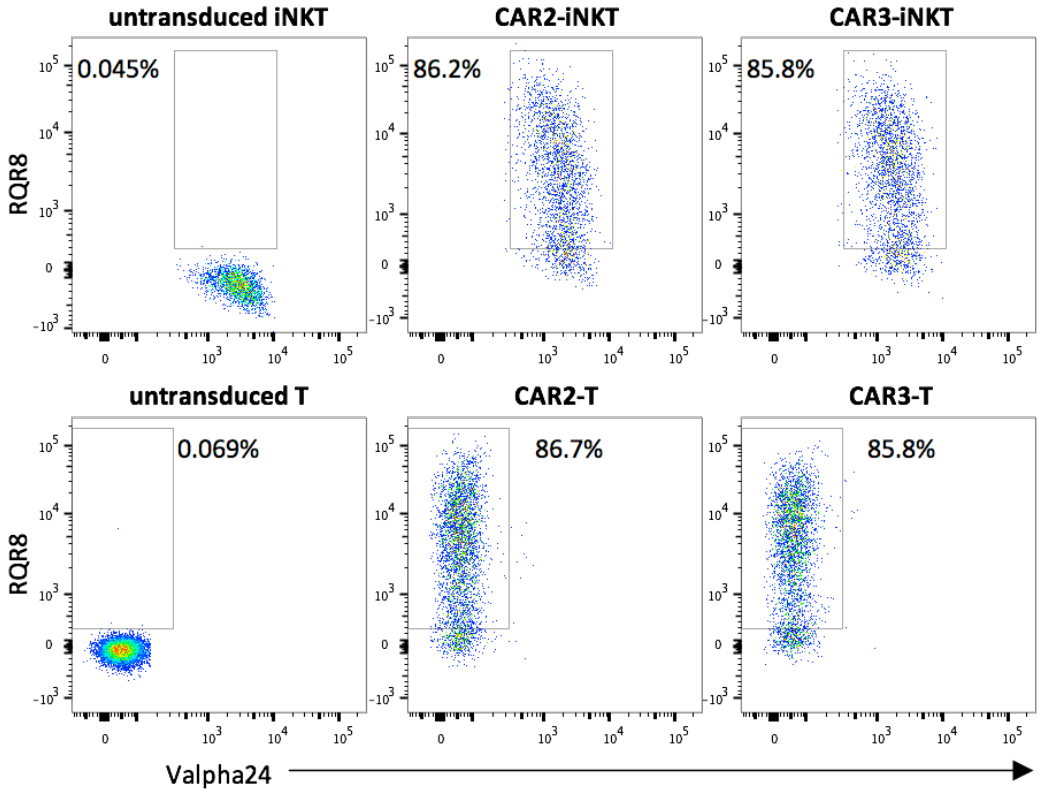


Figure 3-13 2nd and 3rd generation CAR19-iNKT and CAR19-T cells – protocol 5
Representative dots plots of CAR19-iNKT (*top*) and CAR19-T (*bottom*) cells on day +4 post infection (MOI 2), following protocol 5. Transduction efficiency, determined relatively to untransduced control cells, was comparable, irrespective of the vector cell type and CAR design.

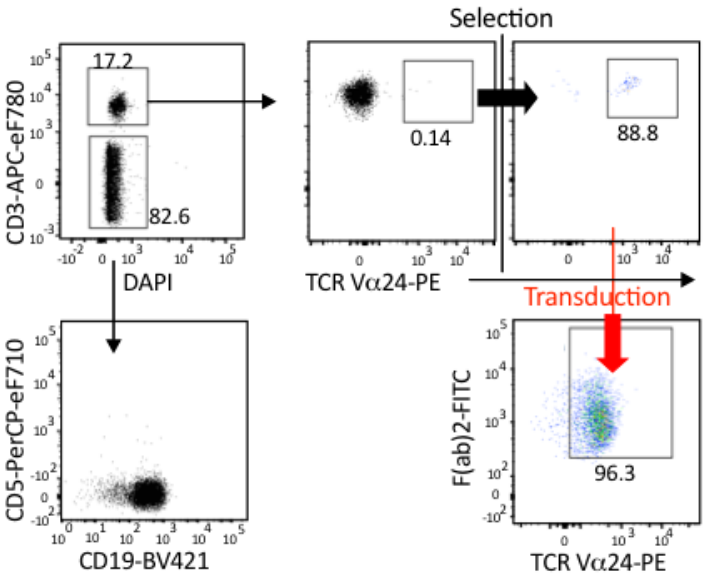


Figure 3-14 Lymphoma patient-derived CAR19-iNKT cells
Example of generation of CAR19-iNKT cells from a patient with active lymphoma using protocol 5. 82% of PBMCs were CD19+ lymphoma cells.

3.4 'Scale-up steps' for clinical scale manufacturing of CAR19-iNKT cells

Next, to address the prospect of clinical translation, I designed a scale-up method to produce clinically relevant numbers of CAR19-iNKT cells. Based on the preliminary experiments with CAR19-T cells, I used the same selection-expansion approach and defined a 2/3-step strategy: (1, optional) RQR8-based (CD34-immunomagnetic) isolation performed immediately after assessment of transduction efficiency, only if <85% pure CAR19-iNKT cells populations, (2) same day stimulation with 1 : 1 irradiated αGalCer-pulsed C1R-CD1d cells in IL-15-supplemented TCM, without any further manipulation until the next assessment, usually occurring 1 week later, occasionally earlier in the case of very highly proliferating cells; (3) IL-15-driven expansion in the absence of APC for another one week, or less if the target number was already achieved.

Results from 7 experiments are shown in **Figure 3-15**, including side-by-side comparison with CAR19-T. In all cases, clinical scale numbers of CAR19-iNKT cells could be produced within 3 weeks, irrespective of the initial cell count. CAR19-iNKT cells outperformed their T counterparts in terms of expandability. Importantly, 3rd generation CAR19-iNKT cells reached the largest cells

numbers, reporting the highest fold-increase, suggesting that, unlike the conventional T, the iNKT platform can be optimal to exploit the activating properties of 3rd generation CAR designs.

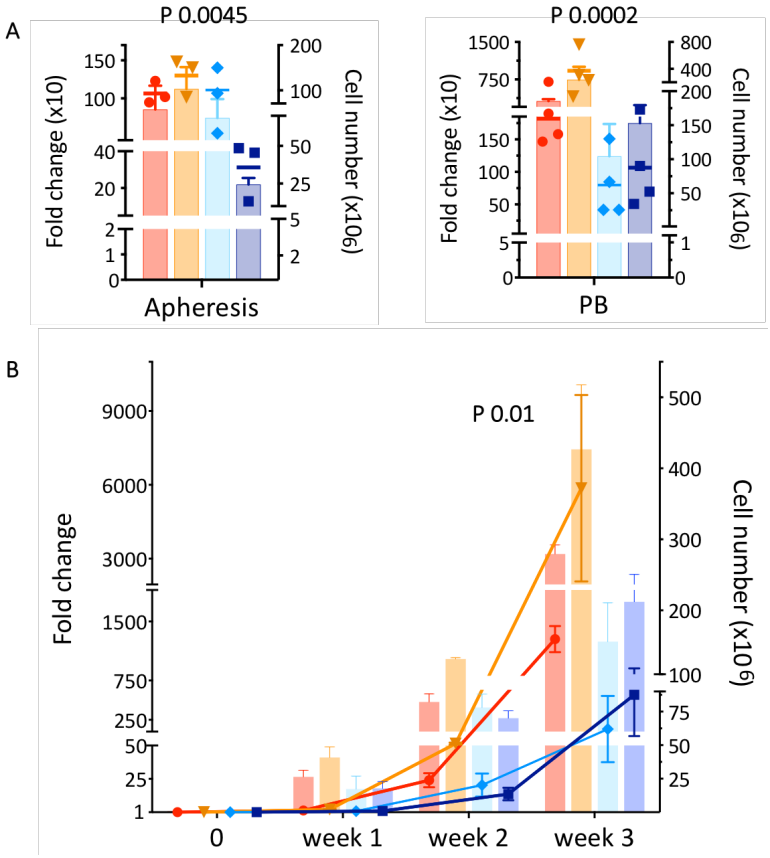


Figure 3-15 CAR19-iNKT expandability and clinical scale expansion

A. End-of-manufacturing expansion and absolute numbers of CAR19 -iNKT and -T cells generated from lymphapheresis (left) or peripheral blood (PB; right) (n=3 and 4 respectively). B. 2nd and 3rd generation CAR19 -iNKT and -T cell fold-change and absolute cell counts over a period of 3 weeks (n=4).

P values are for CAR19-iNKT vs CAR19-T cells using Friedman test. Error bars represent S.E.M.

A timeline summarizing the key steps of the optimised protocol to generate clinical scale CAR19-iNKT cells is provided in **Figure 3-16.**

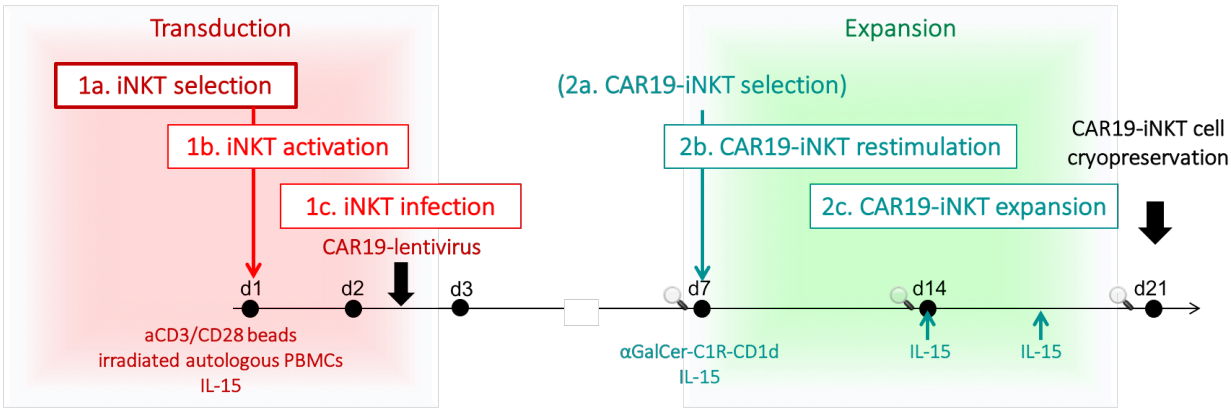


Figure 3-16 Timeline of optimised procedure for manufacturing of large scale CAR19-iNKT cells

🔍 flow cytometry assessment; αGalCer-C1R-CD1d: irradiated αGalCer-pulsed C1R-CD1d cells

3.5 Phenotypic and functional characterisation of CAR19-iNKT cells

CAR19-iNKT cells generated according to my optimised procedure were further characterised by flow cytometry for: (1) relative proportion of $CD4^+$/$CD4^-$ subsets; (2) cytokine profile; (3) PD-1 expression.

3.5.1 Preservation of $CD4^-$ iNKT cell subset

Both $CD8^+$ (cytotoxic) and $CD4^+$ (helper) subsets are important for an optimal anti-tumour T-cell response[181]. Furthermore, there is emerging evidence that the use of balanced CAR19-T cell products may contribute to improving the outcome CAR19-T immunotherapy[40,51,182]. It is conceivable that the same principle could be extended to iNKT-based immunotherapies.

The $CD4^-$ fraction of iNKT cells is characterized by a more polarized Th-1 cytokine profile, expresses higher levels of cytotoxic granules and has been associated with more pronounced anti-tumour functions compared to the $CD4^+$ counterpart[86]. In light of this, preservation of the $CD4^-$ CAR19-iNKT subset would be desirable. Indeed, assessment of CD4 expression on CAR19-iNKT cells confirmed that protocol 5 allows preservation of the $CD4^-$ fraction, resulting in end-of-manufacturing levels comparable to baseline (**Figure 3-17**).

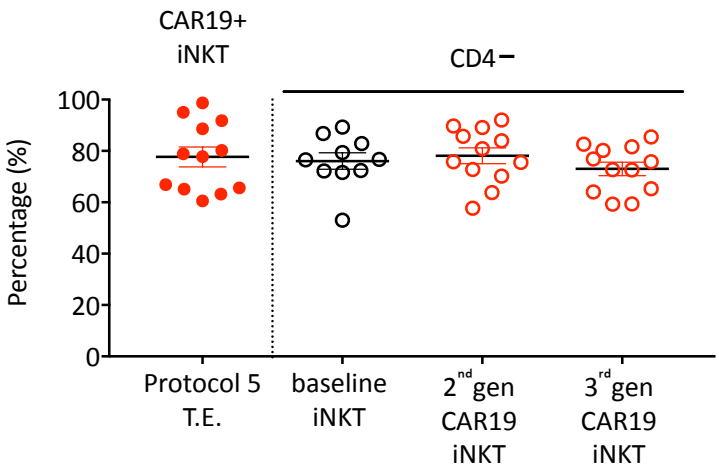


Figure 3-17 CD4⁻ CAR19-iNKT cells – protocol 5 compared to baseline
10 donors presented 76% CD4⁻ cells at baseline. At the end of the scale-up production of 2nd (n=12) and 3rd (n=12) generation CAR19-iNKT cells, CD4⁻ comprised 78% and 73% respectively.
Red: transduced cells; black: parental iNKT cells. Solid symbol: transduction efficiency; clear symbol: CD4⁻ cell percentage. T.E.: transduction efficiency; gen: generation

Furthermore, this seems to be a distinctive feature of protocol 5 since same-donor CAR19-iNKT cells generated according to protocol 2, i.e., the only alternative protocol allowing to generate long-term viable CAR19-iNKT cells, displayed depletion in CD4⁻ cells. (**Figure 3-18**).

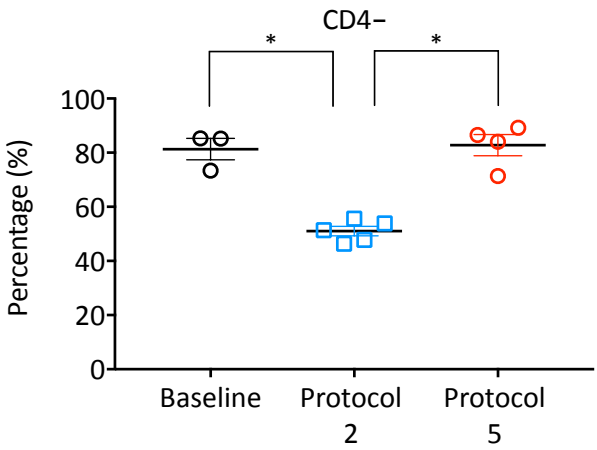


Figure 3-18 CD4⁻ CAR19-iNKT cells – protocol 5 compared to protocol 2
CD4⁻ cells were 81% at baseline (n=3 donors), whereas 51% (n=5) and 83% (n=4) CAR19-iNKT cells were CD4⁻ as assessed at the end of the protocol 2 and 5 respectively. *: P <0.05

3.5.2 CAR-iNKT cells display a Th1-like, poly-functional cytokine profile

Resting $CD4^-$ CAR19-iNKT cells express significantly higher levels of perforin and granzyme B (**Figure 3-19**, **A**) than their $CD4^+$ counterparts, thus preserving an important functional feature of $CD4^-$ unmodified iNKT cells, which have a more pronounced cytotoxic potential than $CD4^+$ iNKT cells. Interestingly, both $CD4^-$ and $CD4^+$ CAR19-iNKT cells displayed larger amounts of newly formed (identified by the moAb D-B48[183]) rather than granule-associated, mature perforin (identified by the moAb δG9[183], $P<0.0001$). Accordingly, the levels of D-B48 perforin were not proportional to the levels of granzyme B ($P<0.0001$) particularly in the $CD4^+$ subset. While demonstrating that both $CD4^-$ and $CD4^+$ CAR19-iNKT cells manufactured according to protocol 5 are armed with pre-made perforin and can potentially kill tumour target cells, these findings also raised the possibility that non-conventional cytolytic pathways, involving perforin exocytosis at the immunological synapse independently on cytotoxic granules[183], may result in a rapid cytotoxic response of CAR19-iNKT cells similar to what has been shown in $CD8^+$ T lymphocytes[183,184].

Upon 4 hour-stimulation with either anti-CD3/CD28 beads or PMA/ionomycin (**Figure 3-19, B-C**), I observed an increase in the levels of mature δG9-perforin as well as Granzyme B, that was particularly pronounced in the $CD4^+$ subset, while D-B48-perforin remained comparable to baseline levels.

Further cytokine profiling included intracellular staining for IFN-γ and IL-4 after stimulation with aCD3/CD28 beads, PMA/ionomycin and APC ($CD19^+$ C1R-CD1d cells), which highlighted a striking Th-0 signature of $CD4^+$ CAR19-iNKT cells, characterized by production of larger amounts of IL-4 than the $CD4^-$ subset (**Figure 3-19**, **B-D**).

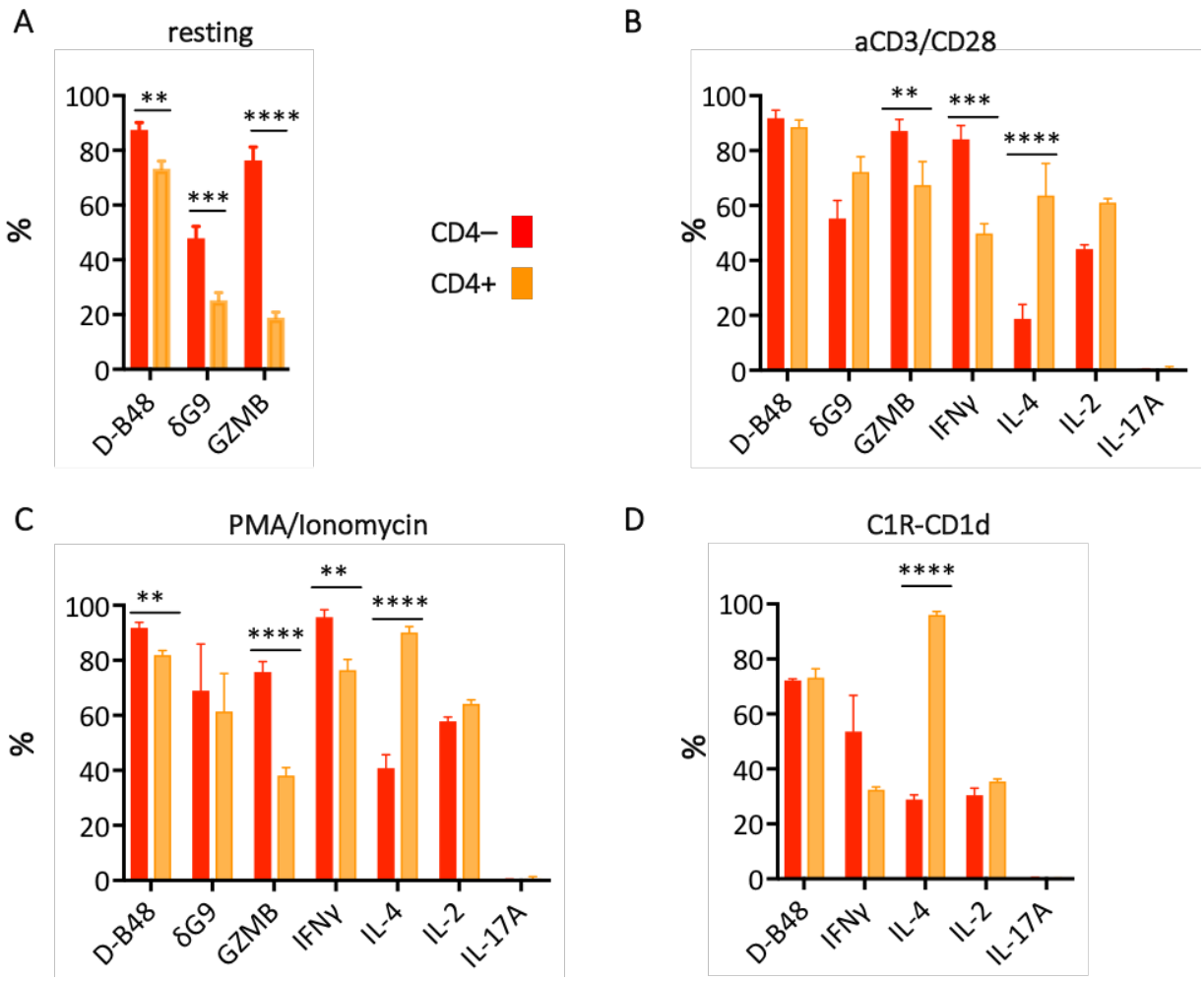


Figure 3-19 CAR19-iNKT intracellular cytokine profile
Intracellular expression of cytokines in resting (n=10, A) and 4 hours activated $CD4^-$ and $CD4^+$ CAR19-iNKT cells with aCD3/CD28-beads (B) and PMA/ionomycin (C) (n=6) or C1R-CD1d targets (n=4, D). D-B48 and δG9 moAbs identify total and granule-associated perforin respectively.
GZMB: granzyme B; IFNγ: interferon-γ.

When compared side-by-side to their CAR19-T counterparts, I found that end-of-manufacturing, resting CAR19-iNKT cells stored more immature ($D\text{-}B48^+$) perforin than their same-donor CAR19-T counterpart, although granzyme B levels were comparable (**Figure 3-20**).

.

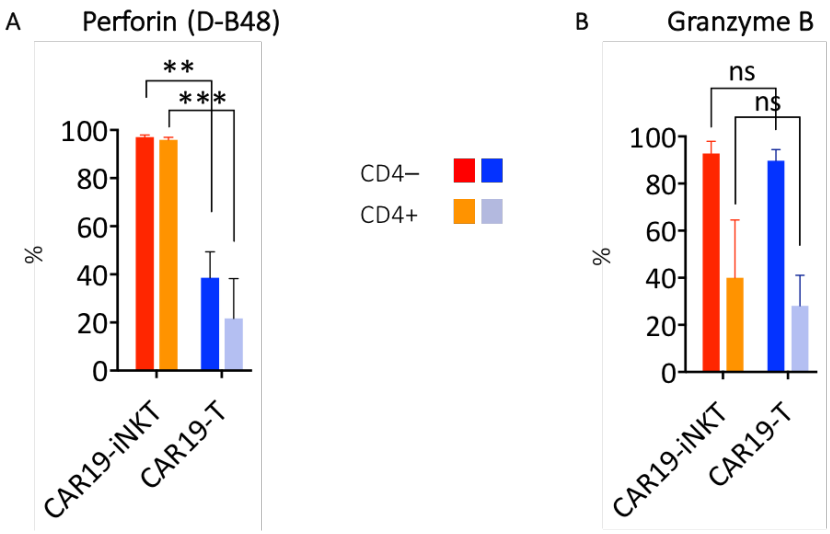


Figure 3-20 CAR19 -iNKT vs -T intracellular cytokine profile – resting cells
Intracellular expression of perforin (D-B48) and granzyme B in resting $CD4^-$ and $CD4^+$ CAR19-iNKT and T cells (n=4).

In addition, upon aCD3/CD28 activation, CAR19-iNKT cells expressed more IFN-γ together with perforin and granzyme B (**Figure 3-21 A**), with a significantly higher proportion of tri-functional effectors, i.e., cells simultaneously expressing IFN-γ, perforin and granzyme B (CAR19-iNKT 40% vs CAR19-T <5%, P<0.01, **Figure 3-21 B-C**). Importantly, >20% CAR19-T vs <3% CAR19-iNKT cells did not produce any the above 3 molecules.

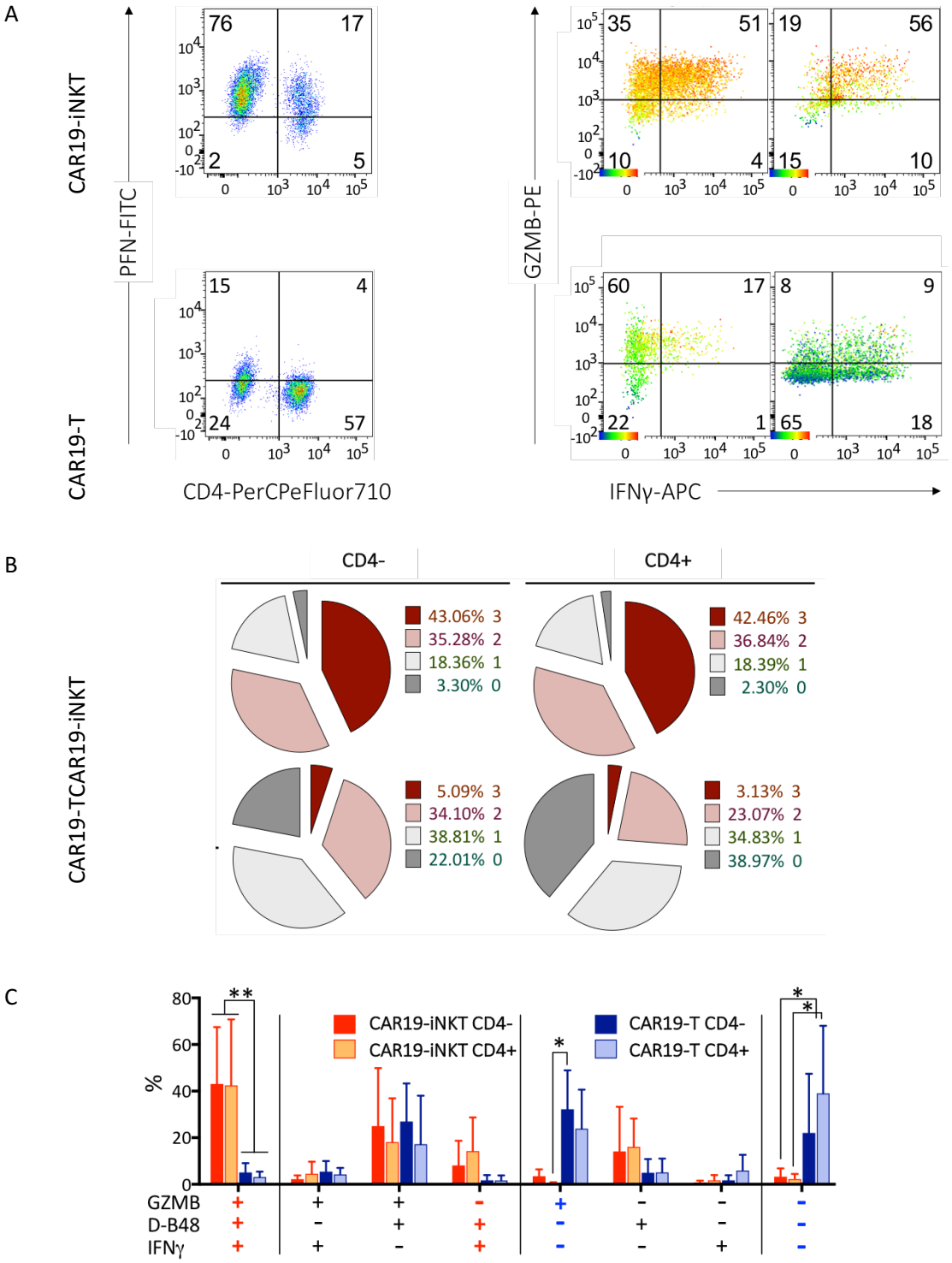


Figure 3-21 Polyfunctional CAR19 -iNKT vs -T cells

A. Representative flow-cytometric analysis of intracellular PFN, GZMB and IFN-γ in $CD4^-/CD4^+$ CAR19-iNKT (*top*) and -T (*bottom*) cells. In GZMB/IFN-γ dot plots, intensity of PFN expression is projected as a heat-map according to the shown colour scale. B. Pie charts summarizing the proportions of cells co-expressing 0-3 cytokines (n=4). C. Proportions of specific cytokines co-expressed by $CD4^-/CD4^+$ CAR19-T and CAR19-iNKT cells (n=4).

Further characterisation by Luminex multiplex cytokine release assay after 3 and 8 hours -stimulation showed that CAR19-iNKT cells produce larger amounts of cytotoxic cytokines with faster kinetics. Moreover, they exhibited a higher propensity to produce Th-1 and Th-2 cytokines but less inhibitory and/or proinflammatory cytokines such as IL-6 and IL-10, that have been associated with CAR19-T-related toxicities (**Figure 3-22**).

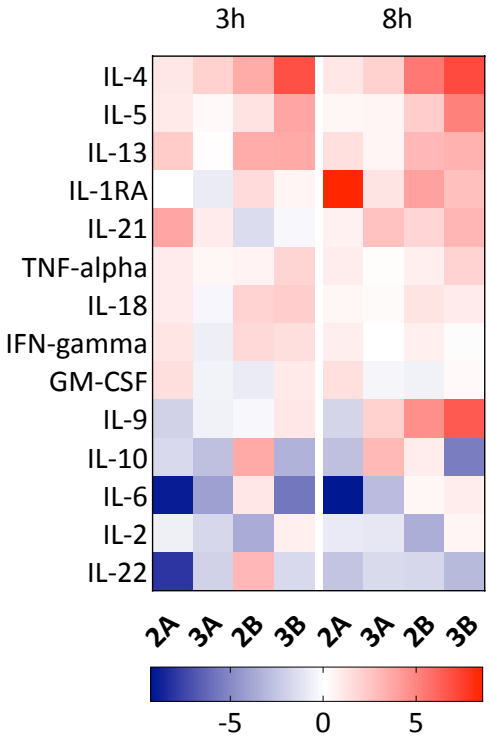


Figure 3-22 CAR19 -iNKT vs -T cytokine release assay
Multiple cytokine secretion after 3 and 8 hrs of activation of 2nd and 3rd (2 & 3) generation CAR19-T and CAR19-iNKT cells from 2 healthy donors (A & B). Heat-map shows normalized CAR19-iNKT/CAR19-T cell ratios (log2 fold change).

3.5.3 Low PD-1 expression by CAR19-iNKT cells

Expression of programmed cell death-1 (PD-1), a major marker of immune cell exhaustion that has been associated with dysfunctional T cells in cancer patients with refractory/relapsed disease[185], was first assessed on resting, end-of-manufacturing CAR19 cells. 8.5% ±1.935 CAR19-iNKT cells were PD-1^{+} (n=4, 2 donors, 2nd gen CAR19: 10.44%; 3rd gen CAR19: 6.57%), with a higher proportion within the CD4^{+} subset (CD4^{+}: 17.88% ±2.077, CD4^{-}:7.01% ±1.453;

P=0.0134). By contrast, 30.23% ±3.55 CAR19-T cells were PD-1^{+} (n=4, 2nd generation CAR19: 25.05% ±0.95; 3rd generation CAR19: 35.4% ±4.60; CAR19 -iNKT vs -T: P=0.0286; **Figure 3-23**).

.

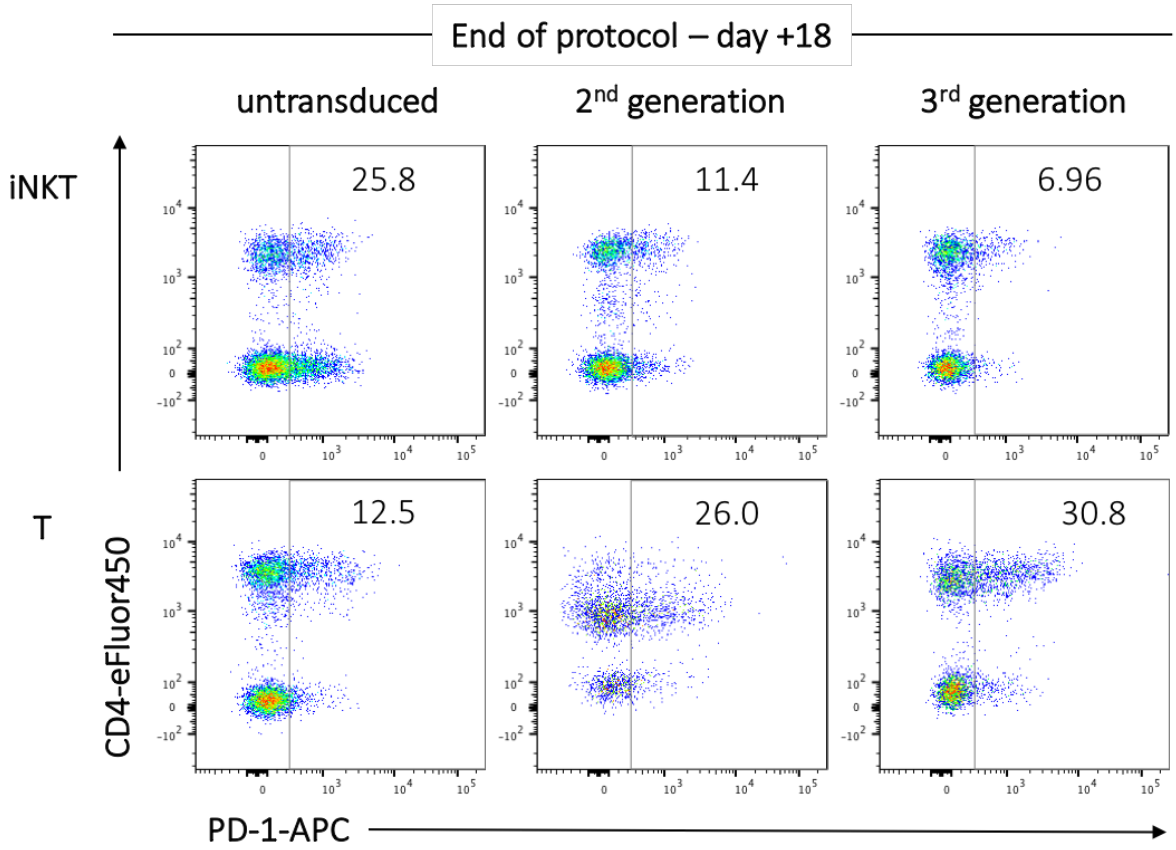


Figure 3-23 End-of-manufacturing PD-1^{+} CAR19-cells
Representative flow-cytometry plots of PD-1^{+} CAR19-cells at the end of the manufacturing process. Gates are relative to isotype control.

Since T cell exhaustion is a state acquired as a result of subsequent antigen stimulations[186,187], I then tested the impact of repeated stimulations on PD-1 expression (**Figure 3-24**, **Figure 3-25, Figure 3-26 and** Figure 3-27
Figure 3-27).

CAR19-iNKT cells generated according to protocol 5 received one or two additional stimulations with αGalCer-pulsed C1R-CD1d cells on day 16 and day 23 respectively. A mild increase in the percentage of PD-1^{+} cells was observed after the second restimulation, although it was not statistically significant. By contrast, PD-1^{+} cells were consistently increased

after each stimulation of CAR19-T cells (63.58% ±4.94 and 83.58% ±6.659 after 1 or 2 additional antigen restimulations 1 week apart respectively; P=0.098). During resting phase, only a partial reversion of the phenotype could be observed, eventually resulting in a significantly larger fraction of PD-1^{+} cells compared to baseline (60.3% ±6.768, P=0.0042).

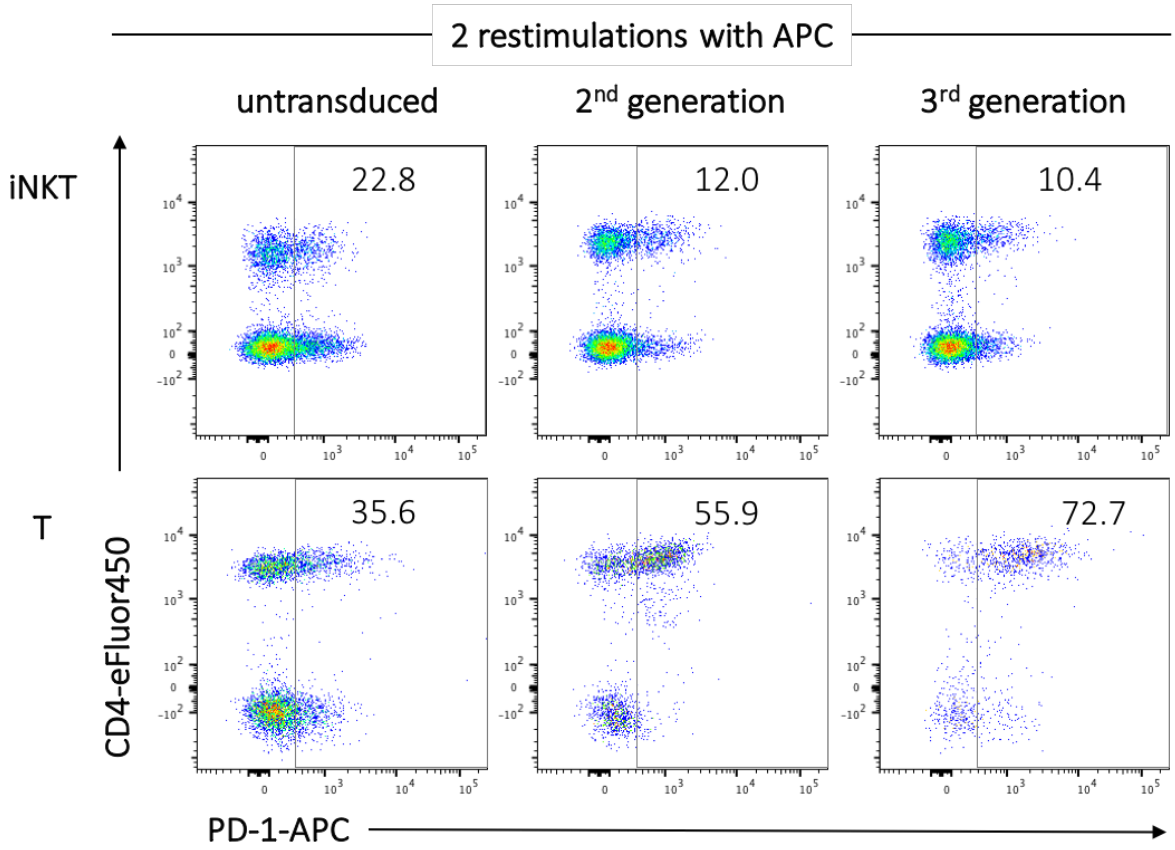


Figure 3-24 PD-1^{+} CAR19-cells after 2 restimulations

CAR19-engineered cells generated according to protocol 5 received 1 additional stimulation with αGalCer-pulsed C1R-CD1d cells on day 16, i.e., 1 week after the restimulation performed according to the engineering protocol. Representative dot plots from 1 out of 4 experiments. Gates are relative to isotype control.

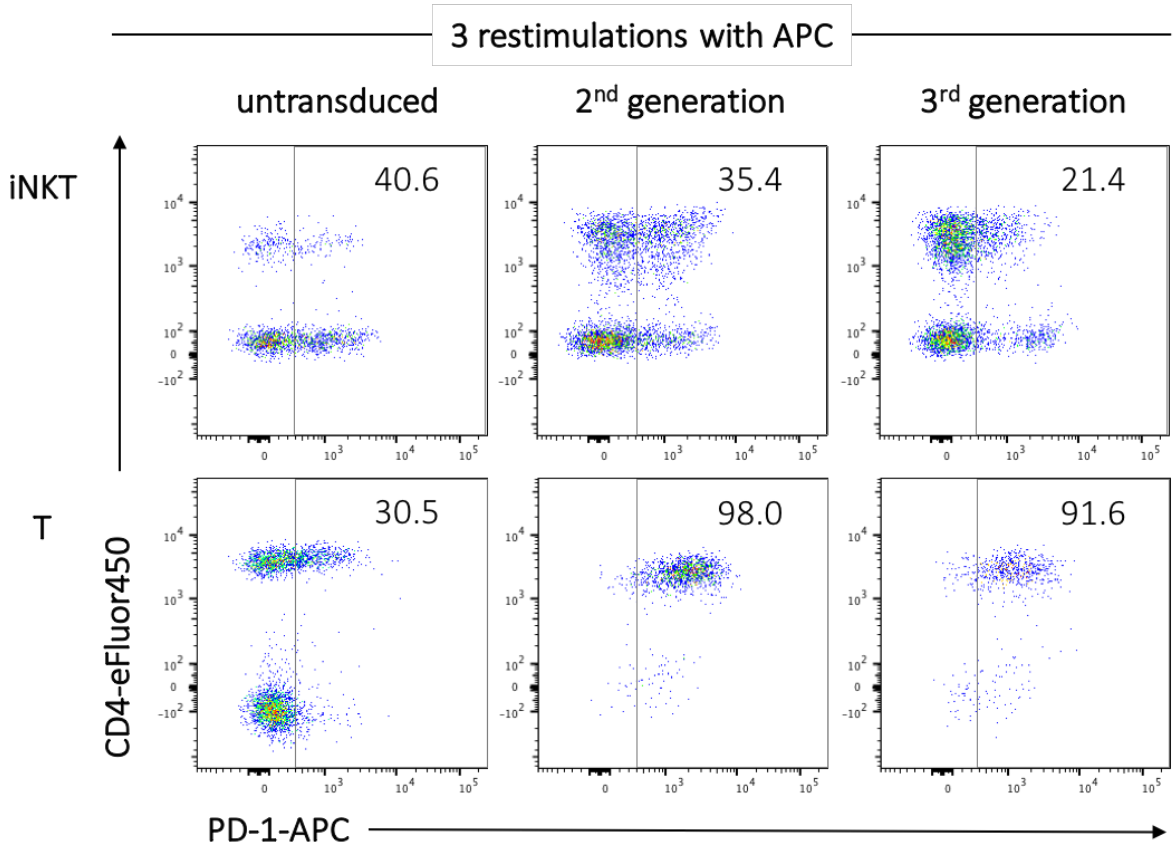


Figure 3-25 PD-1^{+} CAR19-cells after 3 restimulations

CAR19-engineered cells generated according to protocol 5 received 2 additional stimulations with αGalCer-pulsed C1R-CD1d cells on day 16 and 23, starting 1 week after the restimulation performed according to the engineering protocol. Representative dot plots from 1 out of 4 experiments. Gates are relative to isotype control.

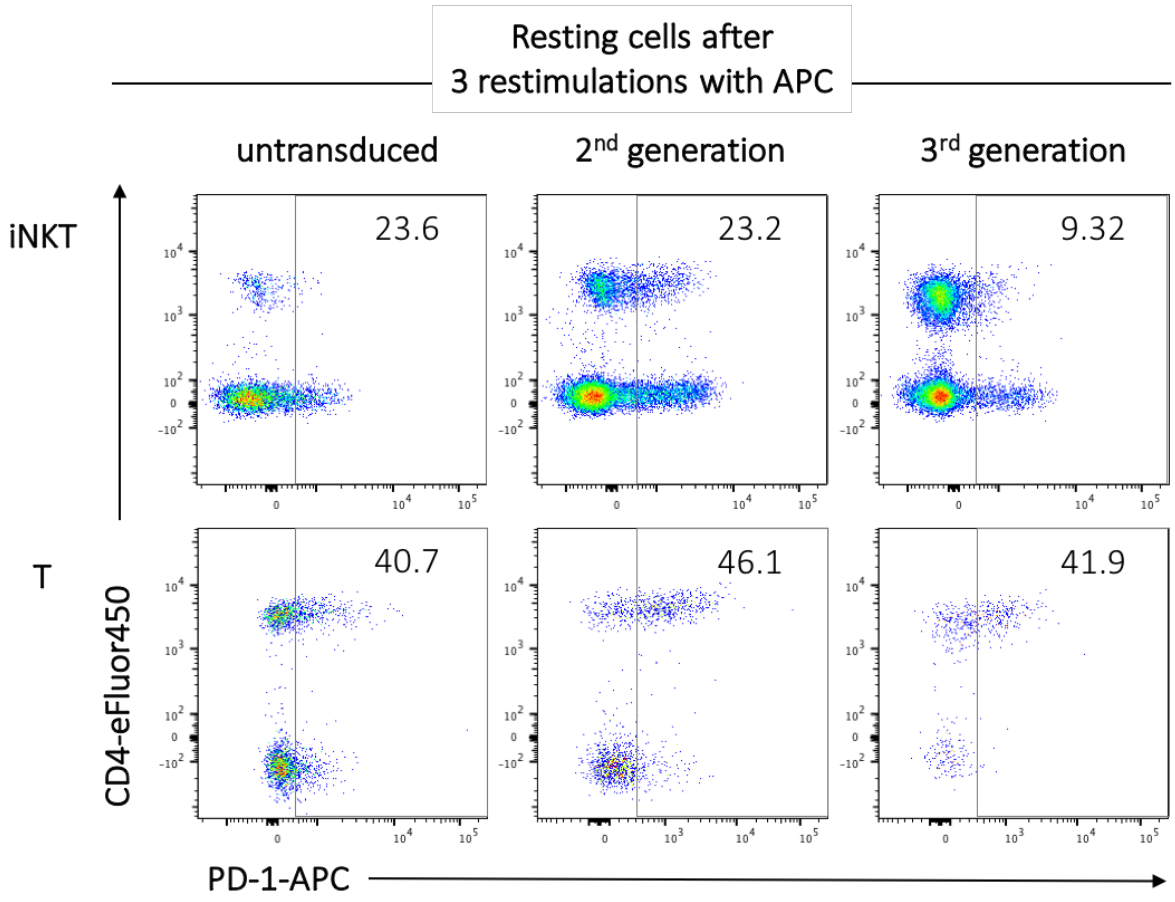


Figure 3-26 PD-1$^+$ CAR19-cells in resting phase after 3 restimulations

Representative dot plots showing PD-1$^+$ cell percentages within resting CAR19-engineered cells restimulated with αGalCer-pulsed C1R-CD1d 3 times 1 week apart, i.e. on day 9, as per protocol 5, and 2 additional times on day 16 and 23. Assessment was performed 1 week after the last restimulation. Gates are relative to isotype control.

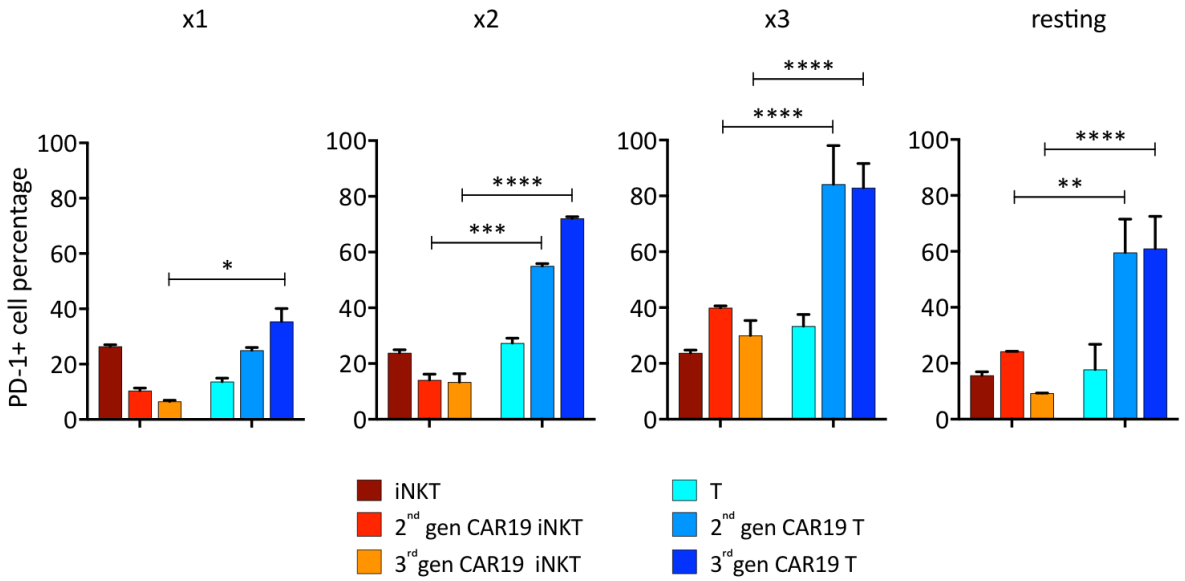


Figure 3-27 PD-1$^+$ CAR19-iNKT vs -T cells after weekly restimulations
Bar graphs showing PD-1$^+$ percentages within CAR19-cell populations restimulated with αGalCer-pulsed C1R-CD1d on day 9 (*x1*), as per protocol 5, day 16 (*x2*) and day 23 (*x3*) and let rest for 1 week (*resting*). Assessment was performed 1 week after restimulation (*x2* and *x3*) or culture in resting conditions (*x1* and *resting*). Gates are relative to isotype control.

Accordingly, expandability was greater and more sustained in CAR19-iNKT cells compared to their T counterparts (**Figure 3-28**).

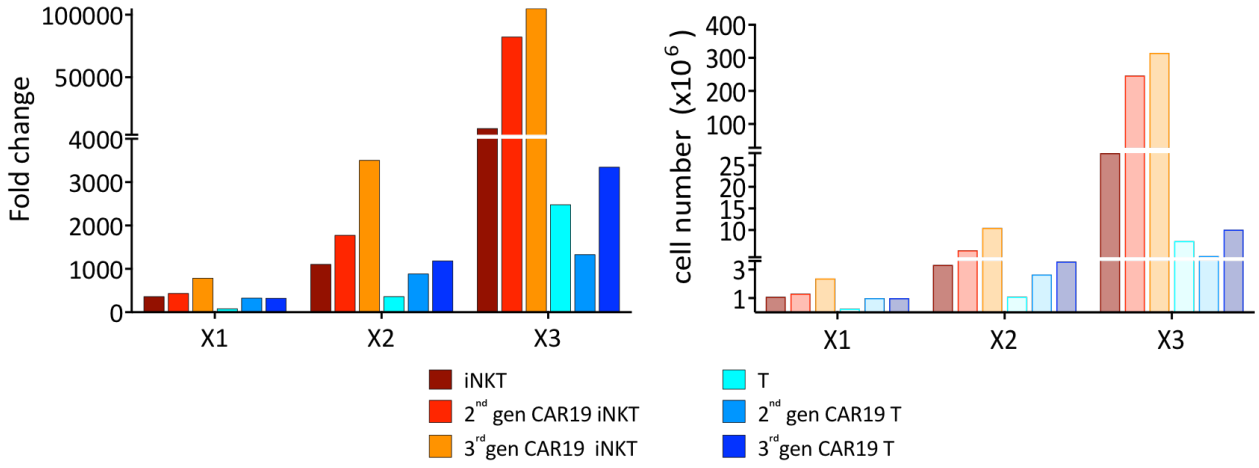


Figure 3-28 CAR19 -iNKT vs -T cell expandability after weekly restimulations
Average fold increase (left) and absolute cell counts (*right*) of CAR19-cells after repeated stimulations. Expandability was inversely correlated with PD-1 expression, shown in **Figure 3-23**, **Figure 3-24** and **Figure 3-25**. n=2, one donor.

3.6 Discussion

Mature B cell lymphomas and chronic B lymphoproliferative disorders (LPD) such as CLL, with the exception of diffuse large B cell lymphoma, are mostly incurable malignancies. CAR19-T cell-based immunotherapy has shown curative potential in some patients with these malignancies, but the overall outcome remains poor. Owing to their unique biological properties, together with the co-expression of CD1d on malignant $CD19^+$ cells, iNKT cells may offer the opportunity to overcome the shortcomings of CAR19-T effectors and represent a more effective platform for CAR19-immunotherapy in $CD1d^+$ B cell lymphomas and LPD. Therefore, the first aim of my work was to develop a novel, bespoke CAR-engineering protocol to generate clinical scale CAR-iNKT cells.

Three main challenges had to be addressed: 1) very low frequency and starting iNKT cell numbers, 2) different reactivity of iNKT cells to conventional T cell mitogens, 3) large-scale expansion in a timed manner. To this end, I took into consideration several variables and I subsequently tested different conditions under 5 main protocols and their derivative modified versions through rigorous step-by-step optimization.

In *protocol 1* upfront expansion from bulk PBMCs was aimed to achieve higher iNKT cell numbers at the time of gene-transfer, similar to standard procedures for CAR-engineering of conventional T cells. This first set of experiments suggested that pure, homogeneous iNKT cell populations are associated with higher transduction efficiencies (*protocol 1b*). Therefore, in *protocol 2* upfront selection followed by expansion as opposed to upfront expansion was adopted. Although successful, the average yield of CAR19-iNKT cells was <50%, while the length of *in vitro* manufacturing remained unsatisfactory, i.e. 4-5 weeks. To shorten the duration of the manufacturing process, from *protocol 3* onwards, CAR19 transduction was incorporated immediately after selection of iNKT cells. Next, different activation strategies were tested to further improve the transduction efficiency, i.e. the iNKT-cell specific agonist αGalCer in *protocol 3* versus the non-specific T cell activator aCD3/CD28-beads in *protocol 4*. CD3/CD28-mediated activation and transduction, in combination with upfront selection, was associated with consistently high percentages of CAR-engineered iNKT cells but severely impacted on their viability. By replacing IL-2 with IL-15, which has been demonstrated to

promote iNKT cell survival through induction of BCL2 family proteins[175], short-term viability CAR19-iNKT cells significantly improved (*protocol 4*$^{IL\text{-}15}$). Eventually, the addition of irradiated autologous PBMCs, as feeders as well as APCs, led to the generation of an optimal *protocol 5.* A summary of the main features of each protocol is provided in **Table 3-7**.

The Metelitsa group first reported the feasibility of CAR-iNKT cells for cancer immunotherapy and patented a procedure, which corresponds to my *protocol 2*[169]. However, my optimal *protocol 5* outperformed Metelitsa's in terms of transduction efficiency and faster scale-up to clinically relevant doses, while presenting several novel aspects and advantages in terms of: (1) upfront (lentivirus) transduction, within the first 24-48h following iNKT cell isolation instead of on day 14, using considerably smaller quantities of virus; (2) aCD3/CD28 versus αGalCer-mediated iNKT cell activation pre-transduction, which is associated with greater gene-transfer efficiency; (3) preferential use of IL-15 in my protocol over IL-2, to improve CAR-iNKT cell viability; (4) minimal *in vitro* manipulation, usually limited to cytokine supplementation once a week instead of every other day; (5) preservation of the $CD4^{-}$, Th-1-like iNKT cell fraction.

Notably, my bespoke micro-scale engineering process, initially designed to fit the rare frequency and low starting numbers of iNKT cells, e.g. 1,000 - 10,000 iNKT cells, with minimal *ex vivo* manipulation, was subsequently combined with a scale-up step to produce large numbers of CAR19-iNKT cells, thus resulting suitable for small clinical samples, e.g. 5-10 ml PB, as well as larger blood volumes or cell apheresis products. Importantly, fresh and frozen blood products may be equally used as a source of cells. Donors can be healthy volunteers or cancer patients either in remission or with active haematological malignancy, i.e., with reduced iNKT cells counts. Furthermore, such micro-scale engineering allowed a drastic reduction of the amounts of reagents and virus required, making the prospect of cutting down the manufacturing-related costs of CAR-immunotherapy likely feasible.

Further *in vitro* validation demonstrated that CAR19-iNKT cells produced according to *protocol 5* were associated with the best anti-tumour potential on the basis of greater CAR19-iNKT cells expandability, preserved $CD4^{+}/CD4^{-}$ ratio, robust Th1 profile and minimal expression of PD-1.

Table 3-7 Overview of optimisation steps towards CAR19-iNKT cell manufacturing protocol

#	Main features	Advantages	Drawbacks	Transduction Efficiency	#	Variants (Transduction Efficiency)
1	MNCs expansion (αGalCer) prior to transduction	Minimal manipulation	• Limited iNKT expansion in the presence of bulk T cells • Loss of iNKT cells fraction upon transduction • Low transduction efficiency	3.17%	1b	Selection pre-transduction (45.76%)
2	a. Upfront selection b. iNKT expansion (αGalCer) prior to transduction ▪ IL-2 every 2-3 days ▪ Re-stimulation (αGalCer) after ≥10 days ▪ Transduction 2 weeks after selection	• Pure iNKT cells • Improved transduction efficiency	• Prolonged in vitro manipulation • CD4+ bias • Transduction efficiency <50%	32.66%		
3	a. Upfront selection b. Upfront transduction c. Pre-activation with αGalCer	Reduced time of in vitro manipulation	Low transduction efficiency	13.12%		
4	a. Upfront selection (>80% 6B11+) b. Upfront transduction c. Pre-activation with aCD3/CD28	Higher transduction efficiency	Cell death	62.20%	4 - 4 - 4 -	IL-2 (81.13%) IL-7 (84.04%) IL-15 (81.90%)
5	a. Upfront selection (>80% 6B11+) b. Uprfront transduction c. Pre-activation with ▪ aCD3/CD28 beads, ▪ autologous iPBMCs ▪ IL-15	• Higher transduction efficiency • Preserved viability • Preserved CD4- • Minimal in vitro manipulation • Minimal virus required • Reduced costs		76.87%		

CAR19-T cell trials proved that the best clinical outcomes are associated with pronounced *in vivo* proliferative responses of CAR19-T cells upon infusion, with a direct correlation between the degree of CAR19-T cells expansion and the depth of the clinical response[34]. Therefore, the excellent *in vitro* expandability of CAR19-iNKT effectors upon co-culture with tumour targets may be predictive of efficacy in patients. In addition, in a side-by-side comparison CAR19-iNKT cells were superior to their T cell counterparts, with 3rd generation CAR19-iNKT cells reaching the highest numbers irrespective of the donor. Importantly, expansion of 3rd generation CAR19-T cells was inconsistent and in some cases poorer than 2nd generation CAR19-T cells due to AICD (**Figure 3-5**), thus suggesting that iNKT cell may represent a more suitable platform for CAR-immunotherapy. Moreover, given their unique ability of tolerating the extraordinary levels of activation induced by 3rd generation CAR constructs, iNKT cell might represent the key to fully exploit the curative potential of the CAR-technology.

T lymphocytes that simultaneously produce multiple cytokines, so-called 'polyfunctional' T cells, provide a more effective immune response to a pathogen or a cancer cell than cells producing a single cytokine[188-190]. Compared to same-donor CAR19-T, a significantly larger proportion of CAR19-iNKT cells produced PFN, granzyme B and IFN-γ in response to 4h aCD3/CD28-bead stimulation (**Figure 3-21**). Importantly, flow cytometry analysis demonstrated higher amounts of PFN, granzyme B and IFN-γ at a single cell level, with a consistent fraction of polyfunctional CAR19-iNKT cells simultaneously producing the three of them, thus predicting a more robust cytotoxic response against cancer targets. Of note, both CD4^{-} and CD4^{+} subsets exhibited the capacity of producing high levels of toxic granules and IFN-γ upon stimulation with different agents (

Figure 3-19). However, while CD4^{-} cells showed a strong Th-1 profile even under resting conditions, CD4^{+} cells displayed a more balanced Th-0 profile, characterized by prominent production of IL-4 (Th-2). This provides another argument in support of the superiority of *protocol 5* over *protocol 2* (Metelitsa's), since only my optimal manufacturing procedure ensures preservation of the CD4^{-} CAR19-iNKT cell population. To complete the functional characterization of my CAR19-iNKT cell product, subsequent dynamic evaluation of cell supernatants confirmed that CAR19-iNKT react faster the conventional CAR19-T cells, releasing more effector and helper mediators that could promote anti-tumour response by bystander,

endogenous immune cells (**Figure 3-22**). However, they did not secrete inhibitory and regulatory cytokines such as IL-10 and IL-6, that have been associated with CAR-T immunotherapy-related neurotoxicity[58-60].

Finally, evaluation of surface expression of PD-1 showed that very few CAR19-iNKT cells manufactured according to my bespoke procedure express it. PD-1 is an inhibitory receptor of the CD28 family, which is known to play a major role in regulating T-cell exhaustion[187]. Specifically, PD-1 has been accepted as a hallmark of the transcriptional programming and epigenetic modifications occurring during the development of T cell exhaustion, leading to a typical 'footprint' which is maintained even after clearance of the specific antigen[185] and represents a main barrier to successful CAR-immunotherapy[191]. For the purposes of my *in vitro* validation, I exposed my CAR19-iNKT cell product to repeated antigen stimulations and found that the proportion of PD-1^{+} effectors was consistently lower compared to control parental iNKT cells as well as CAR19-T counterparts (**Figure 3-24** and **Figure 3-25**). Furthermore, resting CAR19-iNKT exhibited the unique ability to return to pre-stimulation levels of PD-1, whereas the phenotype of their CAR19-T counterparts showed only a partial reversal (**Figure 3-27**), suggesting that unlike conventional T cells, CAR19-iNKT cells may have a unique capacity of bypassing the barrier of immune exhaustion which contribute to disease relapse in patients with B lymphomas[192]. Of note, there are no available data on PD-1 expression on CAR-iNKT cells, although the Metelitsa group reported a >40% PD-1^{+} *untransduced* iNKT cells as assessed 12 days post expansion prior to CAR-engineering.

In summary, I have established a novel, bespoke protocol for CAR-engineering of iNKT cells. The protocol is highly efficient, allows to produce large-scale numbers of pure CAR19-iNKT cells in a relatively short period of time and is suitable for clinical application and translation. The resulting CAR19-iNKT cell product is functional, with anticipated high anti-tumour potential based on excellent expandability, robust Th1-profile and lack of PD-1 associated exhaustion features.

4 *In vitro* validation: dual specificity and cytotoxic activity of CAR19-iNKT cells

4.1 Introduction

CAR immunotherapy is rapidly transforming the treatment of blood cancers. So far, two CAR-T products have been approved for the treatment of relapsed/refractory B cell malignancies: Kymriah (Novartis), for children and young adults with relapsed/refractory B-ALL, with up to 90% CR rates[26-33]; Yescarta (Kite Pharma/Gilead) for patients with relapsed/refractory diffuse large and other high-grade B cell lymphomas, with 51% of CR rates[193]. Only 2/3 of lymphoma patients in CR after CAR19-immunotherapy achieved a sustained remission[34-39]. Therefore, there is a clear need for improving clinical outcomes in $CD19^+$ lymphomas and chronic lymphoproliferative disorders using CAR technology.

Following the paradigm of multi-agent chemotherapy regimens, in order to enhance anti-tumour activity while mitigating antigen escape, ongoing efforts focus on developing multi-specific CAR-based immunotherapies that target simultaneously more than one tumour-associated antigens[194]. CD1d-restricted iNKT cells naturally offer the opportunity for at least dual-specific CAR immunotherapy for CD1d-expressing B cell lymphomas, with several advantages over more conventional dual specific CAR-T cells. Such dual targeting approach would be expected to be enhanced by the inherent innate-like reactivity of iNKT cells, that may promote an earlier and more potent cytotoxic response, thus resulting in swift complete disease eradication at their first shot. In addition, the iNKT cell memory phenotype suggests that CAR-iNKT cells might be less prone to AICD and persist longer at the tumour sites to continuously detect and promptly kill even low numbers of malignant cells, thus preventing clinically evident relapses. Furthermore, the unique iTCR-mediated alloreactivity confers the attractive potential for universal donor use, this emphasising that the preservation of intact

iTCR signalling is a specific forte of CAR-engineered iNKT cells and might be key to streamline the overall CAR-cell manufacturing process.

Hence, having established a highly efficient protocol to produce CAR19-iNKT cells, I planned a set of *in vitro* assays to evaluate CAR19-iNKT cell dual-specific reactivity and test their early cytotoxic response as well as their potential for long term responses. To this end, I have used an array of different CD1d and/or CD19-expressing target cells.

4.2 Optimisation of a flow cytometry based cytotoxicity assay

Natural killer (NK) and T cell-mediated cytotoxicity was traditionally measured in 4–16 h ^{51}Cr-release assays (CRA)[195,196]. Lately, flow cytometry-based methods have been developed to overcome some of the limitations of the CRA, including of safety issues, costs and time of processing, while allowing to dissect the mechanisms and kinetics of killing[197-199]. Specifically, PBMCs from patients can be stained with specific markers for a more accurate quantification of the malignant cell death, while evaluating off-tumour cytotoxicity against bystander healthy cells. In addition, several parameters may be monitored simultaneously on the effector cells as well as the effector-tumour conjugate (ETC) formation, further improving the characterization of the killing process. Therefore, I optimized a flow cytometry-based cytotoxicity assay (FCCA) that allows to simultaneously measure CAR19-cell-mediated cytotoxicity against circulating lymphoma cells, to evaluate potential on-target, off-tumour toxicity against non-malignant cells, to visualize ETC and to determine both effector and target cells immunophenotype.

For validation purposes, I performed a preliminary set of experiments by testing CAR19-T cells against CD19$^+$ B cell line targets, as described in '*Material and Methods'*. Previous work using a similar assay showed that a 3 hour-incubation prior to read-out is optimal and this FCCA is more sensitive than a standard 4-hour CRA to quantify NK or lymphokine-activated killer (LAK) cell-mediated killing of target cells from healthy volunteers and cancer patients[200]. Indeed, in two kinetics studies (1, 2, 3 and 4h) at different CAR19-T effector-to-target cell ratio (E/T; 0.75, 1.5, 3 and 6) I confirmed that a 3 hour-incubation was optimal and that CAR19-engineered T cells effectively killed CD19$^+$ B cell line cells in a dose-dependent manner (**Figure 4-1**), with an

inverse correlation between the E/T ratio and the time required to establish effective immune conjugates (n=2).

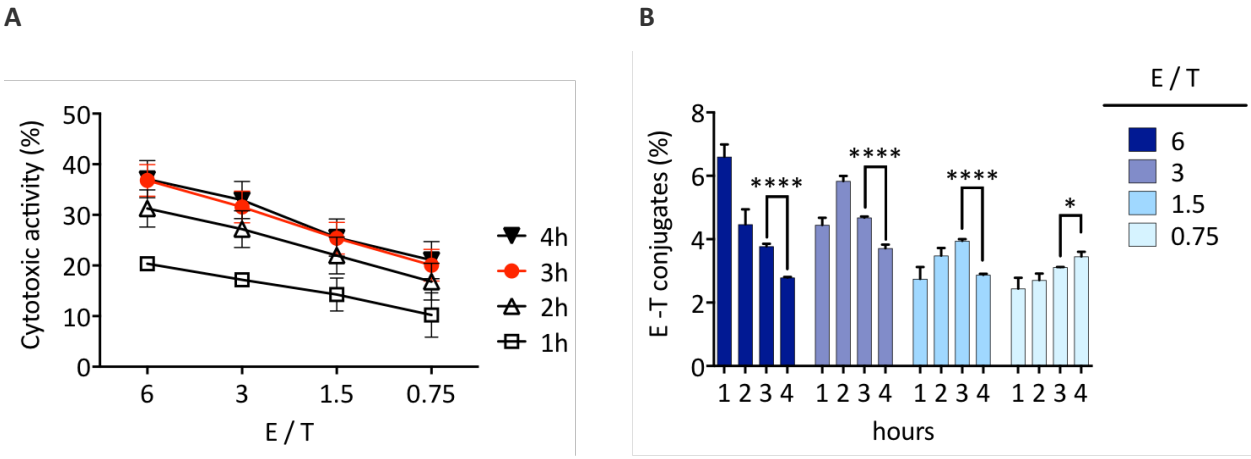


Figure 4-1 Validation of flow-cytometry-based cytotoxicity assay

Representative graphs of CAR19-T cell killing kinetics at different E/T ratios. The final cytotoxicity was comparable at 3 and 4 hours across all E/T ratios (A). However, with the only exeception of the E/T of 0.75, the percentage of effector-target conjugates was higher at 3 hours (B). Error bars represent mean ±S.E.M. of technical triplicates.

4.3 Characterization of CAR19-iNKT cell reactivity

4.3.1 Cooperative killing of $CD1d^{+}CD19^{+}$ targets by dual specific CAR19-iNKT cells

Having validated a robust tool to assess CAR19-cell reactivity and killing potential against target cells, I aimed to functionally validate CAR19-iNKT cells generated according to my optimal manufacturing protocol, i.e. protocol 5.

To this end, first I used the non-B cell lineage K562 cell line, which is naturally $CD1d^{-}CD19^{-}$, and engineered it by retroviral transduction to express either or both antigens (**Figure 4-2**).

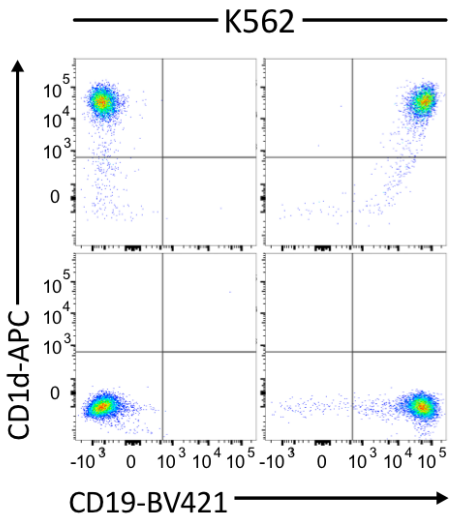


Figure 4-2 CD1d$^+$ and/or CD19$^+$ K562 cells
K562 cells (*bottom left*) were genetically modified with retroviral system to express either CD1d (*top left*) or CD19 (*bottom right*) or both (*top right*)

I found that killing of CD1d$^+$CD19$^-$, CD1d$^-$CD19$^+$ and CD1d$^+$CD19$^+$ targets by 2nd and 3rd generation CAR19-iNKT cells proceeded incrementally (

Figure 4-3). Importantly, (1) engagement of CAR19 effectively activated CAR19-iNKT cells; (2) the endogenous iTCR was functional and both 2nd and 3rd generation CAR19-iNKT cells retained the natural CD1d-restricted reactivity of their parental cells; (3) CAR19-INKT cell reactivity was selective against CD19 and or CD1d -expressing targets, while sparing antigen-negative K562 cells; (4) dual-targeting of CD1d and CD19 resulted in co-operative killing of CD1d$^+$CD19$^+$ cells, thus underscoring the relevance of the endogenous iTCR, together with the exogenous CAR, to determining the final outcome of CAR reactivity. Moreover, in the presence of the iNKT cell selective agonist αGalCer, CAR19-iNKT cell cytotoxicity was further enhanced against CD1d$^+$ and CD1d$^+$CD19$^+$ targets but not against CD1d$^-$CD19$^-$ and CD1d$^-$CD19$^+$ targets (

Figure 4-3 **B**). These findings may support further investigation of integrative approaches combining CAR19-iNKT immunotherapy with administration of clinical grade iNKT cell agonists to enhance CAR19-iNKT cell anti-tumour activity *in vivo*.

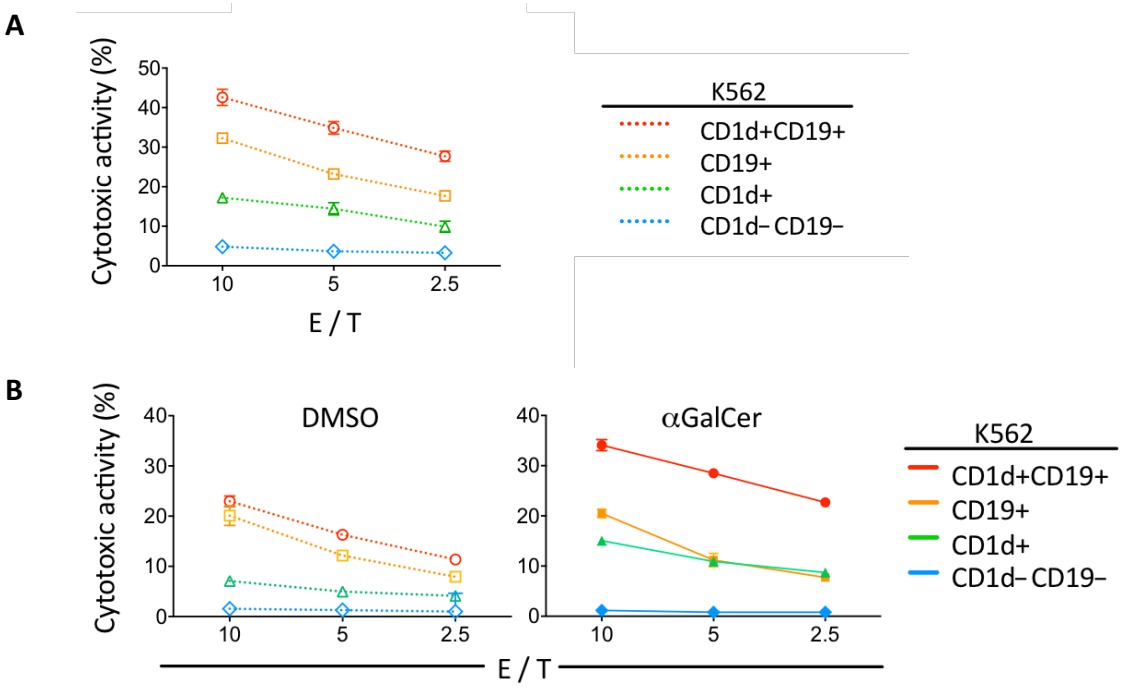


Figure 4-3 CAR19-iNKT cell cytotoxic activity against CD1d$^{+/-}$ and/or CD19 $^{+/-}$ K562 targets

A. Representative cytotoxic activity of 2nd generation CAR19-iNKT cells (generated from donor #4 Laph) against parental CD1d–CD19– K562 cells or K562 cells expressing CD1d and CD19 singly or in combination at the indicated E/T ratios (representative of 3 experiments). B. Representative cytotoxic activity of 3rd generation CAR19-iNKT cells (generated from donor #13 PB) against parental CD1d–CD19– K562 cells or K562 cells expressing CD1d and CD19, singly or in combination, at the indicated E/T ratios. Targets were pulsed overnight with vehicle (*left*) or 100ng/ml αGalCer (*right*) (representative of 2 experiments). Error bars represent S.E.M. of triplicate assays.

4.3.2 Specific killing of B cell lymphoma cell lines by CAR19-iNKT cells

Next, I assessed the *in vitro* reactivity of CAR19-iNKT cells against B cell lines. By using C1R and C1R-CD19 target cells, expressing low or high (exogenous) levels of surface CD19 respectively, I observed that CAR19-iNKT cell cytotoxic activity was proportional to the surface levels of CD19, which is a well-established feature of CAR-mediated specific killing (**Figure 4-4**).

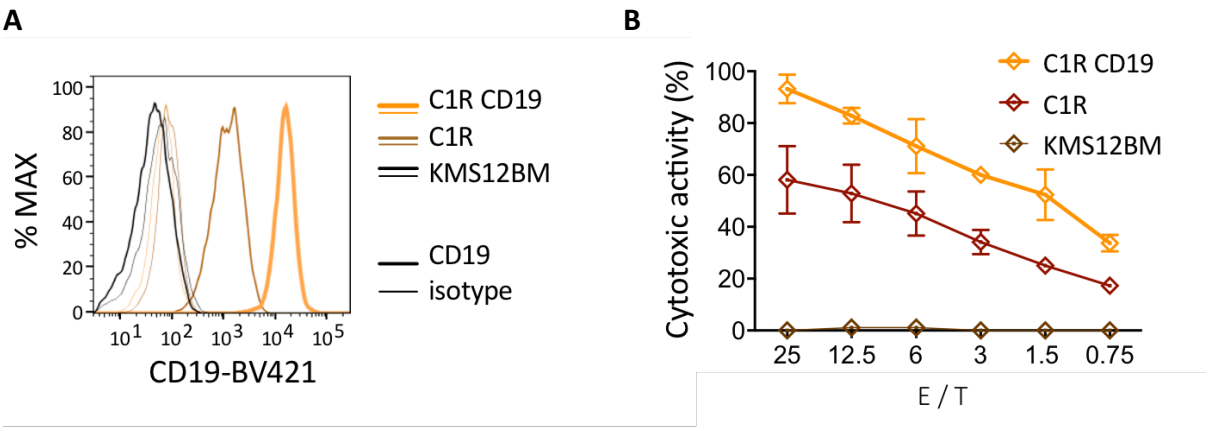


Figure 4-4 CAR19-iNKT cell cytotoxic activity against CD19^{low} and CD19^{high} targets

A. The C1R B cell line (*brown*), which is constitutively CD19^{+} compared to the myeloma KMS12MB cell line (*black*), was engineered with CD19 retrovirus to stably express higher levels of exogenous CD19 (*orange*). Expression levels were determined relative to isotype controls (*hair lines*). B. Representative cytotoxic activity of 2nd generation CAR19-iNKT cells against CD19^{low} and CD19^{high} C1R cells and control CD19^{-} KMS12BM cells. (n=2 experiments). Error bars represent S.E.M. of triplicate assays.

Similarly, in assays where ARH-77 and ARH-77-CD1d cells served as targets, increasing levels of surface CD1d on the cancer cells were associated with a proportional increase in the iTCR-mediated cytotoxic activity (**Figure 4-5**).

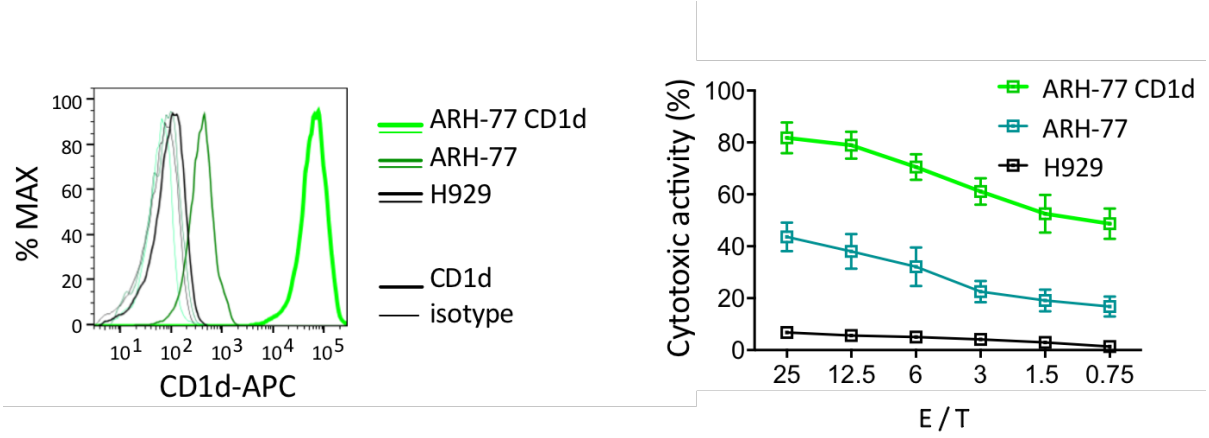


Figure 4-5 CAR19-iNKT cell cytotoxic activity against CD1d^{low} and CD1d^{high} targets

A. The CD19^{dim} ARH-77 plasma cell leukaemia cell line, which is constitutively CD1d^{dim} (*dark green*) compared to the myeloma H929 cell line (*black*), was engineered with CD1d lentivirus to stably express higher levels of exogenous CD1d (*light green*). Expression levels were determined relative to isotype controls (*hair lines*). B**.** Representative cytotoxic activity of 3rd generation CAR19-iNKT cells against CD1d^{dim} and CD1d^{high} ARH-77 cells and control CD1d^{-}CD19^{-} H929 cells. (n=2 experiments). Error bars represent S.E.M. of triplicate assays.

4.3.3 Enhanced reactivity of CAR19-iNKT cells against B cell lymphoma cell lines

Next, I sought to compare side-by-side the reactivity and killing potential of same-donor CAR19- iNKT and -T cells.

In a preliminary set of FCC assays using effectors cells derived from 4 different donors, I tested 2nd generation CAR19-cells against $CD19^{low}$ C1R, $CD19^{high}$ AK, $CD1d^{high}CD19^{low}$ C1R-CD1d and $CD1d^{low}CD19^{high}$ Farage cells at fixed E/T of 1:1. Irrespective of the donor and target cell type, CAR19-iNKT cells killed a higher proportion of tumour cells over 3 hours compared to CAR19-T cells (**Figure 4-6**).

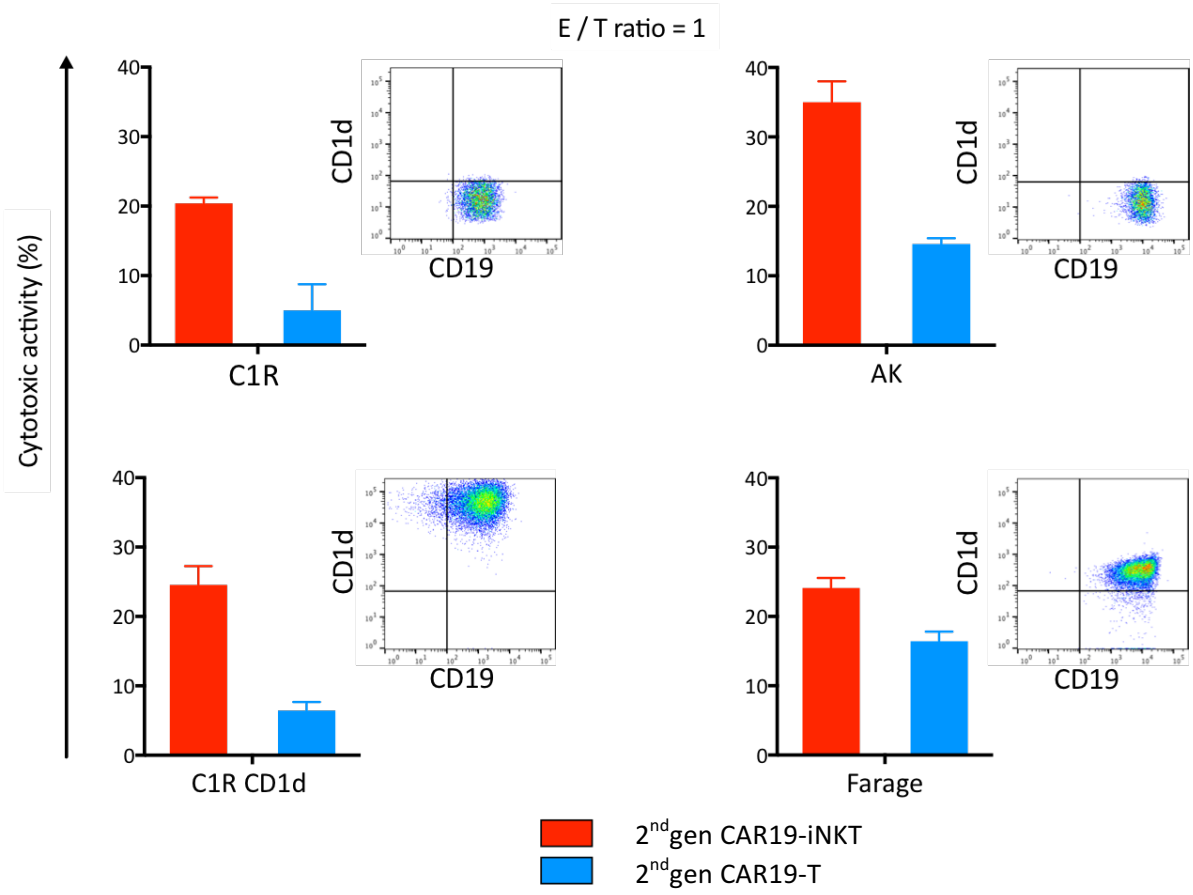


Figure 4-6 Cytotoxicity of 2nd generation CAR19-iNKT vs -T cells at E/T of 1
Representative bar graphs showing cytotoxicity of 2nd generation (2ndgen) CAR19-T and -iNKT cells against $CD19^{low}$ C1R (n=2), $CD19^{high}$ AK (n=2), $CD1d^{high}CD19^{low}$ C1R-CD1d (n=3) and $CD1d^{low}CD19^{high}$ Farage cells (n=2) at fixed E/T of 1:1. Error bars represent S.E.M. of triplicate assays.

The same pattern was observed for 3rd generation CAR19-iNKT cells, with further enhancement in the presence of the iNKT cell agonist αGalCer (**Figure 4-7** and **Figure 4-8**), thus confirming the relative importance of iTCR-mediated reactivity in the context of CAR-iNKT-based immunotherapy.

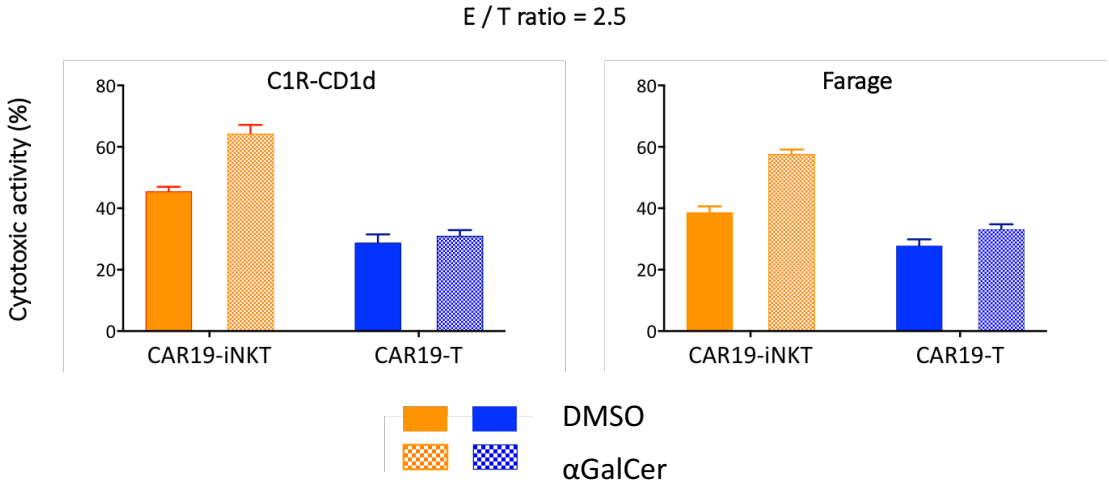


Figure 4-7 Cytotoxicity of 3rd generation CAR19-iNKT vs -T cells at E/T 2.5
Representative cytotoxicity of 3rd generation CAR19-iNKT and -T cells against C1R-CD1d (n=3) and Farage lymphoma cell lines (n=2) pulsed with vehicle or αGalCer. Error bars represent S.E.M. of triplicate assays.

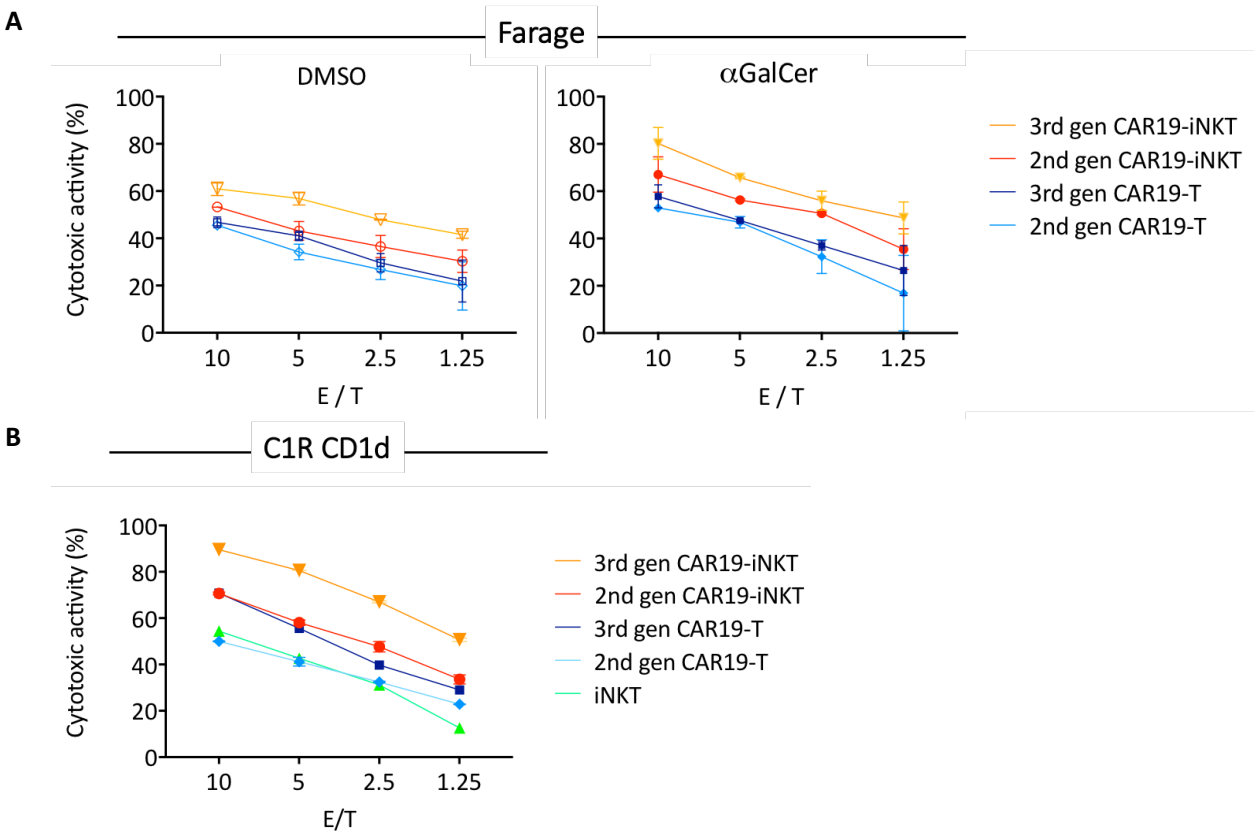
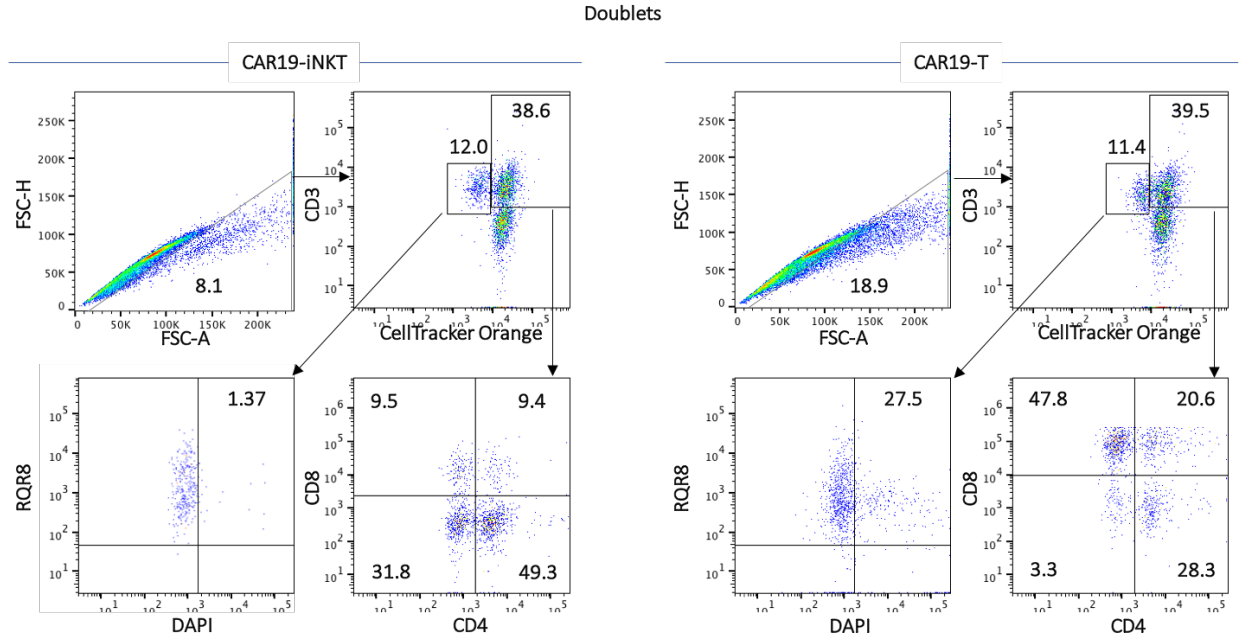


Figure 4-8 Cytotoxicity of 2nd and 3rd generation CAR19-iNKT vs -T cells at E/T of 10, 5, 2.5, 1.25
A. CAR19-iNKT effectively killed Farage cells, 3rd generation CAR19-iNKT outperformed all other groups in terms of cytotoxic activity. The addition of αGalCer further enhanced CAR19-iNKT effector reactivity, resulting in a superior killing by both 2nd and 3rd generation CAR19-iNKT compared to their T counterparts. B. CAR19-iNKT were superior to conventional CAR19-T cells against αGalCer-pulsed C1R-CD1d cells.

Additional analysis of ETC, identified as $CD3^+$ targets within doublets (**Figure 4-9**), showed that, at the end of 3-hour incubation, the proportion of ETC was inversely correlated with the E/T ratio and higher within targets exposed to 2nd generation CAR19-T versus CAR19-iNKT (**Figure 4-10**). These differences were even more pronounced in the case of 3rd generation CAR-engineered cells and upon addition of αGalCer to the culture systems (**Figure 4-10B**). All together, these findings suggest that that dual-specific CAR19-iNKT may be more effective killers as a result of a swifter reactivity characterised by (1) higher avidity (iTCR and CAR19), leading to (2) faster engagement of target cells (conjugate formation), (3) prompt activation and effective lysis, followed by (4) rapid dissociation from the target cells, thus reducing the time of cell-to-cell interactions and the probability of tracking ET conjugates.

A



B

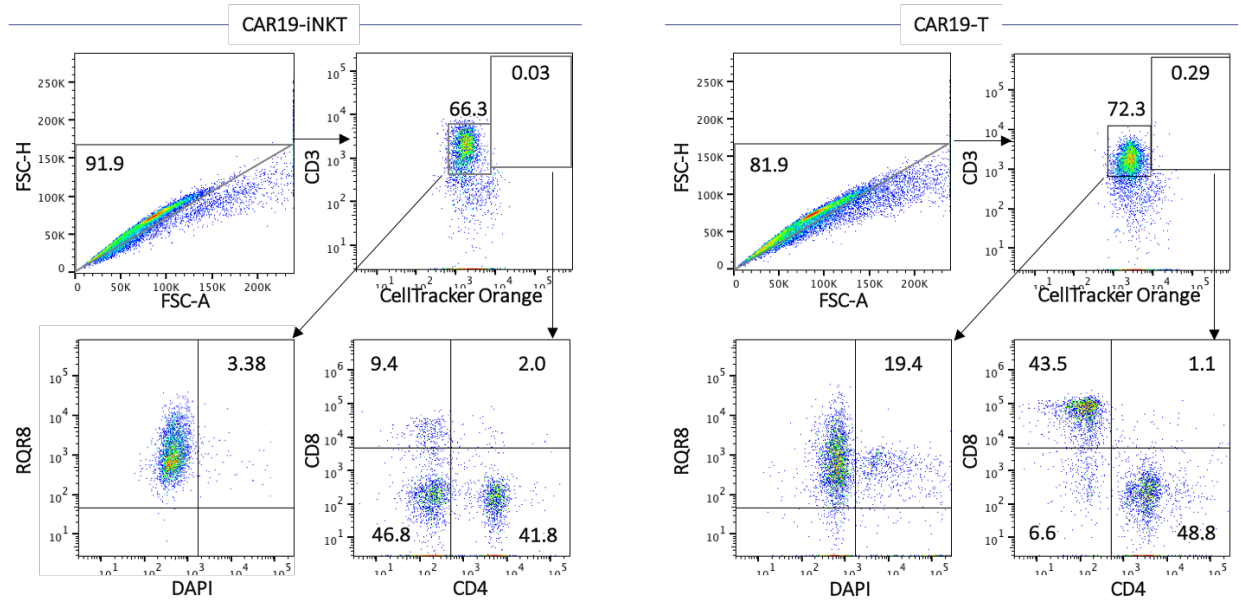


Figure 4-9 Effector-target conjugates analysis

Representative plot from E/T 1.25. A. the percentage of conjugates (FSC-A/H^{high}, CD3^{+}Orange^{+}) and dead CAR19-effectors (DAPI^{+}) was lower in the iNKT cell group. Both cell types showed cooperative killing of CD4^{-} and CD4^{+} subsets (CD4^{+}CD8^{+} events). In the CAR19-iNKT samples (*left panels*), the prominent relative reduction of CD4^{-}CD8^{-} (DN) events within conjugates (*bottom right* plots), i.e. 31.8% (A) vs 46.8% (B), suggests that DN effectors were 'gathering' to kill the cancer cells together with CD4^{+} (CD4^{+} events) and/or CD8^{+} (CD8^{+} and CD4^{+}CD8^{+} events) CAR19-iNKT cells. B. There were less dead CAR19-iNKT cells, which were all expressing high CAR levels and potentially available to re-engage with the targets.

Notably, I found a higher percentage of non-interacting DAPI (or 7-AAD)$^{+}$ 2nd generation CAR19-T cells compared to 2nd generation CAR19-iNKT cells, further corroborating the hypothesis that dual-specific CAR19-iNKT may be more effective killers also as a result of lower AICD.

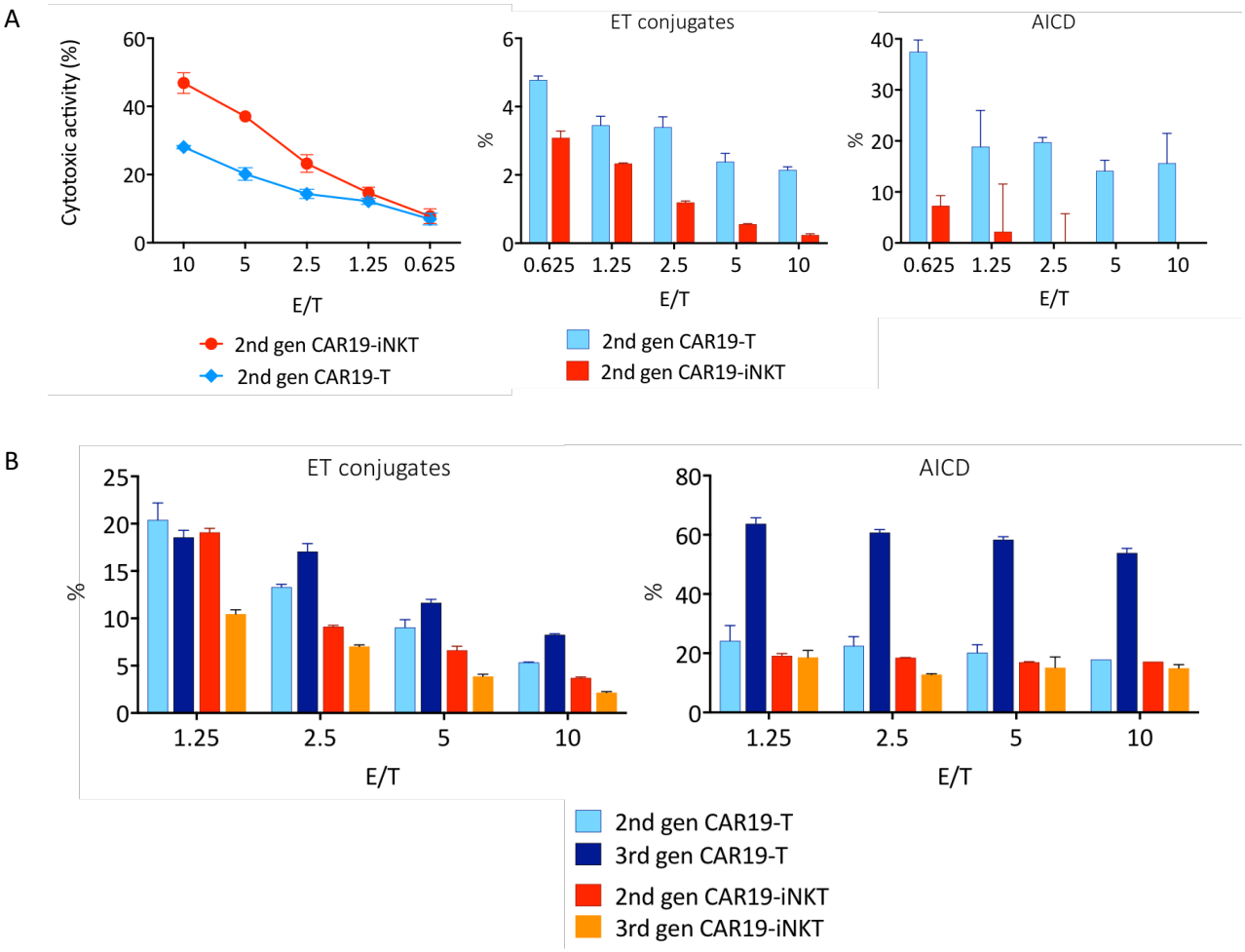


Figure 4-10 Conjugate formation and associated activation-induced effector-cell death

A 2nd generation (2nd gen) CAR19-iNKT and –T cells were tested against C1R-CD1d cells. At the end of 3-hour incubation, CAR19-iNKT cell cytotoxic activity was superior than that of CAR19-T cells (left), more CAR19-T cells were found to be involved in cell-to-cell interactions with target cells (middle) and the proportion of dead effectors within doublets was higher in the CAR19-T wells (right; representative of 2 experiments; error bars represent S.E.M. of technical triplicates). B 2nd and 3rd generation CAR19-iNKT, killing αGalCer-pulsed C1R-CD1d cells as shown in Figure 4-8 B. displayed a lower percentage of effector cells involved in conjugates compared to CAR19-T cells at the same E/T ratio. The fraction of dead effectors within doublets was significantly higher in the third-generation CAR19-T cell samples ($P<0.0001$; 1 experiment; error bars represent S.E.M. of technical triplicates).

Immunophenotypic analysis of CAR19-effector cells confirmed the contribution of both $CD4^+$ and $CD4^-$ subsets to ECT formation (**Figure 4-11**), providing an additional argument in favour of the hypothesis that both $CD4^+$ and $CD4^-$ CAR19-iNKT cells can exert killing functions.

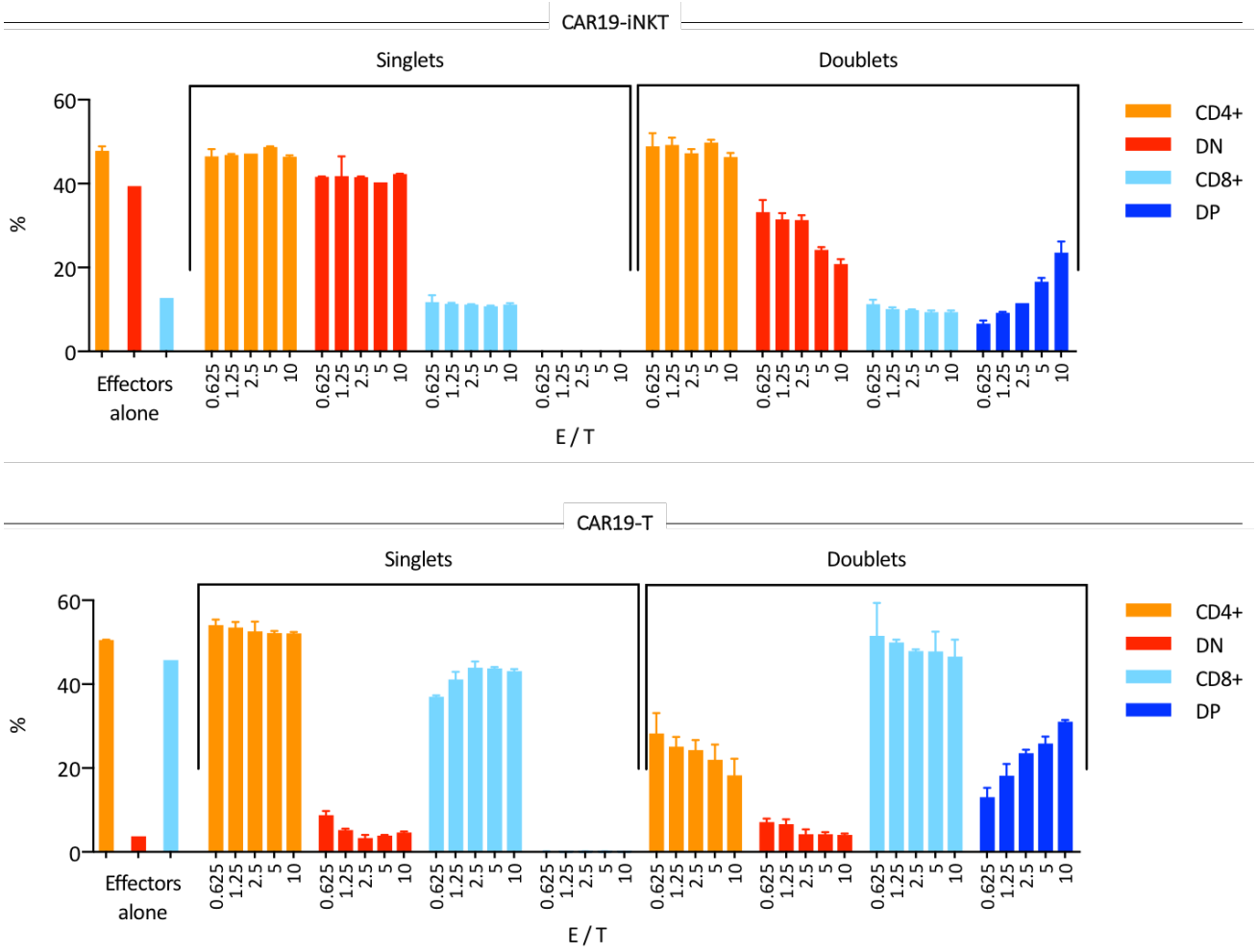


Figure 4-11 $CD4^+$ and $CD4^-$ conjugates
Representative bar graphs showing the distribution of $CD4^{+/-}$ effectors within singlets and conjugates as shown in **Figure 4-9**. Representative of 2 experiments. Error bars represent S.E.M. of technical triplicates.

Indeed, when I measured the cytotoxic activity of sorted end-of-manufacturing $CD4^+$ and $CD4^-$ CAR19-iNKT cells, cultured for an additional week under resting conditions without their CD4 counterpart, I couldn't observe any difference in the final outcome (**Figure 4-12**).

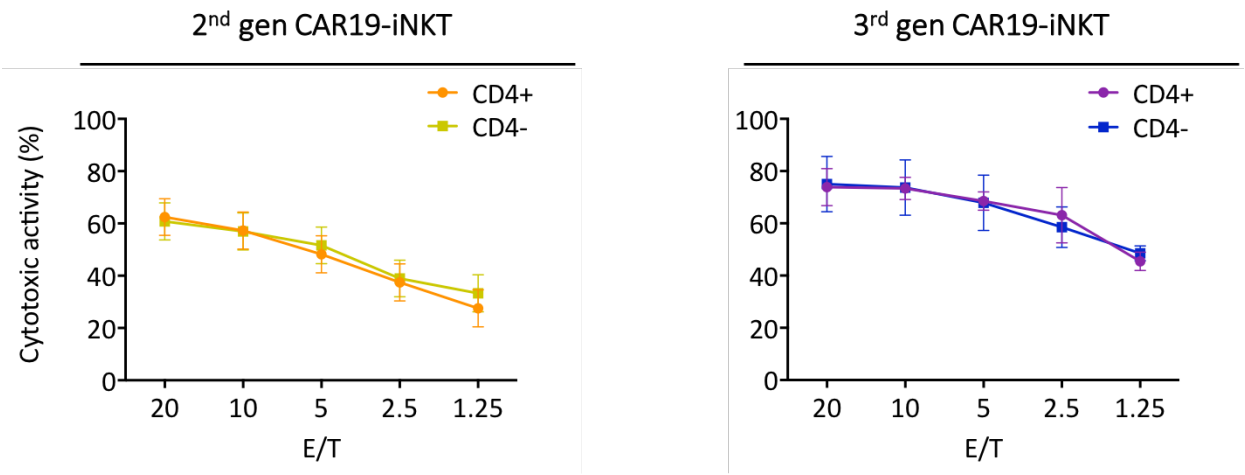


Figure 4-12 CD4$^+$ vs CD4$^-$ CAR19-iNKT cells cytotoxicity against B cell targets
Sorted CD4$^+$ and CD4$^-$ CAR19-iNKT cells were tested against αGalCer-pulsed C1R-CD1d cells. There was no difference in the cytotoxic activity of the two subsets addressed separately (n=1 experiment). Error bars represent S.E.M. of technical triplicates. gen: generation.

4.3.4 Sustained proliferative response coupled to enhanced killing by CAR19-iNKT cells

As mentioned in 3.4 *'Scale-up steps' for clinical scale manufacturing of CAR19-iNKT cells*, CAR19-iNKT cells expand to a greater extent than their T cells counterparts in response to antigen stimulation (**Figure 3-15**). Since the proliferative response to cancer cells has been proved to be a predictive marker of *in vivo* killing activity and clinical outcome[34], I performed a series of 7-day real-time monitoring experiments aiming to evaluate such proliferative response coupled to the cytotoxic activity of CAR19-iNKT cells.

First, by using contrast phase imaging assays I confirmed that CAR19-iNKT cell proliferative response to αGalCer-pulsed irradiated C1R-CD1d cells outperforms that of same-donor CAR19-T cells (**Figure 4-13, Video 1**), with 3rd generation CAR19-iNKT cells reporting the best expansion (n=4, 2 donors).

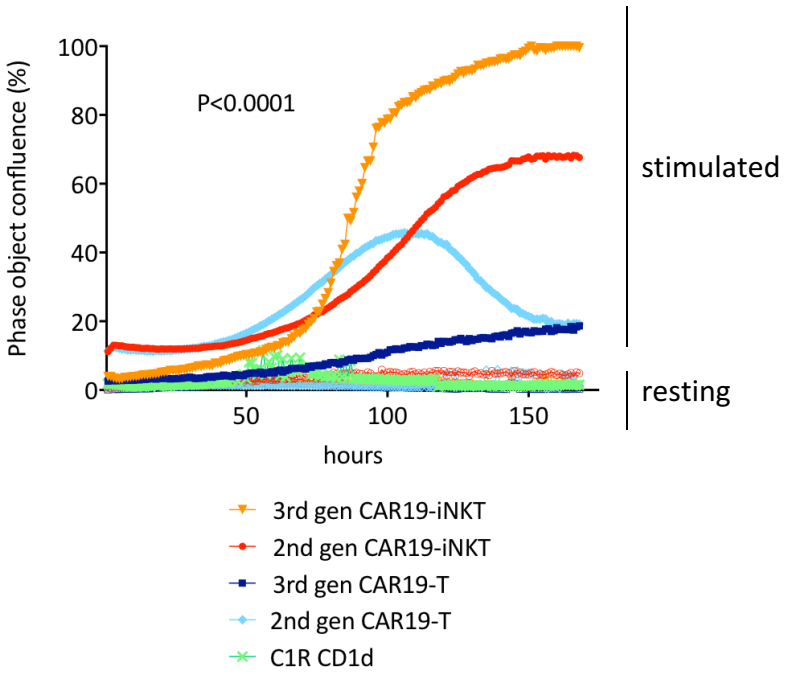
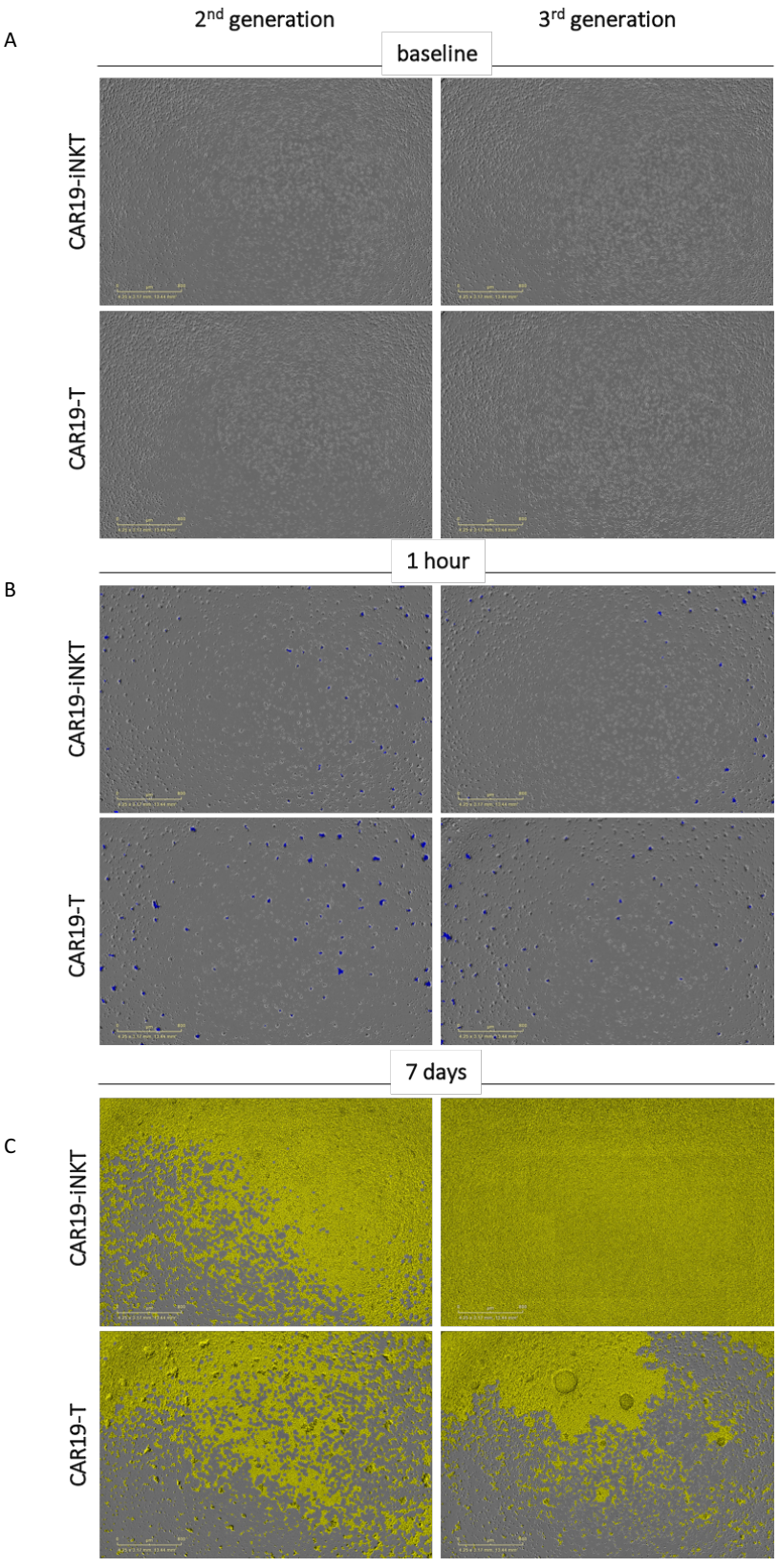


Figure 4-13 Real-time monitoring and analysis of proliferation of CAR19-iNKT vs CAR19-T cells
Seven-day proliferation real-time monitoring and analysis by IncucyteZOOM of 2nd and 3rd generation CAR19-T and CAR19-iNKT cells in the presence (stimulated) or not (resting) of irradiated C1R-CD1d cells. P value is for CAR19-iNKT vs CAR19-T cells using Friedman test.

As shown in **Figure 4-14**, at the beginning of the incubation, single effectors and targets were uniformly distributed across the entire well surface (**A**, grey objects). 60 minutes later, CAR19-T cell wells generally displayed higher levels of large clusters, i.e. interacting cells equivalent to ET conjugates by flow cytometry (**B**, blue masked objects). By contrast, clusters were significantly less and smaller in the CAR19-iNKT wells, particularly in those incubated with the 3rd generation CAR-engineered cells. (**B**). Over the time, 3rd generation CAR19-iNKT cells exhibited the greatest ability to divide and proliferate, thus covering increasing proportions of the well surface (higher phase object confluence) in a more sustained manner compared to all other groups (**C**). 3rd generation CAR19-T cells did exhibit the same predisposition to divide, but failed to effectively proliferate and 'fill in' the available space and mainly persisted as single cells (**C**). That was likely to be due at least in part to AICD, as suggested by the incremental levels of cell debris (**Figure 4-15**). As a control, irradiated C1R-CD1d as well as CAR-effector cells alone did not form clusters and tend to die through the end of the experiment (**Figure 4-16**).

All together, these findings provided some additional data to infer about different kinetics of cytotoxicity according to cell type and CAR design. Specifically, it is well-established that the proportion of ETC at a certain time point and fixed E/T ratios inversely correlates with the ability of the effectors to recognize and successfully attack a target cell[200]. Indeed, as previously mentioned, more potent effectors rapidly kill, swiftly dissociate and are less likely to be tracked in conjugation with their target. Instead, less potent killer cells generally require more time to establish an effective immune synapse and deliver their lethal blow, thus remaining bound longer and dissociating slowly[200]. Accordingly, consistent with previous ETC analysis by flow cytometry, at the beginning of my real-time monitoring I observed a significant proportion of clusters in the wells with 2nd generation but not 3rd generation CAR-engineered cells; this was also in line with the knowledge that 3rd generation constructs trigger more robust activating signals. Remarkably, only iNKT cells proved to tolerate such level of activation, while AICD seemed to undermine the CAR19-T response, leading to a poorer outcome.



Average cell clusters / well

2nd gen CAR19-iNKT
number: 226 ±29.18
area: 669,70 µm2 ±55.57

3rd gen CAR19-iNKT
number: 120 ±8.38
area: 586.86 µm2 ±53.10

2nd gen CAR19-T
number: 269 ±28.03
area: 923.91 ±100.40

3rd gen CAR19-T
number: 236 ±25.52
area: 976.44 µm2 ±120.21

Average cell confluency / well

2nd gen CAR19-iNKT 67.63% ±0.32

3rd gen CAR19-iNKT 99.5% ±1.01

2nd gen CAR19-T 19.21% ±0.82

3rd gen CAR19-T 18.7% ±0.57

Figure 4-14 CAR19-iNKT vs -T cells cell clustering and confluency analysis by IncucyteZOOM

Figure 4-14 CAR19-iNKT vs –T cell clustering and confluency analysis by IncucyteZOOM
A. At the beginning of the incubation, single effectors and targets were uniformly distributed across the entire well surface. B. Clusters were identified by using the IncucyteZOOM cell clustering algorithm as objects with area ≥150µm^2 and eccentricity ≤0.8 and visualised by a blue mask. Images are representative of 2 experiments, 5 technical replicates each. The shown cluster average number per well and area are representative from 1 experiment. C. Cell proliferation was quantified as percentage of single cell confluency and visualised by using a yellow mask.

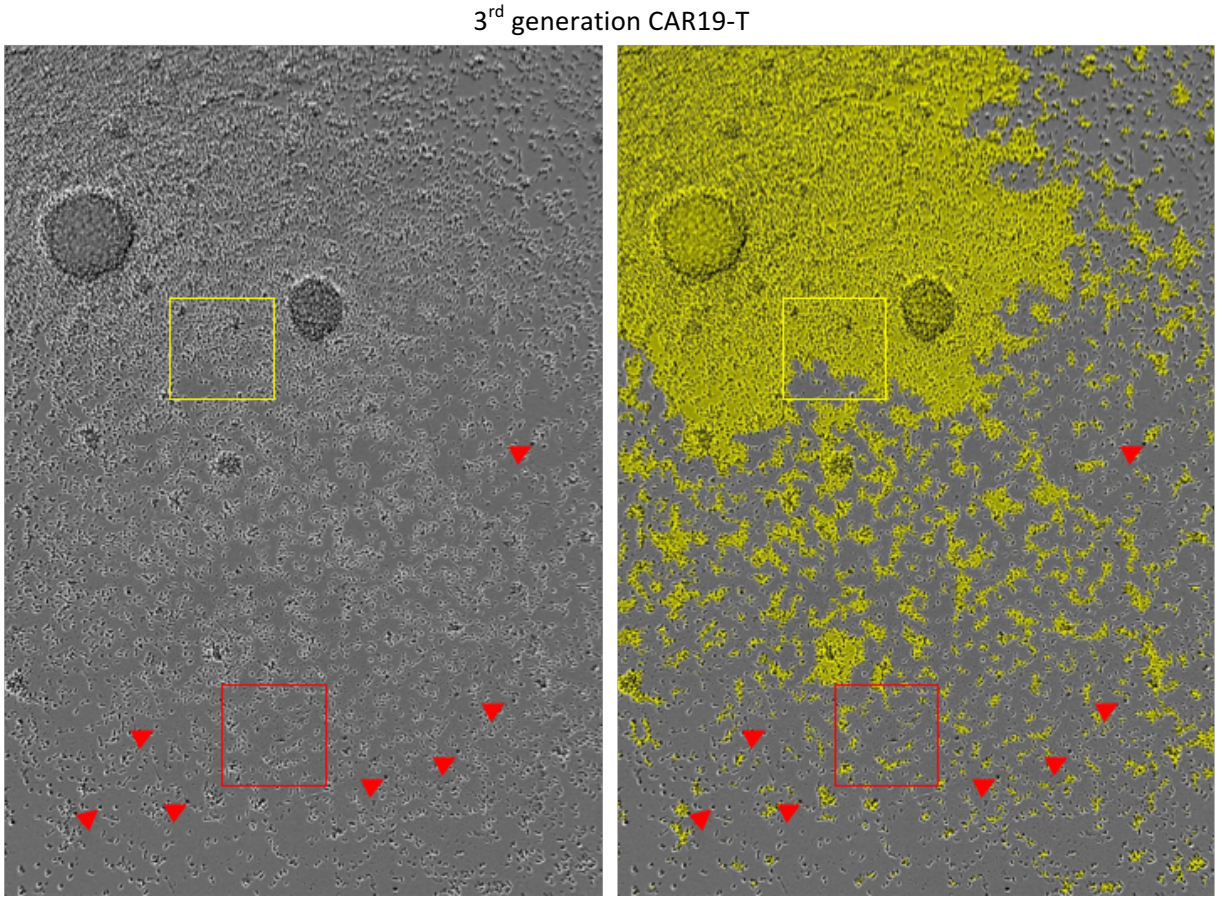


Figure 4-15 Visualization of third CAR19-T cell proliferation by IncucyteZOOM
Real-time monitoring by IncucyteZOOM of CAR19-effectors stimulated with irradiated CD19$^+$ C1R-CD1d targets showed incremental levels of picnotic cells (*red arrows*) and cell debris (*red box*) in 3rd generation CAR19-T cell wells. Note the contrast between healthy proliferating cells, which are oblong and morphologically well-defined while propagating over a 'clean' well floor (*yellow box*), and dying cells, characterised by loss of morphological definition, faded appearance and shrinkage, surrounded by black dots (dead cells, *red arrows*) and cell debris (*red box).*

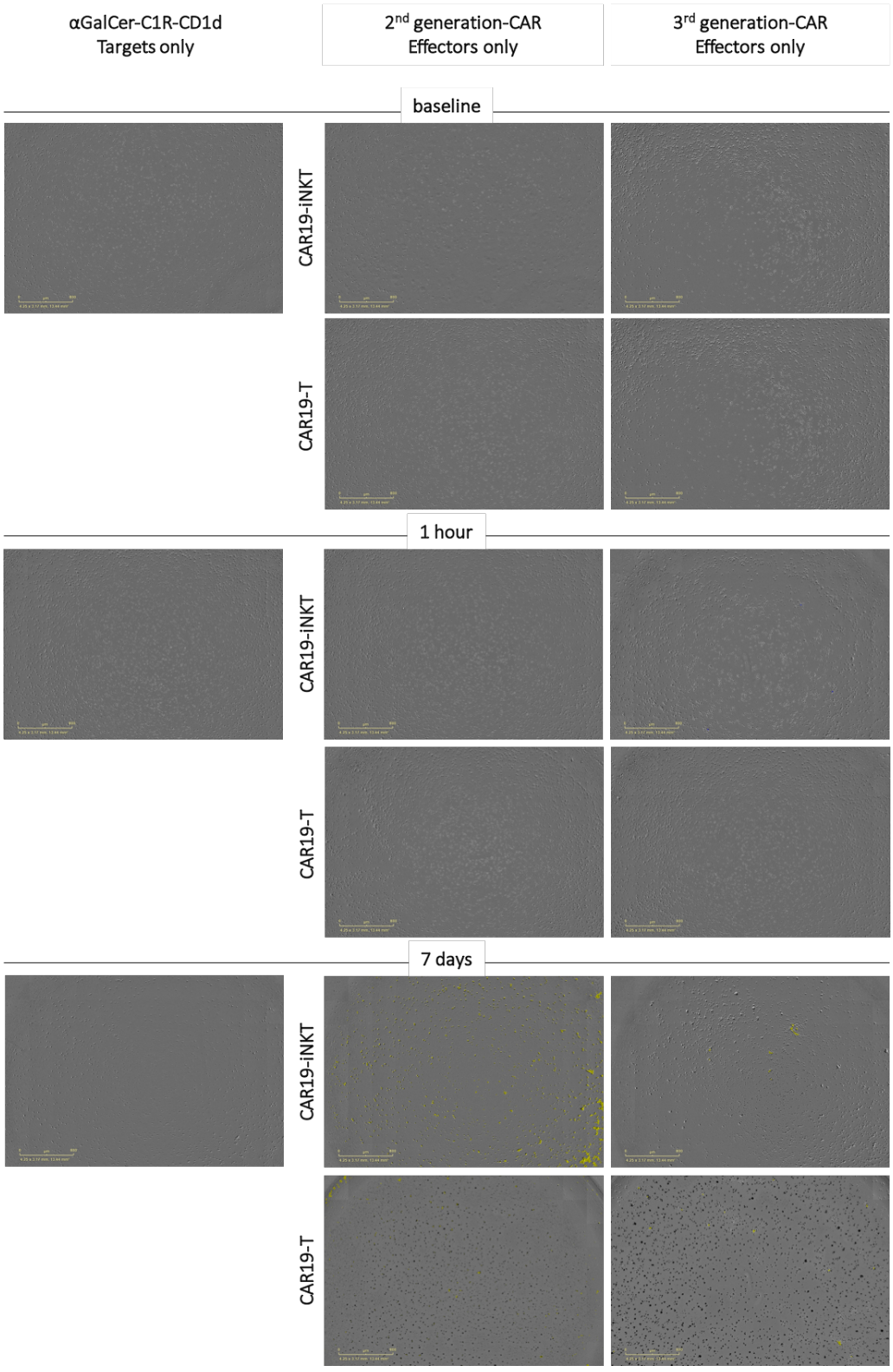


Figure 4-16 Control wells for cell clustering and confluency analysis by IncucyteZOOM
Representative images from control wells of seven-day proliferation assays. Irradiated C1R-CD1d as well as CAR-effector cells alone did not form clusters (no blue mask applicable at 1 hour, *middle panels*) and tend to die (black dots) through the end of the experiment (no or minimal yellow confluency mask, in the case of conglomerate of viable but not proliferating CAR19-iNKT cells).

Next, by using a two-phase channel imaging assay, I real-time monitored both proliferative response of 2nd generation CAR19-effector cells and growth/viability of non-irradiated CD19^{+}CD1d^{+} target cells (ARH-77-CD1d) over a period of 7 days (**Figure 4-17,** and **Video 2**). Cells were incubated at E/T ratios of 1 and 10 without any additional activation, i.e., in low-cytokine medium with 20IU IL-15/ml and no αGalCer**.** No further manipulation was carried out during the experiment. As shown in **Figure 4-17**, CAR19-iNKT cells killed more effectively ARH-77-CD1d cells at both E/T ratios. Notably, only CAR19-iNKT cells displayed the potential for eradicating cancer cells, as suggested by the sustained loss of red fluorescent signal exclusively in the CAR19-iNKT cell wells at E/T 10. Moreover, the final cytotoxic activity of CAR19-iNKT cells at E/T of 1:1 was similar to those of CAR19-T cells at an E/T ratio of 10:1. That was coupled with a more profound and sustained proliferative response of CAR19-iNKT cells, while a proportion of CAR19-T effectors showed evidence of death (amorphous grey ring in the middle of the growing spheroid). As a result, the final outcome of CAR19-iNKT cells at E/T of 1:1 was comparable to that of CAR19-T cells at an E/T ratio of 10:1, suggesting a functional equivalence of CAR19-iNKT : CAR19-T of 10:1.

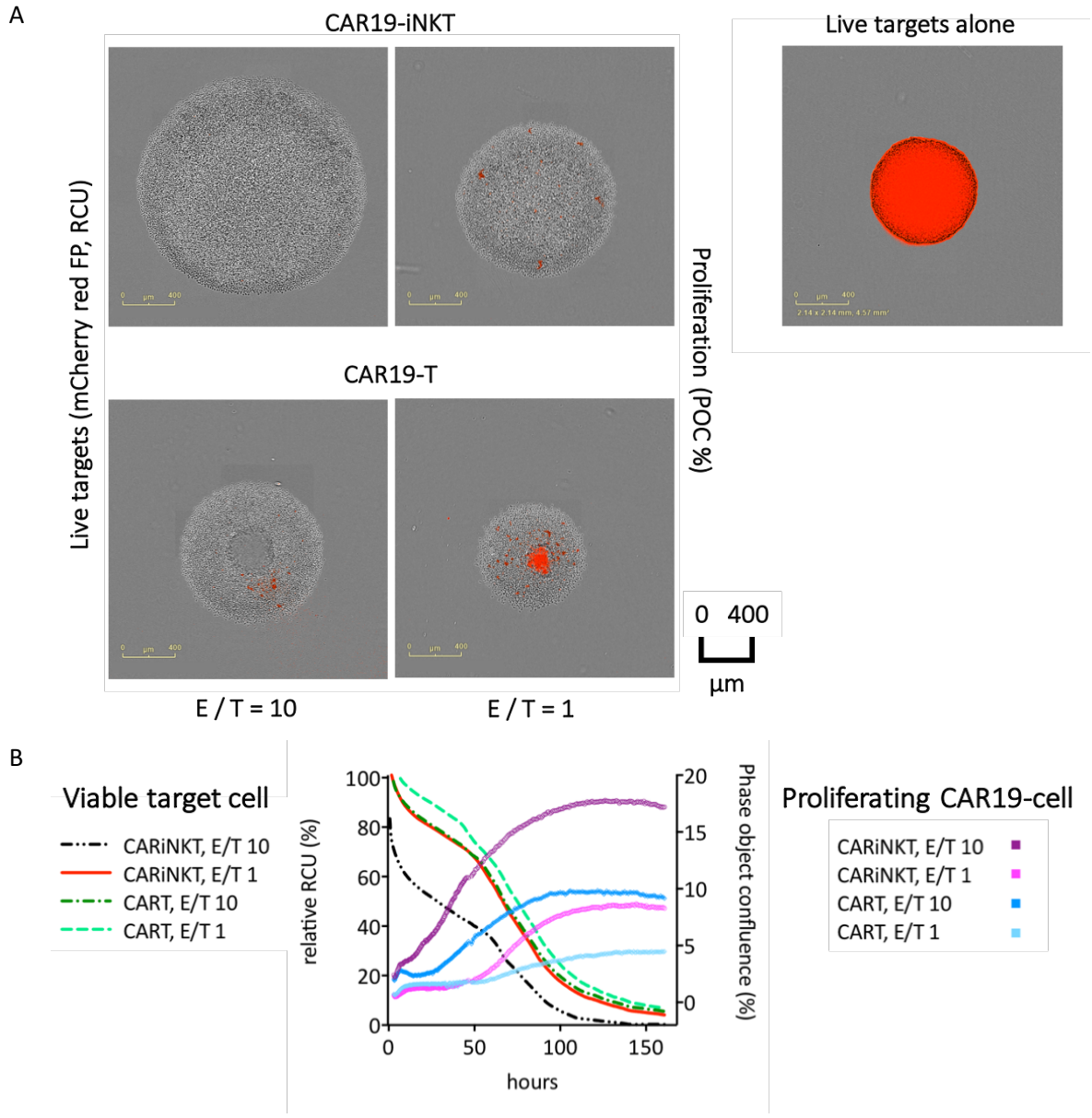


Figure 4-17 Real-time monitoring of proliferation and cytotoxicity of CAR19-iNKT vs CAR19-T cells

A. Combined Incucyte images of representative wells showing the final effectors (grey objects) and live targets (red objects) after seven-day co-culture. Effectors were 2nd generation CAR19 -T and -NKT cells. Targets were ARH-77-CD1d cells labelled with mCherry red fluorescent protein. B. Seven-day trajectory of effector and target cell proliferation and elimination respectively ($P<0.0001$ for CAR19-iNKT vs CAR19-T cells according to Friedman test).

4.3.5 Enhanced reactivity of CAR19-iNKT cells against primary B cell lymphoma cells

Finally, to better reflect the clinical context, I set up cytotoxicity assays using as targets primary CD1d^{+} B lymphoma cells from one patient with blastic variant of MCL and two patients with MZL, which co-express CD1d and CD19[131] (**Figure 4-18**)

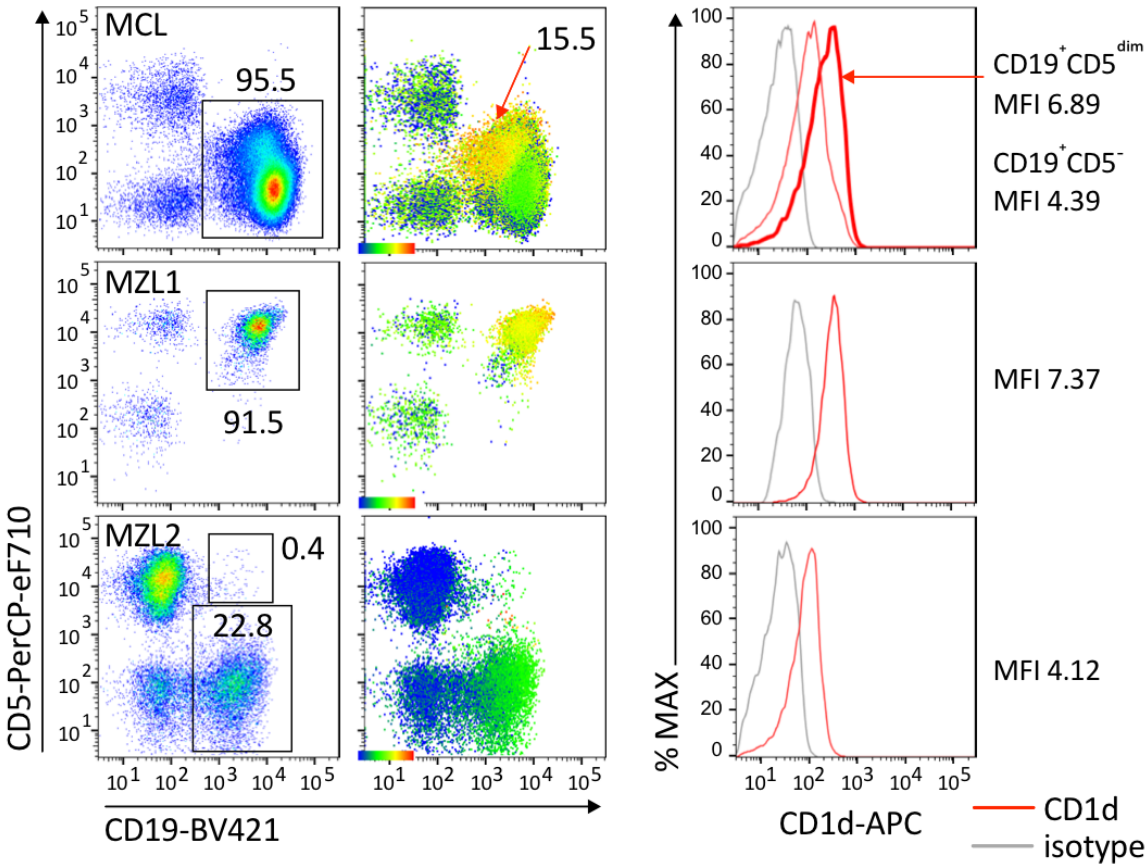


Figure 4-18 CD1d surface expression on primary B cell lymphoma cells

Flow-cytometric analysis of CD19 and CD1d co-expression on peripheral blood lymphoma cells from one patient with blastic variant of MCL (*top*) and two patients with MZL (*middle* and *bottom*). CD19^{+} malignant cells (boxed in pseudocolor plots, *left* panels) expressed low-to-intermediate levels of surface CD1d, as shown in the colour maps on CD5/CD19 dot plots (*middle* panels, MFI increasing from the blue-green tone towards the red tone) and histograms (*right* panels). Note the presence of 2 different lymphoma populations with different levels of CD1d expression in the MCL patient.

In 6 out of 7 assays involving 3 healthy donors, CAR19-iNKT cells were more cytotoxic than CAR19-T cells (**Figure 4-19**).

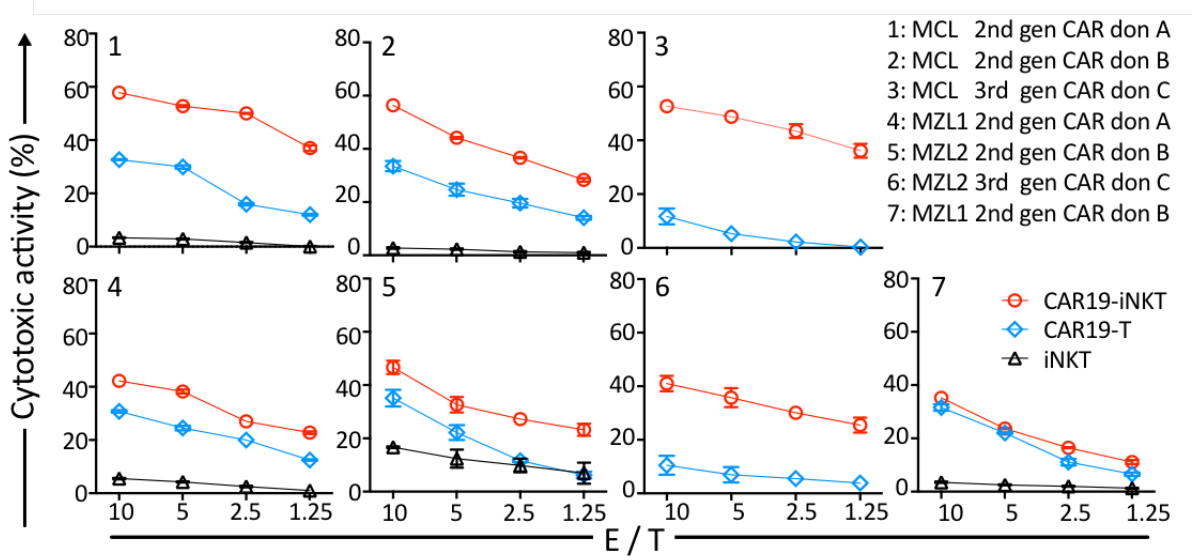


Figure 4-19 CAR19-iNKTvs CAR19-T vs iNKT cell cytotoxicity against primary B cell lymphoma cells
Cytotoxicity of CAR19-iNKT, CAR19-T and of untransduced iNKT cells against lymphoma cells from one patient with MCL (*top*) and two patients with MZB lymphoma (*bottom*) using three different T/iNKT cell healthy donors. Error bars represent S.E.M. of triplicate assays.

Further assessment of cell size and 7-AAD retention (as shown in **Figure 4-20**) confirmed superior killing by CAR19-iNKT cells of all patient lymphoma cells (**Figure 4-21A-B**).

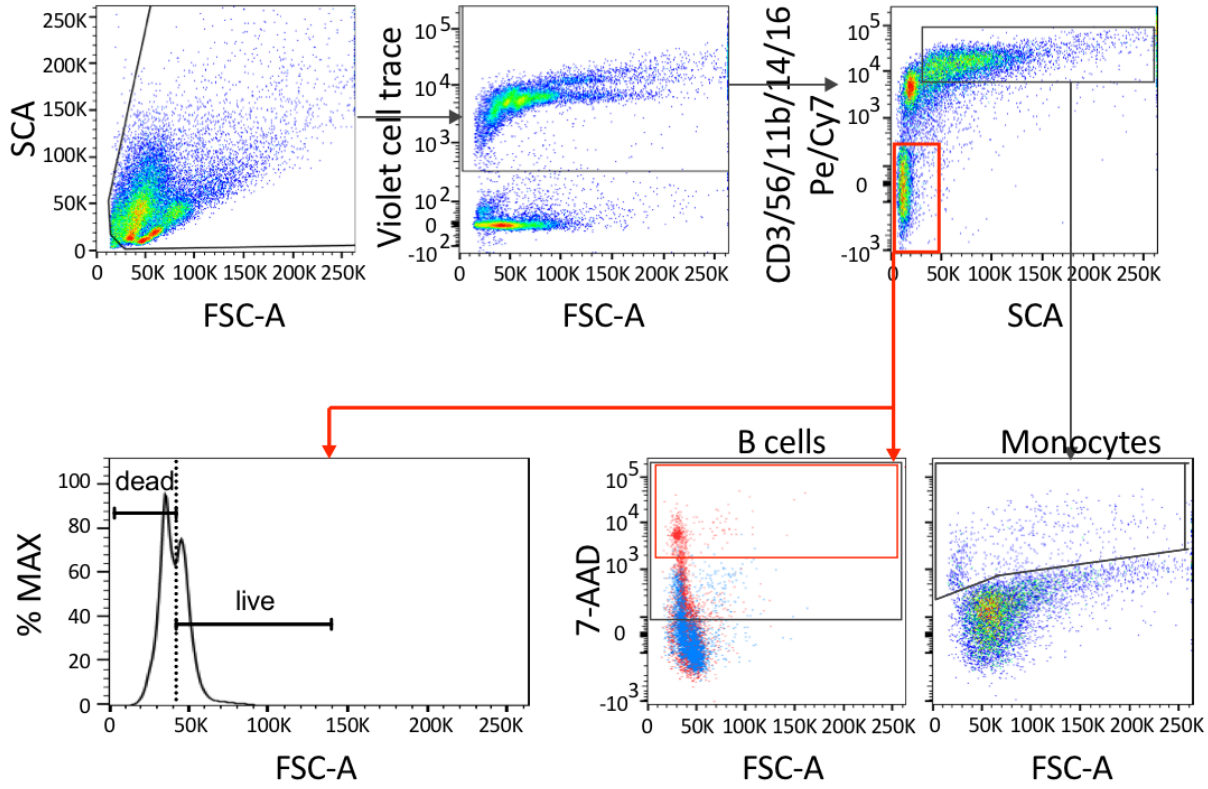


Figure 4-20 Gating strategy of FCCA with lymphoma cell targets

Patients PBMCs were labeled with violet cell tracer and subsequently stained with a PeCy7-conjugated antibody mix to allow identification of lymphoma cells (Violet+, CD19+CD3/56/11b/14/16–, SCA^{low}) and monocytes (Violet+, CD3/56/11b/14/16+, SCA^{high}) within the same sample. Dead cells were identified as 7-AAD+ events, with high and intermediate 7-AAD intensity corresponding to necrotic and apoptotic cells respectively[201]. Cell death was also assessed by cell size (FSC-A) with smaller cells corresponding to apoptotic/necrotic cells.

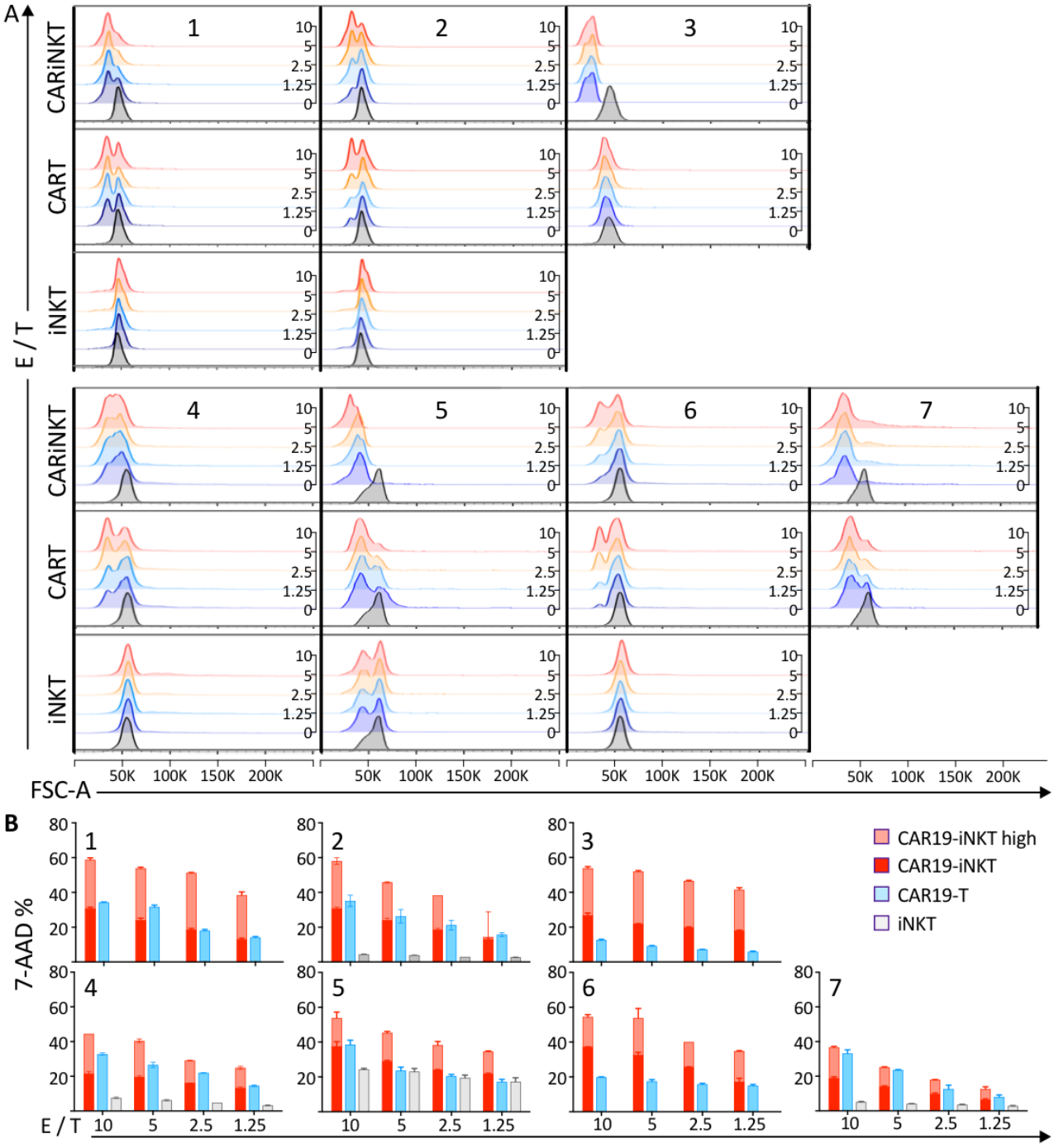


Figure 4-21 Primary B cell lymphoma cell death analysis by FCCA

A. Flow-cytometry histograms showing FSC-A-based cell size analysis of primary lymphoma target cells in cytotoxicity assays with CAR19-iNKT, CAR19-T and untransduced iNKT cells. B. Fraction of 7-AAD^{high} and 7-AAD^{dim} primary lymphoma cells in cytotoxicity assays with CAR19-iNKT, CAR19-T and untransduced iNKT cells. Error bars represent S.E.M. of triplicate assays

In these ‘same-tube' assays we also observed low-to-no killing of monocytes (

Figure 4-23), which express high levels of CD1d[202] but not CD19 (

Figure 6-24), suggesting a low ‘*on-target, off-tumour*’ reactivity of CAR19-iNKT cells.

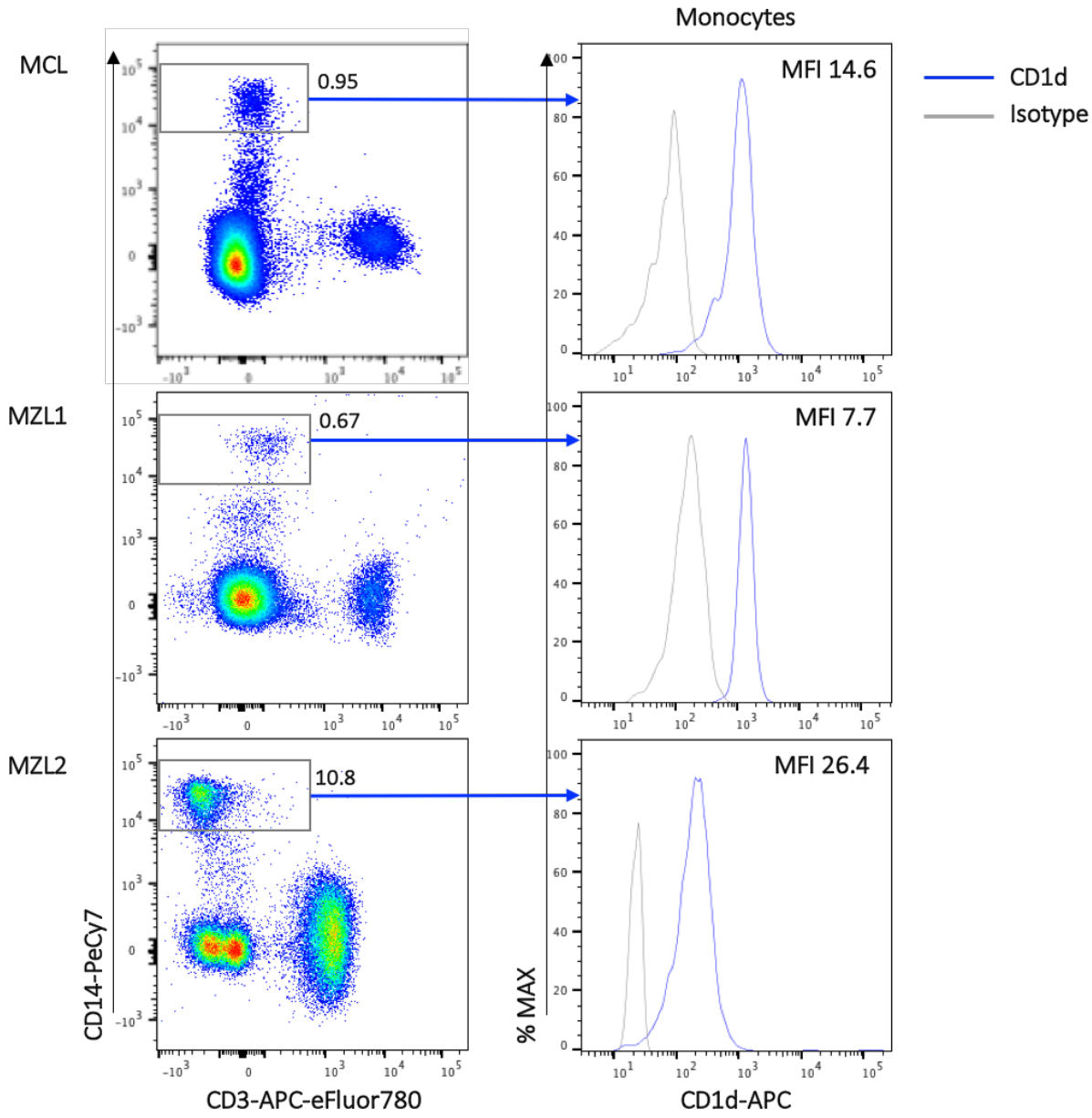


Figure 4-22 CD1d expression on primary monocytes

Flow-cytometric analysis of CD1d expression on peripheral blood monocytes from the same patients as **Figure 4-18**.

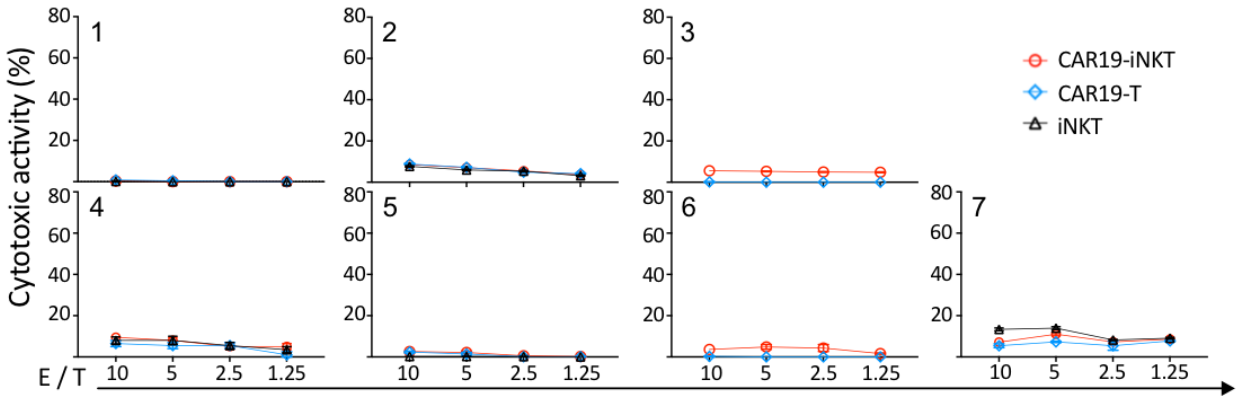


Figure 4-23 Monocyte specific cell death in lymphoma patients derived PBMCs
Cytotoxic activity of CAR19-iNKT, CAR19-T and untransduced iNKT cells against monocytes in assays shown in **Figure 4-19**.

4.4 Discussion

Conventional CAR19-T cells induce CR in up to 90% relapsed/refractory (r/r) ALL patients with late-stage disease[26-33]. However, antigen-negative relapses have been reported in up to 30% of CAR-T-treated ALL patients. Similarly, lack of efficacy and CD19 loss/downregulation represent the main cause of failure in CAR-T treated patients with advanced r/r B cell lymphoma and LPD[31,203-209].

Targeting two (or more) antigens simultaneously has been regarded as one of the most effective approaches to enhance anti-tumour activity while mitigating against the risk of immune evasion by cancer cells[194]. In pre-clinical studies, co-expression of two (or more) CAR constructs with distinct antigen specificities in the same T cell led to higher cytotoxic activity compared to mixed populations of two (or more) T cell lines each endowed with a mono-specific CAR[46]. However, packaging size of viral vectors may limit the feasibility of such approach[210]. Moreover, cross-interactions between scFv of different constructs may impact on the CAR-antigen affinity, dampen the effector-cell avidity and promote CAR-cell non-specific activation and immune exhaustion[210]. The same limitations apply to tandemCARs, i.e., CARs incorporating multiple antigen-binding domains in series[210]. By contrast, CD1d-restricted iNKT cells would naturally offer the opportunity for at least dual-specific CAR-iTCR-immunotherapy for CD1d-expressing targets, provided the iTCR signalling is preserved in CAR-engineered iNKT cells, without the shortcomings of dual-specific conventional CAR-T cells and the related manufacturing constraints.

In order to characterise and functionally validate the dual-specific reactivity of CAR19-iNKT cells produced according to my optimal protocol, I evaluated the anti-tumour response of CAR19-iNKT cells *in vitro* in the context of different CD1d and/or CD19-expressing tumour models.

First, I used an artificial system based on the K562 cell line. K562 is a human erythroleukaemic cell line that was derived from a patient with chronic myelogenous leukaemia in blast crisis[211,212]. K562 cells do not express endogenous HLA A, B, DR or CD1 molecules, thus minimising the induction of allo-/non-specific T lymphocytes[213]. In addition, they do not express costimulatory molecules such as CD86, CD83, 4-1BBL, OX40L, ICOSL or CD40L[214], they

lack the expression of PDL1/2 and B7H3/4 inhibitory ligands and do not secrete activating/regulatory cytokines, including IFN-γ, GM-CSF, IL-10 or common γ-chain receptor cytokines[214]. However, they do present the adhesion molecules ICAM-1 (CD54) and LFA-3 (CD58), which are required to form an effective immunological synapse[214], and they are easy to transduce[215]. Therefore, K562 cells represent a very controlled system to assess the inherent reactivity of antigen-specific T cells and have been widely used as a backbone cell line to generate artificial APCs[216,217].

On this basis, I genetically modified K562 cells to express CD1d and/or CD19, singly or in combination, and tested CAR19-iNKT cell cytotoxic activity against these targets by means of 3h flow cytometry-based cytotoxicity assays. While viability of parental K562 cells co-cultured with CAR19-iNKT effectors was comparable to that of control targets incubated alone, $CD1d^{+}CD19^{-}$, $CD1d^{-}CD19^{+}$ and $CD1d^{+}CD19^{+}$ K562 cells exposed to CAR19-iNKT cells presented incremental proportions of dead cells. This demonstrated that in CAR19-engineered iNKT cells the iTCR remains functional, the CAR19 can trigger a response against $CD19^{+}$ targets that lack the natural iNKT cell antigen, and simultaneous engagement of iTCR and CAR19 co-operatively activates CAR19-iNKT cells. Importantly, the addition of the specific iNKT cell agonist αGalCer enhanced CAR19-iNKT cell cytotoxicity exclusively against CD1d-expressing K562 cells, further corroborating the evidence of a fully functional iTCR with CD1d-restricted activity.

Next, I performed a series of assays using B lymphoid cell lines as targets. Previous work showed that in the absence of exogenous glycolipid antigens, $CD1d^{intermediate/low}$ human B cell lymphoma cell lines, including Farage cells, do not activate unmodified iNKT cells[218]. Furthermore, unmodified iNKT cell cytotoxicity correlates with the levels of surface CD1d, with minimal lysis of tumour cell lines expressing low levels of CD1d[219]. However, in the presence of αGalCer, both cytokine and cytotoxic responses are enhanced and equally robust, irrespective of the levels of CD1d[218,219]. Likewise, the reactivity of conventional CAR19-T cells against $CD19^{+}$ targets has been proved to be proportional to the level of expression of CD19 on the plasma membrane. When I tested dual-specific CAR19-iNKT cells against B cell targets differentially expressing CD1d and/or CD19, only tumour cells expressing the relevant antigens were killed, with a correlation between the percentage of death and the antigen levels (**Figure 4-4** and **Figure 4-5**). Notably, in the absence of αGalCer CAR19-iNKT cells resulted effective against the

iNKT cell-resistant Farage B cell line (**Figure 4-6**, **Figure 4-7** and **Figure 4-8A**) and superior to CAR19-T cells against $CD19^{high}$ B cells targets which were $CD1d^{-}$ (AK cells, **Figure 4-6**). Furthermore, the addition of αGalCer consistently led to potent enhancement of CAR19-iNKT cell cytotoxicity, irrespective of the levels of CD1d. Hence, on the basis of these observations it could be envisioned a combinatorial approach including adjuvant administration of an iNKT agonist, e.g. at the time of CAR19-iNKT immunotherapy and/or after the infusion of CAR19-iNKT cells, to enhance the efficacy and improve the clinical outcome of CAR19-iNKT immunotherapy in patients with B cell malignancies.

Conjugate analysis by flow cytometry allowed to integrate quantitative assessment of cytotoxic activity with qualitative characterization of killing kinetics. Specifically, the superior cytotoxicity of CAR19-iNKT cells was at least in part underpinned by swift engagement and rapid dissociation from the targets as a result of effective lysis, with fewer trackable conjugates at a defined time point (**Figure 4-10**). While prompt killing responses are inherent in the innate-like reactivity of iNKT cells, this was also consistent with the hypothesis of higher avidity of dual specific CAR19-iNKT effectors using both iTCR and CAR19 to attack $CD1d^{+}CD19^{+}$ targets. Notably, the excellent viability of CAR19-iNKT cells within conjugates, in striking contrast with the high rate of CAR19-T AICD (**Figure 4-10**), suggests that CAR19-iNKT cells may persist longer and patrol the tumour site to prevent disease relapse more effectively than conventional CAR19-T cells.

Real-time monitoring further corroborated the evidence of faster CAR19-iNKT cell reactivity (cluster analysis, **Figure 3-11B**) and improved viability, that was associated with outstanding proliferative response to tumour cell targets, particularly in the case of 3^{rd} generation CAR19-iNKT cells. By comparison, CAR19-T cell performance was poorer, thus emphasising that indeed the iNKT cell platform meets the requirements for a more effective CAR-immunotherapy[41], i.e., potential for fast clearance of the tumour cells and longer persistence associated with greater antigen-dependent expandability. Furthermore, the greater proliferation in the presence of high tumour load (E/T 1:1, **Figure 4-17**) as well as the more sustained killing activity against residual low-numbers of lymphoma cells (E/T 10:1, **Figure 4-17**) suggest that CAR19-iNKT rather than T cells have the capacity to completely deplete malignant B cells.

Finally, I tested my CAR19-iNKT cells against primary lymphoma cells.

Previous work reported that, in the absence of exogenous glycolipid ligands, the Th1 response of allogeneic iNKT cells isolated from healthy donors is more robust against MCL-derived rather than normal B cells[218]. Moreover, αGalCer-pulsed B cells from MCL activated allogeneic iNKT cells from healthy donors more effectively than normal B cells[218], confirming that iNKT cell are capable of recognizing malignant B cells and reacting against them, when effectively activated, according to mechanisms that might allow different outcomes in response to tumour versus non-tumour cells.

When I performed cytotoxicity assays using primary PBMCs from MCL and MZL patients as targets (in the absence of αGalCer), I found that CAR19-iNKT cells from healthy donors effectively killed the clonal cells, which were $CD19^{+}CD1d^{+}$, to a greater extent than CAR19-T effectors in all but one case. It is conceivable that, at least in the case of MCL-derived targets, the inherent iTCR-mediated reactivity of iNKT cells against malignant $CD1d^{+}$ B cells could have contributed to the better outcome associated with the CAR19-iNKT effectors. Importantly, 3rd generation CAR19-iNKT cells outperformed their 3rd generation CAR19-T counterparts in terms of killing activity, similar to my previous observations in cell line-based assays.

Of note, CAR19-iNKT (but not CAR19-T) cell cytotoxic activity seemed to be higher against MCL than against MZL-derived targets, irrespective of the donor and the costimulatory configuration of the CAR (CAR19-iNKT $P<0.0001$ vs CAR19-T $P=0.27$). This cannot be entirely explained by the surface levels of CD1d, since CD1d expression was higher on MZL1 than on MCL B cells. It might be that MCL and MZL are characterised by different lipid profiles and the glycolipid antigens of MZL are less antigenic than those of MCL B cells. In addition, the antigen presentation apparatus of MZL cells might present some defects that variably affect the ability to assemble and expose the CD1d-glycolipid complexes on the surface for the scrutiny of CAR19-iNKT cells. Finally, there is emerging evidence suggesting that different B cell malignancies are characterised by distinct patterns of co-stimulatory/inhibitory molecules as well as inhibitory/regulatory cytokines that determine different outcomes of immunotherapy strategies[220-222].

Interestingly, 2nd generation CAR19-iNKT cells generated from the same healthy donor killed more effectively MZL B cells from patient 2 (assay 5) compared to patient 1 (assay 7). This could be simply explained by the higher proportion of malignant cells in patient 1 and the resulting actual E/T ratios, lower in assay 7 than assay 5. However, it should be noted that patient 1 had an atypical splenic MZL ($CD5^+$), that might be inherently more resistant than typical MZL to CAR19-iNKT cytotoxicity. Finally, it cannot be excluded that autologous immune cells in MZL2 (assays 5) but not MZL1 (assay 7) were actively recruited in the battle against cancer cells, a phenomenon referred to as iNKT cell-induced transactivation of downstream effector cells to enhance the endogenous anti-tumour response. Specifically, in assay 5 approximately 9% of all mononuclear cells were $CD56^+CD3^-$ (**Figure 4-24**).

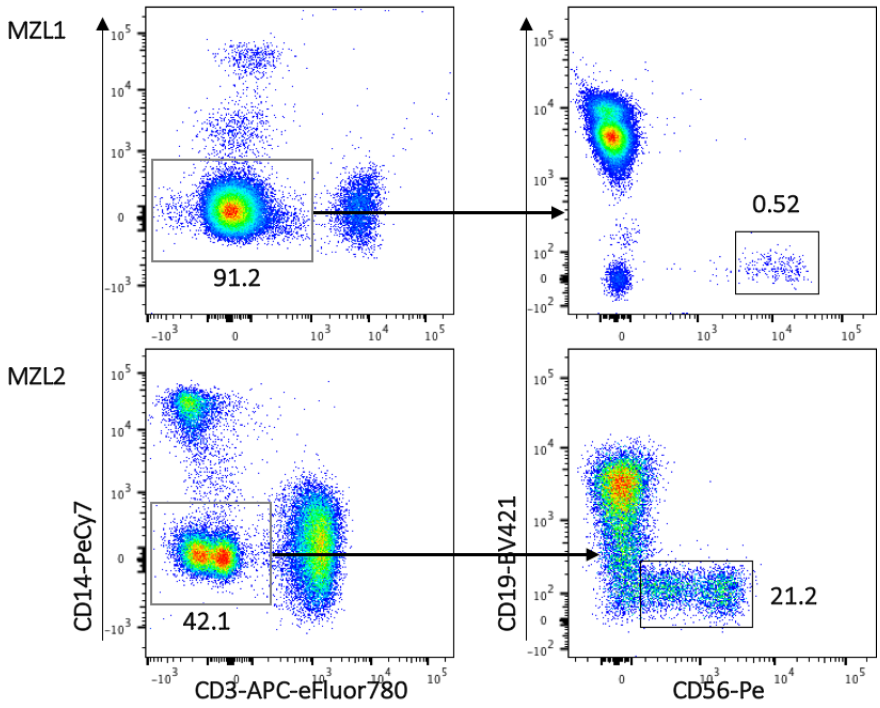


Figure 4-24 Flow cytometry analysis of MZL-derived PBMCs
$CD3^+$ T cells and $CD14^+$ monocytes were excluded from the analysis (*left*). Within non-malignant ($CD19^-$) cells, there was a $CD56^+$ population of NK cells representing nearly 9% of all live mononuclear cells in patient 2 (*bottom right*), while that was negligible in patient 1 (*top right*)

iNKT cells strongly activated by αGalCer-pulsed $CD1d^+$ tumour cells can exert their anti-tumour activity both directly by lysing the $CD1d^+$ cells and indirectly by activating NK ($CD56^+$) effectors, that can kill even malignant cells which are not directly targeted by iNKT cells[219]. Therefore, NK-

mediated cytotoxicity might have contributed at least to a certain extent to the final outcome of assay 5, thus emphasizing that immune cell transactivation could represent another important mechanism of *in vivo* amplification of CAR19-iNKT cell therapeutic activity in clinical settings. On the other hand, the poorer outcome of assay 7 underscores the need to explore strategies to enhance CAR19-iNKT immunotherapy in patients with bulk disease. Further investigation should include cytotoxicity assays using αGalcer-pulsed primary lymphoma cells. Alternatively, other combinatorial strategies could serve the scope (see chapter 5, Transcriptional and epigenetic basis for enhancing CAR-iNKT cell reactivity).

Last, the finding that CAR19-iNKT cells did not kill patients' monocytes within the 3h timeframe period of the cytotoxicity assay, despite expressing CD1d at comparable or higher levels than malignant $CD19^+$ B cells, requires some explanation.

With respect to this topic, there may be several reasons.

One possibility could be that 3h-incubation was too short to elicit effective activation of CAR19-iNKT cells exclusively through the low affinity interaction between CD1d and iTCR at those fixed E/T ratios. Another possibility could be that, in the context of B lymphomas/LPD (and their related glycolipid antigens), the outcome of the exclusive iTCR-CD1d interaction between (CAR19-)iNKT cells and circulating monocytes, in the absence of CD19 and other exogenous stimulations, could be rather a non-cytotoxic, regulatory-like response, possibly reminiscent of the natural physiological cross-talk between iNKT cells and DCs[223]. Alternatively, the lack of monocyte specific cell death could be related to inherent features of $CD14^+$ cells in cancer patients, less effective/defective at cross presenting tumour-associated glycolipid antigens [224,225]. More recently, it has been suggested that circulating monocytes in lymphoma patients can deliver inhibitory signals that may prevent IFN-γ and cytotoxic iNKT cell responses in the absence of opposing strong stimulations in an indoleamine 2,3-dioxygenase (IDO)1-dependent manner[226-229]. Beyond enzymatic mechanisms, IDO1 can also act as a signalling molecule, involved in dendritic cell reprogramming[230,231] and pro-survival/antiapoptotic pathways[232], thus conferring survival advantage to IDO1 hyper-expressing cells and resistance to conventional apoptotic signals. Therefore, it cannot be excluded that these patients with end-stage, pluri-refractory disease had dysfunctional monocytes that could not be eliminated by CAR19-iNKT

cells in the absence of an effective CD19-induced activation and cytotoxic response, irrespective of the expression levels of CD1d.

Further functional studies would be required to better address this issue and investigate the potential for off-target toxicity by CAR19-iNKT cells, including long-term *in vitro* (and *in vivo*) assays with monocytes as well as other potential $CD1d^{+}CD19^{-}$ targets (see below Transcriptional and epigenetic basis for enhancing CAR-iNKT cell reactivity chapter).

5 Transcriptional and epigenetic basis for enhancing CAR-iNKT cell reactivity

5.1 Introduction

CLL is the most prevalent leukaemia of adults in the West, with a median age at diagnosis of 70 years[12]. It is characterized by relentless accumulation of malignant B cells in peripheral blood, bone marrow and lymphoid tissues. Where indicated, first line chemo-immunotherapy can induce sustained remissions only in a small minority of patients, the prognosis remaining poor in the case of relapsed/refractory disease[13]. Allo-HSCT could be curative, but due to transplant-related morbidity/mortality it is not suitable for most patients. More recently, the BCR signalling pathway inhibitors idelalisib[14] and ibrutinib[15] have shown the potential to induce CRs, but as yet not cures. In contrast, CAR19-T cells appear to have curative potential in CLL, with evidence of >4 years sustained CR in some heavily pre-treated patients[34]. Despite such exciting results, the overall outcomes of CAR-T immunotherapy for CLL remain unsatisfactory compared to those achieved in ALL patients, with approximately 50% versus 70-90% CR rates in CLL and ALL respectively[233]. In addition, antigen escape following CAR19-T therapy has been reported[234]. All together, these data emphasise the need for further optimisation of CAR-based technologies for the treatment of CLL.

B-CLL cells express no or lower CD1d surface levels compared to their normal counterparts[131]. They also express lower levels of CD1d compared to MCL and MZL malignant B cells. Moreover, microarray gene expression profiling demonstrated a significant down-regulation of CD1d in B-CLL cells isolated from patients with early/stable disease compared to normal B cells[235], although advanced/progressive disease has been associated with higher surface and transcript levels[236]. Hence, it has been proposed that in advanced disease increased expression of CD1d may facilitate presentation of endogenous/exogenous lipids, possibly specific to the leukemic clone, leading to cognate interactions with iNKT cells, which remain functional in CLL and can

promote survival of the leukemic cells[237]. Furthermore, the dynamic CD1d expression pattern in CLL patients provides the evidence that *CD1D* is not permanently silenced in B-CLL cells and suggests that perhaps the still intact iNKT/CD1d immunoregulatory axis could be exploited to develop a novel dual target-specific approach combining transcriptional modulation of CD1d on cancer cells with CAR19-iNKT immunotherapy.

The mechanisms underlying CD1d transcriptional regulation are incompletely understood in both normal and pathological B cells. Previous work showed that the retinoic acid (RA) signalling might be involved. Specifically, the distal promoter of *CD1D,* 1.5 kb upstream the ATG translational start site, contains a RA response element (RARE) motif[137] (**Figure 5-1**).

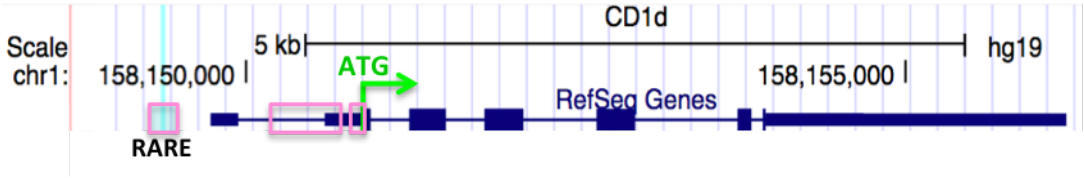


Figure 5-1 Transcriptional regulation of *CD1D* gene
Adapted from the UCSC genome browser**.**

Decrease/loss of RA signalling has been linked with transcriptional down-modulation of *CD1D* in activated and EBV-infected human B lymphoblastoid cell lines (B-LCLs). Similarly, *in vitro* treatment with RA agonists such as all-trans RA (ATRA) restores *CD1D* transcription and expression in these cells[138,139].

There is also evidence of a bivalent chromatin state at the CD1d promoter in B-LCL and murine GC B cells. Bivalent histone modifications are defined by the co-existence of repressing and activating histone marks in the same chromatin domain, i.e. trimethylation on histone 3 of lysine 27 (H3K27me3) and lysine 4 (H3K4me3) respectively. The Polycomb group (PcG) protein EZH2 within the Polycomb-repressive complex 2 (PRC2) catalyses the formation of the repressive H3K27me3, whereas Trithorax group (TrxG) proteins catalyse the formation of activating H3K4me3 marks. The presence of seemingly opposing epigenetic marks in the same region is required in undifferentiated embryonic stem cells to ensure temporal and spatial control of developmental gene programs[238]. There is evidence that the notion of bivalency can be also applied to other normal and pathological states, including activated germinal centre (GC) B lymphocytes[239], malignant cells[240] and in inherited disease[163]. Although there are no

reports linking bivalent histone modifications to *CD1D* regulation, previous *in silico* analysis performed at the Karadimitris lab (M.S. Chaudhry, **Figure 5-2**) revealed the presence of both H3K4me3 and H3K27me3 at the location of the RARE in the distal *CD1D* promoter in EBV-infected B-LCLs and murine GC B cells.

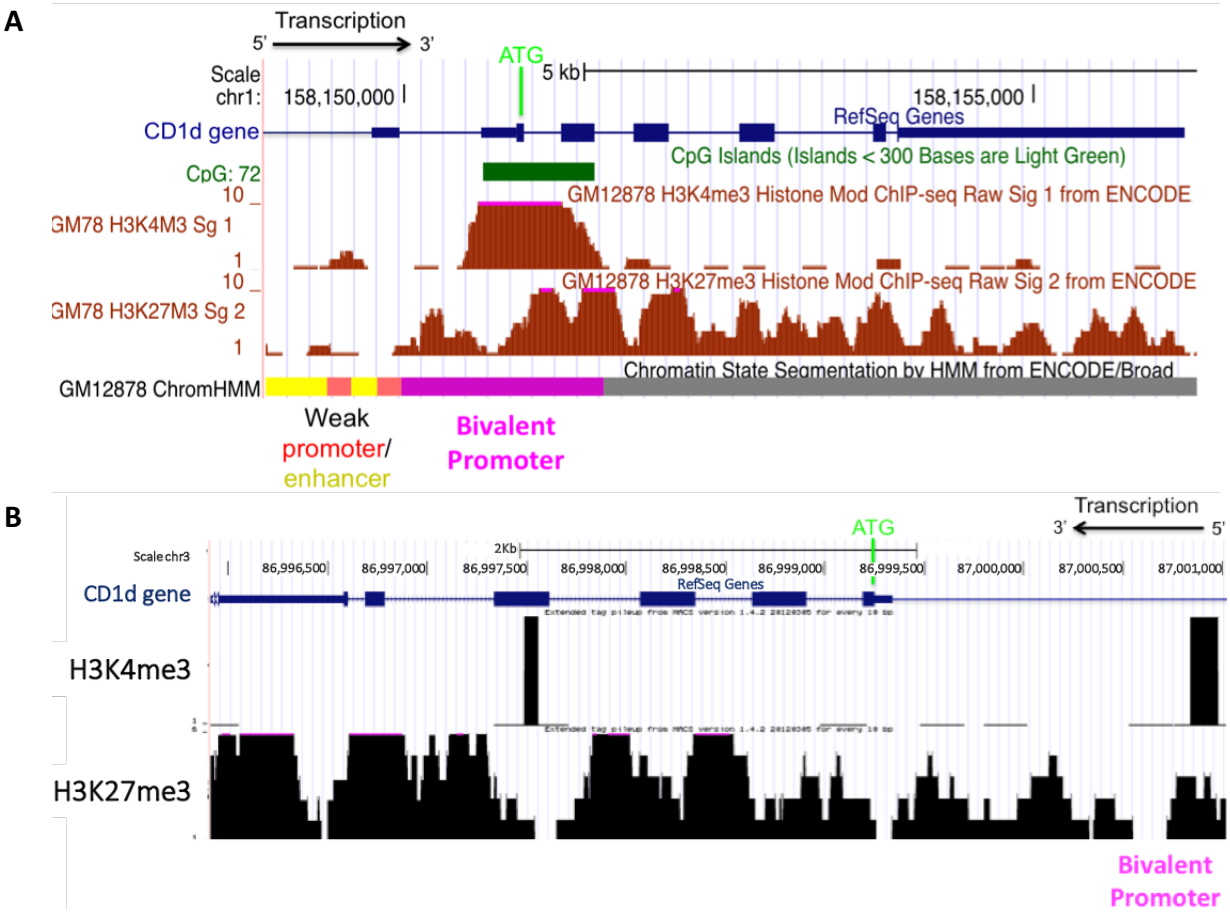


Figure 5-2 In silico analysis of the CD1D promoter in B-LCLs and murine GC B cells.
ChIP-seq data for the B-LCL GM12878 (A, provided by the Broad Institute) and for murine GC B cells (B, available from the GEO database GSE50912) obtained by interrogating the UCSC genome browser. The upstream regulatory region of the CD1D gene showed H3K4me3 and H3K27me3 marks, consistent with a bivalent poised promoter.

Remarkably, unlike normal resting B cells, both EBV-infected B-LCLs and GC B cells do not express CD1d[202]. Moreover, activated, GC and EBV-infected B cells share some common features with CLL cells, including activation of the B cell receptor pathways. Therefore, it is conceivable that the finding of bivalent *CD1D* promoter in B-LCLs and murine GC B cells could

be extended to CLL cells. Importantly, if repression of *CD1D* through imposition of bivalent marking were confirmed, this would raise the prospect of modulating *CD1D* transcription by pharmacological inhibition of PRC2 components, such as EZH2. Notably, EZH2 inhibitors are in clinical development for mature B lymphoid malignancies[239] and their use may represent a novel strategy to restore CD1d expression in CLL cells.

5.2 CAR19-iNKT cells effectively kill B-CLL cells *in vitro*

B-CLL cells express no or lower CD1d surface levels compared to their normal counterparts (**Figure** 5-3)

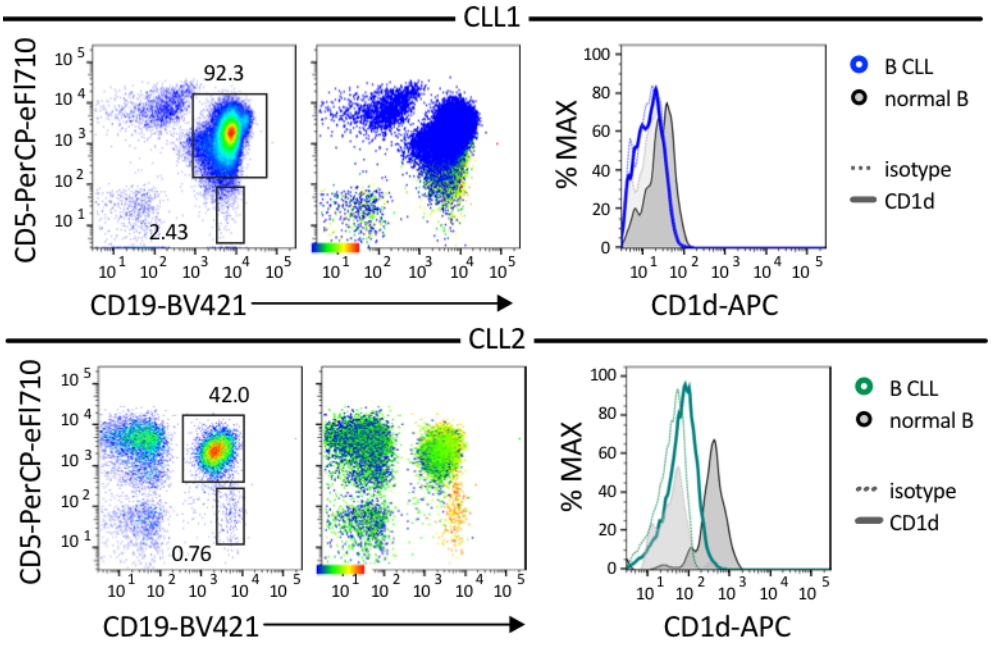


Figure 5-3 CD1d surface expression on CLL malignant and normal B cells
No (CLL1) or low (CLL2) CD1d expression in CLL cells ($CD19^{+}CD5^{+}$) from 2 patients in comparison to normal B cells ($CD19^{+}CD5^{-}$). CD1d expression is shown as a heat-map on CD19/CD5 dot plots and as histogram overlays.

In order to confirm that the iNKT/CD1d axis is functional in CLL, I tested CAR19-iNKT cells against $CD1d^{low}$ B-CLL cells that had been pulsed with αGalCer or control vehicle and found that CAR19-iNKT effectively killed malignant B-CLL cells irrespective of the low expression levels of CD1d (

Figure 5-4).

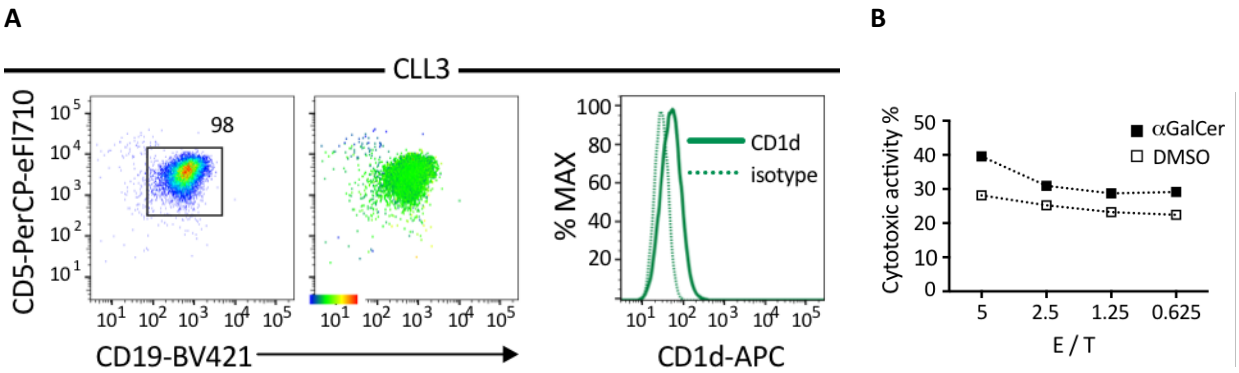


Figure 5-4 CAR19-iNKT cell cytotoxicity against CLL cells

A. Flow cytometry analysis of CD1dlow B-CLL cells, identified as $CD19^{+}CD5^{+}$ cells in pseudocolour dot plots (*left*), with superimposed CD1d color-map (*middle*) and histogram representing CD1d expression relative to isotype control. B. Cytotoxic activity of 2nd generation CAR19-iNKT cells against B-CLL in A. in the presence of DMSO control or αGalCer. Error bars represent S.E.M. of triplicate assays.

Since CAR19-iNKT cell cytotoxicity directly correlates with the expression levels of CD1d (**Figure 4-5**), I sought to investigate whether I could enhance CAR19-iNKT cell reactivity against B-CLL cells by inducing upregulation of CD1d via pharmacological means. Based on the evidence that ATRA treatment restores *CD1D* transcription and expression in activated GC and EBV-infected B cells [138,139], which have some biological similarities with CLL cells, I hypothesized that *in vitro* treatment of CLL cells with ATRA could also restore CD1d expression on malignant B-CLL cells. Indeed, clinically relevant doses of ATRA led to restoration of CD1d expression both at a transcript and protein level in B CLL cells without affecting cell viability (**Figure 5-5**).

.

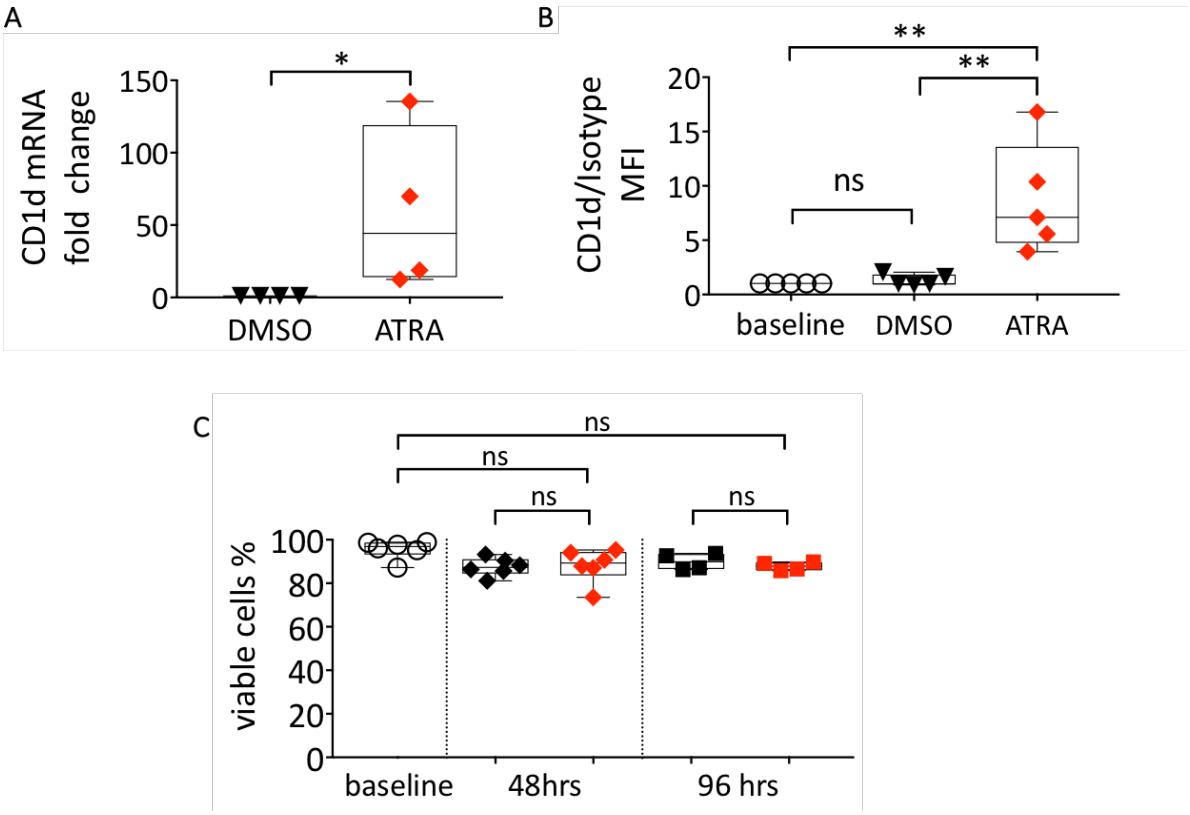


Figure 5-5 Effect of ATRA treatment on CD1d expression and viability in B-CLL cells

A. Relative increase of CD1d mRNA as assessed by qPCR expression on CLL cells treated with 0.01% DMSO or 10^{-6}M ATRA for 0 or 48hrs (n=4 patients). B. Relative increase of CD1d cell surface expression as assessed by CD1d/isotype ratio (n=5 patients). C. No effect of ATRA on CLL cell viability as assessed by trypan blue staining.

Next, I tested CAR19-iNKT and -T cells against ATRA-treated B-CLL cells. As shown in **Figure 5-6**, CAR19-iNKT cells killed αGalCer-pulsed B-CLL cells more effectively that CAR19-T cells irrespective of whether CLL cells had been exposed (48h) to pharmacological dose of ATRA or not. However, CAR19-iNKT but not CAR19-T cells cytotoxicity was further enhanced against ATRA-treated, $CD1d^{high}$ B-CLL cells.

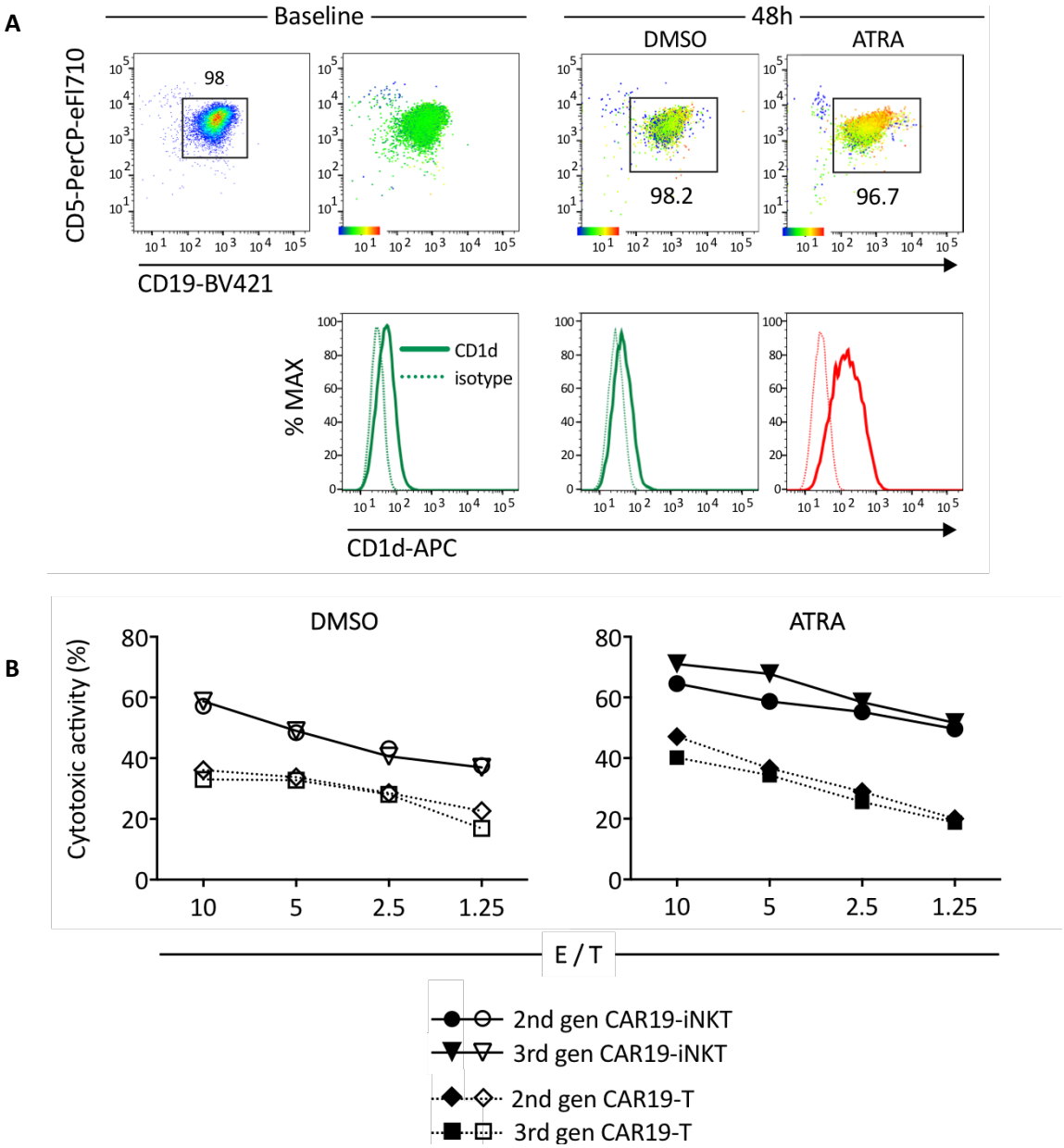


Figure 5-6 CAR19-iNKT vs CAR19-T cytotoxicity against ATRA-treated B-CLL cells

A. Upregulation of surface CD1d upon 48h after treatment with 10^{-6}M ATRA compared to baseline levels and 0.01% DMSO control. B. Cytotoxic activity of 2nd and 3rd generation CAR19-iNKT and -T cells against DMSO (*left*) or αGalCer (*top*)-pulsed B-CLL cells.

5.3 Molecular basis of CD1d expression in B-CLL cells

I then aimed to further evaluate the molecular basis of CD1d regulation in B-CLL cells. B-CLL cells with no (patient CLL4) and very low (patient CLL5) baseline expression of surface CD1d were exposed to ATRA for up to 96hours.

Assessment of CD1d transcript levels at different time points demonstrated prompt upregulation of CD1d mRNA at 3-5 hours, steady increase over the next 24 hours, followed by a plateau or further milder increase up to 96hours. Flow cytometry analysis at the same time points confirmed a time-dependent expression of surface CD1d protein. These findings further confirmed that the retinoid pathway is involved in the regulation of CD1d expression at a transcriptional level.

Finally, the promoter of CD1d was analysed with the aim to test the hypothesis of bivalency and verify whether successful induction by ATRA was occurring on a background of 'permissive' epigenetic configuration that poised expression of CD1d for swift restoration upon ATRA exposure.

Indeed, ChIP assays in baseline B-CLL cells from patients 4 and 5 demonstrated enrichment of both H3K4me3 activating and H3K27me3 repressive histone marks at the CD1d promoter, thus for the first time providing evidence of bivalency at the CD1d promoter in primary CLL cells (**Figure 5-8**).

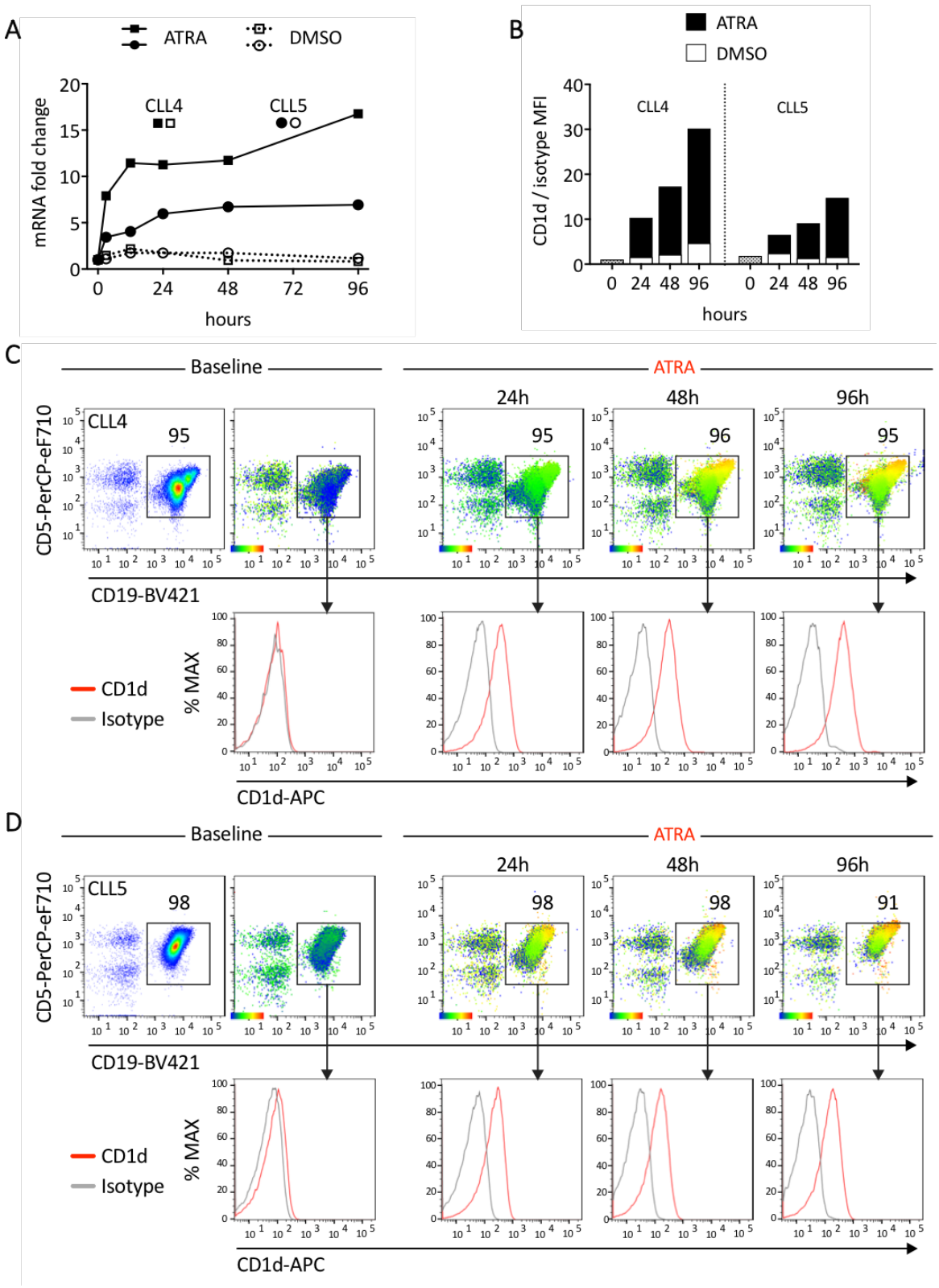


Figure 5-7 CD1d expression in CLL cells pre and post treatment with ATRA

Representative mRNA levels (A), MFI summary (B) and FACS plots (C) showing restoration of CD1d expression post 48 hours ATRA ($1x10^{-6}$M) relative to control DMSO (0.01%).

Red line: CD1d (clone 42); grey line: isotype control antibody.

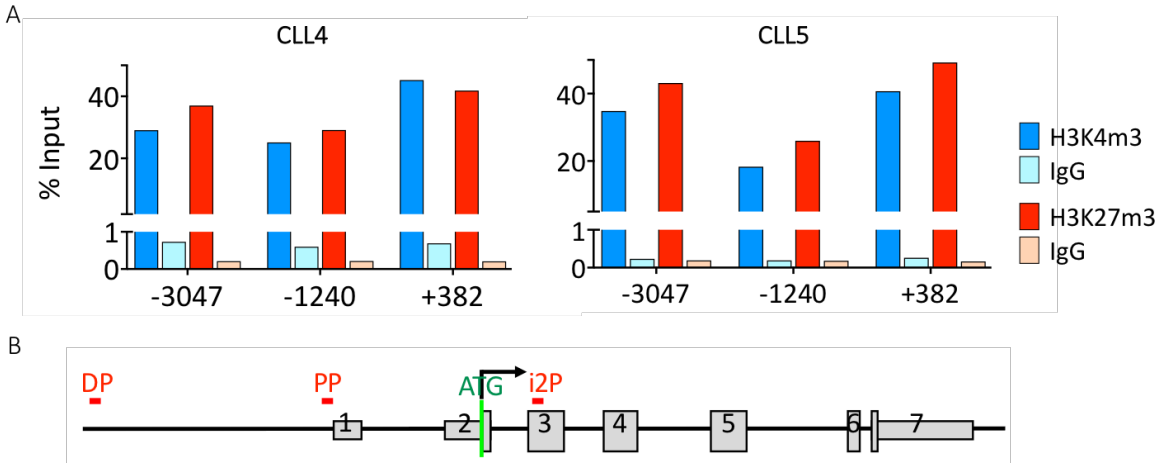


Figure 5-8 ChIP-qPCR assay in baseline B-CLL cells

A. ChIP-qPCR assay showing bivalent histone state of CD1D in primary CLL cells from the same 2 patients shown in **Figure 5-7.** There was relative enrichment for H3K4m3 and H3K27m3 marks in relation to Ig control. B. Scheme of the 3 qPCR amplicons spanning the 5' UTR (DP: distal; PP: proximal, relative to the ATG start codon) and the gene body (i2P: within exon 2) of CD1D. Representative of 2 independent experiments.

5.4 Discussion

As discussed in the previous chapter, CAR19-iNKT cells are capable of killing $CD1d^+$ MCL and MZL B cells more effectively than conventional CAR19-T cells even in the absence of αGalCer. Given that the iTCR, which is functional in CAR19-engineered iNKT cells, can recognize tumour cell-associated glycolipid antigens presented by CD1d and subsequently trigger Th-1 responses against malignant B cells[218], it is likely that the iTCR-CD1d interaction co-operates to the final activation of CAR19-iNKT effectors.

Compared to the levels of cytotoxicity measured in the assays with cell lines, the specific cell death within primary lymphoma cells was lower, suggesting that strategies to enhance the anti-lymphoma activity of CAR19-iNKT immunotherapy should be explored. One option is represented by co-administration of glycolipid compounds such as αGalCer, that can be effectively presented by primary tumour cells[218] and consistently allowed to enhance CAR19-iNKT cell cytotoxic activity against $CD1d^+$ B cell lines (**Figure 4-7** and **Figure 4-8**). Furthermore, on the basis that the reactivity of CAR19-iNKT cells is proportional to the density of their target antigens on the cancer cell surface (**Figure 4-4** and **Figure 4-5**), it could be anticipated that upregulation of CD1d would lead to improved outcome of CAR19-iNKT immunotherapy in B cell lymphomas.

CLL represents an ideal model to evaluate the effect of CD1d modulation on CAR19-iNKT reactivity. CLL is a lymphoproliferative disorder characterized by low-to-no expression of CD1d on malignant B cells[131,241]. However, the iNKT/CD1d axis is still functional, i.e. B CLL cells can present glycolipids in complex with CD1d and autologous (as well as allogeneic[242]) iNKT cells remain capable of producing a proliferative, cytokine and cytotoxic response when activated[241]. Furthermore, the presence of higher surface levels of CD1d in cases of aggressive, progressive disease[236] suggests that CD1d may be repressed but not permanently silenced in B CLL cells and its expression could be restored in patients with constitutive low/no protein.

In a first series of experiments, I verified that primary B CLL cells express very low levels of CD1d compared to their normal counterparts (**Figure 5-3**). Irrespective of the negligible baseline expression, these cells were capable of eliciting a significant cytotoxic response by

CAR19-iNKT cells, demonstrating that CAR19-iNKT cell immunotherapy could be suitable also for CLL patients. Importantly, the addition of αGalCer led to a better outcome, thus confirming the hypothesis of functional CAR19-iNKT/CD1d axis.

Next, I tested whether pre-treatment with ATRA could induce higher surface expression of CD1d and subsequently improve the performance of CAR19-iNKT cell effectors. The choice of ATRA was based on the notion that the CD1d promoter contains a RARE motif[137] and the demonstration that ATRA restores CD1d in human EBV-transformed and murine activated GC B cells, where it is down-regulated[138,139]. A study published at the end of 2017 showed for the first time in primary B CLL cells that ATRA can induce CD1d in malignant B cells, followed by enhanced iNKT cell reactivity in vitro in the absence of exogenous agonists[242]. Similarly, I observed that CD1d could be effectively modulated by treating CLL cells with ATRA in a time dependent manner (**Figure 5-7**). Importantly, clinically relevant doses, which are employed as a standard differentiating treatment for acute promyelocytic leukaemia (APL), did not affect in vitro viability of B-CLL cells (**Figure 5-5**). By contrast, subsequent co-culture with CAR19-iNKT effectors resulted in significant death of these cells. Furthermore, side-by-side comparison with the CAR19-T counterparts showed that CAR19-iNKT cells can kill αGalCer-pulsed CLL targets with baseline (low) CD1d levels more effectively than CAR19-T effectors and their cytotoxic activity can be specifically improved by treating B-CLL cells with ATRA, with no effect on the CAR19-T cell performance.

While these findings can be directly attributed to the larger amounts of surface CD1d molecules and the subsequent increase in the iTCR-mediated reactivity of dual specific CAR19-iNKT effectors, differences in the lipids presented by CD1d might play a role too. Quantitative and qualitative changes in the cellular content of gangliosides have been described in neuroblastoma cell lines treated with 5-10 μM retinoic acid as a result of ATRA-induced transcription and subsequent increased enzymatic activity of the GD1b/GM1a ganglioside synthase beta-1,3-galactosyltransferase[243]. Glycosphingolipid profiling of CLL cells upon exposure to ATRA would be an interesting line of investigation in the future.

It would be also important to address whether ATRA would have the same effect on other cell types. Increased levels of functional CD1d on the surface of healthy cells which naturally express CD1d, such as monocytes, or *de novo* expression in healthy tissues which are constitutively negative could promote unwanted on-target, off-tumour toxicity. On the other end, 'unlocking' the transcription of CD1d in incurable $CD1d^{-}$ disorders, could offer the opportunity to extend an ATRA/CAR-iNKT based immunotherapy to a broader range of cancers, including poor-prognosis solid tumours.

Finally, the demonstration of bivalency at the CD1d promoter for the first time in primary B-CLL cells may open up to exploring even combinatorial therapeutic strategies.

Bivalent domains are considered to poise expression of developmental genes, allowing timely activation while maintaining repression in the absence of differentiation signals[244]. Furthermore, ATRA-induced differentiation in embryonic stem cells (ESCs) is conditioned by the co-existence of H3K4me3 activating signatures at the transcription starting site (TSS) of lineage commitment genes with H3K27me3-marked promoter, thus demonstrating an overlapping relationship between bivalency and ATRA-induction[245]. Bivalent chromatin domains have a well-recognised role also in cancer progression, where loss of H3K27me3 marks from bivalent promoters has been frequently linked with activation of relevant oncogenes[246,247]. More recently, formation of new bivalent chromatin domains has been described as a main mechanism of lymphomagenesis in germinal centre (GC)-derived follicular lymphoma (FL) and diffuse large B cell lymphoma (DLBCL), with *de novo* generation of H3K27me3 marks in over 1,000 H3K4me3-only promoters and subsequent repression of the related genes as a result of hyper-expression/gain-of-function mutations EZH2[239].

There is little evidence concerning the role of bivalency and bivalent genes in CLL, the status of EZH2 and the transcriptional effects of ATRA in malignant B CLL cells. Higher levels of EZH2 mRNA and protein have been described in B-CLL cells from poor-prognosis patients compared to more indolent cases[248]. Furthermore, the pattern of H3K27me3 was found to correlate with EZH2 expression and activity in B-CLL cells and could be pharmacologically modulated by means of clinically available EZH2 inhibitors such as GSK-343 and EPZ-6438[248]. More recently, *de novo* EZH2-driven bivalency characterised by new H3K27me3 marks at the CD20 promoter was induced in B-CLL cells[249], suggesting that EZH2-dependent bivalency may potentially exert

some control on gene expression in CLL cells. This, together with the demonstration of bivalency at the CD1d promoter, raise the prospect of new therapeutic options for CLL patients. The combination of ATRA with EZH2 inhibitors might co-operatively restore CD1d expression and lead to higher surface levels, resulting in further enhancement of CAR19-iNKT cell immunotherapy and improved outcome compared to the administration of ATRA alone. Additional studies would be required to dissect the configuration of the CD1d promoter in B-CLL cells at baseline and in response to ATRA and EZH2 inhibitors, possibly including assessment of co-occupancy by RARα/RXR and EZH2 transcription factors in association with repressor/activating histone marks. This could provide the foundation for a clinically applicable pharmacological approach to develop a more effective iTCR/CAR immunotherapy. Furthermore, since the concept of bivalency is not restricted to CD1d and CLL, a similar approach could be extended to other genes and/or haematological malignancies as solid tumours, opening new exciting avenues for the treatment of cancer patients.

6 *In vivo* validation: enhanced anti-tumour activity of CAR19-iNKT cells

6.1 Introduction

Involvement of iNKT cells in anti-tumour responses against B-cell lymphoma *in vivo* was first studied in the iNKT cell-deficient TCR Jα18KO murine model, in which adoptive transfer of murine iNKT cells specifically prolonged survival of animals with CD1d-expressing lymphoma[250]. Subsequently, Bagnara et al. reported a proof-of-principle study demonstrating the *in vivo* anti-tumour activity of *in vitro* expanded human iNKT cells against the C1R-CD1d B lymphoblastoid cell line, that was attributable to direct and specific CD1d-medited killing of neoplastic cells[251]. Thereafter, several studies have sought to ascertain the role of iNKT cells in modulating anti-lymphoma responses[218,250,252-257]. Importantly, Li et al. showed that during lymphomagenesis, iNKT cells, when appropriately stimulated, are capable of effectively killing malignant cells as well as eliciting robust responses by the adaptive arm of the immune system[218], thus providing further evidence in support of the notion that iNKT cell adoptive transfer in B cell lymphoma can directly control tumour growth, while restoring and enhancing the endogenous adaptive anti-tumour immunity. However, lymphoma progression was associated with progressive loss of iNKT cell function, including reduced IFN-γ production *in vivo* as well as reduced cytokine production upon αGalCer stimulation *ex vivo*[218]. Taken together, these observations make a strong case for genetically enhancing iNKT cells to ensure sustained activation in the context of active, progressing lymphoma.

Current evidence of anti-lymphoma activity of CAR-engineered iNKT cells is limited. To date, only one group has reported on CAR-iNKT cells for cancer immunotherapy in systemic cancer xenograft models. Specifically, the Metelitsa group tested GD2- and CD19-specific CAR-iNKT cells against neuroblastoma and B cell lymphoma cell lines. By using a CD28-ζ and CD28-41BB- ζ CAR configuration, they found no difference in the *in vivo* anti-tumour activity of 2nd

generation CAR-iNKT versus 2nd generation CAR-T cells, although CAR-iNKT cells were proved to home to the tumour sites at a higher frequency than their T cell counterparts.

Xenoreactivity to murine tissues is known to support persistence of T but not iNKT cells, irrespective of their anti-tumour specific reactivity. Furthermore, T cell xenoreactivity contributes to a variable extent to tumour rejection and may result in overwhelming activation of immune cells, which culminates in indiscriminate attack of healthy tissues, referred to as xeno-GvHD. Indeed, the Metelitsa group observed the occurrence of xeno-GvHD in CAR-T- but not CAR-iNKT-treated mice, suggesting that the control of disease by CAR-T effectors could be attributed at least in part to a xenoreactivity-related effect. In line with this, successful CAR-iNKT cell immunotherapy in their models required either repeated, weekly cell dosing (neuroblastoma) or adjuvant IL-2 ($CD19^{+}CD1d^{-}$ lymphoma) administered iv every 3 days. Eventually, by using repeated administrations of GD2-specific, 3rd generation-CAR-iNKT versus single injections of 3rd generation CAR-T cells, survival of neuroblastoma-bearing NSG xenografts could be improved and prolonged from 5 weeks up to 10 weeks.

While highlighting some important limitations concerning the fitness of their CAR-iNKT cell product, this work did not provide a robust side-by-side comparison of CAR19-iNKT vs CAR19-T cells against B lymphoma cells *in vivo*. Hence, in my work I aimed not only to functionally validate my CAR19-iNKT cell product *in vivo* but also to obtain a robust comparison of CAR-iNKT vs CAR-T cells. To this end, I adopted a conventional approach, generally employed in CAR-T preclinical studies, involving use of an NSG systemic xenograft model, a 2nd generation CAR design and a single infusion of CAR-modified cells without administration of exogenous IL-2.

6.2 Establishment of luciferase-expressing C1R-CD1d cells

The use of BLI as a non-invasive procedure in evaluating tumour growth requires luciferase-expressing cell lines. Therefore, I transduced the C1R-CD1d and Farage cell lines with a firefly luciferase construct (**Figure 6-1**) and purified luciferase-expressing cells by FACS (**A**), attaining stable cell lines within two weeks.

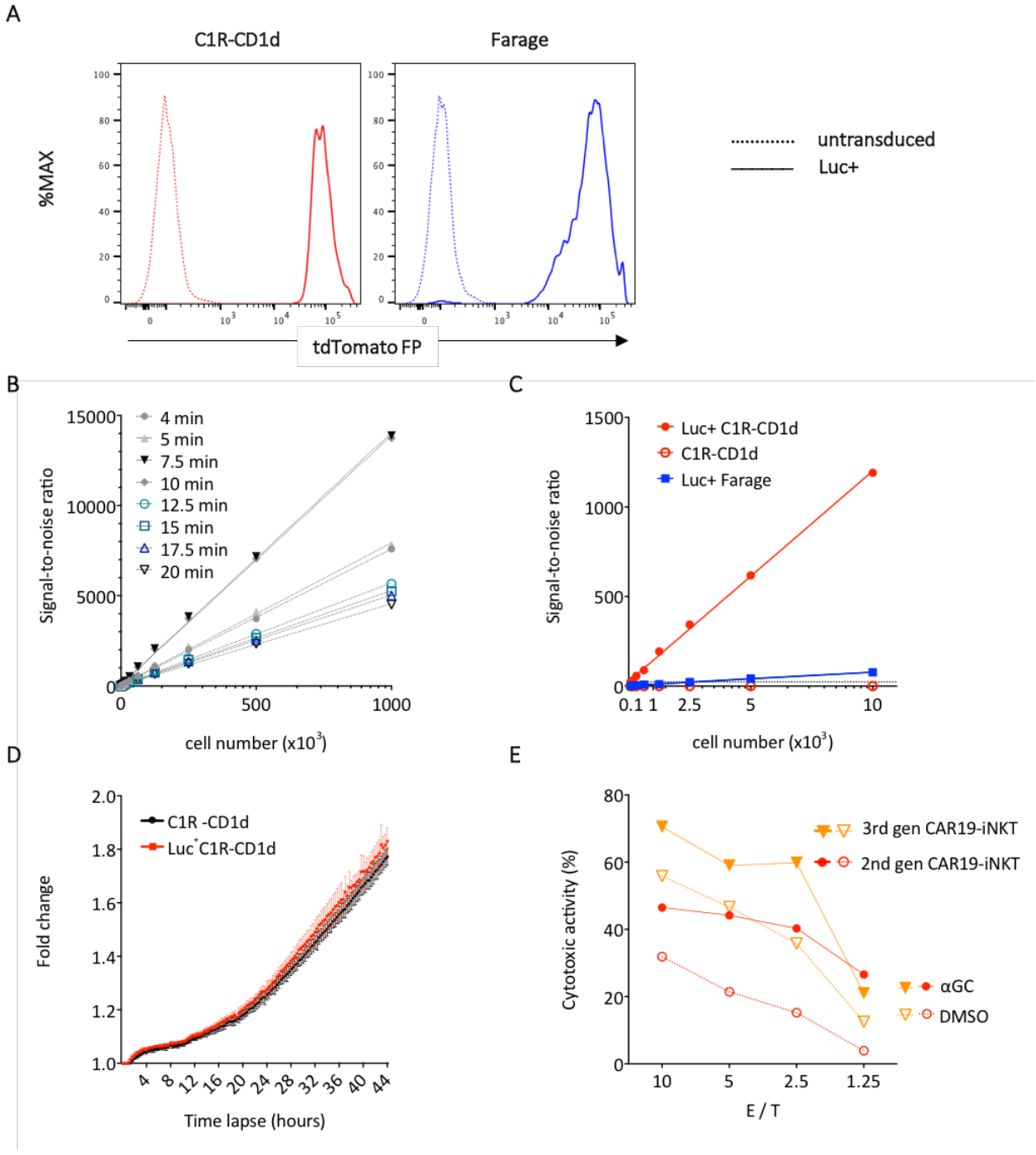


Figure 6-1 Generation and *in vitro* validation of luciferase expressing C1R-CD1d cell line

A. C1R-CD1d and Farage cells were transduced with firefly luciferase co-expressed with tandem dimer Tomato red fluorescent protein (tdRFP) in a single SFG vector obtained from John Maher. B. Dose-response studies demonstrated a strong luciferase activity associated with C1R-CD1d cells. C. By contrast, transduced Farage cells produced a weak photon signal, nearly comparable to background from untransduced cells. D-E Transduction and expression of a functional luciferase protein did not alter the growth rate of C1R-CD1d cells (D) and their sensitivity to CAR19-iNKT cell cytotoxic activity in vitro (assessed by bioluminescence) (E).

In vitro validation confirmed a strong luciferase activity associated with C1R-CD1d cells (**B**) but not Farage cells (**C**), suggesting that the latter were not suitable for *in vivo* application. Further *in vitro* testing confirmed that luc^{+}C1R-CD1d cells had growth rates comparable to the parental cell lines (**D**) and could be effectively killed by CAR19-effectors (**E**).

6.3 Luc^{+}C1R-CD1d cells are capable of xenografting NSG mice

In a first pilot experiment, 1 to 2.5×10^{6} Luc^{+} C1R-CD1d cells were iv injected into three 7-week old NSG mice, 2 females and 1 male. 1 extra male served as a healthy control. No irradiation conditioning was used. No injection-related adverse events were observed. From day 3, tumour growth was monitored by bioluminescent imaging (BLI) every 3-4 days (**Figure 6-2**).

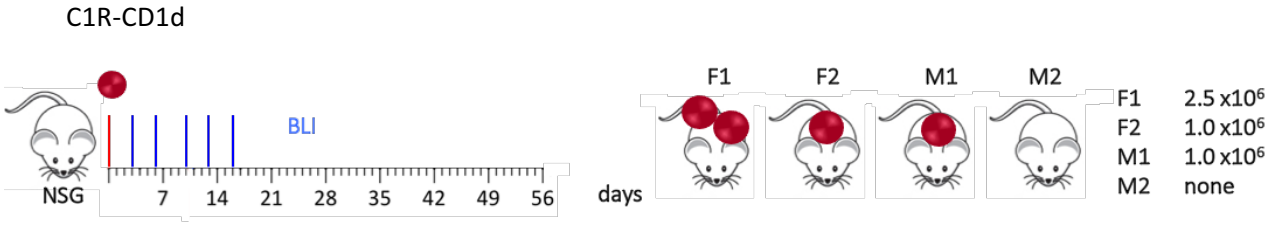


Figure 6-2 *In vivo* pilot experiment 1
Layout of *in vivo* titration of Luc^{+}C1R-CD1d cells in a systemic xenograft. NSG mice received 1 to 2.5×10^{6} Luc^{+}C1R-CD1d cells via tail injection. Firefly luciferase activity as a marker of tumour growth was determined by BLI, i.e., by quantifying the number of photons originated from tumour-bearing animals upon intra-peritoneal (ip) administration of D-Luciferin.

In order to define the best settings and conditions of imaging, anesthetized mice were imaged in ventral position beginning approximately 2.5 minutes after intraperitoneal (ip) injection of 15µg/g mouse aqueous solution of D-luciferin potassium salt. Up to ten sequential scans per mouse were performed at each time point. Each animal was serially imaged at the same relative time point after D-luciferin injection. Images were generated by acquiring a fixed total number of 10,000 photons using (variable) auto-exposure time and default (fixed) medium binning to allow the highest sensitivity associated with good image resolution.

To quantify bioluminescence, measurement regions of interest (ROIs) were drawn around the positive areas and photon signal quantified as total photon flux, i.e. the radiance

(photons/sec/cm2/steradian) in each pixel summed over the ROI area (cm2) x 4π, taking into account the background when needed.

A bioluminescence peak was generally observed 12 minutes after ip injection of D-luciferin (**Figure 6-3**). However, a delayed peak was reported in F1 on day 13 and F2 on day 16, that could be explained by different wash-in and wash-out kinetics of hypoxic tissues[258].

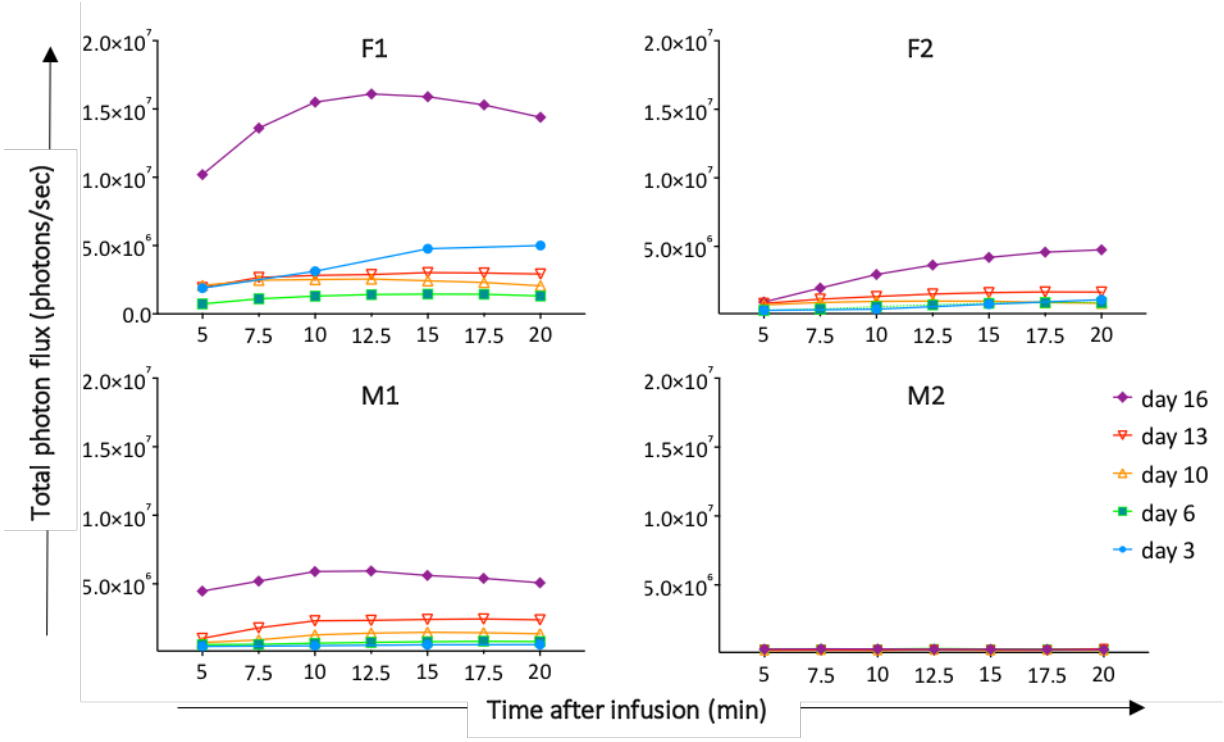


Figure 6-3 *In vivo* C1R-CD1d bioluminescence titration
At each time point, mice were scanned every 2.5 minutes to define the best timing to acquire images in terms of highest photon emission with the most favourable signal-to-noise ratio.

Tumour engraftment was defined as increasing luciferase-mediated photon flux over two consecutive imaging sessions. Engraftment could be confirmed in all C1R-CD1d recipients on day 13 irrespective of the cell dose. A stronger photon signal could be detected from the caudal body segment up to day 16 (**Figure 6-4**). During the following 2 weeks, mouse F1 stopped growing and eventually developed hind limb paralysis on day 38. F2 and M1 suffered from alopecia since day 42 and prolapsed penis from day 53 respectively and were culled on day 46 and 53, meeting the criteria of humane endpoints. Terminal BLI showed tumour progression in all mice, consistent with spine involvement (**Figure 6-5**).

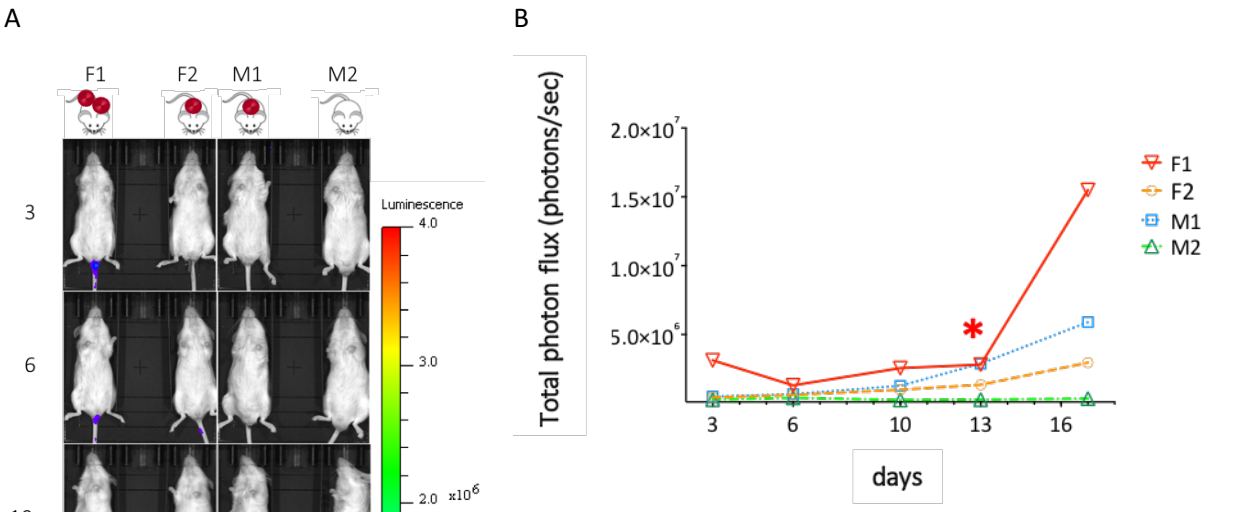


Figure 6-4 *In vivo* tumour burden monitoring

Tumour burden was monitored by bioluminescent imaging on the indicated days. Bioluminescent images (A) and photon count (B) at 12.5 min after luciferin injection.

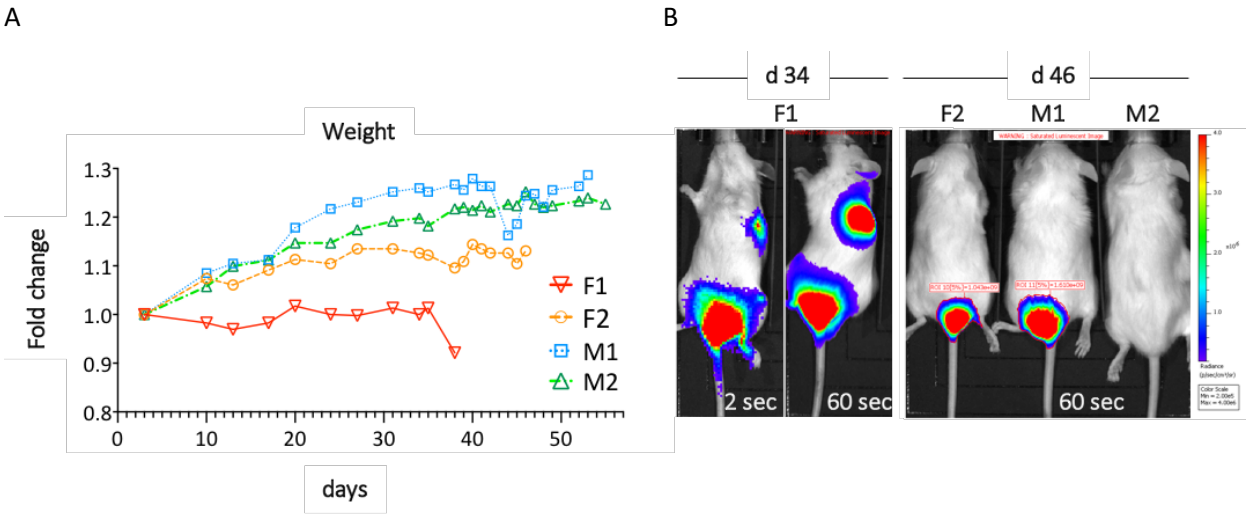


Figure 6-5 Weight chart and terminal BLI scans

A F1, which received the highest tumour cell dose, stopped growing earlier compared to the other animals. B Terminal scans demonstrated disease progression in all tumour xenografts, with more extensive spine involvement in F1.

6.4 Single infusions of CAR19-iNKT cells are feasible and well tolerated in NSG xenografts.

The first pilot suggested that optimal imaging requires BLI scanning approximately 12 min after ip D-luciferin injection using a fixed medium binning. In order to accommodate detection of early stage (engraftment) as well as advanced disease without reaching saturation, a target number of 10,000 photons per image with autoexposure time was chosen for the next experiments. An additional 1 sec and, where required, 60 sec images were planned to allow comparison of larger and smaller lesions respectively at different time points, as well as ventral and dorsal scans, to avoid underestimation of low-burden tumours involving the spine.

Next, I set up a second pilot experiment to verify that the same settings were also suitable to evaluate the therapeutic potential of CAR19-iNKT cell immunotherapy compared to CAR19-T cells. Specifically, I aimed to confirm the feasibility of a scheme widely used to test CAR-T immunotherapy, i.e., 10×10^6 CAR-cell dose administered as a single infusion in early disease setting (xenograft engraftment)[259-262] (**Figure 6-6**). In order to induce a more aggressive systemic disease with shorter time to engraftment, I intravenously injected 8 animals (7-week old NSG mice, 5 females and 3 males) with a tumour cell dose of 5×10^6 Luc^+ C1R-CD1d cells.
All mice were scanned from day 2 every 3 days. On day 8, engraftment could be confirmed in 7 out of 8 animals. Therefore, mice were randomized to no immunotherapy (infusion of equivalent volume of saline) or CAR19-T or CAR19-iNKT treatment (10×10^6 cells). Primary endpoints were overall survival and tumour burden. Secondary endpoints were GvHD and post-xenograft tumour cell phenotype.

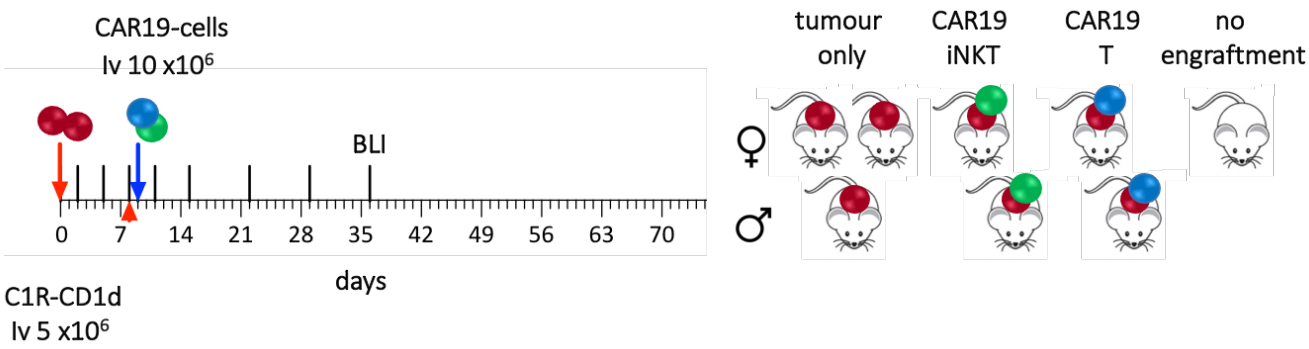


Figure 6-6 *In vivo* pilot 2 experiment

Layout of *in vivo* pilot 2 experiment. Age- and sex-matched NSG mice received 5 ×10^6 Luc+C1R-CD1d cells (red) via tail injection. Engraftment (red arrow edge) was confirmed on day 8. Subsequently, mice were randomized to no treatment or CAR19-immunotherapy with 10 x10^6 third-generation CAR19-iNKT (green) or –T (blue). Engraftment failure occurred in one animal.

The CAR-cell infusion was well tolerated. None of the mice developed early pathological symptoms or signs that could be attributed to CAR19-cell adoptive transfer. During BLI follow-up, the tumour-only control mice develop advanced, progressive disease, with active photon signal from several body segments. Subsequent histological analysis demonstrated that the biophotonic positive regions were infiltrated by tumour cells (**Figure 6-7** and **Figure 6-8**).

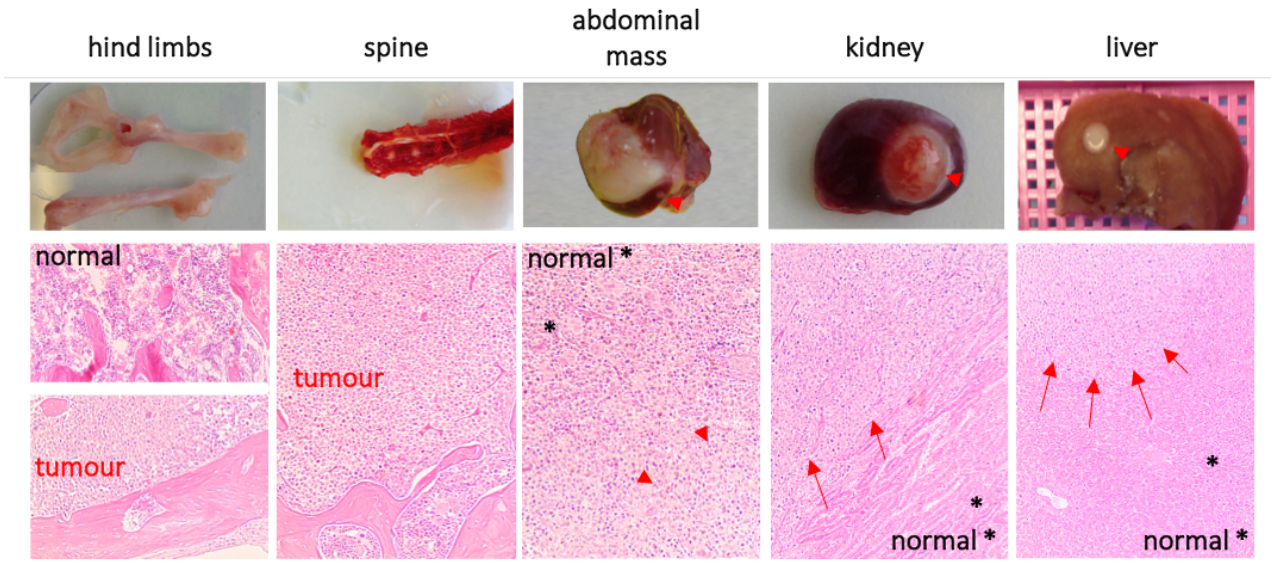
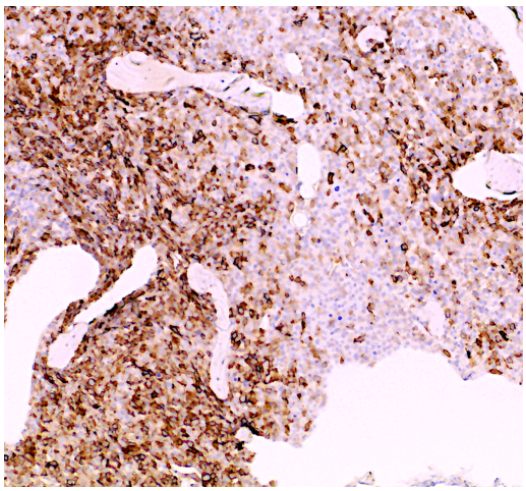


Figure 6-7 Systemic infiltration by C1R-CD1d cells

Representative images showing macroscopic (*top*) and microscopic (*bottom*) tumour infiltration in BM from hind limbs and spine, spleen (arrow) and abdominal lymph nodes, kidney and liver. Tumour cells (red arrows) are shown side-by-side with normal tissue cells (black asterisk).

A



B

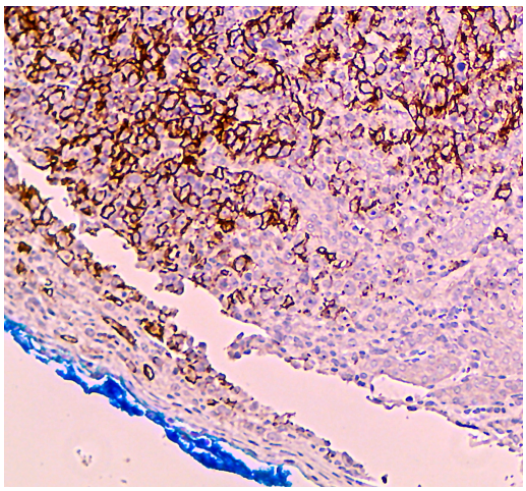


Figure 6-8 IHC analysis of xenograft tissues
Representative images from tumour-only mice showing positive IHC staining for CD19 on BM (A, 10X) and kidney (B, 20x) sections. Solid tissues were marked with ink (blue staining) prior to sampling.

By contrast, the rate of tumour growth was reduced in CAR19-treated mice after a single injection compared to untreated animals. CAR19-iNKT cell transfer was associated with a more profound reduction of luc^{+} C1R-CD1d masses compared to CAR19-T treated mice despite the use of a single injection schedule and the absence of previous or concomitant administration of adjuvant αGalCer/IL-2 (**Figure 6-9**). That was associated with a longer tumour-free survival and better overall survival up to day 75 (**Figure 6-10**). No clinical GvHD or other CAR-therapy related adverse events were observed during the experiment.

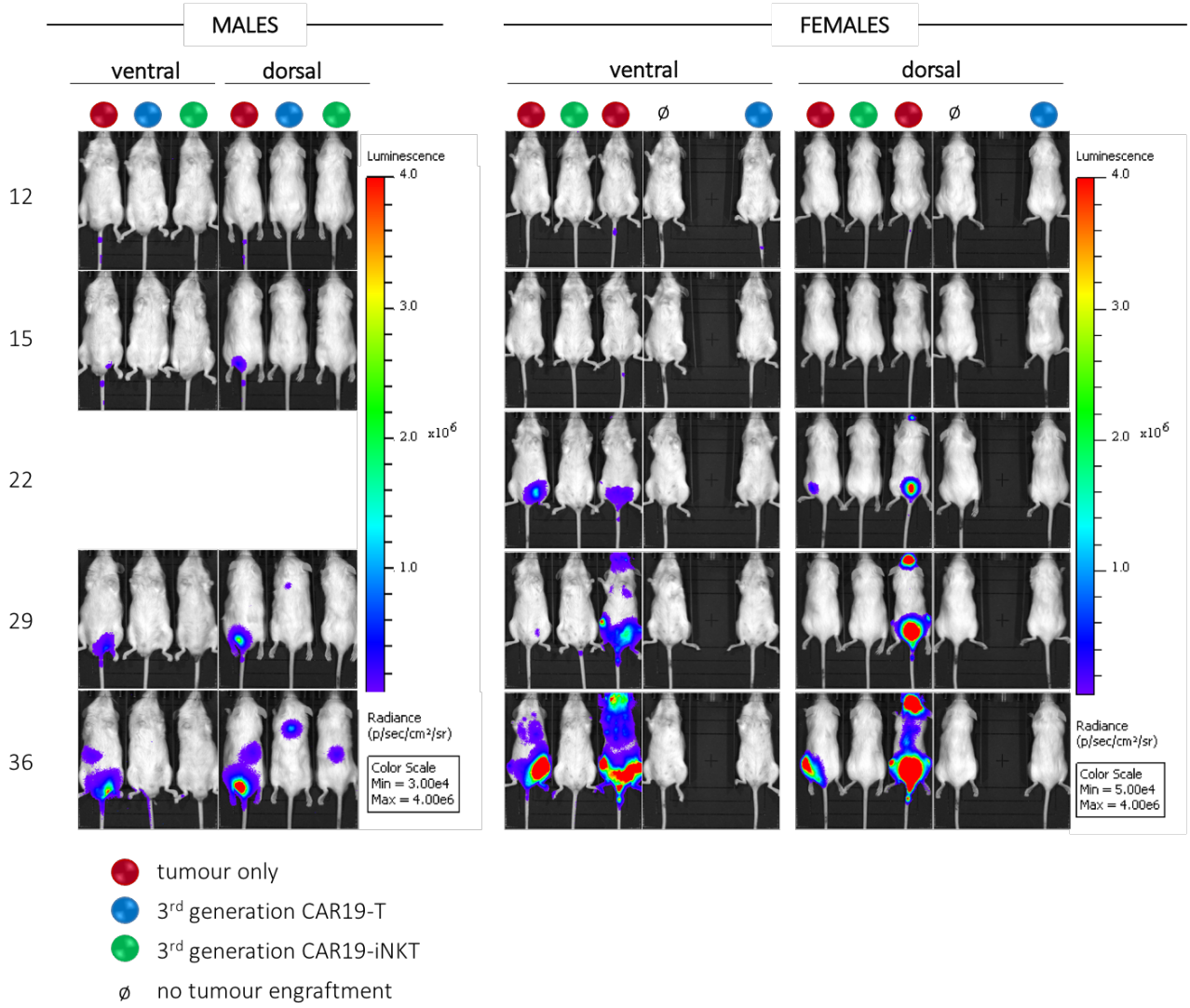


Figure 6-9 Tumour burden monitoring in pilot 2 experiment

Age- and sex-matched NSG mice received iv injection of 5 x10^6 firefly luc$^+$C1R-CD1d. On day 8, C1R-CD1d cell engraftment was confirmed in 7 mice. 4 xenografts were subsequently treated with a single iv infusion of 3rd generation CAR19-iNKT (green) or -T (blue) cells. Three mice served as tumour-only controls (red). Thereafter, tumour growth was monitored using weekly bioluminescent imaging.
Ø = no C1R-CD1d cell engraftment.

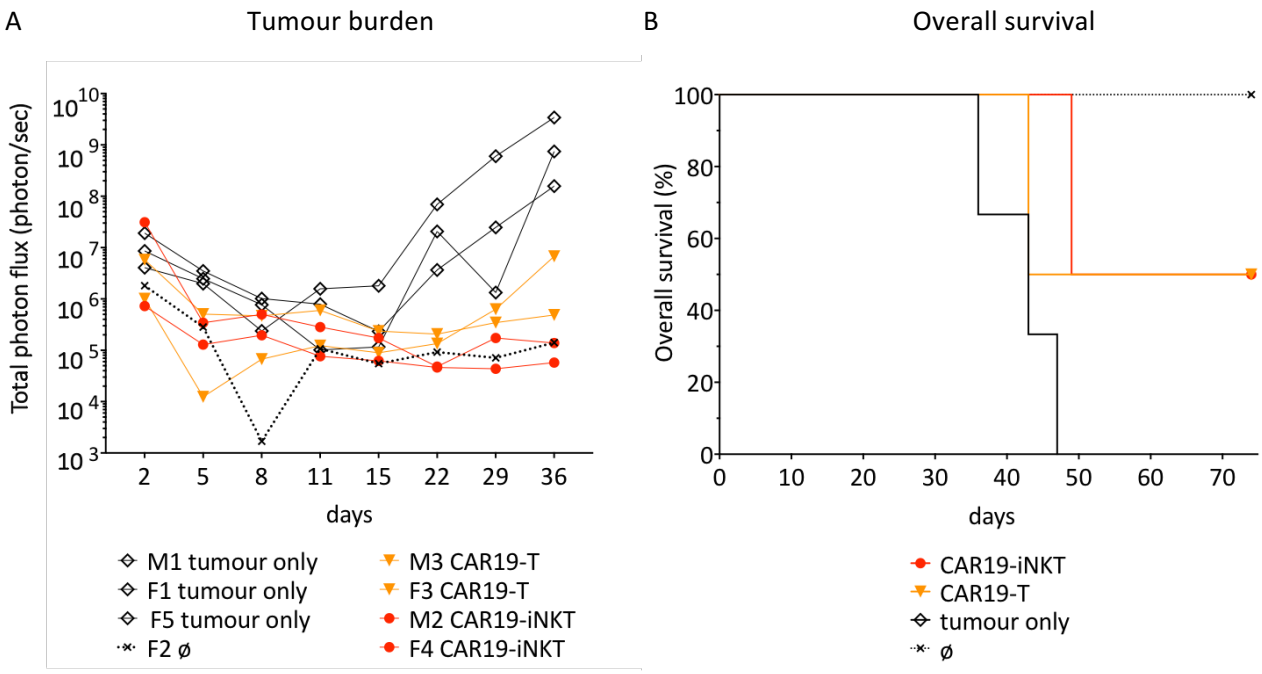


Figure 6-10 Feasibility study for preclinical *in vivo* investigation of CAR19-iNKT cell immunotherapy for B lymphoma

A. Summary of tumour burden profile per each mouse as assessed by BLI. B. Overall survival plot showing that 2 out of 4 preliminary CAR19-treated animals but none of tumour-only control mice were still alive on day 75 after a single injection of either CAR19-iNKT or CAR19-T.

Final flow cytometry analysis confirmed preserved CD19 and CD1d expression in CAR19-iNKT animals (**Figure 6-11**). HE histology sections didn't show any sign of GvHD (**Figure 6-12**).

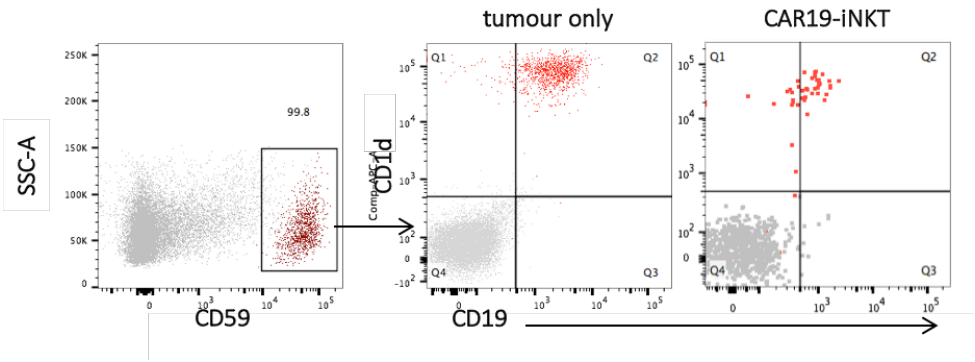
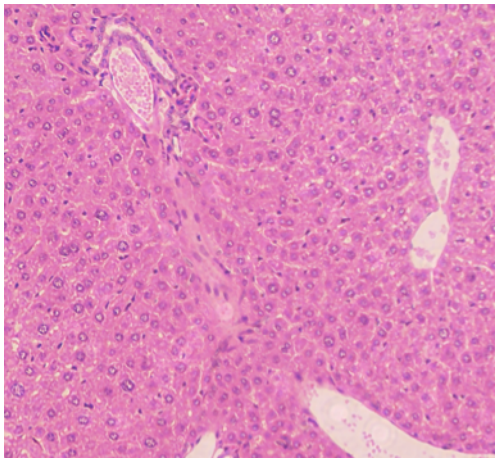


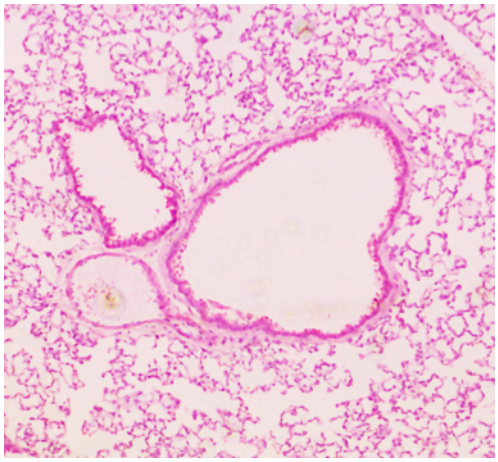
Figure 6-11 CD19 and CD1d expression on xenograft-derived C1R-CD1d cells

Representative flow cytometry plots showing expression of CD19 and CD1d on C1R-CD1d cells obtained from the spleen of the CAR19-iNKT-treated mouse with active bioluminescent signal. Human cells were identified as human CD59+ cells (*left*) within the live, single cells. Compared to C1R-CD1d cells isolated from a tumour-only control mouse (*middle*), the very few cells retrieved from the CAR19-iNKT-treated animal showed comparable levels of CD19 and CD1d (*right*).

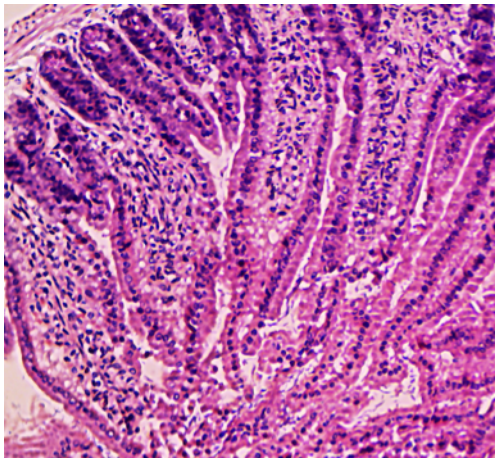
A



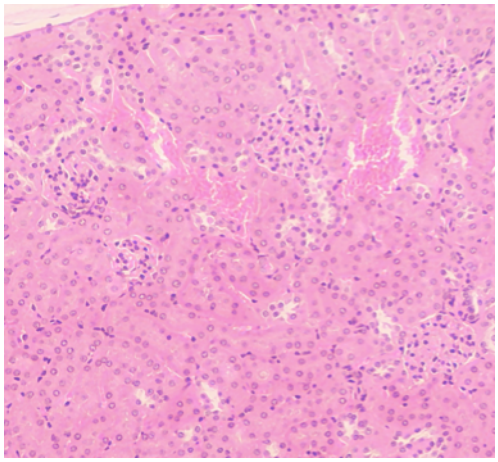
B



C



D



E

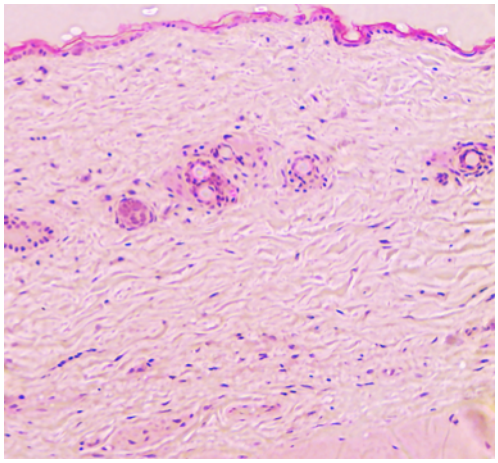


Figure 6-12 Histological analysis of GvHD target organs in CAR19-iNKT-treated xenografts

Microscopic examination of liver (A), lungs (B), gut (C), kidney (D) and skin (E) did not show any abnormalities in CAR19-iNKT-treated mice.

6.5 Enhanced anti-lymphoma activity of CAR19-iNKT cell *in vivo*

Having defined the conditions for evaluating my CAR19-iNKT cell product in a systemic B-lymphoma xenograft model, I performed two experiments aimed to compare the anti-lymphoma activity of 2nd generation CAR19-iNKT with 2nd generation CAR19-T cells (**Figure 6-13)**. Primary endpoints were overall survival (OS) and tumour-free survival (TFS).

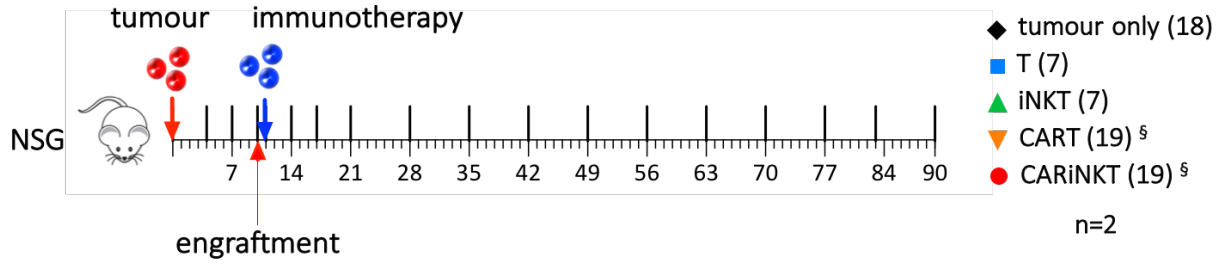


Figure 6-13 Layout for characterisation of *in vivo* anti-lymphoma activity of CAR19-iNKT cells
6-week old NSG mice were injected intravenously with 5 x10^6 luciferase-expressing C1R-CD1d on day 0. By day 4 after injection, tumour growth was monitored by BLI. Tumour engraftment was defined as increasing luciferase-mediated photon flux over two consecutive imaging sessions 3 days apart. Tumour xenografts were then randomised to control or immunotherapy arm. Treated animals were randomly assigned to 1 of 4 treatments, i.e., unmodified T/iNKT cells or CAR19-engineered T/iNKT cells. Tumour burden was monitored twice a week until day 21 and once a week thereafter.

A total of 73 animals received 5 x10^6 luciferase-expressing C1R-CD1d, 70 were engrafted, corresponding to 96% engraftment rate, as confirmed by BLI. Tumour xenografts were then randomised to control or immunotherapy, with 4 comparison arms, i.e., unmodified T, unmodified iNKT, CAR19-T and CAR19-iNKT cells. 10 x10^6 effector cells were administered by tail injection in all cases.

The procedures were well tolerated, no adverse events were observed during the tumour induction. The CAR-cell infusion was well tolerated. However, in the next few hours following immunotherapy the CAR19-iNKT group suffered from 5% weight loss, mild hypoactivity and changes in the fur, that appeared to be darker and ruffled. Such adverse event was transient and mild, did not require any specific action apart from close monitoring, and by 48 hours all mice were fully recovered.

Throughout the experiment, T and CAR19-T mice developed signs of low-grade GvHD, that was limited to skin involvement. Specifically, almost all mice developed facial and dorsal alopecia lesions and whiskers loss (**Figure 6-14**) during the second month of monitoring. Some of them recovered during the third month. None of them evolved to moderate/severe syndrome, defined as non-tumour related loss of weight, hunching, hypoactivity, ruffled fur and scaling[263]. Eventually, all animals that received immunotherapy were evaluable for analysis at the end of the study.

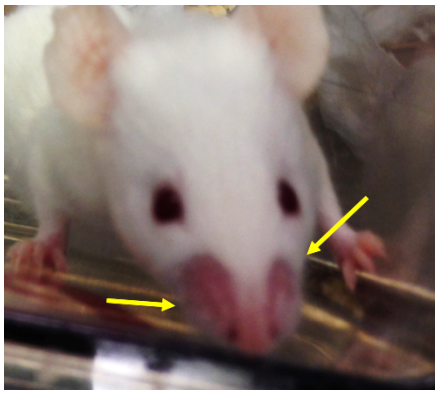


Figure 6-14 Skin GvHD
Representative facial coin lesions in a CAR19-T mouse.

The most frequent symptoms associated with tumour progression in any group were hunching, hypoactivity/hyporeactivity, hind limb paresis/paralysis. Less frequently, anorexia and dehydration led to rapid weight loss up to 20% in 24 hours. Some mice developed more pronounced neurological features characterised by stereotypic circling, loss of balance and seizures. Skin tumours presented with loss of skin integrity. In few cases, a palpable mass was associated with abdominal distension and/or urinary retention.

Animals treated with unmodified T or iNKT cells had poorer OS compared to mice receiving CAR19-engineered cells (**Figure 6-15**). However, compared to CAR19-T cell recipients, the CAR19-iNKT cell-treated group displayed a significantly improved OS ($P=0.01$) and TFS ($P<0.0001$).

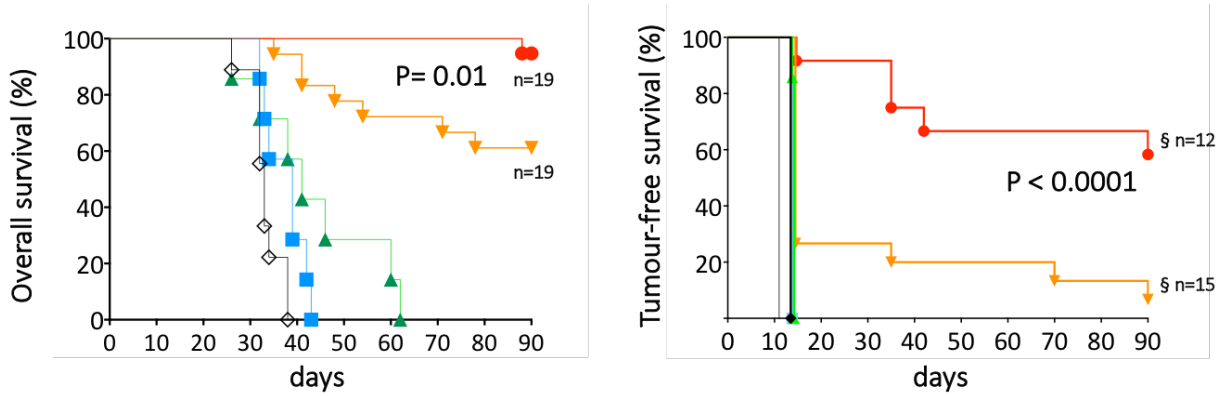


Figure 6-15 Anti-tumour activity of CAR19-iNKT cells in a systemic B-lymphoma xenograft model
Summary of OS and TFS of tumour-bearing mice untreated (n=12) or treated with untransduced T cells (n=7), untransduced iNKT cells (n=7), second-generation CAR19-T cells (n=19, of which 4 excluded from TFS analysis; see **§**) or CAR19-iNKT cells (n=19, of which 7 excluded from TFS analysis; see **§**). **§** In 4 and 7 CAR19-T and CAR19-iNKT-treated animals respectively, tumour burden could not be monitored by BLI from day 70 (+59 post itx) during the first experiment due to restricted access to the IVIS instrument. However, all mice were maintained in the study until achievement of humane endpoint or the end of experiment. Data are from two independent experiments using two distinct cohorts of animals. Effector cells generated in different times from two different donors. Shown P values are for comparison of CAR19-T vs CAR19-iNKT cell-treated animals.

As shown in **Figure 6-16**, 3 out of 7 CAR19-T-treated mice within the first cohort died due to tumour progression on day 41, 48 and 78, while there were no tumour-related deaths among the CAR19-iNKT treated mice. One CAR19-iNKT animal died due to middle ear infection on day 88. Notably, all CAR19-T mice had detectable bioluminescent signal above the background threshold throughout the first experiment, never achieving complete disease remission (CR).

In a second independent experiment, 4 out of 12 CAR19-T and 1 out of 12 CAR19-iNKT -treated mice died due to tumour progression, the former on day 35, 41, 54 and 71 whereas the latter on day 88 respectively. Remarkably, only one CAR19-T-recipient achieved a sustained CR, defined as drop of biophotonic signal below background, while most of them never underwent CR and 3 had evidence of disease relapsed on day 35, 70 and 90. By contrast, all CAR19-iNKT-treated mice but 1 achieved CR. Most of them maintained CR until the end of experiment, with the exception of 3 relapses occurring on day 35 (two animals) and 42 (one animal) and another mouse showing evidence of disease for the first time at the last scan on day 90.

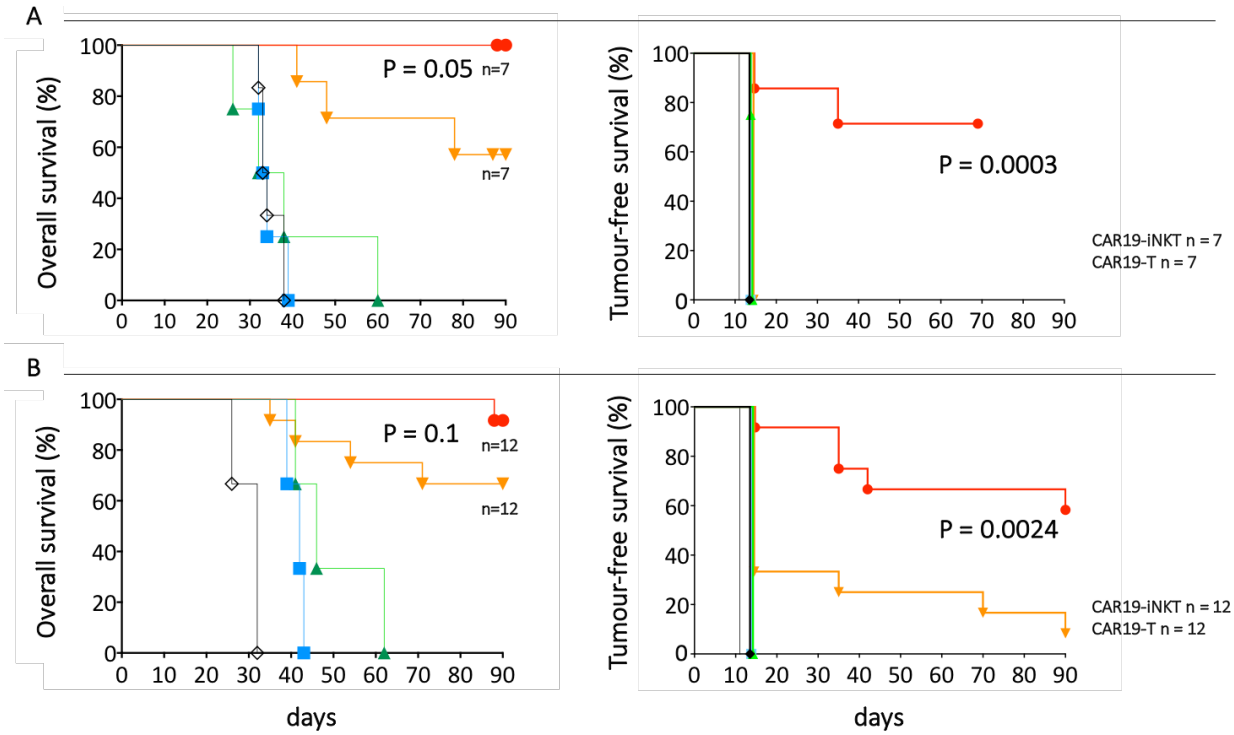


Figure 6-16 Overall and tumour-free survival according to experiment
A. Results from cohort 1. B. Results from cohort 2

The improved OS and TFS could be at least in part explained by a significantly swifter decline of tumour burden observed within 3 days following transfer of CAR19-iNKT cells (**Figure 6-17)**.

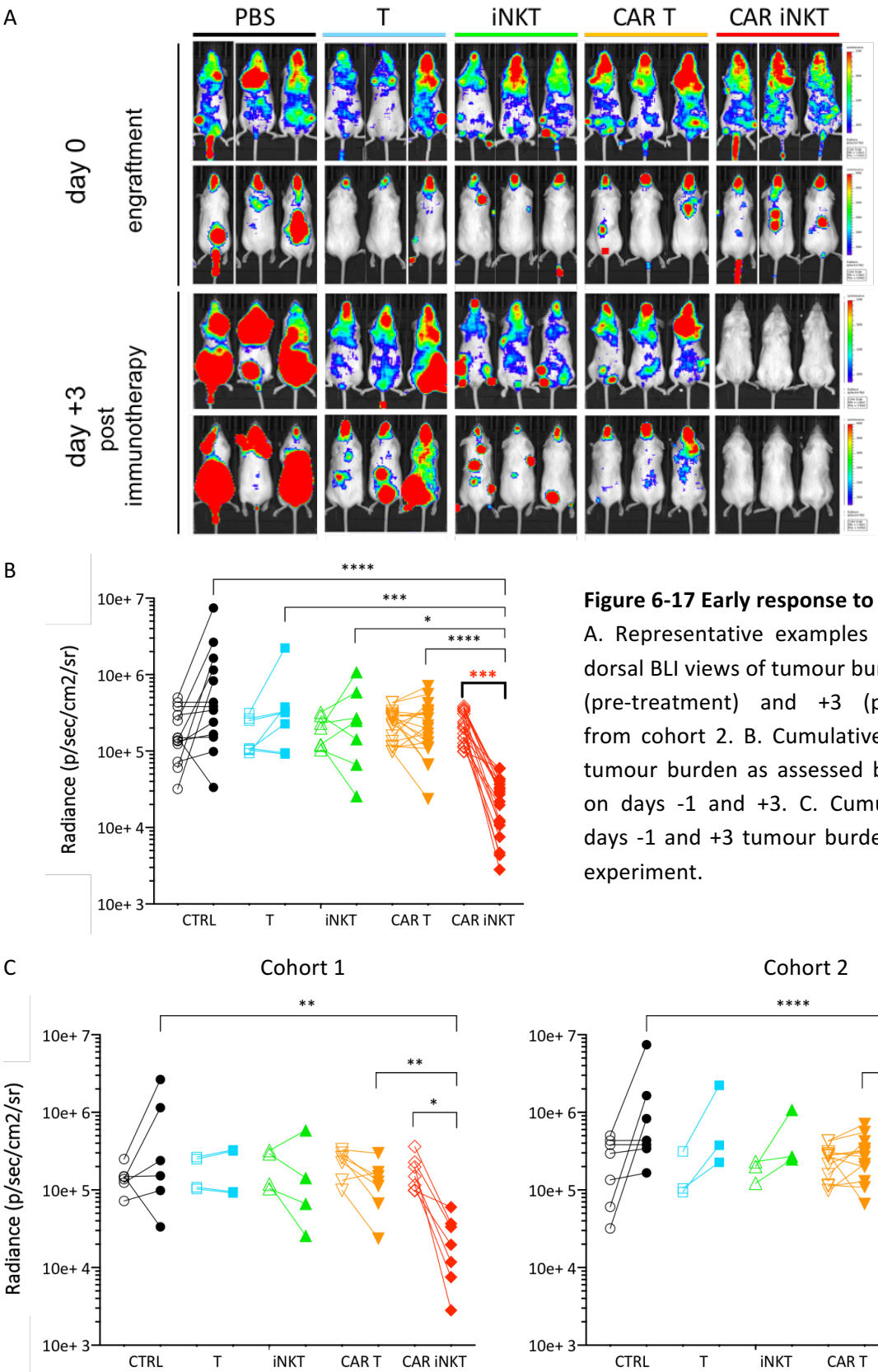


Figure 6-17 Early response to treatment

A. Representative examples of ventral and dorsal BLI views of tumour burden on days -1 (pre-treatment) and +3 (post-treatment) from cohort 2. B. Cumulative data showing tumour burden as assessed by BLI radiance on days -1 and +3. C. Cumulative data of days -1 and +3 tumour burden according to experiment.

6.6 CAR19-iNKT cell eradicate brain tumour

As shown in **Figure 6-17A**, in my established C1R-CD1d tumour model I observed enhanced bioluminescent activity over the head even at the time of engraftment. In order to better characterize the head signal, I performed brain MR studies. MRI sequences, acquired using Gadolinium-based contrast agent in 3 scanning projections (**Figure 6-18**), demonstrated areas of Gadolinium uptake and brain tissue enhancement consistent with tumour involvement in animals with BLI evidence of head photon signal (**Figure 6-19** and **Figure 6-20**).

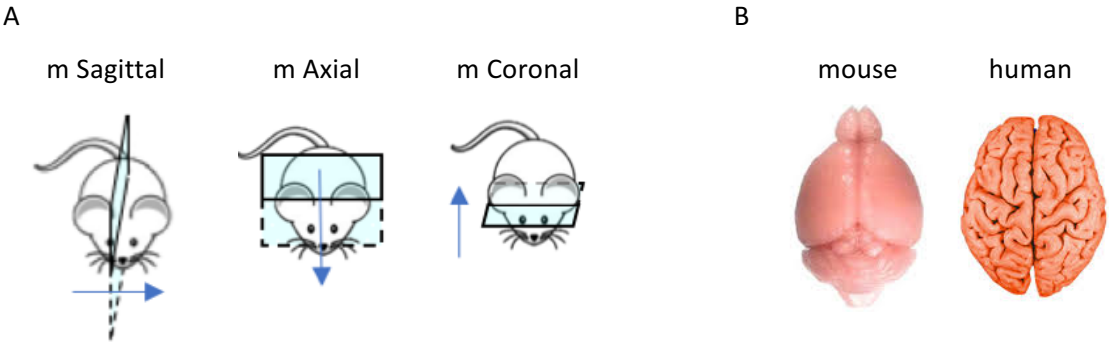


Figure 6-18 Mouse MRI brain sections and macroscopic anatomy
A. MRI section orientation as defined relative to the mouse spine. m: mouse B. Macroscopic anatomy of mouse brain compared to human brain. The murine brain surface is smoother, with less cortical convolutions and prominent olfactory bulb (*left panel*, apical lobe). Modified from https://medicalxpress.com/news/2014-02-dino-brains-thought-control10-fascinating.html

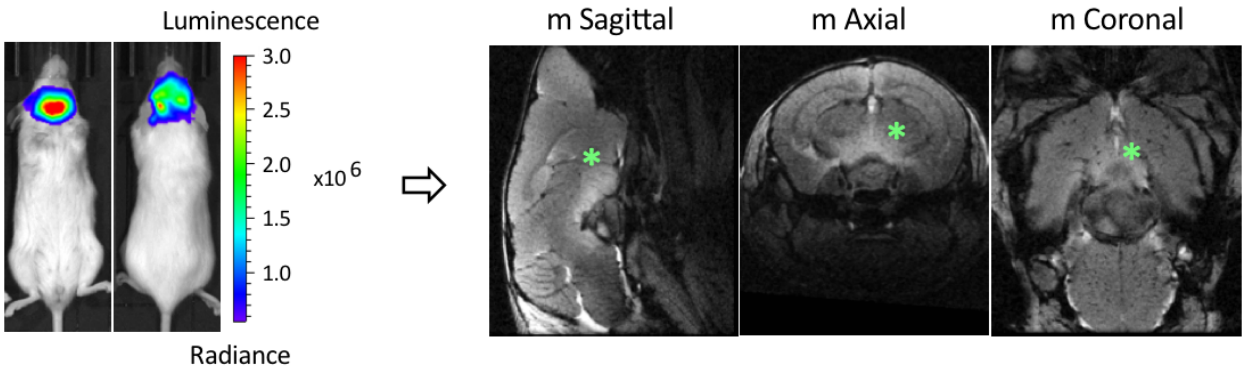


Figure 6-19 Representative MRI images of brain tumour
Correlation of BLI signal with brain MRI study in a CAR19-T cell-treated animal. *Left*: BLI images obtained on day+21 post immunotherapy. *Right*: Representative mouse (m) sagittal, axial and coronal MRI sections obtained on day+23 post immunotherapy after contrast injection (Gadovist 3mmol/kg iv) and acquired with T1 FLASH sequence to maximize the Gadolinium signal. The terminal MRI study showed a sellar mass of 21.4mm3 (±0.2) and suprasellar parenchymal enhancement (green asterisks), suggestive of lymphomatous growth in the in the pituitary gland and surrounding parenchymal tissue infiltration by tumour cells.

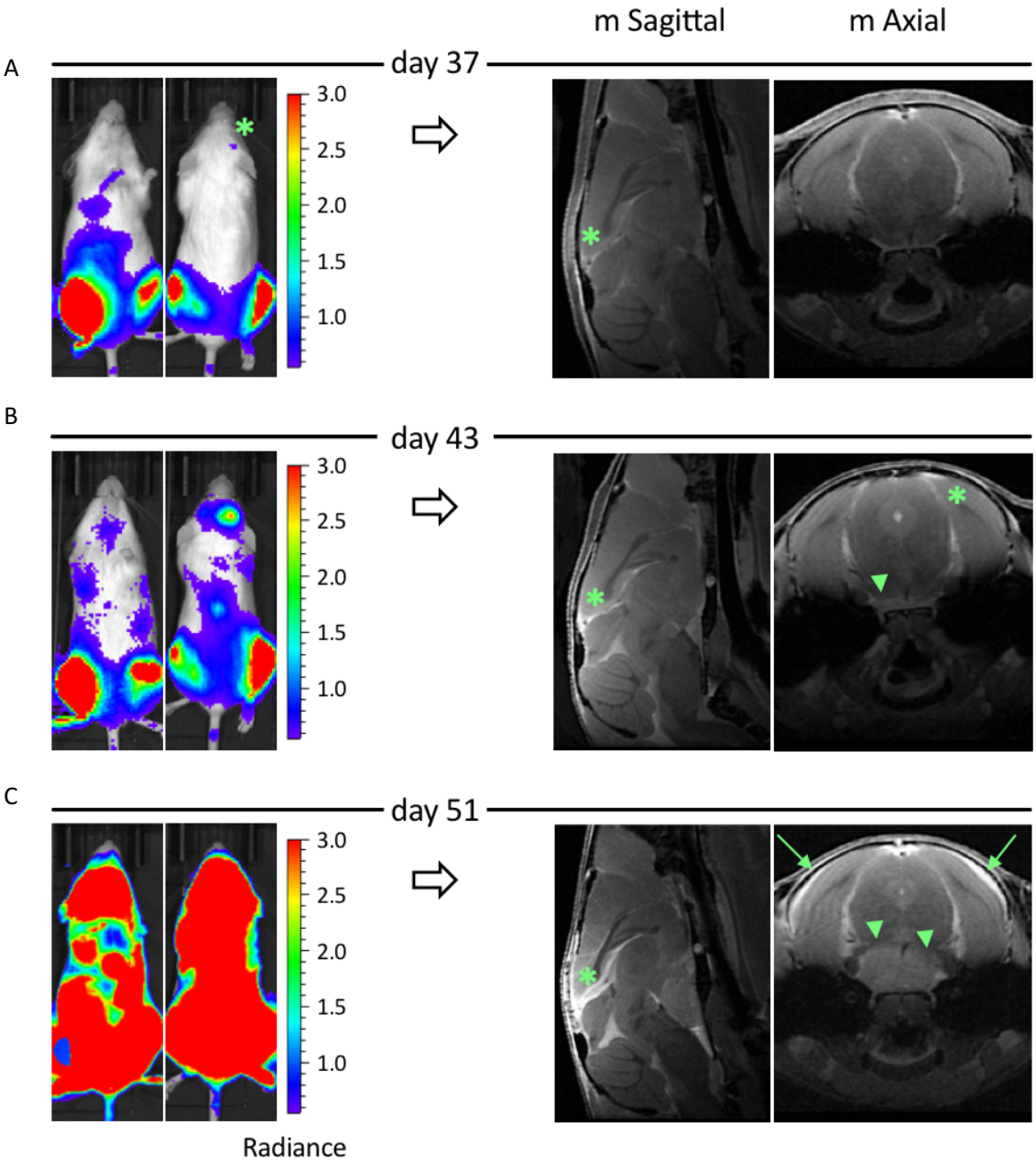


Figure 6-20 Representative MRI monitoring of brain tumour

Correlation of BLI images with brain MRI monitoring in an iNKT cell-treated animal. The animal stopped gaining weight from day +36 post-immunotherapy. Longitudinal MRI study showed a steadily growing mass in the pituitary region (B, green arrow ends), with an estimated volume of 4.72mm3, 7.79mm3 and 28.2mm3 on day +37 (*top*), +43 (*middle*) and +51 (*bottom*) respectively. Eventually, the mouse became hypoactive, which was associated with the appearance of diffuse, smooth extra-axial contrast enhancement along the cerebral convexity bilaterally (C, green arrows), suggestive of meningeal infiltration by tumour cells.

Gadolinium uptake was mainly observed in supratentorial regions, especially isocortex and deep grey matter, with cases of meningeal involvement and cerebrospinal fluid (CSF) disease. Contrast-to-noise (CNR) determination confirmed a direct correlation between the tumour burden in the head as assessed by BLI and either the isocortex or the hypothalamus CNR (**Table 6-1**). While healthy control mice had an isocortex CNR of 21.77 ±1.07 and a hypothalamus CNR of 3.54 ±0.40, tumour bearing xenografts with active head photon signal displayed values consistently higher than the maximum observed in controls, i.e., larger than 23.55 and/or 4.22 respectively according to the brain site.

Further MR spectroscopy confirmed the presence of aberrant metabolic activity associated with the sellar masses identified by MRI, characterized by relative increase of choline (Cho, peak at 3.2ppm) and lipid macromolecules (peak at 0.8-0.9ppm), as assessed by long and short echo time (LTE and STE) respectively, and parallel decrease of creatine (Cr, LTE peak at 3.0ppm,) and NAA (LTE peak at 2.0ppm, **Figure 6-21**). Moreover, quantification of the relevant peaks at LTE demonstrated a correlation between the magnitude of the change and the tumour growth (**Figure 6-21**, **Table 6-1**). Specifically, in same-sex and age healthy animals with comparable weight, the mean pituitary gland volume was 1.838mm^3 ±0.137 (range 1.450 - 2.048). In all but CAR19-iNKT-treated xenografts the pituitary gland volume was larger than the max value among healthy mice. Similarly, an abnormal metabolic profile could be detected and measured only in xenografts with enlarged hypophysis, with a Cho/Cr and/or Cho/NAA ratio consistently higher than 0.1. The presence of a prominent choline peak together with a lipid peak seemed to be a distinctive feature associated with neoplastic growth, similar to what has been recently described in patients with CNS primary neoplasms[264-266].

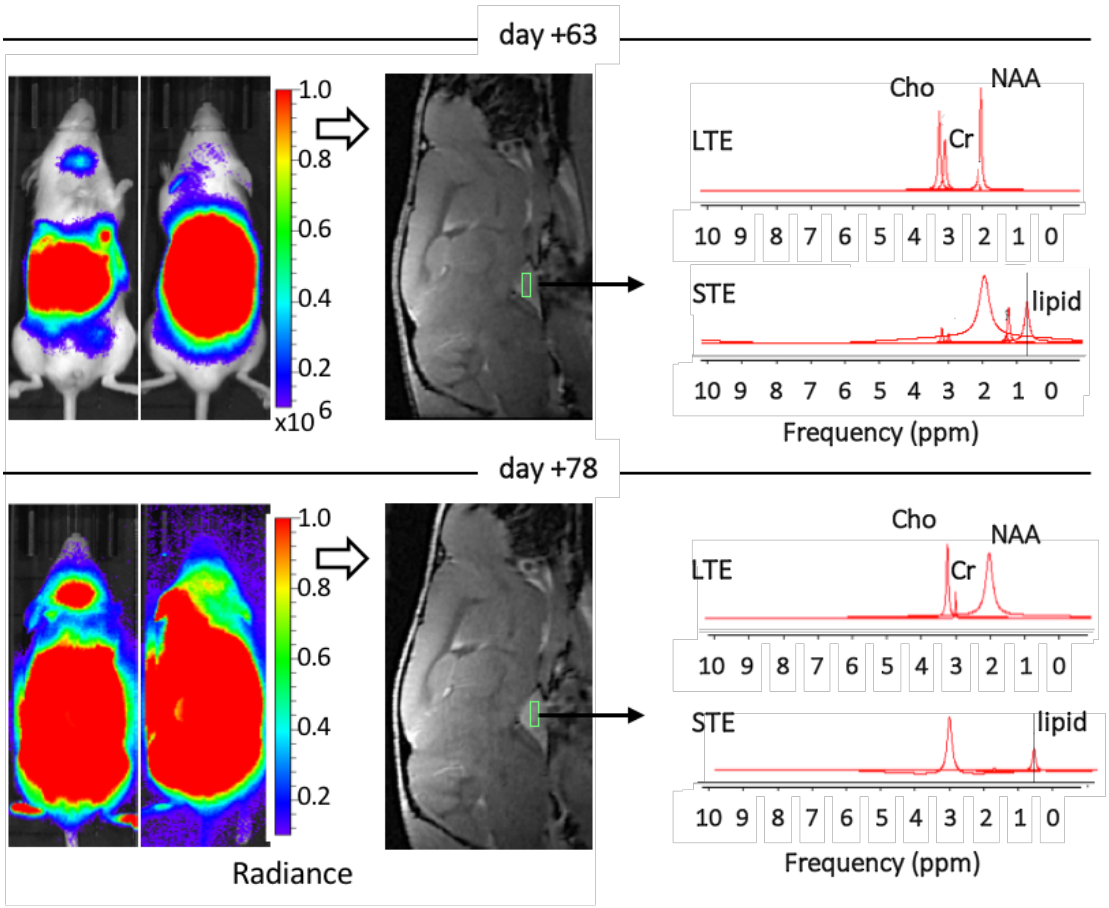


Figure 6-21 Representative MR Spectroscopy of sellar mass

Longitudinal MRI and MR Spectroscopy study in a CAR-T cell treated animal. *Top*: MRS assessment on day+63 post-immunotherapy underpinned low burden head disease, which upon MR spectroscopic analysis was characterized by inversion of the Choline/Creatine (frequency: 3.2/3.0) and Choline/NAA (frequency:3.2/2.0) peaks at LTE compared to normal control and lipid peak at STE (**Table 6-1**). *Bottom*: Head disease progression was confirmed by BLI, MRI and MR Spectroscopy on day+78, showing increased bioluminescent signal from the head, enlarged sellar mass (from 6.382mm3 ±0.235 to 7.429 ±0.033) and elevated Choline/Creatine and Choline/NAA ratios and lipid peak. MR Spectroscopy data are shown as chemical shifts expressed in parts per million (ppm) relative to the reference Tetramethylsilane (TMS, frequency 0.00 ppm).

Table 6-1 MRI study – all animals

#	Mouse ID	Treatment	Time point	Brain					Pituitary gland		Cho /Cr	Cho /NAA	0.8 0.9
			Day post tumour (treatment)	Head BLI	Isocortex CNR		Hypothalamus CNR		Volume (mm^3) Mean ± SEM				
Healthy animals													
1	F38	none	44 days old	7.34E+03	18.673	±2.076	2.395	0.785	1.843	±0.119	0.042	0.023	No
2	F38	none	58 days old	2.34E+04	22.757	±1.362	3.845	1.885	2.048	±0.023	0.000	0.000	No
3	F39	none	44 days old	1.26E+04	22.110	±2.730	3.715	1.745	2.010	±0.180	0.063	0.096	No
4	F39	none	58 days old	1.22E+04	23.545	±11.114	4.215	0.505	1.450	±0.027	0.000	0.000	No
Tumor xenografts													
5	F35	none	29 (NA)	2.77E+06	111.973	±2.863	21.087	0.937	4.995	±0.445	NA	NA	NA
6	F35	none	35 (NA)	2.14E+08	142.635	±12.735	39.751	0.311	9.945	±0.255	3.750	NA	NA
7	F33	T	29 (+18)	1.06E+08	130.114	±8.904	112.372	4.729	3.675	±0.205	NA	NA	NA
8	F32	iNKT	48 (+37)	4.21E+05	31.569	±9.810	10.200	1.180	4.610	±0.110	1.396	0.737	Yes
9	F32	iNKT	54 (+43)	1.10E+07	102.635	±8.365	13.070	0.680	7.365	±0.425	1.662	1.857	Yes
10	F32	iNKT	62 (+51)	2.52E+08	136.166	±32.833	14.025	0.535	28.050	±0.150	66.194	8.800	Yes
11	F13	CAR19-T	32 (+21)	1.02E+08	14.477	±0.183	21.192	0.192	21.400	±0.200	NA	NA	NA
12	F37	CAR19-T	74 (+63)	2.28E+06	93.260	±37.67	9.860	1.650	6.385	±0.235	1.346	0.750	Yes
13	F37	CAR19-T	89 (+78)	3.49E+07	125.140	±38.58	24.085	1.405	7.430	±0.033	7.343	3.980	Yes
14	F4	CAR19-T	68 (+57)	2.02E+06	53.195	±3.305	24.755	3.495	4.115	±0.066	1.198	0.636	Yes
15	F25	CAR19-T	90 (+79)	5.84E+04	90.545	±5.355	5.695	2.395	4.605	±0.466	2.675	2.174	Yes
16	F27	CAR19-T	90 (+79)	5.46E+04	32.250	±12.17	4.995	0.995	3.385	±0.495	2.093	3.788	Yes
17	F7	CAR19-iNKT	90 (+79)	9.84E+03	13.765	±1.505	4.005	1.195	1.713	±0.112	0.000	0.000	No
18	F9	CAR19-iNKT	90 (+79)	9.78E+03	15.82	±0.760	3.115	1.125	1.496	±1.378	0.000	0.000	No

Cho: choline; Cr: creatine; NAA: N-Acetylaspartate; NA: not available

In addition, diffusion weighted imaging (DWI) allowed to confirm the absence of disease when there was no clear evidence of tumour growth by BLI, MRI and MR spectroscopy (**Figure 6-22**).

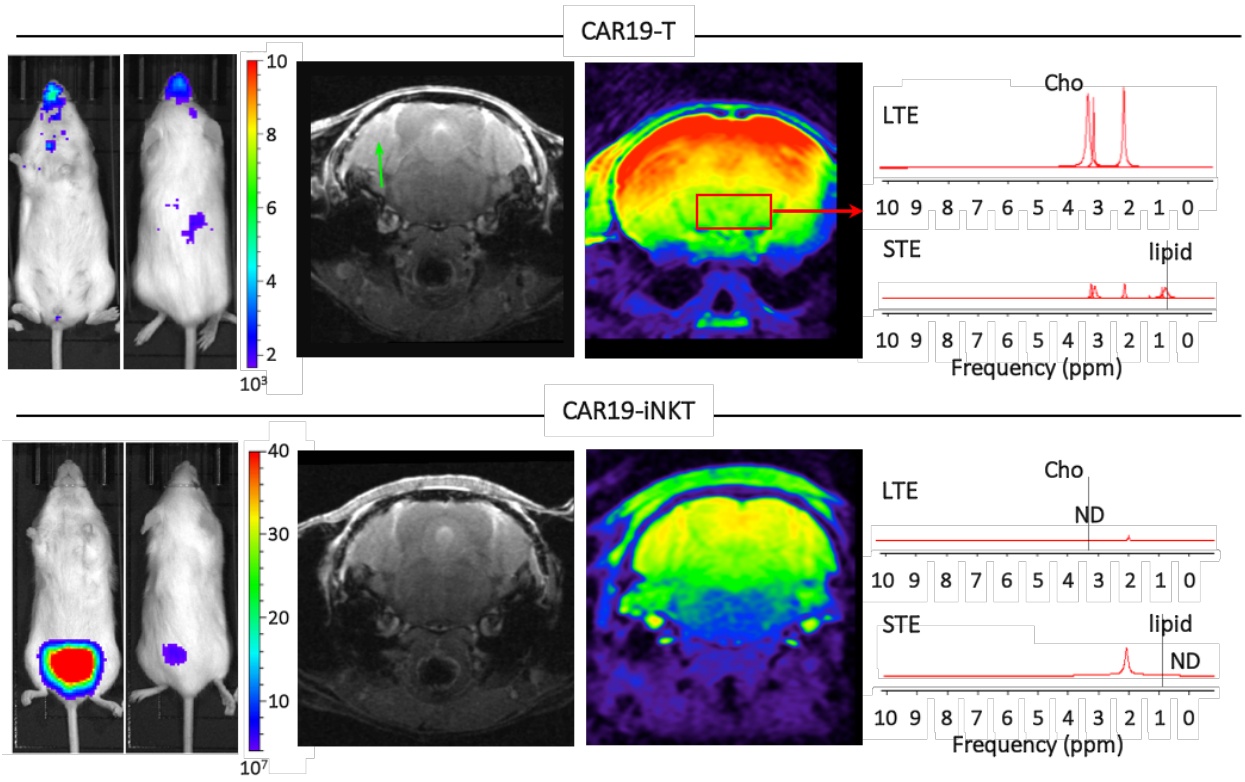


Figure 6-22 Representative DWI analysis of low-burden brain disease
Heatmap representation of apparent diffusion coefficients (ADCs). Red areas represent regions characterized by higher cellular density (lower ADCs), consistent with the presence of tumour cells. Green-yellow areas represent normal tissues (higher ADCs). Low-burden lesions with borderline contrast enhancement by MRI were associated with lower ADCs by DWI and abnormal MR Spectroscopy profile (*top*). By contrast, in the absence of active BLI photon signal, there was no Gadolinium uptake with normal ADCs and metabolic profile (*bottom*).

Based on the above findings, final correlation of bioluminescence study with MR modalities and histologic analysis suggested the presence of intracranial meningeal, brain and pituitary disease in most animals at the time of engraftment (**Figure 6-23**, **Figure 6-24** and **Table 6-2**). While brain lymphomas persisted above the threshold of detection in all but one animals receiving CAR19-T cells as well as in all untreated animals, they were cleared in 13/18 CAR19-iNKT cell-treated animals. This suggests that CAR19-iNKT cells cross the blood-brain barrier and effectively control brain disease, a property that could be of significant clinical value in the immunotherapy of brain lymphomas and other brain cancers.

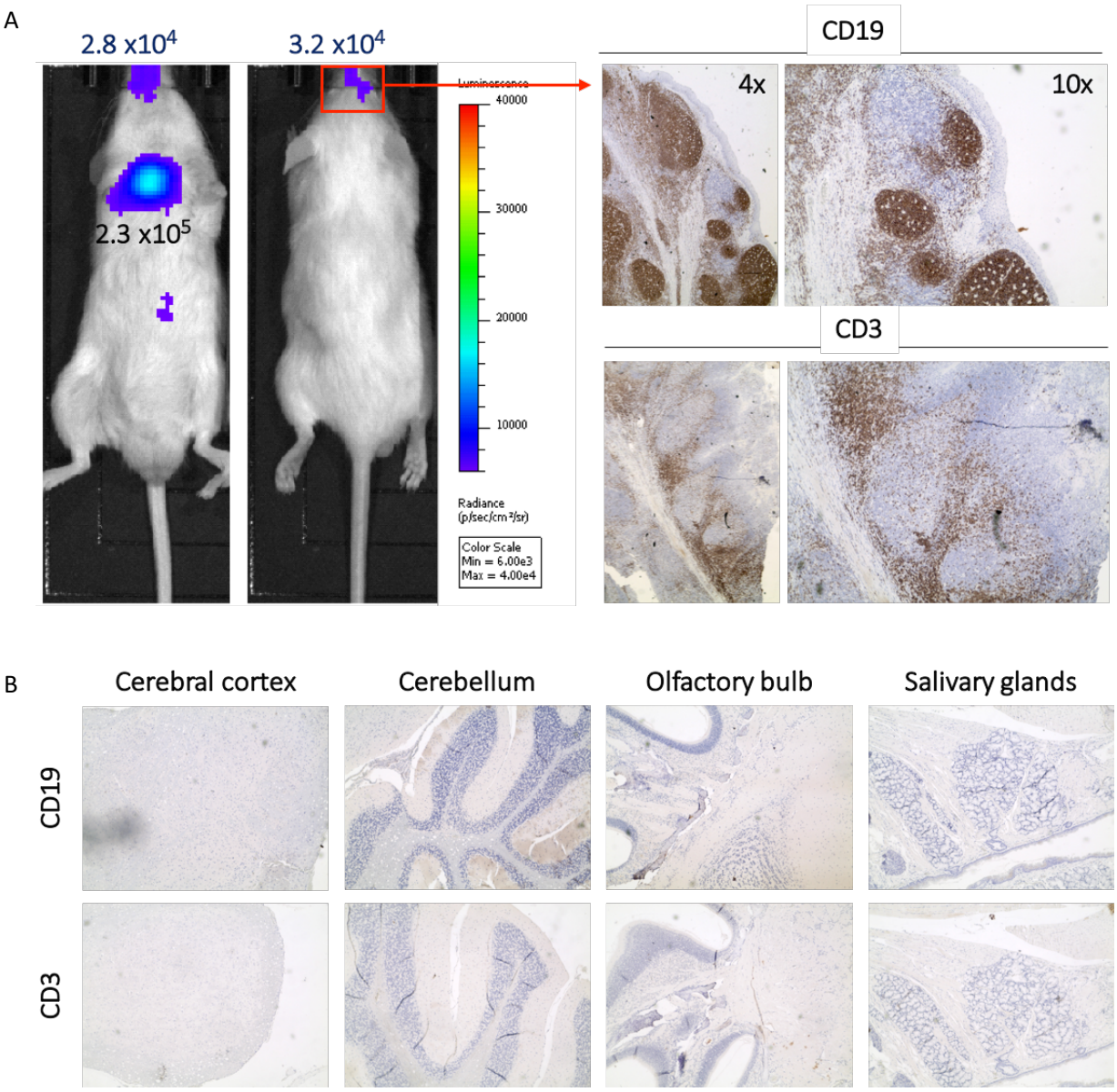


Figure 6-23 Correlation of BLI images with immunohistochemistry

A. Representative example of staining with anti-human CD19 (hCD19) and CD3 (hCD3) of olfactory bulb brain tissue of a mouse treated with CAR19-T cells. The tumour cells were identified by bright CD19 staining, whereas CAR19-T cells were revealed by $CD3^+$ staining at the edge of the tumour areas. B. There was no evidence of tumour and/or T cells in all other assessed areas.

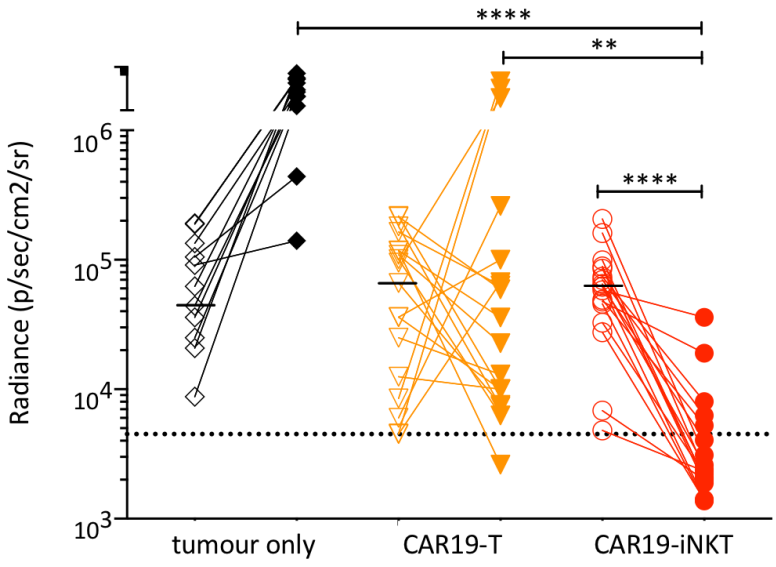


Figure 6-24 Head tumour burden as assessed by BLI

Photon activity in the head of control (n=11), CAR19-T (n=18) and CAR19-iNKT (n=18) cell-treated animals at engraftment and at completion of the experiment. Detection threshold (dotted line) was set as the lowest BLI activity value recorded in the head at engraftment in the whole cohort of animals used (see table Table 6-2).

Table 6-2 Head tumour burden

	Tumour only		CAR19-T		CAR19-iNKT	
	Engraftment	Endpoint	Engraftment	Endpoint	Engraftment	Endpoint
Number of values	11	11	18	18	18	18
Minimum radiance	8.74E+03	1.40E+05	4.50E+03	2.61E+03	4.80E+03	1.37E+03
Maximum radiance	1.91E+05	2.56E+09	2.18E+05	4.65E+08	2.07E+05	3.59E+04
Mean radiance	8.25E+04	4.33E+08	8.43E+04	3.23E+07	6.92E+04	5.74E+03
Median radiance	6.24E+04	4.94E+07	8.06E+04	2.93E+04	6.21E+04	2.37E+03
Std. Error of Mean	1.98E+04	2.35E+08	1.74E+04	2.61E+07	1.17E+04	2.03E+03
Lower 95% CI of mean radiance	3.84E+04	-9.02E+07	4.77E+04	-2.27E+07	4.46E+04	1.46E+03
Upper 95% CI of mean radiance	1.27E+05	9.56E+08	1.21E+05	8.73E+07	9.38E+04	1.00E+04
Threshold radiance	4.50E+03	4.50E+03	4.50E+03	4.50E+03	4.50E+03	4.50E+03
Discrepancy of mean radiance	7.80E+04	4.33E+08	7.98E+04	3.23E+07	6.47E+04	1.24E+03
Discrepancy of median radiance	5.79E+04	4.94E+07	7.61E+04	2.48E+04	5.76E+04	-2.14E+03
Statistic tests						
Kruskal-Wallis test	tumour only vs CAR19-T vs CAR19-iNKT at engraftments: ns (P=0.9144)					
Kruskal-Wallis test	tumour only vs CAR19-T vs CAR19-iNKT at endpoint: P<0.0001					
Wilcoxon test (paired)	CAR19-iNKT at engraftments vs endpoint: P<0.0001					

Radiance: p/sec/cm2/sr

6.7 CAR19-iNKT cell second complete responses of lymphoma relapse

In 4 CAR19-iNKTcell-treated mice, after initial clearance of systemic lymphoma, relapse including brain disease developed at a later stage. Remarkably, in all 4 mice this secondary disease eventually regressed leading to long-term survival (**Figure 6-26**) and consistent with long-term persistence and ability for secondary anti-tumour responses by CAR19-iNKT cells.

Further immunohistochemistry analysis confirmed the absence of residual disease and any sign of neurological damage, suggesting that CAR19-iNKT cells may deliver anti-tumour therapeutic activity in the brain without significant neurotoxicity (**Figure 6-27**).

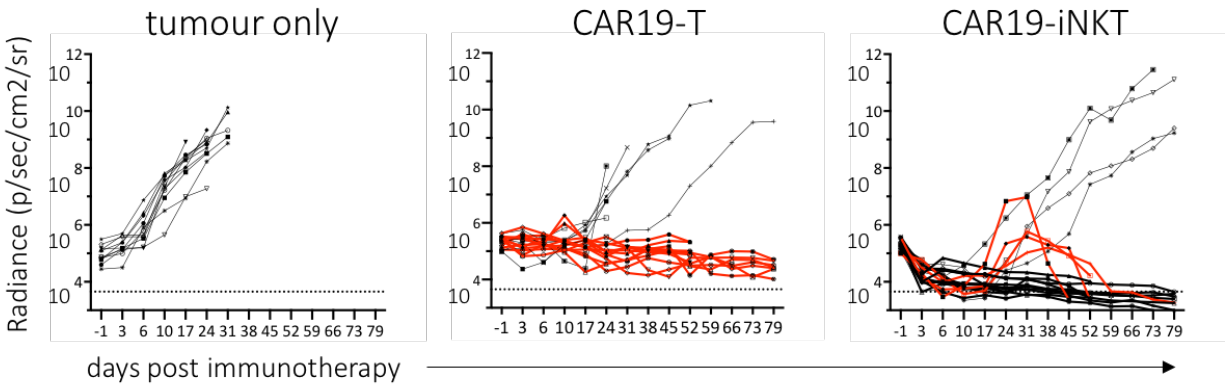


Figure 6-25 Tumour burden profiles

Whole body BLI activity recorded throughout the duration of the experiment from tumour-only control, CAR19-T and CAR19-iNKT treated groups. A typical 'hump' profile, associated with robust, sustained second remission, was observed in 4 animals receiving CAR19-iNKT immunotherapy but in none within the other groups.

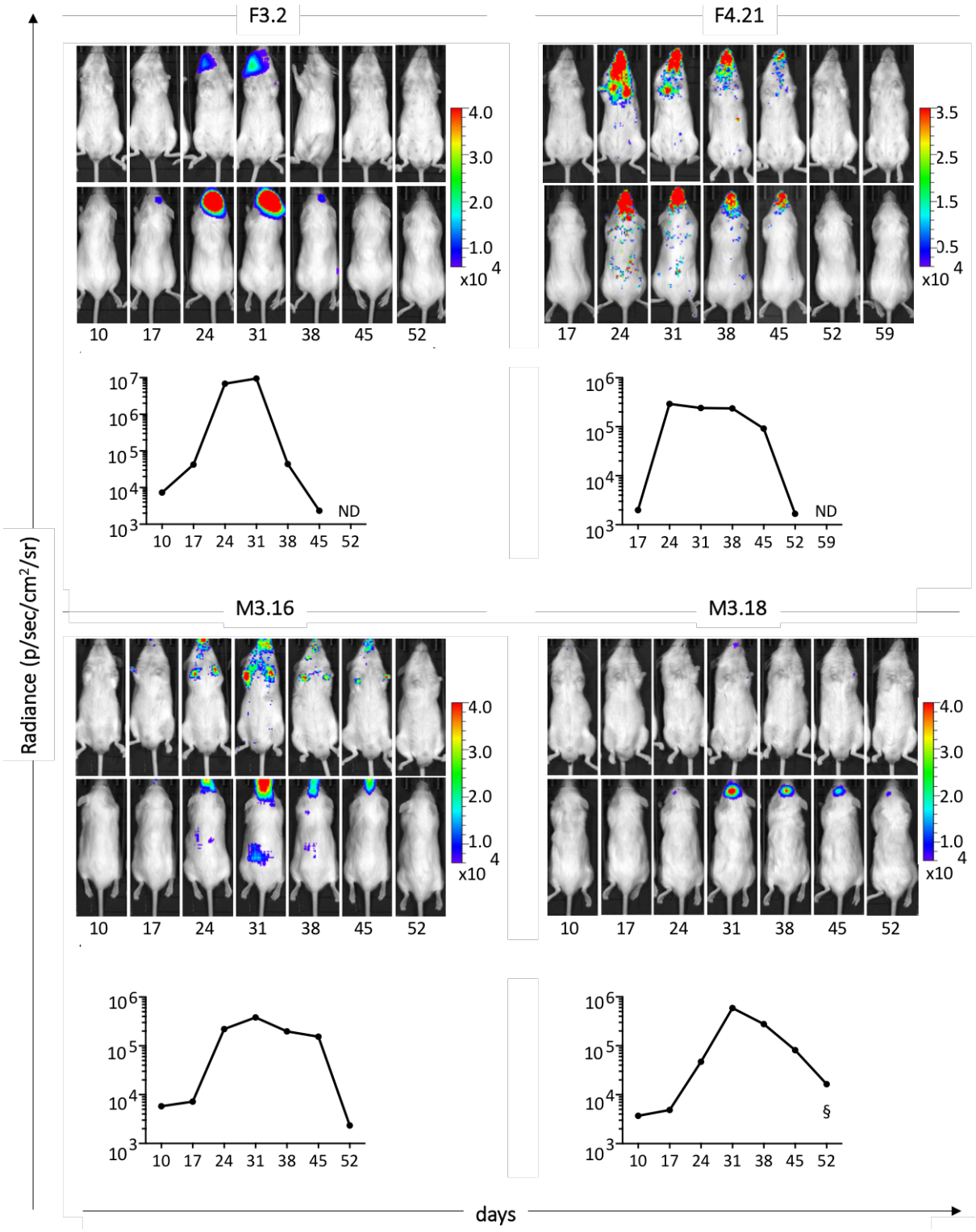


Figure 6-26 Second remissions in CAR19-iNKT mice

Longitudinal BLI images and dynamics of radiance activity are shown for each animal. Relapse occurred between 17 and 26 days following immunotherapy. In 3 mice, a second CR was documented by BLI. In the 4th mouse a partial remission could be documented, due to restricted access to the IVIS instrument from day 70 (+59 post itx) (§). However, all mice survived until the end of the experiment with no clinical signs of tumour progression as assessed post mortem by fluorescence imaging, flow cytometry or immunohistochemistry (not shown). ND: not detectable.

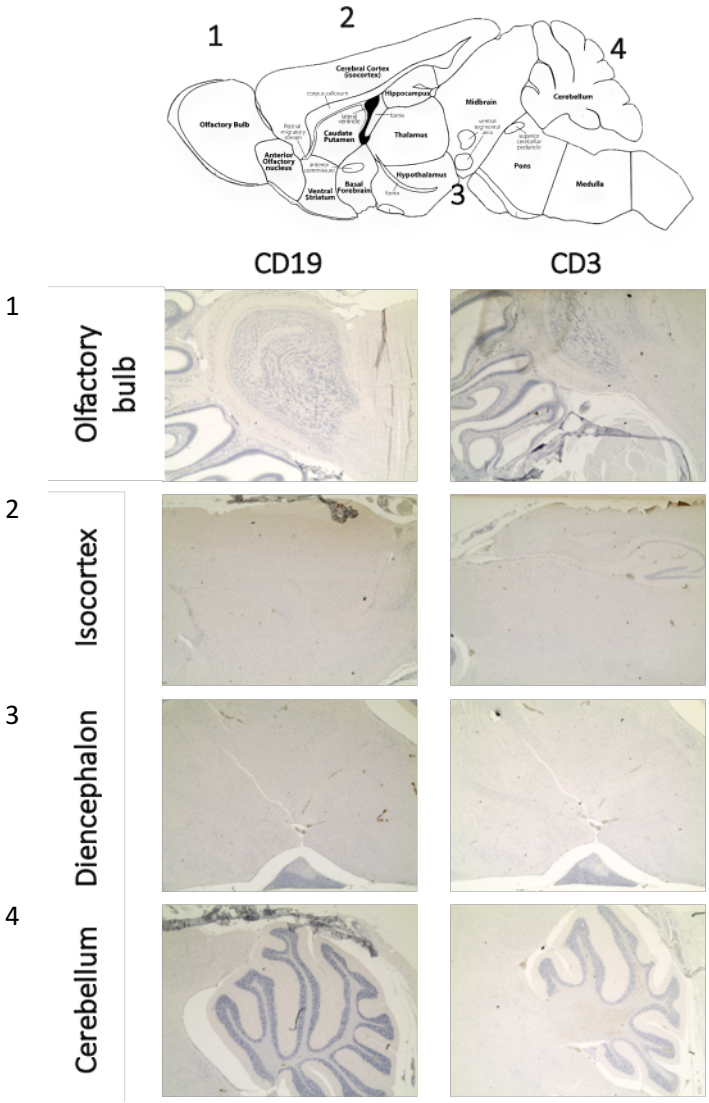


Figure 6-27 Absence of CAR19-iNKT related neurotoxicity

Representative immunohistochemistry analysis of brain tissues from F3.2 mouse at the end of experiments

6.8 Discussion

Assessment and validation of CAR-T therapies in *in vivo* models has been a key component of current clinical trial success, providing valuable information for the optimization of CAR-T technology[267]. Different experimental approaches addressed specific questions, e.g. 'stress-test' models, based on T cell doses purposefully reduced to levels where CAR therapy begins to fail, address the potency associated with different CAR co-stimulatory configurations[268]; humanized xenograft models evaluate cancer growth and response to CAR-based treatments in the context of a human immune system and resultant tumour microenvironment[48]; patient-derived xenografts (PDX) recapitulate the heterogeneity and complexity of patients' disease for more accurate prediction of CAR immunotherapy outcome[269]. Therefore, there is not a gold standard and the choice of the 'appropriate' setting, e.g. in terms of host, target cells and therapeutic schedule, is largely dependent on the contingent scientific question.

For the purposes of my study, I aimed to functionally validate my novel CAR19-iNKT cell product *in vivo* and confirm the potential to eradicate human $CD1d^+$ B cell lymphoma cells in the long term.

To date, there is no literature describing the use of a systemic xenograft model of $CD1d^+$ B cell lymphoma. A number of studies addressed the CD1d-mediated anti-lymphoma activity of iNKT cells only in orthotopic murine systems, mainly due to the poorer persistence of human iNKT compared to conventional T lymphocytes in mouse xenografts[218,250,252-257].

The C1R-CD1d cell line has been largely employed in functional studies involving iNKT cells[218,270-273]. On this basis, C1R-CD1d cells served as targets for part of my *in vitro* cytotoxicity tests. Bagnara et al. first reported on the feasibility of an *in vivo* assay based on human C1R-CD1d engrafted mice to evaluate the therapeutic efficacy of adoptively transferred human iNKT cells[251]. Hence, having successfully engineered C1R-CD1d cells to express firefly luciferase, I established a novel C1R-CD1d xenograft model. Importantly, while Bagnara et al. used the NOD/scid strain and induced subcutaneous disease, I chose NSG mice and iv tumour injections. Compared to NOD/scid, in NSG mice the innate immunity is more severely compromised, with complete lack of NK cells, associated with defective DC and macrophages as well as absent mature B and T cells[274,275]. Therefore, the risk of observing spontaneous tumour remissions due

to residual host immunity is virtually eliminated. In addition, by using the iv route, I could establish a clinically more relevant model of systemic disease. A first set of titration experiments confirmed that administration of 1-5 x10^6 cells, i.e., the same dose used by Bagnara et al., was well tolerated upon iv injection and was appropriate to ensure engraftment in multiple body segments, with diffuse active photon signal in the head, chest, abdomen and limbs areas.

For CAR19-iNKT cell adoptive transfer, I chose to test 2nd generation CAR-engineered cells with a schedule of 10 x10^6 cells per mouse in a single infusion without adjuvant therapies, namely αGalCer and IL-2. This scheme was purposely aimed to validate the fitness and efficacy of my CAR19-iNKT product in a '*stress-test*'-like setting for iNKT cells, using lower cell doses than those effective in xenograft models[251], while being suitable for simultaneous comparison with conventional CAR19-T cells. With respect to the anticipated response in a hypothetical iNKT cell scenario, Bagnara et al. observed a reduction of C1R-CD1d masses in their model only after using repeated iv infusions of 2×10^7 iNKT cells in combination with αGalCer[251]. Schedules based on fewer effectors or single administrations were generally ineffective or led to only transient reduction of low-burden nodules (1 x10^6 C1R-CD1d cells) for about 48-72h prior to rebound tumour progression[251]. Therefore, a better disease control in my model would indirectly suggest a superior anti-lymphoma activity of my CAR19-engineered compared to unmodified iNKT cells. Notably, the Metelitsa group reported that the therapeutic activity of their CAR-iNKT product at the dose of 1x10^7 cells required weekly iv infusions or adjuvant IL-2 every 3 days[48,49]. In addition, such schedule seemed to effectively prolong survival of cancer-bearing xenografts treated with 3rd generation but not 2nd generation CAR-engineered iNKT cells. Finally, the surprisingly limited success of their CAR-iNKT immunotherapy was reported in the context of a humanized model where, owing to iNKT cell regulatory and trans-activating functions, the co-existing human immune cells would be expected to amplify the CAR-iNKT cells anti-tumour activity[48]. Hence, a better outcome in my model would be also suggestive of improved fitness and superiority of my CAR19-iNKT cell product over the only other one available in the literature.

In relation to the comparison with CAR19-T cells, my model was suitable for a fair side-by-side assessment. First, since the best clinical results have been achieved in CAR-T trials using 2nd generation configurations and AICD may undermine the long-term performance of 3rd generation CAR-T[41] but not CAR-iNKT cells, I focused on 2nd generation CAR19-engineered cells. In addition, CD28-based CAR constructs have been successfully used to engineer iNKT and T cells. Specifically, one of the only two FDA-approved CAR19-T products is CD28-based (Yescarta) and CAR-iNKT cells carrying diverse 2nd generation configurations did not exhibit any major functional disparity[48], thus CD28 resulting appropriate for both effectors.
Second, proof-of-principle studies often employed single infusions of $1x10^{7}$[261,276] (and sometimes higher doses[277,278] of) CAR-T cells to investigate their therapeutic activity at their maximum potential.

With respect to the matter of xenogeneic GvHD (xeno-GvHD), the estimated risk associated with the use of T and CAR19-T cells in my model was minimum, with no concerns about bias that could potentially influence the experimental outcome. Xeno-GvHD is generally associated with slow tumour models. The longer the survival of tumour-only control mice, the longer the follow-up required to observe a survival advantage in the treated group. C1R-CD1d engrafted animals exhibited a tumour growth rate similar to Raji and Daudi B cells models, with an anticipated period of observation of 2-3 months[49,260,279]. Some authors described the occurrence of xeno-GvHD in NSG mice as early as 50-55 days after engraftment of CAR-T cells, with an average of 79 days[280]. As a result, the affected mice had to be culled in partial/complete disease remission because of the onset of xeno-GvHD symptoms, i.e., too early to confirm a tumour-free survival advantage compared to tumour-bearing control-only animals. However, those cases were reported in association with CAR-T cell doses as high as $2x10^{7}$ cells or more and *in vitro* culture with IL-7 and IL-15 but not IL-15 alone[280]. By contrast, I planned to infuse lower CAR-cell doses, manufactured with IL-15 only. Furthermore, given that iNKT cells do not incite xenoreactivity, there was actually the opposite risk, if any, that the CAR19-T cell bias could play 'against' CAR19-iNKT cells and generate artifactually better outcomes in favour of CAR-T immunotherapy.

Indeed, in all my three experiments I observed signs of xenoreactivity in CAR19-T but not CAR19-iNKT recipients, consisting of very well-defined, coin-like alopecia lesions on the face (**Figure 6-14**) and dorsum, with intact skin and no associated BLI signal. However, no mouse developed GvHD syndrome, as defined by more than 10% loss of weight and any degree of hunching, hypoactivity, ruffled fur and scaling skin that could not be attributed to tumour progression[263]. Eventually, all animals that received immunotherapy were evaluable for analysis at the end of the study.

Primary endpoints were overall survival and tumour-free survival. In concordance with the *in vitro* findings, my *in vivo* model of $CD1d^{+}CD19^{+}$ B lineage malignancy demonstrated the enhanced anti-tumour effect of CAR19-iNKT over CAR-T cells in terms of both overall and tumour-free survival. To my knowledge, this is the first time that human iNKT cell-based adoptive cell therapy results to be superior to T cell-based strategy in a xenograft model. This is likely to be due to the significantly more robust anti-tumour effect of CAR19-iNKT cells in the first few days post-immunotherapy and was perhaps a reflection of both the combined iTCR/CAR19-mediated cytotoxicity and the inherent innate-like reactivity of iNKT lymphocytes, which act to orchestrate emerging immune responses well before conventional T cells[281]. Of note, in line with this, Bagnara et al. demonstrated a reduction in the size of C1R-CD1d-derived tumours within 48-72 hour after iNKT cell transfer[251]. Likewise, Heczey et al. found that in CAR-iNKT treated-xenografts clinical responses were associated with early cytokine release by CAR-iNKT cells *in vivo*[48], suggesting that the iNKT cell platform has indeed the potential for a swift reactivity that is highly predictive of positive outcome. Notably, the ability to clear the malignant cells early after CAR-immunotherapy, without requiring long-term persistence of CAR-cell effectors, has been identified as a key determinant of complete disease eradication and prevention of antigen negative relapses[41].

Finally, CAR19-iNKT cells likely effectively eliminate brain and relapsed lymphoma. Again, this represents the first pre-clinical evidence of a CAR-based approach controlling brain lymphomas, which complicate the course of up to 10% NHL patients[282] and make up 3% of primary CNS neoplasms[283], thus being an unmet challenge in B cell malignancies. While CAR-T cells failed to control brain disease, which caused death in a number of CAR19-T treated

animals, in CAR19-iNKT cell recipients an almost uniform eradication of brain lymphoma was seen with no residual neurotoxicity, consistent with the ability of CAR-iNKT cells to safely cross the blood-brain barrier. Furthermore, only CAR19-NKT recipients experienced regression until complete remission of relapsed brain disease, suggesting long-term persistence of functional CAR19-iNKT cells.

One argument against the hypothesis that CAR19-iNKT cells can control better brain disease could be that I have never demonstrated the presence of CAR19-iNKT cells *in vivo*.
In my model, BLI monitoring was used to follow tumour growth. Flow cytometry and histological analysis were performed only at humane endpoints or at the end of the experiment to confirm the cause of death and the tumour phenotype. As such, I could confirm the presence of human $CD19^+$ ($hCD19^+$) cells in all tumour-only, T- and iNKT- treated animals. The group of CAR19-T recipients that died with active progressive BLI signal, yielded $hCD19^+$ cells by both methods and in a fraction I could demonstrate the presence of human $CD3^+$ ($hCD3^+$), i.e., CAR19-T cells, in brain tissue sections by IHC. Interestingly, $hCD3^+$ cells had a characteristic 'inter-follicular' pattern, reminiscent of that of exhausted T cells unable to infiltrate into foci of lymphoma B cells[284]. By contrast, most CAR19-iNKT mice were culled at the end of the planned 90-days monitoring in complete remission. The very few animals showing signs of lymphoma at their last follow-up resulted consistently $hCD19^+$ but $hCD3^-$ upon flow cytometry/IHC assessment. One explanation could be that these animals reflected cases where CAR19-iNKT cells failed to engraft/persist and therefore could not be detected. On the other hand, it cannot be excluded that the therapeutic efficacy of CAR19-iNKT cells was independent on their long-term persistence in tumour-engrafted animals and was rather determined by early clearance of all malignant cells upon immunotherapy. On this assumption, no $hCD3^+$ cells could be detected in any CAR19-iNKT cell recipient and the mice that died reflected the cases of animals with incomplete eradication *ab initio*. Such hypothesis would be also supported by observations in CAR19-T trials where patients in complete remission maintain long-term responses, compatible with cure, irrespective of the lack of detectable CAR19-T cells relatively early after immunotherapy, associated with parallel recovery of normal but not malignant B cells[285-287 39,288].

Yet, this would not explain the 2nd remission after late relapses. In this regard, it is unlikely that disease elimination could be attributed to spontaneous tumour regression. None of the 18 tumour-only control mice, including 3 animals engrafted with lower C1R-CD1d cell numbers in the first pilot experiment, exhibited reduction/loss of photon signal throughout the experiment. Similarly, an equal number of CAR19-T animals developed late relapses at the same time of CAR19-iNKT cell-treated mice, but none of them achieved a second remission. Those CAR19-T animals died early after relapse and cyto/histological analysis confirmed the presence of $CD19^+$ cells. By contrast, CAR19-iNKT did not undergo extensive cyto/histological assessment early after relapse due to achievement of second remission within two weeks, a timeframe similar to that of the first remissions. Moreover, by the end of the 90-days monitoring there were no signs of active disease by BLI.

Although it remains to be formally demonstrated, it is conceivable that CAR19-iNKT cells directly drove those relapsed mice into remission. Specifically, it can be hypothesized that few residual C1R-CD1d cells survived to the first CAR19-iNKT cell attack and were responsible for the late clinical relapse. On the other hand, few reactive CAR-iNKT cells persisted and when the stimulator-to-responder ratio *in vivo* became 'effective', CAR19-iNKT cells activation and expansion led to an effector-to-target ratio capable to control disease till eradication. In fact, this is what has been observed in patients who developed the deepest and more sustained responses in CAR19-T trials. Moreover, the ability to patrol the tumour site and prevent or control clinical relapses, even in the absence of first complete elimination of cancer cells, have been regarded as one of the key for successful outcome of CAR-immunotherapy.

Finally, it cannot be rule out the possibility of organ segregation and lack of CAR19-iNKT cell detection due to tissue sampling. Of note, in keeping with all the above, Bagnara et al. could never demonstrate the presence of iNKT cells in C1R-CD1d-free mice culled at the end of their experiments[251].

7 Conclusions & Perspectives

Chimeric antigen receptor T cell immunotherapy has dramatically changed the therapeutic prospects for B cell malignancies[17]. Over the last decade, CD19-redirected T lymphocytes have been proven to have the ability to induce deep, long-lasting remissions and possibly cure in patients with acute and chronic B cell neoplasms where all previous lines of treatment had failed[26-39]. Such impressive results led to the first approvals for autologous CAR19-engineered T cell products[193,289] and also fostered efforts to even extend the CAR technology to other incurable malignancies[46,290]. However, definite progress has been hampered by the high rate of lack of efficacy[233] and disease relapse[40,41], including CD19-negative relapses[234], as well as severe, life-threatening toxicity, mainly cytokine release syndrome and neurotoxicity[54,58-70]. In refractory patients, active disease may also negatively impact on the ability to manufacture CAR-T cells in a timely manner, while in the case of disease remission, autologous T cells may be defective and not compatible with the generation of fully functional CAR-cell products as a result of previous lines of treatment[41]. In an effort to improve efficacy and versatility of the CAR technology, allogeneic T lymphocytes have been regarded as a suitable alternative to patients' own cells, although the risk of aGvHD remains a main concern and, together with important logistical difficulties, represents the main limitation to widespread application[41]. Finally, long-term financial sustainability may put at risk the future of CAR-T therapies, thus emphasizing the need for cheaper platforms[41].

For all the above reasons, iNKT cells represent an attractive, promising alternative to conventional T cells in cancer immunotherapy. Importantly, their direct and indirect anti-tumour activity[92,103-113] as well as potential for universal use[144,147,148], combined with the feasibility of *in vitro* and *in vivo* manipulation by means of an iNKT-specific MoAb (6B11) and agonist (αGalCer)[106,114-121,168], suggest that they can be exploited to develop a more effective CAR-immunotherapy. Central to iNKT cell biology is their restriction by the non-polymorphic HLA I-like molecule CD1d, which is mainly expressed on antigen presenting cells, including normal B cells and their $CD19^{+}$ malignant counterparts[127-131]. Therefore, I hypothesized that equipping iNKT cells with a CAR19 would potentially achieve dual targeting of CD1d and CD19

on the same clonal cells by the endogenous iTCR and the CAR19 respectively, thus enhancing the overall anti-lymphoma effect.

Previous studies demonstrated the feasibility of CAR-engineering of iNKT cells and their pre-clinical activity against neuroblastoma[48] and $CD1d^{-}CD19^{+}$ B cell lymphoma cell lines[49]. Yet, successful manufacturing of CAR-iNKT cells remains a relatively recent achievement and limited to the expertise of a single group, with a dearth of information about how best to manufacture CAR-iNKT cells. In addition, CAR-iNKT cells have not been tested against patient-derived lymphoma cells and there are no data generated from direct comparative analysis of CAR-T and CAR-iNKT cells.

Thus, during my PhD work, I aimed to develop and optimise a protocol to manufacture clinical scale CAR19-iNKT cells and test the hypothesis that CAR19-engineered iNKT cells may deliver a more effective immunotherapy than conventional T effectors in $CD1d^{+}$ B cell malignancies.

First, by testing five different protocols (and relative variants) through meticulous step-by-step optimization, I found that upfront selection followed by lentiviral CAR19 transduction of CD3/CD28-activated iNKT cells, in the presence of IL-15 and autologous irradiated PBMCs, consistently generates highly transduced CAR19-iNKT cells. Such procedure is substantially different from the only other one available in the literature, it is more efficient, versatile and cost-effective and suitable for fresh and frozen materials, equally derived from healthy donors and cancer patients, in remission as well as with active disease. Importantly, as low as 1,000 starting iNKT cells are sufficient to ensure large scale numbers of pure CAR19-iNKT cells in a relatively short time of *ex vivo* manipulation, while offering the opportunity to dramatically cut the costs related to the manufacturing reagents. Further *in vitro* validation highlighted 4 distinctive features of my CAR19-iNKT cell product: 1) excellent expandability, greater than conventional CAR19-T, predictive of higher therapeutic efficacy in relation to the more pronounced and sustained proliferative response to target cells; 2) preservation of the $CD4^{-}$ fraction, which, compared to $CD4^{+}$ iNKT cells, displays a more polarized Th1 cytokine profile; 3) more robust cytotoxic potential than same-donor CAR19-T cells on the basis of the production of larger amounts of toxic granules and interferon-γ and the presence of a significantly higher

proportion of polyfunctional effectors cells; 4) resistance to immune cell exhaustion upon repeated stimulation and exposure to cancer targets.

Next, I functionally characterized and *in vitro* validated my CAR19-iNKT effectors by testing their cytotoxic activity against an array of cancer cell targets expressing different combinations of CD1d and CAR19. By using the non-lymphoid $CD1d^{-}CD19^{-}$ K562 cells engineered to express CD1d and CD19 singly or in combination, I found that the iTCR and CAR19 are both functional and mediate co-operative killing by CAR19-engineereed iNKT cells, thus demonstrating that CAR19-iNKT are dual specific, they are capable of killing single positive $CD1d^{+}CD19^{-}$ and $CD1d^{-}$ $CD19^{+}$ targets and more effectively $CD1d^{+}CD19^{+}$ co-expressing cancer cells, and their cytotoxic activity is further enhanced by their glycolipid ligand αGalCer against $CD1d^{+}$ targets. When tested against B cell lineage targets displaying different levels of CD1d and CD19 antigens, I demonstrated that CAR19-iNKT cell cytotoxicity correlates with the antigen density and is potentiated in association with higher exogenous expression compared to constitutive lower levels of CD1d and/or CD19. Side-by-side comparison with same-donor CAR19-T cells showed that CAR19-iNKT cells kill more effectively $CD1d^{+}$ B cell lymphoma cell lines. Subsequent dissection by conjugate analysis and assessment of long-term killing activity coupled with proliferative response to cancer cells, suggested that CAR19-iNKT cell superior cytotoxicity is underpinned by faster reactivity, minimal susceptibility to AICD and striking proliferation upon target engagement, particularly for 3^{rd} generation CAR19-iNKT, with a unique potential for complete disease eradication. Finally, evaluation against primary $CD1d^{+}CD19^{+}$ malignant cells from patients with relapsed, refractory MCL and MZL, confirmed that dual specific targeting of lymphoma cells by CAR19-iNKT effectors can lead to better outcome than conventional CAR19-T immunotherapy, even in the absence of iNKT-specific agonists, with low risk of on-target, off-tumour toxicity as suggested by the lack of specific cell death within autologous patients' monocytes.

I then explored the feasibility of combinatorial approaches that would allow to further enhance the anti-lymphoma activity against difficult-to-treat diseases, and possibly exploit the anti-tumour potential of CAR-iNKT cells against $CD1d^{low}$ and $CD1d^{-}$ disorders, by using primary B CLL cells, which express constitutively low or no CD1d relative to normal as well as MCL and MZL

malignant cells. Importantly, I confirmed that CAR19-iNKT cells can effectively kill B CLL cells, with further enhancement in the presence of αGalCer, and transcriptional modulation of CD1d by clinically relevant doses of ATRA, which are widely used for treatment of other blood cancers and solid tumours, such as APL and poor-prognosis neuroblastoma, led to additional, CD1d-driven improvement of CAR19-iNKT but not CAR19-T cell cytotoxicity against ATRA-treated CLL cells.

Finally, in a systemic *in vivo* model of $CD1d^{+}CD19^{+}$ B cell malignancy, a single infusion of CAR19-iNKT cells, without any adjuvant treatment, was associated with significantly improved overall and tumour-free survival of lymphoma-bearing mice and better overall outcome compared to CAR19-T treated animals. That could be at least in part explained by a swifter and more robust reactivity of CAR19-iNKT cell *in vivo*, with subsequent complete disease eradication early upon infusion. Remarkably, control of brain tumour and induction of second complete remissions without any residual neurotoxicity was only observed in CAR19-iNKT cell-treated animals. This would be consistent with CAR19-iNKT cells having the capacity to effectively cross the blood-brain barrier, co-existing with a potentially safe profile and the propensity to persist and resist immune exhaustion to a greater extent than conventional T cells, all features of high clinical value for the development of effective immunotherapy of brain lymphoma and other brain cancers.

To conclude, my PhD work has generated some new piece of evidence relevant to the field of cancer immunotherapy. In the future, my results might have important implications.

First, the demonstration for the first time of the superiority of CAR19-iNKT over CAR19-T cells against CD1d+ B malignancies, together with the confirmation of the feasibility of iNKT cells engineering, lay the foundations for further clinical translation and investigation in clinical trials.

Second, similar manufacturing processes, while allowing to work with more 'homogeneous' T cell populations and improve the unpredictable outcomes associated with heterogeneous bulk T populations, might be in principle applied to successfully manipulate other rare T cell subsets with different biological properties.

Third, employment of iNKT cells would be associated with the almost unique opportunity for a more versatile, off-the-shelf and ready-to-use reagent, since unlike conventional allogeneic T lymphocytes, allogeneic iNKT cells protect from aGVHD, thus being suitable for manufacturing from third-party, universal healthy donors.

Fourth, the inherent iNKT cell regulatory properties and innate-like reactivity suggest that lower cell doses might be required than those currently infused in CAR-T trials, resulting in a more sustainable technology in a long-term.

Finally, molecular dissection of CD1d regulation gives hope for combinatorial strategies with transcriptional and possibly epigenetic treatments that may allow surface CD1d restoration in CD1d-negative diseases, thus broadening the landscape of potential disorders that might benefit from a CAR-iNKT based immunotherapy. Similar mechanistic approaches may provide new insights to '*on demand switch-on/switch-off*' relevant target antigens, without the need of extra genetic manipulation, thus opening up to novel, exciting avenues for seriously ill patients.

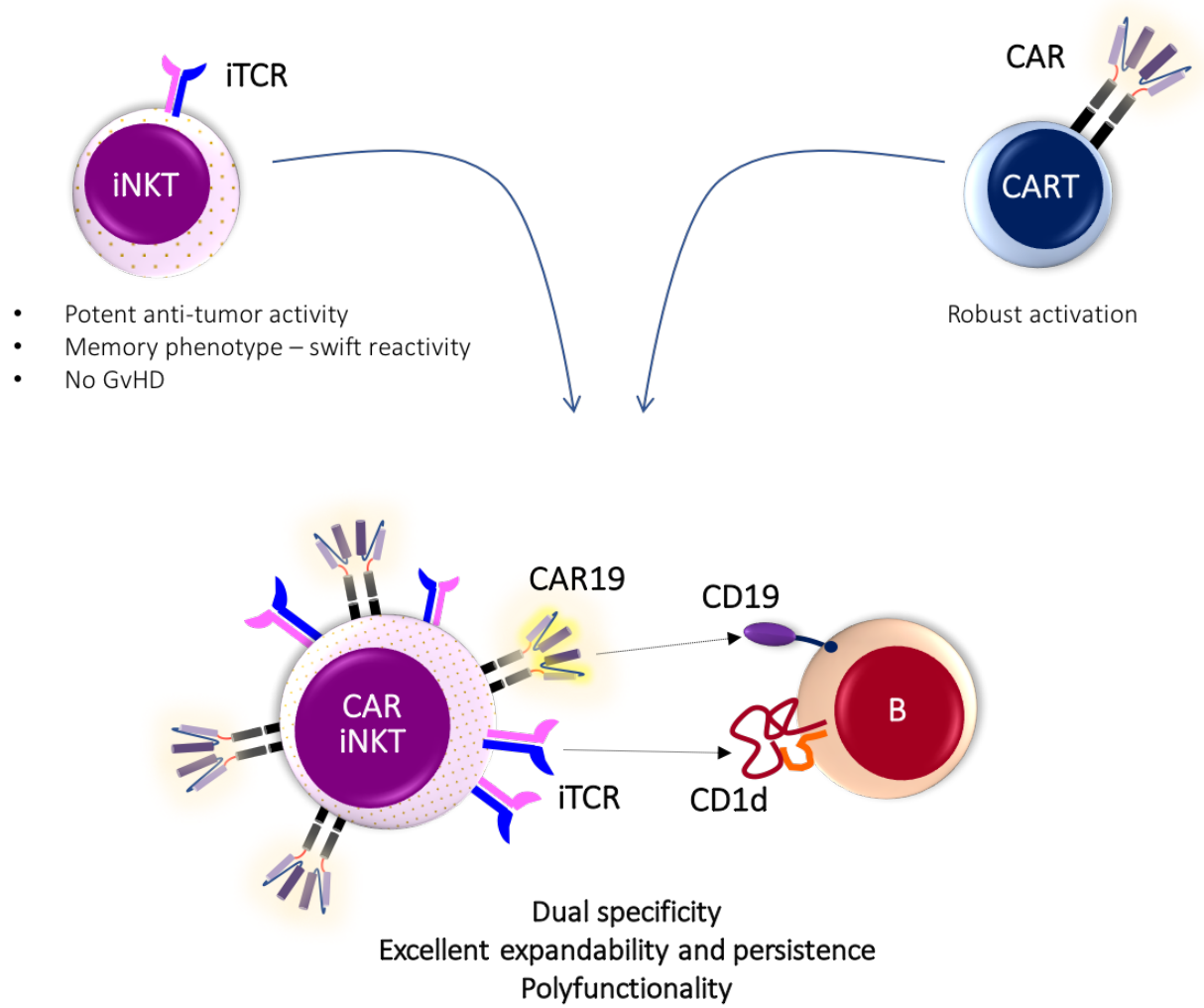


Figure 7-1 CAR19-iNKT cell overview

8 References

1. (IARC), G. United Kindom, All cancers excluded non-melanoma skin cancer, Number of new cancers in 2015 (all ages, both sexes). (2018).
2. (IARC), G. World, Non-Hodgkin lymphoma, Number of new cancers in 2015 (all ages, both sexes). (2018).
3. GLOBOSCAN2012(IARC). World, Multiple Myeloma, Number of cancer deaths in 2015. (2015).
4. (IARC), G. World, Non-Hodgkin lymphoma, Incidence map (ASR, both sexes). (2018).
5. (IARC), G. World, Non-Hodgkin lymphoma, Number of cancer deaths in 2020 (all ages, both sexes). (2018).
6. Harris, N.L.*, et al.* New approaches to lymphoma diagnosis. *Hematology / the Education Program of the American Society of Hematology. American Society of Hematology. Education Program*, 194-220 (2001).
7. Perez-Galan, P., Dreyling, M. & Wiestner, A. Mantle cell lymphoma: biology, pathogenesis, and the molecular basis of treatment in the genomic era. *Blood* **117**, 26-38 (2011).
8. Epperla, N., Hamadani, M., Fenske, T.S. & Costa, L.J. Incidence and survival trends in mantle cell lymphoma. *British journal of haematology*, n/a-n/a.
9. Jaffe, E.S., Harris, N.L., Stein, H. & Vardiman, J.W. *WHO Classification of Tumours of Haematopoietic and Lymphoid Tissues*, (IARC, Lyon, 2017).
10. Noy, A.*, et al.* Targeting Bruton tyrosine kinase with ibrutinib in relapsed/refractory marginal zone lymphoma. *Blood* **129**, 2224-2232 (2017).
11. Zinzani, P.L. The many faces of marginal zone lymphoma. *ASH Education Program Book* **2012**, 426-432 (2012).
12. **http://seer.cancer.gov/statfacts/html/clyl.html** (accessed September 2016).
13. Dreger, P.*, et al.* Indications for allogeneic stem cell transplantation in chronic lymphocytic leukemia: the EBMT transplant consensus. *Leukemia* **21**, 12-17 (2006).
14. Furman , R.R.*, et al.* Idelalisib and Rituximab in Relapsed Chronic Lymphocytic Leukemia. *New England Journal of Medicine* **370**, 997-1007 (2014).
15. Burger, J.A.*, et al.* Ibrutinib as Initial Therapy for Patients with Chronic Lymphocytic Leukemia. *New England Journal of Medicine* **373**, 2425-2437 (2015).
16. Wang, M.L.*, et al.* Targeting BTK with ibrutinib in relapsed or refractory mantle-cell lymphoma. *The New England journal of medicine* **369**, 507-516 (2013).
17. Ruella, M. & June, C.H. Chimeric Antigen Receptor T cells for B Cell Neoplasms: Choose the Right CAR for You. *Curr Hematol Malig Rep* (2016).
18. Gross, G., Waks, T. & Eshhar, Z. Expression of immunoglobulin-T-cell receptor chimeric molecules as functional receptors with antibody-type specificity. *Proceedings of the National Academy of Sciences of the United States of America* **86**, 10024-10028 (1989).
19. Kuwana, Y.*, et al.* Expression of chimeric receptor composed of immunoglobulin-derived V regions and T-cell receptor-derived C regions. *Biochemical and biophysical research communications* **149**, 960-968 (1987).

20. Lim, W.A. & June, C.H. The Principles of Engineering Immune Cells to Treat Cancer. *Cell* **168**, 724-740 (2017).
21. Barrett, D.M., Singh, N., Porter, D.L., Grupp, S.A. & June, C.H. Chimeric antigen receptor therapy for cancer. *Annual review of medicine* **65**, 333-347 (2014).
22. Hege, K.M.*, et al.* Safety, tumor trafficking and immunogenicity of chimeric antigen receptor (CAR)-T cells specific for TAG-72 in colorectal cancer. *Journal for ImmunoTherapy of Cancer* **5**, 22 (2017).
23. Lamers, C.H.J.*, et al.* Treatment of Metastatic Renal Cell Carcinoma With Autologous T-Lymphocytes Genetically Retargeted Against Carbonic Anhydrase IX: First Clinical Experience. *Journal of Clinical Oncology* **24**, e20-e22 (2006).
24. Kochenderfer, J.N., Wilson, W.H. & Janik, J.E. Eradication of B-lineage cells and regression of lymphoma in a patient treated with autologous T cells genetically engineered to recognize CD19. *Blood* **116**, 4099-4102 (2010).
25. Kochenderfer, J.N., Dudley, M.E. & Feldman, S.A. B-cell depletion and remissions of malignancy along with cytokine-associated toxicity in a clinical trial of anti-CD19 chimeric-antigen-receptor-transduced T cells. *Blood* **119**, 2709-2720 (2012).
26. Brentjens, R.J.*, et al.* CD19-targeted T cells rapidly induce molecular remissions in adults with chemotherapy-refractory acute lymphoblastic leukemia. *Sci Transl Med* **5**, 177ra138 (2013).
27. Maude, S.L.*, et al.* Chimeric antigen receptor T cells for sustained remissions in leukemia. *The New England journal of medicine* **371**(2014).
28. Brudno, J.N.*, et al.* Allogeneic T Cells That Express an Anti-CD19 Chimeric Antigen Receptor Induce Remissions of B-Cell Malignancies That Progress After Allogeneic Hematopoietic Stem-Cell Transplantation Without Causing Graft-Versus-Host Disease. *Journal of Clinical Oncology* **34**, 1112-1121 (2016).
29. Lee, D.W.*, et al.* T cells expressing CD19 chimeric antigen receptors for acute lymphoblastic leukaemia in children and young adults: a phase 1 dose-escalation trial. *The Lancet* **385**, 517-528.
30. Turtle, C.J.*, et al.* CD19 CAR-T cells of defined CD4+:CD8+ composition in adult B cell ALL patients. *The Journal of clinical investigation* **126**, 2123-2138 (2016).
31. Grupp, S.A.*, et al.* Chimeric antigen receptor-modified T cells for acute lymphoid leukemia. *New England Journal of Medicine* **368**, 1509-1518 (2013).
32. Maude, S.L.*, et al.* Tisagenlecleucel in Children and Young Adults with B-Cell Lymphoblastic Leukemia. *The New England journal of medicine* **378**, 439-448 (2018).
33. Park, J.H.*, et al.* Long-Term Follow-up of CD19 CAR Therapy in Acute Lymphoblastic Leukemia. *The New England journal of medicine* **378**, 449-459 (2018).
34. Porter, D.L.*, et al.* Chimeric antigen receptor T cells persist and induce sustained remissions in relapsed refractory chronic lymphocytic leukemia. *Science Translational Medicine* **7**, 303ra139-303ra139 (2015).
35. Neelapu, S.S.*, et al.* A Phase 2 Multicenter Trial of KTE-C19 (anti-CD19 CAR T Cells) in Patients With Chemorefractory Primary Mediastinal B-Cell Lymphoma (PMBCL) and Transformed Follicular Lymphoma (TFL): Interim Results From ZUMA-1. *Blood* **128**, 998 (2016).
36. Locke, F.L.*, et al.* Phase 1 Results of ZUMA-1: A Multicenter Study of KTE-C19 Anti-CD19 CAR T Cell Therapy in Refractory Aggressive Lymphoma. *Molecular Therapy* **25**, 285-295 (2017).

37. Kochenderfer, J.N., *et al.* Chemotherapy-Refractory Diffuse Large B-Cell Lymphoma and Indolent B-Cell Malignancies Can Be Effectively Treated With Autologous T Cells Expressing an Anti-CD19 Chimeric Antigen Receptor. *J Clin Oncol* (2014).
38. Neelapu, S.S., *et al.* Axicabtagene Ciloleucel CAR T-Cell Therapy in Refractory Large B-Cell Lymphoma. *N Engl J Med* **377**, 2531-2544 (2017).
39. Schuster, S.J., *et al.* Chimeric Antigen Receptor T Cells in Refractory B-Cell Lymphomas. *The New England journal of medicine* **377**, 2545-2554 (2017).
40. Turtle, C.J., *et al.* Immunotherapy of non-Hodgkin's lymphoma with a defined ratio of CD8+ and CD4+ CD19-specific chimeric antigen receptor-modified T cells. *Science translational medicine* **8**(2016).
41. Brudno, J.N. & Kochenderfer, J.N. Chimeric antigen receptor T-cell therapies for lymphoma. *Nature Reviews Clinical Oncology* **15**, 31 (2017).
42. Wang, X., *et al.* Phase 1 studies of central memory–derived CD19 CAR T–cell therapy following autologous HSCT in patients with B-cell NHL. *Blood* **127**, 2980-2990 (2016).
43. Till, B.G., *et al.* CD20-specific adoptive immunotherapy for lymphoma using a chimeric antigen receptor with both CD28 and 4-1BB domains: pilot clinical trial results. *Blood* **119**(2012).
44. Sadelain, M., Riviere, I. & Riddell, S. Therapeutic T cell engineering. *Nature* **545**, 423-431 (2017).
45. Ruella, M., *et al.* Overcoming the Immunosuppressive Tumor Microenvironment of Hodgkin Lymphoma Using Chimeric Antigen Receptor T Cells. *Cancer discovery* (2017).
46. Rotolo, A., Karadimitris, A. & Ruella, M. Building upon the success of CART19: chimeric antigen receptor T cells for hematologic malignancies. *Leukemia & lymphoma*, 1-16 (2017).
47. Eyquem, J., *et al.* Targeting a CAR to the TRAC locus with CRISPR/Cas9 enhances tumour rejection. *Nature* **543**, 113-117 (2017).
48. Heczey, A., *et al.* Invariant NKT cells with chimeric antigen receptor provide a novel platform for safe and effective cancer immunotherapy. *Blood* **124**, 2824-2833 (2014).
49. Tian, G., *et al.* CD62L+ NKT cells have prolonged persistence and antitumor activity in vivo. *The Journal of clinical investigation* **126**, 2341-2355 (2016).
50. Capsomidis, A., *et al.* Chimeric Antigen Receptor-Engineered Human Gamma Delta T Cells: Enhanced Cytotoxicity with Retention of Cross Presentation. *Molecular therapy : the journal of the American Society of Gene Therapy* **26**, 354-365 (2018).
51. Turtle, C.J., *et al.* CD19 CAR-T cells of defined CD4+:CD8+ composition in adult B cell ALL patients. *The Journal of clinical investigation* **126**(2016).
52. Tran, E., Longo, D.L. & Urba, W.J. A Milestone for CAR T Cells. *New England Journal of Medicine* **377**, 2593-2596 (2017).
53. Scholler, J., *et al.* Decade-long safety and function of retroviral-modified chimeric antigen receptor T cells. *Science translational medicine* **4**(2012).
54. Lee, D.W., Gardner, R. & Porter, D.L. Current concepts in the diagnosis and management of cytokine release syndrome. *Blood* **124**, 188-195 (2014).
55. Maude, S.L., Frey, N. & Shaw, P.A. Chimeric antigen receptor T cells for sustained remissions in leukemia. *The New England journal of medicine* **371**, 1507-1517 (2014).
56. Davila, M.L., Riviere, I. & Wang, X. Efficacy and toxicity management of 19-28z CAR T cell therapy in B cell acute lymphoblastic leukemia. *Science translational medicine* **6**, 224ra225 (2014).

57. Maude, S.L., Barrett, D., Teachey, D.T. & Grupp, S.A. Managing cytokine release syndrome associated with novel T cell-engaging therapies. *Cancer J* **20**, 119-122 (2014).
58. Topp, M.S*., et al.* Safety and activity of blinatumomab for adult patients with relapsed or refractory B-precursor acute lymphoblastic leukaemia: a multicentre, single-arm, phase 2 study. *The Lancet. Oncology* **16**(2015).
59. Wu, J., Fu, J., Zhang, M. & Liu, D. Blinatumomab: a bispecific T cell engager (BiTE) antibody against CD19/CD3 for refractory acute lymphoid leukemia. *Journal of hematology & oncology* **8**(2015).
60. Fan, G., Wang, Z., Hao, M. & Li, J. Bispecific antibodies and their applications. *Journal of hematology & oncology* **8**(2015).
61. Wang, Z., Guo, Y. & Han, W. Current status and perspectives of chimeric antigen receptor modified T cells for cancer treatment. *Protein & cell* **8**, 896-925 (2017).
62. Neelapu, S.S*., et al.* Axicabtagene Ciloleucel CAR T-Cell Therapy in Refractory Large B-Cell Lymphoma. *New England Journal of Medicine* **377**, 2531-2544 (2017).
63. Buechner, J*., et al.* Global registration trial of efficacy and safety of CTL019 in pediatric and young adult patients with relapsed/refractory (R/R) acute lymphoblastic leukemia (ALL): update to the interim analysis. *Clinical Lymphoma Myeloma Leuk* **17**(2017).
64. Gust, J*., et al.* Endothelial activation and blood-brain barrier disruption in neurotoxicity after adoptive immunotherapy with CD19 CAR-T cells. *Cancer discovery* **7**(2017).
65. Schuster, S.J*., et al.* Global pivotal phase 2 trial of the Cd19-targeted therapy Ctl019 in adult patients with relapsed or refractory (R/R) diffuse large B-cell lymphoma (Dlbcl)-an interim analysis. *Hematological oncology* **35**(2017).
66. Gardner, R.A*., et al.* Intent-to-treat leukemia remission by CD19 CAR T cells of defined formulation and dose in children and young adults. *Blood* **129**(2017).
67. Abramson, J.S*., et al.* High durable CR rates in relapsed/refractory (R/R) aggressive B-NHL treated with the CD19-directed CAR T cell product JCAR017 (TRANSCEND NHL 001): defined composition allows for dose-finding and definition of pivotal cohort. *Blood* **130**(2017).
68. Mei, H*., et al.* Neurological toxicities and coagulation disorders in the cytokine release syndrome during CAR-T therapy. *British journal of haematology* (2017).
69. Prudent, V. & Breitbart, W.S. Chimeric antigen receptor T-cell neuropsychiatric toxicity in acute lymphoblastic leukemia. *Palliat Support Care* **15**(2017).
70. Fry, T.J*., et al.* CD22-targeted CAR T cells induce remission in B-ALL that is naive or resistant to CD19-targeted CAR immunotherapy. *Nat Med* **24**, 20-28 (2018).
71. Wang, Z. & Han, W. Biomarkers of cytokine release syndrome and neurotoxicity related to CAR-T cell therapy. *Biomarker Research* **6**, 4 (2018).
72. Mackall, C.L. & Miklos, D.B. CNS endothelial cell activation emerges as a driver of CAR T cell-associated neurotoxicity. *Cancer discovery* **7**(2017).
73. Bonifant, C.L., Jackson, H.J., Brentjens, R.J. & Curran, K.J. Toxicity and management in CAR T-cell therapy. *Molecular therapy oncolytics* **3**, 16011 (2016).
74. Kochenderfer, J.N*., et al.* B-cell depletion and remissions of malignancy along with cytokine-associated toxicity in a clinical trial of anti-CD19 chimeric-antigen-receptor–transduced T cells. *Blood* **119**(2012).

75. Kochenderfer, J.N.*, et al.* Eradication of B-lineage cells and regression of lymphoma in a patient treated with autologous T cells genetically engineered to recognize CD19. *Blood* **116**, 4099-4102 (2010).
76. Di Stasi, A.*, et al.* Inducible apoptosis as a safety switch for adoptive cell therapy. *The New England journal of medicine* **365**(2011).
77. Greco, R.*, et al.* Improving the safety of cell therapy with the TK-suicide gene. *Frontiers in Pharmacology* **6**, 95 (2015).
78. Kenderian, S.S.*, et al.* CD33-specific chimeric antigen receptor T cells exhibit potent preclinical activity against human acute myeloid leukemia. *Leukemia* **29**, 1637-1647 (2015).
79. Johnson, L.A. & June, C.H. Driving gene-engineered T cell immunotherapy of cancer. *Cell Res* **27**, 38-58 (2017).
80. Sadelain, M., Rivière, I. & Riddell, S. Therapeutic T cell engineering. *Nature* **545**, 423-431 (2017).
81. Qasim, W.*, et al.* Molecular remission of infant B-ALL after infusion of universal TALEN gene-edited CAR T cells. *Sci Transl Med* **9**, pii: eaaj2013. (2017).
82. Sun, J.*, et al.* Early transduction produces highly functional chimeric antigen receptor-modified virus-specific T-cells with central memory markers: a Production Assistant for Cell Therapy (PACT) translational application. *J Immunother Cancer* **3**, 5 (2015).
83. Cruz, C.R., Micklethwaite, K.P. & Savoldo, B. Infusion of donor-derived CD19-redirected virus-specific T cells for B-cell malignancies relapsed after allogeneic stem cell transplant: a phase 1 study. *Blood* **122**, 2965-2973 (2013).
84. Poirot, L.*, et al.* Multiplex Genome-Edited T-cell Manufacturing Platform for "Off-the-Shelf" Adoptive T-cell Immunotherapies. *Cancer research* **75**, 3853-3864 (2015).
85. Wang, X.*, et al.* CMVpp65 Vaccine Enhances the Antitumor Efficacy of Adoptively Transferred CD19-Redirected CMV-Specific T Cells. *Clinical cancer research : an official journal of the American Association for Cancer Research* **21**, 2993-3002 (2015).
86. Gumperz, J.E., Miyake, S., Yamamura, T. & Brenner, M.B. Functionally distinct subsets of CD1d-restricted natural killer T cells revealed by CD1d tetramer staining. *J. Exp. Med.* **195**, 625-636 (2002).
87. Exley, M.A. Selective activation, expansion, and monitoring of human iNKT cells with a monoclonal antibody specific for the TCR α-chain CDR3 loop. *Eur. J. Immunol.* **38**, 1756-1766 (2008).
88. Exley, M.A., Wilson, B. & Balk, S.P. Isolation and functional use of human NKT cells. *Current protocols in immunology* **Chapter 14**, Unit 14.11 (2010).
89. Bendelac, A., Savage, P.B. & Teyton, L. The biology of NKT cells. *Annu. Rev. Immunol.* **25**, 297-336 (2007).
90. Matsuda, J.L.*, et al.* Tracking the response of natural killer T cells to a glycolipid antigen using CD1d tetramers. *The Journal of experimental medicine* **192**, 741-754 (2000).
91. Salio, M., Silk, J.D., Jones, E.Y. & Cerundolo, V. Biology of CD1- and MR1-restricted T cells. *Annu Rev Immunol* **32**, 323-366 (2014).
92. Exley, M.A.*, et al.* Developing understanding of the roles of CD1d-restricted T cell subsets in cancer: reversing tumor-induced defects. *Clinical immunology* **140**, 184-195 (2011).
93. Godfrey, D.I. & Kronenberg, M. Going both ways: immune regulation via CD1d-dependent NKT cells. *J. Clin. Invest.* **114**, 1379-1388 (2004).

94. Berzins, S.P., Smyth, M.J. & Baxter, A.G. Presumed guilty: natural killer T cell defects and human disease. *Nature Rev. Immunol.* **11**, 131-142 (2011).
95. Wang, X.*, et al.* Human invariant natural killer T cells acquire transient innate responsiveness via histone H4 acetylation induced by weak TCR stimulation. *The Journal of experimental medicine* **209**, 987-1000 (2012).
96. Lee, P.T., Benlagha, K., Teyton, L. & Bendelac, A. Distinct functional lineages of human V(alpha)24 natural killer T cells. *The Journal of experimental medicine* **195**, 637-641 (2002).
97. Takahashi, T.*, et al.* Cutting edge: analysis of human V alpha 24+CD8+ NK T cells activated by alpha-galactosylceramide-pulsed monocyte-derived dendritic cells. *Journal of immunology* **168**, 3140-3144 (2002).
98. O'Reilly, V.*, et al.* Distinct and overlapping effector functions of expanded human CD4+, CD8alpha+ and CD4-CD8alpha- invariant natural killer T cells. *PloS one* **6**, e28648 (2011).
99. Tahir, S.M. Loss of IFN-γ production by invariant NK T cells in advanced cancer. *J. Immunol.* **167**, 4046-4050 (2001).
100. Yanagisawa, K. Impaired proliferative response of Vα24 NKT cells from cancer patients against α-galactosylceramide. *J. Immunol.* **168**, 6494-6499 (2002).
101. Dhodapkar, M.V.*, et al.* A reversible defect in natural killer T cell function characterizes the progression of premalignant to malignant multiple myeloma. *The Journal of experimental medicine* **197**, 1667-1676 (2003).
102. Fujii, S.*, et al.* Severe and selective deficiency of interferon-gamma-producing invariant natural killer T cells in patients with myelodysplastic syndromes. *British journal of haematology* **122**, 617-622 (2003).
103. Molling, J.W.*, et al.* Peripheral blood IFN-gamma-secreting Valpha24+Vbeta11+ NKT cell numbers are decreased in cancer patients independent of tumor type or tumor load. *International journal of cancer. Journal international du cancer* **116**, 87-93 (2005).
104. Molling, J.W.*, et al.* Low levels of circulating invariant natural killer T cells predict poor clinical outcome in patients with head and neck squamous cell carcinoma. *Journal of clinical oncology : official journal of the American Society of Clinical Oncology* **25**, 862-868 (2007).
105. Schneiders, F.L. Clinical experience with α-galactosylceramide (KRN7000) in patients with advanced cancer and chronic hepatitis B/C infection. *Clin. Immunol.* **140**, 130-141 (2011).
106. Motohashi, S., Okamoto, Y., Yoshino, I. & Nakayama, T. Anti-tumor immune responses induced by iNKT cell-based immunotherapy for lung cancer and head and neck cancer. *Clinical immunology* **140**, 167-176 (2011).
107. Shaulov, A.*, et al.* Peripheral blood progenitor cell product contains Th1-biased noninvariant CD1d-reactive natural killer T cells: implications for posttransplant survival. *Experimental hematology* **36**, 464-472 (2008).
108. Cui, J.*, et al.* Requirement for Valpha14 NKT cells in IL-12-mediated rejection of tumors. *Science* **278**, 1623-1626 (1997).
109. Nakagawa, R.*, et al.* Treatment of hepatic metastasis of the colon26 adenocarcinoma with an alpha-galactosylceramide, KRN7000. *Cancer research* **58**, 1202-1207 (1998).
110. Toura, I.*, et al.* Cutting edge: inhibition of experimental tumor metastasis by dendritic cells pulsed with alpha-galactosylceramide. *Journal of immunology* **163**, 2387-2391 (1999).

111. Nishimura, T*., et al.* The interface between innate and acquired immunity: glycolipid antigen presentation by CD1d-expressing dendritic cells to NKT cells induces the differentiation of antigen-specific cytotoxic T lymphocytes. *International immunology* **12**, 987-994 (2000).
112. Kawano, T*., et al.* CD1d-restricted and TCR-mediated activation of valpha14 NKT cells by glycosylceramides. *Science* **278**, 1626-1629 (1997).
113. Nowak, M*., et al.* Defective NKT cell activation by CD1d+ TRAMP prostate tumor cells is corrected by interleukin-12 with alpha-galactosylceramide. *PloS one* **5**, e11311 (2010).
114. Giaccone, G. A phase I study of the natural killer T-cell ligand α-galactosylceramide (KRN7000) in patients with solid tumors. *Clin. Cancer Res.* **8**, 3702-3709 (2002).
115. Nicol, A.J., Tazbirkova, A. & Nieda, M. Comparison of clinical and immunological effects of intravenous and intradermal administration of alpha-galactosylceramide (KRN7000)-pulsed dendritic cells. *Clinical cancer research : an official journal of the American Association for Cancer Research* **17**, 5140-5151 (2011).
116. Richter, J*., et al.* Clinical regressions and broad immune activation following combination therapy targeting human NKT cells in myeloma. *Blood* **121**, 423-430 (2013).
117. Motohashi, S*., et al.* A phase I-II study of alpha-galactosylceramide-pulsed IL-2/GM-CSF-cultured peripheral blood mononuclear cells in patients with advanced and recurrent non-small cell lung cancer. *Journal of immunology* **182**, 2492-2501 (2009).
118. Schneiders, F.L*., et al.* Clinical experience with alpha-galactosylceramide (KRN7000) in patients with advanced cancer and chronic hepatitis B/C infection. *Clinical immunology* **140**, 130-141 (2011).
119. Chang, D.H*., et al.* Sustained expansion of NKT cells and antigen-specific T cells after injection of alpha-galactosyl-ceramide loaded mature dendritic cells in cancer patients. *The Journal of experimental medicine* **201**, 1503-1517 (2005).
120. Ishikawa, A*., et al.* A phase I study of alpha-galactosylceramide (KRN7000)-pulsed dendritic cells in patients with advanced and recurrent non-small cell lung cancer. *Clinical cancer research : an official journal of the American Association for Cancer Research* **11**, 1910-1917 (2005).
121. Nieda, M*., et al.* Therapeutic activation of Valpha24+Vbeta11+ NKT cells in human subjects results in highly coordinated secondary activation of acquired and innate immunity. *Blood* **103**, 383-389 (2004).
122. Kunii, N*., et al.* Combination therapy of in vitro-expanded natural killer T cells and alpha-galactosylceramide-pulsed antigen-presenting cells in patients with recurrent head and neck carcinoma. *Cancer science* **100**, 1092-1098 (2009).
123. Motohashi, S. A phase I study of in vitro expanded natural killer T cells in patients with advanced and recurrent non-small cell lung cancer. *Clin. Cancer Res.* **12**, 6079-6086 (2006).
124. Yamasaki, K*., et al.* Induction of NKT cell-specific immune responses in cancer tissues after NKT cell-targeted adoptive immunotherapy. *Clin Immunol* **138**, 255-265 (2011).
125. Exley, M.A*., et al.* Adoptive Transfer of Invariant NKT Cells as Immunotherapy for Advanced Melanoma: A Phase I Clinical Trial. *Clinical cancer research : an official journal of the American Association for Cancer Research* **23**, 3510-3519 (2017).
126. Exley, M.A., Balk, S.P. & Wilson, S.B. Isolation and functional use of human NK T cells. *Curr Protoc.Immunol* **Chapter 14**, Unit (2003).
127. Nickoloff, B.J., Wrone-Smith, T., Bonish, B. & Porcelli, S.A. Response of murine and normal human skin to injection of allogeneic blood-derived psoriatic immunocytes: detection of T cells

expressing receptors typically present on natural killer cells, including CD94, CD158, and CD161. *Archives of dermatology* **135**, 546-552 (1999).

128. Brigl, M. & Brenner, M.B. CD1: antigen presentation and T cell function. *Annu Rev Immunol* **22**, 817-890 (2004).
129. Kotsianidis, I.*, et al.* The diagnostic value of CD1d expression in a large cohort of patients with B-cell chronic lymphoproliferative disorders. *Am.J Clin Pathol.* **136**, 400-408 (2011).
130. Spanoudakis, E.*, et al.* Regulation of multiple myeloma survival and progression by CD1d. *Blood* **113**, 2498-2507 (2009).
131. Kotsianidis, I.*, et al.* The diagnostic value of CD1d expression in a large cohort of patients with B-cell chronic lymphoproliferative disorders. *American journal of clinical pathology* **136**, 400-408 (2011).
132. Fais, F.*, et al.* CD1d is expressed on B-chronic lymphocytic leukemia cells and mediates alpha-galactosylceramide presentation to natural killer T lymphocytes. *Int.J Cancer* **109**, 402-411 (2004).
133. Gorini, F.*, et al.* Invariant NKT cells contribute to chronic lymphocytic leukemia surveillance and prognosis. *Blood* **129**, 3440-3451 (2017).
134. Chen, Q.Y. & Jackson, N. Human CD1D gene has TATA boxless dual promoters: an SP1-binding element determines the function of the proximal promoter. *Journal of immunology* **172**, 5512-5521 (2004).
135. Yang, P.M., Lin, P.J. & Chen, C.C. CD1d induction in solid tumor cells by histone deacetylase inhibitors through inhibition of HDAC1/2 and activation of Sp1. *Epigenetics* **7**, 390-399 (2012).
136. Chen, Q.Y.*, et al.* Human CD1D gene expression is regulated by LEF-1 through distal promoter regulatory elements. *Journal of immunology* **184**, 5047-5054 (2010).
137. Chen, Q. & Ross, A.C. Retinoic acid regulates CD1d gene expression at the transcriptional level in human and rodent monocytic cells. *Experimental biology and medicine* **232**, 488-494 (2007).
138. Allan, L.L.*, et al.* CD1d and CD1c Expression in Human B Cells Is Regulated by Activation and Retinoic Acid Receptor Signaling. *The Journal of Immunology* **186**, 5261-5272 (2011).
139. Chung, B.K.*, et al.* Innate immune control of EBV-infected B cells by invariant natural killer T cells. *Blood* **122**, 2600-2608 (2013).
140. Szatmari, I.*, et al.* PPARgamma controls CD1d expression by turning on retinoic acid synthesis in developing human dendritic cells. *The Journal of experimental medicine* **203**, 2351-2362 (2006).
141. Ferrara, J.L., Levine, J.E., Reddy, P. & Holler, E. Graft-versus-host disease. *Lancet* **373**(2009).
142. Ferrara, J.L. Pathogenesis of acute graft-versus-host disease: cytokines and cellular effectors. *J.Hematother.Stem Cell Res.* **9**, 299-306 (2000).
143. Teshima, T., Reddy, P. & Zeiser, R. Acute Graft-versus-Host Disease: Novel Biological Insights. *Biology of blood and marrow transplantation : journal of the American Society for Blood and Marrow Transplantation* (2015).
144. Hongo, D., Tang, X., Dutt, S., Nador, R.G. & Strober, S. Interactions between NKT cells and Tregs are required for tolerance to combined bone marrow and organ transplants. *Blood* **119**, 1581-1589 (2012).
145. Yao, Z., Liu, Y., Jones, J. & Strober, S. Differences in Bcl-2 expression by T-cell subsets alter their balance after in vivo irradiation to favor CD4+Bcl-2hi NKT cells. *European journal of immunology* **39**, 763-775 (2009).

146. Kohrt, H.E., Pillai, A.B., Lowsky, R. & Strober, S. NKT cells, Treg, and their interactions in bone marrow transplantation. *European journal of immunology* **40**, 1862-1869 (2010).
147. Karadimitris, A. & Chaidos, A. The role of invariant NKT cells in allogeneic hematopoietic stem cell transplantation. *Critical reviews in immunology* **32**, 157-171 (2012).
148. Leveson-Gower, D.B*., et al.* Low doses of natural killer T cells provide protection from acute graft-versus-host disease via an IL-4-dependent mechanism. *Blood* **117**, 3220-3229 (2011).
149. Schneidawind, D*., et al.* CD4+ invariant natural killer T cells protect from murine GVHD lethality through expansion of donor CD4+CD25+FoxP3+ regulatory T cells. *Blood* **124**, 3320-3328 (2014).
150. Chaidos, A*., et al.* Graft invariant natural killer T-cell dose predicts risk of acute graft-versus-host disease in allogeneic hematopoietic stem cell transplantation. *Blood* **119**, 5030-5036 (2012).
151. Strober, S. & Lowsky, R. Rare cells predict GVHD. *Blood* **119**, 4820-4821 (2012).
152. Rubio, M.T*., et al.* Early posttransplantation donor-derived invariant natural killer T-cell recovery predicts the occurrence of acute graft-versus-host disease and overall survival. *Blood* **120**, 2144-2154 (2012).
153. de Lalla, C*., et al.* Invariant NKT cell reconstitution in pediatric leukemia patients given HLA-haploidentical stem cell transplantation defines distinct CD4+ and CD4- subset dynamics and correlates with remission state. *Journal of immunology* **186**, 4490-4499 (2011).
154. Patterson, S*., et al.* Human invariant NKT cells display alloreactivity instructed by invariant TCR-CD1d interaction and killer Ig receptors. *Journal of immunology* **181**, 3268-3276 (2008).
155. Pillai, A.B., George, T.I., Dutt, S., Teo, P. & Strober, S. Host NKT cells can prevent graft-versus-host disease and permit graft antitumor activity after bone marrow transplantation. *Journal of immunology* **178**, 6242-6251 (2007).
156. Dellabona, P., Casorati, G., de, L.C., Montagna, D. & Locatelli, F. On the use of donor-derived iNKT cells for adoptive immunotherapy to prevent leukemia recurrence in pediatric recipients of HLA haploidentical HSCT for hematological malignancies. *Clinical immunology* **140**, 152-159 (2011).
157. Guan, P., Bassiri, H., Patel, N.P., Nichols, K.E. & Das, R. Invariant natural killer T cells in hematopoietic stem cell transplantation: killer choice for natural suppression. *Bone marrow transplantation* **51**, 629-637 (2016).
158. Almasbak, H*., et al.* Inclusion of an IgG1-Fc spacer abrogates efficacy of CD19 CAR T cells in a xenograft mouse model. *Gene therapy* (2015).
159. Philip, B*., et al.* A highly compact epitope-based marker/suicide gene for easier and safer T-cell therapy. *Blood* **124**, 1277-1287 (2014).
160. Whilding, L.M*., et al.* Targeting of Aberrant alphavbeta6 Integrin Expression in Solid Tumors Using Chimeric Antigen Receptor-Engineered T Cells. *Molecular therapy : the journal of the American Society of Gene Therapy* **25**, 259-273 (2017).
161. Chomienne, C*., et al.* All-trans retinoic acid in acute promyelocytic leukemias. II. In vitro studies: structure-function relationship. *Blood* **76**, 1710 (1990).
162. Kutner, R.H., Zhang, X.-Y. & Reiser, J. Production, concentration and titration of pseudotyped HIV-1-based lentiviral vectors. *Nature protocols* **4**, 495 (2009).
163. Caputo, V.S*., et al.* Mechanism of Polycomb recruitment to CpG islands revealed by inherited disease-associated mutation. *Human molecular genetics* **22**, 3187-3194 (2013).
164. Spanoudakis, E*., et al.* Regulation of multiple myeloma survival and progression by CD1d. *Blood* **113**, 2498-2507 (2009).

165. Kawano, T*., et al.* Antitumor cytotoxicity mediated by ligand-activated human V alpha24 NKT cells. *Cancer research* **59**, 5102-5105 (1999).
166. Tahir, S.M*., et al.* Loss of IFN-gamma production by invariant NK T cells in advanced cancer. *Journal of immunology* **167**, 4046-4050 (2001).
167. Chaidos, A*., et al.* Graft invariant natural killer T-cell dose predicts risk of acute graft-versus-host disease in allogeneic hematopoietic stem cell transplantation. *Blood* (2012).
168. Exley, M.A*., et al.* Selective activation, expansion, and monitoring of human iNKT cells with a monoclonal antibody specific for the TCR alpha-chain CDR3 loop. *European journal of immunology* **38**, 1756-1766 (2008).
169. METELITSA, L.S., Liu, D., Dotti, G. & HECZEY, A. Targeting the tumor microenvironment using manipulated nkt cells. (Google Patents, 2013).
170. Better, M., Feldman, S.A. & Rosenberg, S.A. METHODS FOR PRODUCING AUTOLOGOUS T CELLS USEFUL TO TREAT B CELL MALIGNANCIES AND OTHER CANCERS AND COMPOSITIONS THEREOF. (U.S.A., 2015).
171. Hollyman, D*., et al.* Manufacturing validation of biologically functional T cells targeted to CD19 antigen for autologous adoptive cell therapy. *J Immunother* **32**, 169-180 (2009).
172. Li, Y. & Kurlander, R.J. Comparison of anti-CD3 and anti-CD28-coated beads with soluble anti-CD3 for expanding human T cells: Differing impact on CD8 T cell phenotype and responsiveness to restimulation. *Journal of translational medicine* **8**, 104-104 (2010).
173. Bilal, M.Y., Vacaflores, A. & Houtman, J.C.D. Optimization of Methods for the Genetic Modification of Human T Cells. *Immunology and cell biology* **93**, 896-908 (2015).
174. Marks-Konczalik, J*., et al.* IL-2-induced activation-induced cell death is inhibited in IL-15 transgenic mice. *Proceedings of the National Academy of Sciences* **97**, 11445-11450 (2000).
175. Gordy, L.E*., et al.* IL-15 regulates homeostasis and terminal maturation of NKT cells. *Journal of immunology* **187**, 6335-6345 (2011).
176. Chetoui, N., Boisvert, M., Gendron, S. & Aoudjit, F. Interleukin-7 promotes the survival of human CD4(+) effector/memory T cells by up-regulating Bcl-2 proteins and activating the JAK/STAT signalling pathway. *Immunology* **130**, 418-426 (2010).
177. Park, J.-Y., Keller, H., Sato, N. & Park, J.-H. NKT cells require IL-7, not IL-15, for survival and homeostasis (LYM4P.761). *The Journal of Immunology* **192**, 65.18 (2014).
178. Bendelac, A., Matzinger, P., Seder, R.A., Paul, W.E. & Schwartz, R.H. Activation events during thymic selection. *The Journal of experimental medicine* **175**, 731-742 (1992).
179. Matulis, G*., et al.* Innate-like control of human iNKT cell autoreactivity via the hypervariable CDR3beta loop. *PLoS biology* **8**, e1000402 (2010).
180. Better, M*., et al.* Rapid cell expansion (RACE) technology for production of engineered autologous T-cell therapy: Path toward manageable multicenter clinical trials in aggressive NHL with anti-CD19 CAR. *ASCO Meeting Abstracts* **32**, 3079 (2014).
181. Rocha, B. & Tanchot, C. Towards a cellular definition of CD8+ T-cell memory: the role of CD4+ T-cell help in CD8+ T-cell responses. *Current opinion in immunology* **16**, 259-263 (2004).
182. Sommermeyer, D*., et al.* Chimeric antigen receptor-modified T cells derived from defined CD8(+) and CD4(+) subsets confer superior antitumor reactivity in vivo. *Leukemia* **30**, 492-500 (2016).

183. Makedonas, G.*, et al.* Rapid up-regulation and granule-independent transport of perforin to the immunological synapse define a novel mechanism of antigen-specific CD8+ T cell cytotoxic activity. *J Immunol* **182**, 5560-5569 (2009).
184. Menager, M.M.*, et al.* Secretory cytotoxic granule maturation and exocytosis require the effector protein hMunc13-4. *Nature immunology* **8**, 257-267 (2007).
185. Lee, J., Ahn, E., Kissick, H.T. & Ahmed, R. Reinvigorating Exhausted T Cells by Blockade of the PD-1 Pathway. *Forum on immunopathological diseases and therapeutics* **6**, 7-17 (2015).
186. Utzschneider, D.T.*, et al.* T cells maintain an exhausted phenotype after antigen withdrawal and population reexpansion. *Nature immunology* **14**, 603-610 (2013).
187. Buggert, M., Tauriainen, J. & Karlsson, A.C. Genetic footprints of T cell exhaustion. *Translational Cancer Research*, S65-S67 (2017).
188. Foley, J.F. Polyfunctional T Cells. *Science signaling* **5**, ec42 (2012).
189. Haining, W.N. Travels in time: Assessing the functional complexity of T cells. *Proceedings of the National Academy of Sciences of the United States of America* **109**, 1359-1360 (2012).
190. Attig, S.*, et al.* Simultaneous infiltration of polyfunctional effector and suppressor T cells into renal cell carcinomas. *Cancer research* **69**, 8412-8419 (2009).
191. Ghoneim, H.E., Zamora, A.E., Thomas, P.G. & Youngblood, B.A. Cell-Intrinsic Barriers of T Cell-Based Immunotherapy. *Trends in molecular medicine* **22**, 1000-1011.
192. Xu-Monette, Z.Y., Zhou, J. & Young, K.H. PD-1 expression and clinical PD-1 blockade in B-cell lymphomas. *Blood* (2017).
193. U.S. F. a. D. Administration, YESCARTA (axicabtagene ciloleucel). Vol. 2018 (**https://www.fda.gov/biologicsbloodvaccines/cellulargenetherapyproducts/approvedproducts/ucm581222.htm**, 2018).
194. Navai, Shoba A. & Ahmed, N. Targeting the tumour profile using broad spectrum chimaeric antigen receptor T-cells. *Biochemical Society Transactions* **44**, 391 (2016).
195. Roder, J.C.*, et al.* A new immunodeficiency disorder in humans involving NK cells. *Nature* **284**, 553-555 (1980).
196. Morales, A. & Ottenhof, P.C. Clinical application of a whole blood assay for human natural killer (NK) cell activity. *Cancer* **52**, 667-670 (1983).
197. Goldberg, J.E., Sherwood, S.W. & Clayberger, C. A novel method for measuring CTL and NK cell-mediated cytotoxicity using annexin V and two-color flow cytometry. *Journal of immunological methods* **224**, 1-9 (1999).
198. Ozdemir, O., Ravindranath, Y. & Savasan, S. Cell-mediated cytotoxicity evaluation using monoclonal antibody staining for target or effector cells with annexinV/propidium iodide colabeling by fluorosphere-adjusted counts on three-color flow cytometry. *Cytometry. Part A : the journal of the International Society for Analytical Cytology* **56**, 53-60 (2003).
199. Liu, L.*, et al.* Visualization and quantification of T cell-mediated cytotoxicity using cell-permeable fluorogenic caspase substrates. *Nature medicine* **8**, 185-189 (2002).
200. Kim, G.G., Donnenberg, V.S., Donnenberg, A.D., Gooding, W. & Whiteside, T.L. A novel multiparametric flow cytometry-based cytotoxicity assay simultaneously immunophenotypes effector cells: comparisons to a 4 h 51Cr-release assay. *Journal of immunological methods* **325**, 51-66 (2007).

201. Philpott, N.J*., et al.* The use of 7-amino actinomycin D in identifying apoptosis: simplicity of use and broad spectrum of application compared with other techniques. *Blood* **87**, 2244-2251 (1996).
202. Exley, M*., et al.* CD1d structure and regulation on human thymocytes, peripheral blood T cells, B cells and monocytes. *Immunology* **100**, 37-47 (2000).
203. Lee, D.W*., et al.* T cells expressing CD19 chimeric antigen receptors for acute lymphoblastic leukaemia in children and young adults: a phase 1 dose-escalation trial. *Lancet* **385**(2015).
204. Sotillo, E*., et al.* Convergence of acquired mutations and alternative splicing of CD19 enables resistance to CART-19 immunotherapy. *Cancer discovery* **5**(2015).
205. Jacoby, E*., et al.* CD19 CAR immune pressure induces B-precursor acute lymphoblastic leukaemia lineage switch exposing inherent leukaemic plasticity. *Nature communications* **7**(2016).
206. Gardner, R*., et al.* Acquisition of a CD19 negative myeloid phenotype allows immune escape of MLL-rearranged B-ALL from CD19 CAR-T cell therapy. *Blood* **127**(2016).
207. Perna, F. & Sadelain, M. Myeloid leukemia switch as immune escape from CD19 chimeric antigen receptor (CAR) therapy. *Transl Cancer Res* **5**(2016).
208. Turtle, C.J*., et al.* CD19 CAR-T cells of defined CD4+:CD8+ composition in adult B cell ALL patients. *The Journal of clinical investigation* **126**(2016).
209. Wang, Z., Wu, Z., Liu, Y. & Han, W. New development in CAR-T cell therapy. *Journal of hematology & oncology* **10**, 53 (2017).
210. De Munter, S*., et al.* Nanobody Based Dual Specific CARs. *International journal of molecular sciences* **19**, 403 (2018).
211. Lozzio, B.B. & Lozzio, C.B. Properties of the K562 cell line derived from a patient with chronic myeloid leukemia. *International journal of cancer. Journal international du cancer* **19**, 136 (1977).
212. Lozzio, C.B. & Lozzio, B.B. Human chronic myelogenous leukemia cell-line with positive Philadelphia chromosome. *Blood* **45**, 321-334 (1975).
213. Turtle, C.J. & Riddell, S.R. Artificial antigen presenting cells for use in adoptive immunotherapy. *Cancer journal (Sudbury, Mass.)* **16**, 374-381 (2010).
214. Butler, M.O*., et al.* Long-lived antitumor CD8+ lymphocytes for adoptive therapy generated using an artificial antigen-presenting cell. *Clinical cancer research : an official journal of the American Association for Cancer Research* **13**, 1857-1867 (2007).
215. Butler, M.O. & Hirano, N. Human cell-based artificial antigen-presenting cells for cancer immunotherapy. *Immunological reviews* **257**, 10.1111/imr.12129 (2014).
216. Kim, J.V., Latouche, J.B., Riviere, I. & Sadelain, M. The ABCs of artificial antigen presentation. *Nature biotechnology* **22**, 403-410 (2004).
217. Turtle, C.J. & Riddell, S.R. Artificial antigen-presenting cells for use in adoptive immunotherapy. *Cancer J* **16**, 374-381 (2010).
218. Li, J*., et al.* NKT Cell Responses to B Cell Lymphoma. *Medical sciences : open access journal* **2**, 82-97 (2014).
219. Metelitsa, L.S*., et al.* Human NKT cells mediate antitumor cytotoxicity directly by recognizing target cell CD1d with bound ligand or indirectly by producing IL-2 to activate NK cells. *Journal of immunology* **167**, 3114-3122 (2001).

220. Merryman, R.W., Armand, P., Wright, K.T. & Rodig, S.J. Checkpoint blockade in Hodgkin and non-Hodgkin lymphoma. *Blood advances* **1**, 2643-2654 (2017).
221. Boice, M.*, et al.* Loss of the HVEM Tumor Suppressor in Lymphoma and Restoration by Modified CAR-T Cells. *Cell* **167**, 405-418.e413 (2016).
222. Dranoff, G. Cytokines in cancer pathogenesis and cancer therapy. *Nat Rev Cancer* **4**, 11-22 (2004).
223. Hegde, S.*, et al.* NKT cells direct monocytes into a DC differentiation pathway. *Journal of leukocyte biology* **81**, 1224-1235 (2007).
224. Sriram, V.*, et al.* Inhibition of glycolipid shedding rescues recognition of a CD1⁺ T cell lymphoma by natural killer T (NKT) cells. *Proceedings of the National Academy of Sciences* **99**, 8197 (2002).
225. Sallusto, F., Nicolò, C., De Maria, R., Corinti, S. & Testi, R. Ceramide Inhibits Antigen Uptake and Presentation by Dendritic Cells. *The Journal of experimental medicine* **184**, 2411 (1996).
226. Lin, Y.*, et al.* Immunosuppressive CD14(+)HLA-DR(low/−) monocytes in B-cell non-Hodgkin lymphoma. *Blood* **117**, 872-881 (2011).
227. Chang, C.I., Liao, J.C. & Kuo, L. Macrophage arginase promotes tumor cell growth and suppresses nitric oxide-mediated tumor cytotoxicity. *Cancer research* **61**, 1100-1106 (2001).
228. Theate, I.*, et al.* Extensive profiling of the expression of the indoleamine 2,3-dioxygenase 1 protein in normal and tumoral human tissues. *Cancer immunology research* **3**, 161-172 (2015).
229. Molano, A., Illarionov, P.A., Besra, G.S., Putterman, C. & Porcelli, S.A. Modulation of invariant natural killer T cell cytokine responses by indoleamine 2,3-dioxygenase. *Immunology letters* **117**, 81-90 (2008).
230. Orabona, C., Pallotta, M.T. & Grohmann, U. Different partners, opposite outcomes: a new perspective of the immunobiology of indoleamine 2,3-dioxygenase. *Molecular medicine* **18**, 834-842 (2012).
231. Pallotta, M.T.*, et al.* Indoleamine 2,3-dioxygenase is a signaling protein in long-term tolerance by dendritic cells. *Nature immunology* **12**, 870-878 (2011).
232. Mei, J.*, et al.* Indoleamine 2,3-dioxygenase-1 (IDO1) enhances survival and invasiveness of endometrial stromal cells via the activation of JNK signaling pathway. *International journal of clinical and experimental pathology* **6**, 431-444 (2013).
233. Singh, N., Frey, N.V., Grupp, S.A. & Maude, S.L. CAR T Cell Therapy in Acute Lymphoblastic Leukemia and Potential for Chronic Lymphocytic Leukemia. *Current Treatment Options in Oncology* **17**, 1-11 (2016).
234. Porter, D.L.*, et al.* Randomized, phase II dose optimization study of chimeric antigen receptor (CAR) modified T cells directed against CD19 in patients (pts) with relapsed, refractory (R/R) CLL. in *2016 ASCO Annual Meeting* (J Clin Oncol 34, 2016 (suppl; abstr 3009), Chicago, 2016).
235. Zheng, Z., Venkatapathy, S., Rao, G. & Harrington, C.A. Expression profiling of B cell chronic lymphocytic leukemia suggests deficient CD1-mediated immunity, polarized cytokine response, altered adhesion and increased intracellular protein transport and processing of leukemic cells. *Leukemia* **16**, 2429-2437 (2002).
236. Bojarska-Junak, A.*, et al.* CD1d expression is higher in chronic lymphocytic leukemia patients with unfavorable prognosis. *Leukemia research* **38**, 435-442 (2014).
237. Chaudhry, M.S. & Karadimitris, A. Role and regulation of CD1d in normal and pathological B cells. *J Immunol* **193**, 4761-4768 (2014).

238. Mahmoudi, T. & Verrijzer, C.P. Chromatin silencing and activation by Polycomb and trithorax group proteins. *Oncogene* **20**, 3055-3066 (2001).
239. Beguelin, W.*, et al.* EZH2 is required for germinal center formation and somatic EZH2 mutations promote lymphoid transformation. *Cancer cell* **23**, 677-692 (2013).
240. Caganova, M.*, et al.* Germinal center dysregulation by histone methyltransferase EZH2 promotes lymphomagenesis. *The Journal of clinical investigation* **123**, 5009-5022 (2013).
241. Weinkove, R., Brooks, C.R., Carter, J.M., Hermans, I.F. & Ronchese, F. Functional invariant natural killer T-cell and CD1d axis in chronic lymphocytic leukemia: implications for immunotherapy. *Haematologica* **98**, 376-384 (2013).
242. Ghnewa, Y.G.*, et al.* Retinoic acid induction of CD1d expression primes chronic lymphocytic leukemia B cells for killing by CD8+ invariant natural killer T cells. *Clinical immunology* **183**, 91-98 (2017).
243. Hettmer, S., McCarter, R., Ladisch, S. & Kaucic, K. Alterations in neuroblastoma ganglioside synthesis by induction of GD1b synthase by retinoic acid. *British journal of cancer* **91**, 389-397 (2004).
244. Azuara, V.*, et al.* Chromatin signatures of pluripotent cell lines. *Nature cell biology* **8**, 532-538 (2006).
245. Denissov, S.*, et al.* Mll2 is required for H3K4 trimethylation on bivalent promoters in embryonic stem cells, whereas Mll1 is redundant. *Development* **141**, 526 (2014).
246. Hahn, M.A.*, et al.* Loss of the polycomb mark from bivalent promoters leads to activation of cancer-promoting genes in colorectal tumors. *Cancer research* **74**, 3617-3629 (2014).
247. Bernhart, S.H.*, et al.* Changes of bivalent chromatin coincide with increased expression of developmental genes in cancer. *Scientific reports* **6**, 37393 (2016).
248. Papakonstantinou, N.*, et al.* Overexpression of the Histone Methyltransferase EZH2 in Chronic Lymphocytic Leukemia Confers Protection from Apoptosis and Is Linked to Clinical Aggressiveness. *Blood* **124**, 1956 (2014).
249. Scialdone, A.*, et al.* The HDAC inhibitor valproate induces a bivalent status of the CD20 promoter in CLL patients suggesting distinct epigenetic regulation of CD20 expression in CLL in vivo. *Oncotarget* **8**, 37409-37422 (2017).
250. Renukaradhya, G.J.*, et al.* Type I NKT cells protect (and type II NKT cells suppress) the host's innate antitumor immune response to a B-cell lymphoma. *Blood* **111**, 5637-5645 (2008).
251. Bagnara, D. Adoptive immunotherapy mediated by ex vivo expanded natural killer T cells against CD1d-expressing lymphoid neoplasms. *Haematologica* **94**, 967-974 (2009).
252. Fujii, S., Shimizu, K., Smith, C., Bonifaz, L. & Steinman, R.M. Activation of natural killer T cells by [alpha]-galactosylceramide rapidly induces the full maturation of dendritic cells in vivo and thereby acts as an adjuvant for combined CD4 and CD8 T cell immunity to a coadministered protein. *J. Exp. Med.* **198**, 267-279 (2003).
253. Mattarollo, S.R.*, et al.* NKT cell adjuvant-based tumor vaccine for treatment of myc oncogene-driven mouse B-cell lymphoma. *Blood* **120**, 3019-3029 (2012).
254. Bjordahl, R.L., Gapin, L., Marrack, P. & Refaeli, Y. iNKT cells suppress the CD8+ T cell response to a murine Burkitt's-like B cell lymphoma. *PloS one* **7**, e42635 (2012).
255. Chung, Y.*, et al.* An NKT-mediated autologous vaccine generates CD4 T-cell dependent potent antilymphoma immunity. *Blood* **110**, 2013-2019 (2007).

256. Renukaradhya, G.J*., et al.* Inhibition of antitumor immunity by invariant natural killer T cells in a T-cell lymphoma model in vivo. *International journal of cancer. Journal international du cancer* **118**, 3045-3053 (2006).
257. Hong, S*., et al.* Tumor cells loaded with alpha-galactosylceramide promote therapeutic NKT-dependent anti-tumor immunity in multiple myeloma. *Immunology letters* **156**, 132-139 (2013).
258. Khalil, A.A*., et al.* The Influence of Hypoxia and pH on Bioluminescence Imaging of Luciferase-Transfected Tumor Cells and Xenografts. *International journal of molecular imaging* **2013**, 287697 (2013).
259. Tasian, S.K*., et al.* Optimized Depletion of Chimeric Antigen Receptor T-Cells in Murine Xenograft Models of Human Acute Myeloid Leukemia. *Blood* (2017).
260. Zheng, L*., et al.* Lym-1 Chimeric Antigen Receptor T Cells Exhibit Potent Anti-Tumor Effects against B-Cell Lymphoma. *International journal of molecular sciences* **18**, 2773 (2017).
261. Hoyos, V*., et al.* Engineering CD19-specific T lymphocytes with interleukin-15 and a suicide gene to enhance their anti-lymphoma/leukemia effects and safety. *Leukemia* **24**, 1160-1170 (2010).
262. Zah, E., Lin, M.-Y., Silva-Benedict, A., Jensen, M.C. & Chen, Y.Y. T Cells Expressing CD19/CD20 Bispecific Chimeric Antigen Receptors Prevent Antigen Escape by Malignant B Cells. *Cancer immunology research* **4**, 498-508 (2016).
263. Cooke, K.R*., et al.* An experimental model of idiopathic pneumonia syndrome after bone marrow transplantation: I. The roles of minor H antigens and endotoxin. *Blood* **88**, 3230-3239 (1996).
264. Al-Okaili, R.N., Krejza, J., Wang, S., Woo, J.H. & Melhem, E.R. Advanced MR Imaging Techniques in the Diagnosis of Intraaxial Brain Tumors in Adults. *RadioGraphics* **26**, S173-S189 (2006).
265. Kim, J.h*., et al.* 3T ¹H-MR Spectroscopy in Grading of Cerebral Gliomas: Comparison of Short and Intermediate Echo Time Sequences. *American Journal of Neuroradiology* **27**, 1412 (2006).
266. Verma, A., Kumar, I., Verma, N., Aggarwal, P. & Ojha, R. Magnetic resonance spectroscopy — Revisiting the biochemical and molecular milieu of brain tumors. *BBA Clinical* **5**, 170-178 (2016).
267. Abate-Daga, D. & Davila, M.L. CAR models: next-generation CAR modifications for enhanced T-cell function. *Molecular therapy oncolytics* **3**, 16014 (2016).
268. Zhao, Z*., et al.* Structural design of engineered costimulation determines tumor rejection kinetics and persistence of CAR T cells. *Cancer cell* **28**, 415-428 (2015).
269. Guo, Y., Feng, K., Wang, Y. & Han, W. Targeting cancer stem cells by using chimeric antigen receptor-modified T cells: a potential and curable approach for cancer treatment. *Protein & cell* (2017).
270. Brossay, L*., et al.* CD1d-mediated recognition of an alpha-galactosylceramide by natural killer T cells is highly conserved through mammalian evolution. *The Journal of experimental medicine* **188**, 1521-1528 (1998).
271. Corgnac, S*., et al.* CD1d-antibody fusion proteins target iNKT cells to the tumor and trigger long-term therapeutic responses. *Cancer Immunology, Immunotherapy* **62**, 747-760 (2013).
272. Jervis, P.J*., et al.* Design, Synthesis, and Functional Activity of Labeled CD1d Glycolipid Agonists. *Bioconjugate chemistry* **24**, 586-594 (2013).
273. Van Rhijn, I*., et al.* CD1d-restricted T cell activation by nonlipidic small molecules. *Proceedings of the National Academy of Sciences of the United States of America* **101**, 13578-13583 (2004).

274. Coughlan, A.M.*, et al.* Myeloid Engraftment in Humanized Mice: Impact of Granulocyte-Colony Stimulating Factor Treatment and Transgenic Mouse Strain. *Stem cells and development* **25**, 530-541 (2016).
275. Shultz, L.D.*, et al.* Human lymphoid and myeloid cell development in NOD/LtSz-scid IL2R gamma null mice engrafted with mobilized human hemopoietic stem cells. *Journal of immunology* **174**, 6477-6489 (2005).
276. Budde, L.E.*, et al.* Combining a CD20 chimeric antigen receptor and an inducible caspase 9 suicide switch to improve the efficacy and safety of T cell adoptive immunotherapy for lymphoma. *PloS one* **8**, e82742 (2013).
277. Qin, H.*, et al.* Eradication of B-ALL using chimeric antigen receptor–expressing T cells targeting the TSLPR oncoprotein. *Blood* **126**, 629 (2015).
278. Poirot, L.*, et al.* Multiplex Genome-Edited T-cell Manufacturing Platform for "Off-the-Shelf" Adoptive T-cell Immunotherapies. *Cancer research* **75**, 3853 (2015).
279. Tsukahara, T.*, et al.* CD19 target-engineered T-cells accumulate at tumor lesions in human B-cell lymphoma xenograft mouse models. *Biochemical and biophysical research communications* **438**, 84-89 (2013).
280. Alcantar-Orozco, E.M., Gornall, H., Baldan, V., Hawkins, R.E. & Gilham, D.E. Potential limitations of the NSG humanized mouse as a model system to optimize engineered human T cell therapy for cancer. *Human gene therapy methods* **24**, 310-320 (2013).
281. Brigl, M., Bry, L., Kent, S.C., Gumperz, J.E. & Brenner, M.B. Mechanism of CD1d-restricted natural killer T cell activation during microbial infection. *Nature immunology* **4**, 1230-1237 (2003).
282. Herr, M.M., Barr, P.M., Rich, D.Q. & Mohile, N. Clinical Features, Treatment, and Survival of Secondary Central Nervous System Lymphoma. *Blood* **124**, 5389 (2014).
283. Baraniskin, A.*, et al.* MicroRNA-30c as a novel diagnostic biomarker for primary and secondary B-cell lymphoma of the CNS. *Journal of neuro-oncology* (2018).
284. Myklebust, J.H.*, et al.* High PD-1 expression and suppressed cytokine signaling distinguish T cells infiltrating follicular lymphoma tumors from peripheral T cells. *Blood* **121**, 1367-1376 (2013).
285. Kochenderfer, J.N.*, et al.* Lymphoma Remissions Caused by Anti-CD19 Chimeric Antigen Receptor T Cells Are Associated With High Serum Interleukin-15 Levels. *Journal of Clinical Oncology* **35**, 1803-1813 (2017).
286. Xiao, W.*, et al.* Early recovery of circulating immature B cells in B-lymphoblastic leukemia patients after CD19 targeted CAR T cell therapy: A pitfall for minimal residual disease detection. *Cytometry. Part B, Clinical cytometry* (2017).
287. Brentjens, R.J.*, et al.* CD19-Targeted T Cells Rapidly Induce Molecular Remissions in Adults with Chemotherapy-Refractory Acute Lymphoblastic Leukemia. *Science translational medicine* **5**, 177ra138 (2013).
288. Garfall, A.L.*, et al.* Chimeric Antigen Receptor T Cells against CD19 for Multiple Myeloma. *New England Journal of Medicine* **373**, 1040-1047 (2015).
289. U. S. F. a. D. Administration, KYMRIAH (tisagenlecleucel). Vol. 2018 (**https://www.fda.gov/BiologicsBloodVaccines/CellularGeneTherapyProducts/ApprovedProducts/ucm573706.htm**, 2017).
290. June, C.H. & Powell Jr, D.J. CAR-EXPRESSING CELLS AGAINST MULTIPLE TUMOR ANTIGENS AND USES THEREOF. (USA, 2016).